UNIVERSITY OF CALIFORNIA, IRVINE

Techno-Economic Analysis of IGCCs Employing Novel Warm Gas Carbon Dioxide Separation and Carbon Capture Enhancements for High-Methane Syngas

THESIS

submitted in partial satisfaction of the requirements
for the degree of

MASTER OF SCIENCE
in Mechanical and Aerospace Engineering

by

Fabian Rosner

Thesis Committee:
Professor Scott Samuelsen, Ph.D., Chair
Professor Jack Brouwer, Ph.D.
Professor Jaeho Lee, Ph.D.

2018

DEDICATION

To

the environment;

hopefully no one is going to print this and if, only double sided.

"*The people who are crazy enough to think they can change the world are the ones who do.*"

Steve Jobs

TABLE OF CONTENTS

LIST OF FIGURES

LIST OF TABLES

NOMENCLATURE

Roman Symbols

a	Reaction Constant	–
a	Equilibrium Correction Factor	–
a_c	Specific External Surface Area of Catalyst	$\frac{\mathrm{m}^2}{\mathrm{g}}$
A	Surface Area	m^2
b	Reaction Order Exponent	–
Bi	Biot Number	–
Bo	Bodenstein Number	–
c	Concentration	$\frac{\mathrm{mol}}{\mathrm{m}^3}$
C	Cross-Sectional Area	m^2
Ca	Carberry Number	–
c_p	Heat Capacity at Constant Pressure	$\frac{\mathrm{kJ}}{\mathrm{mol\,K}}$
d	Catalyst Pellet Diameter	m
d_k	Molecule's Kinetic Diameter	m
d_pore	Pore Diameter	m
D	Reactor Diameter	m
D_{12}	Binary Diffusivity	$\frac{\mathrm{m}^2}{\mathrm{s}}$
D_ax	axial Dispersion	$\frac{\mathrm{m}^2}{\mathrm{s}}$
D_eff	Effective Diffusivity	$\frac{\mathrm{m}^2}{\mathrm{s}}$
D_K	Knudsen Diffusivity	$\frac{\mathrm{m}^2}{\mathrm{s}}$
E_A	Activation Energy	$\frac{\mathrm{kJ}}{\mathrm{kg\,K}}$
F	Pressure Correction Factor	–
h	Reaction Enthalpy	$\frac{\mathrm{kJ}}{\mathrm{mol}}$
J_D	Colburn Factor Mass Transport	–
J_H	Colburn Factor Heat Transport	–
k	Reaction Constant	$\frac{\mathrm{mol\,kPa}^{\mathrm{m+n+o+p}}}{\mathrm{g_{cat}\,s}}$
k	Turbine Pressure Constant	–
k_0	Frequency Factor	$\frac{\mathrm{mol\,kPa}^{\mathrm{m+n+o+p}}}{\mathrm{g_{cat}\,s}}$
k_B	Boltzmann Constant	$\frac{\mathrm{J}}{\mathrm{K}}$
K	Equilibrium Constant	atm
K'	Modified Equilibrium Constant	atm

Kn	Knudsen Number	$\frac{\mathrm{m}^2}{\mathrm{s}}$
L	Length	m
m	Carbon Monoxide Reaction Order Exponent	–
M	Molecular Weight	$\frac{\mathrm{g}}{\mathrm{mol}}$
$\overline{M}$	Average Molecular Weight	$\frac{\mathrm{g}}{\mathrm{mol}}$
n	Water Reaction Order Exponent	–
$\dot{n}$	Molar Flux	$\frac{\mathrm{mol}}{\mathrm{m}^2\mathrm{s}}$
$\dot{N}$	Molar Flow Rate	$\frac{\mathrm{mol}}{\mathrm{s}}$
o	Carbon Dioxide Order Reaction Exponent	–
p	Hydrogen Reaction Order Exponent	–
p	Pressure	atm
Pe	Peclet number	–
$\dot{Q}$	Energy Flow	kW
r^{g}	Gravimetric Reaction Rate	$\frac{\mathrm{mol}}{\mathrm{g}_{\mathrm{cat}}\mathrm{s}}$
r^{v}	Volumetric Reaction Rate	$\frac{\mathrm{mol}}{\mathrm{m}^3_{\mathrm{cat}}\mathrm{s}}$
R	Gas Constant	$\frac{\mathrm{kJ}}{\mathrm{kg}}$
R	Radius	m
R_{FT}	Fischer-Tropsch Constant	–
Re	Reynolds Number	–
Ro	Rate Optimization Number	–
S	Catalyst Pellet Surface Area	m^2
Sc	Schmidt Number	–
Sh	Sherwood Number	–
T	Temperature	K
T_{m}	Equilibrium Temperature Approach	K
u	Superficial Velocity	$\frac{\mathrm{m}}{\mathrm{s}}$
u	Scaling Exponent	–
v	Velocity	$\frac{\mathrm{m}}{\mathrm{s}}$
V	Volume of Element	m^3
V_{pellet}	Catalyst Pellet Volume	m^3
$\dot{V}$	Volumetric Flow Rate	$\frac{\mathrm{m}^3}{\mathrm{s}}$
X	Conversion	–
y	Gas Phase Volume Fraction	–
z	Direction of Reactor Axis	m

Greek Symbols

α	Heat Transfer Coefficient	$\frac{\mathrm{W}}{\mathrm{m}^2\mathrm{K}}$
β	Mass Transfer Coefficient	$\frac{\mathrm{m}}{\mathrm{s}}$
Γ	Mears Modulus for Intra-Particle Heat Transfer	

$\Delta\ c$	Concentration Change	Pa
$\Delta\ p$	Pressure Drop	$\frac{\mathrm{mol}}{\mathrm{m}^3}$
$\Delta\ x$	Height of Volume Element	m
$\Delta\ y$	Width of Volume Element	m
$\Delta\ z$	Depth of Volume Element	m
$\varepsilon_{\mathrm{bed}}$	Bed Void Fraction	–
$\varepsilon_{\mathrm{pellet}}$	Catalyst Porosity	–
ζ	Friction Coefficient	–
η	Catalyst Effectiveness	–
μ	Kinematic Viscosity	Pa s
π	Circle Constant	–
ρ	Density	$\frac{\mathrm{kg}}{\mathrm{m}^3}$
Σ_v	Diffusion Volume	–
τ_{bed}	Catalyst Bed Tortuosity	–
τ_{pellet}	Catalyst Pellet Tortuosity	–
τ	Residence Time	s
Φ_{b}	Thiele Modulus	–
Φ_{g}	Generalized Thiele Modulus	–
χ	Shape Factor	–
Ψ	Weisz-Prater Modulus	–
Ω	Mears Modulus for Extra-Particle Heat Transfer	

Subscripts

1	Reverse Hydrogasification
2	Boudouard Reaction
3	Water Gas Reaction
C	Carbon Species
FT	Fischer-Tropsch
H	Hydrogen Species
HC	Binary Mixture Hydrogen-Carbon
q	Cell Number q
i	Component i
Net Gen	Net Generation
OC	Binary Mixture Oxygen-Carbon
p	Pellet
R	Reference Case
t	Thermal

Abbreviations

AER	Annual Escalation Rate
AGR	Acid Gas Removal
aMDEA	Activated Methyl-Diethanol-Amine
ar	As Received
ASU	Air Separation Unit
CCF	Capital Charge Factor
CF	Plant Capacity Factor
COE	Cost of Electricity
daf	Dry and Ash Free
DoE	Department of Energy
dmmf	Dry and Mineral Matter Free
EAGLE	Energy Application for Gas, Liquid and Electricity
EPC	Engineering Services, Procurement and Construction
GE	General Electric
GT	Gas Turbine
HHV	Higher Heating Value
HRSG	Heat Recovery Steam Generator
HT	High Temperature
IGCC	Integrated Gasification Combined Cycle
IRS	Isothermal Shift Reactor
LHV	Lower Heating Value
LT	Low Temperature
MDEA	Methyl-Diethanol-Amine
MEA	Monoethanolamine
MHI	Mitsubishi Heavy Industry
MT	Medium Temperature
MWH	Annual Net-Megawatt-Hours at CF 100 %
NETL	National Energy Technology Laboratory
OC_{fix}	Fixed Annual Operating Cost
OC_{var}	Total Variable Annual Operating Cost
PC	Pulverized Coal
PM	Particulate Matter
PRB	Powder River Basin
PSA	Pressure Swing Adsorption
RC	Reference Cost
RP	Reference Parameter
RTI	Research Triangle Institute
RY	Reference Year
SC	Scaled Cost

SMR	Steam Methane Reforming
SP	Scaled Parameter
ST	Steam Turbine
SY	Scaled Year
TDA	TDA Research, Inc.
TIT	Turbine Inlet Temperature
TOC	Total Overnight Capital
TPC	Total Plant Cost
TR	Number of Trains/Equipment Reference
TRIG™	Transport Integrated Gasification
TS	Number of Trains/Equipment Scaled
TSA	Temperature Swing Adsorption
TS&M	Transport, Storage & Monitoring
WGS	Water Gas Shift

ACKNOWLEDGMENTS

I would like to express the deepest appreciation to my committee chair, Professor Scott Samuelsen. His immense support during the entire time was exceptional. His balanced guidance allowed me to dive deep into research questions following my personal interests but steered me into the right direction whenever needed. Without his guidance and persistent help this thesis would not have been possible.

Highest gratitude goes to Dr. Rao whose technical expertise from over 30 years of industry experience contributed a lot to this work. Dr. Rao was available any time to discuss research questions and conversations with him were always very productive.

I would like to thank my committee members, Professor Jack Brouwer and Professor Jaeho Lee, for serving on my thesis committee. I admire each of them for their outstanding teaching inspiring me to follow their example of conducting research at the highest level.

In addition, a thank you to TDA Research Inc. TDA has been an outstanding and reliable partner for the entire time of this project providing information and technical expertise about the CO_2-PSA.

Conclusively, I would like to thank my fellow student at the Advanced Power and Energy Program for the great support and constructive conversations about my research outcomes.

ABSTRACT OF THE THESIS

Techno-Economic Analysis of IGCCs Employing Novel Warm Gas Carbon Dioxide Separation and Carbon Capture Enhancements for High-Methane Syngas

By

Fabian Rosner

MASTER OF SCIENCE in Mechanical and Aerospace Engineering

University of California, Irvine, 2018

Professor Scott Samuelsen, Ph.D., Chair

The utilization of coal worldwide for electric power generation portends a need for advanced technologies to mitigate the release of carbon. To this end, a novel PSA-based warm gas CO_2-removal technology is compared to a state-of-the-art integrated gasification combined cycle (IGCC) power plant with dual-stage Selexol^{TM} unit for carbon capture using computational methods. The carbon capture in the Selexol^{TM} case is limited to 83.40 % due to the high methane content in the syngas. The Selexol^{TM} efficiency is $31.11\,\% - \text{HHV}$ resulting in a cost-of-electricity (COE) of 148.6 $\frac{\$}{\text{MWh}}$ with transport, storage, and monitoring (TS&M). Integration of the warm gas CO_2-removal technology increases the efficiency to $34.20\,\% - \text{HHV}$. Optimization of the water gas shift reactors using thermodynamic gas stability analysis and kinetic reaction modeling results in an efficiency of 35.63 % leading to a reduction in COE to 127.2 $\frac{\$}{\text{MWh}}$ with TS&M. With the here introduced Ro number, the catalyst volume of isothermal shifting can be reduced by up to 73 %. Due to a higher capture yield of the PSA-technology, carbon capture of 88.6 % can be achieved. In order to reach the U.S. Department of Energy target of 90 % carbon capture, three options are addressed: (1) combustion of syngas in the CO_2 purification section while raising steam, (2) syngas reforming in an external adiabatic reformer and (3) syngas recycling to the gasifier. While the syngas recycling option reveals the highest efficiency, the combustion of syngas option is the most economical with a COE of 138.1 $\frac{\$}{\text{MWh}}$ with TS&M.

Keywords: Integrated Gasification Combined Cycle (IGCC), Transport Gasifier (TRIG^{TM}), Water Gas Shift, Isothermal Shifting, Carbon Deposition, Carbon Capture, Warm Gas Cleanup, CO_2-Adsorption, High Methane Syngas.

Chapter 1

Introduction

1.1 Motivation

Energy is a key component for the development of human society and economic growth. Modern industry heavily relies on the availability of energy and is concerned about costs associated with energy procurement, especially in large economies like the United States, China, Japan, Germany and the United Kingdom. Emerging markets like India have, as well, large energy demands which greatly depend upon fossil primary energy and energy carriers. Particularly in developing countries like China and India, where large coal reserves exist, coal provides an inexpensive and reliable energy source. Coal is one of the most abundant fossil energy sources. Worldwide coal reserves surpass oil and gas reserves and will last a very long time into the future. The easy accessibility and uncomplicated handling for shipping make it an attractive fuel around the globe. Coal is more evenly distributed worldwide than other fossil fuels and it can be found in many countries, which reduces the dependence on oil and oil supplier countries. However, coal has the biggest environmental impact among the fossil energy carriers. Coal with its heavy carbon content per unit of released energy

leads to higher carbon dioxide emissions increases compared to other fossil fuels. In addition, traditional combustion of coal produces gaseous and solid criteria pollutants (e.g., nitrogen- and sulfur-oxides, particulate matter). This raises concerns regarding air pollution and greenhouse gas emissions.

In 2012, carbon dioxide emissions worldwide reached a value of 31.7 $\frac{\text{Gt}}{\text{year}}$ which represents an increase of 1.2 % compared to the previous year. The electricity generation and heating sectors account for 42 % of the carbon dioxide emissions, by far the largest carbon dioxide emitting sectors [1]. The World Energy Outlook 2011 warns that, under current development, carbon dioxide emissions will increase to 43 $\frac{\text{Gt}}{\text{year}}$ by 2035 [2]. This development is due to the increasing demand for energy and its strong reliance on fossil energy carriers, predominantly coal. In 2012, coal was responsible for 44 % of the worldwide carbon dioxide emissions from fossil fuels, primarily in electricity generation whereby coal accounted for 29 % of the total electricity generated [1]. As a result, the development of technologies for reducing emissions associated with fossil fuel based power plants is required.

In 2012, coal accounted for 29 % of the total electricity generation [1]. The reasons for utilizing coal in electricity generation are versatile. Coal is one of the most abundant energy sources. Worldwide coal reserves surpass oil and gas reserves and will last a very long time into the future. Its low cost, easy accessibility and uncomplicated handling for shipping make it an attractive fuel for use around the globe. The distribution of coal is more geographically even than other fossil fuels and it can be found in many countries, which reduces the dependence on oil and their supplier countries. With respect to grid stability and energy supply reliability, coal based energy technologies as used in power plants are extremely reliable and adjustable in electricity generation in contrast to many renewable technologies like solar or wind power.

In order to overcome emission and pollution problems associated with coal combustion, two different approaches for future generation power plants have attracted great interest in the research community; which include integrated gasification combined cycles (IGCC) and

blending coal with biomass. IGCCs enable highly efficient pre-combustion CO_2 cleanup, whereas biomass co-gasification reduces the environmental impact.

Integrated gasification combined cycles have shown to be an important development on the way to clean power generation from coal and biomass, combining the advantages of coal and/or biomass usage with low air pollution, low carbon dioxide emission, and high efficiency (for details see section 2.2). Instead of combusting coal directly and operating a Rankine-cycle based on the created temperature difference between the hot flue gas and a working fluid, commonly water, IGCC power plants operate on a Brayton-cycle with a bottoming Rankine-Cycle. The integrated gasification process converts solid coal into a mixture of methane, carbon monoxide, carbon dioxide, hydrogen, water and many more components in smaller concentrations; also known as synthesis gas or syngas. The syngas is fed into a gas turbine (Brayton-cycle) where it is mixed with air and transformed to high-temperature gas through combustion under high pressure. The high-temperature, high-pressure gas from the gas turbine is then expanded through a turbine that, in turn, powers an electric generator and compressor. The hot exhaust gas is used to generate high-pressure steam for the bottoming Rankine-cycle. This way, higher efficiencies can be reached compared to conventional coal power plants because of the thermal coupling between the combustion process in the gas turbine (where heat is available for conversion to work at a much higher temperature) and the Rankine-Cycle utilizing the waste heat to drive a steam generator. One of the leading advantages of IGCC plants is pre-combustion cleanup which removes components like sulfur and mercury. In addition, carbon dioxide can be removed from the feed stream prior to combustion. In the high-pressure syngas, these components are present in much higher concentrations than after combustion when the exhaust stream is diluted with nitrogen and excess oxygen from the air. As a result, much higher sulfur, mercury and carbon dioxide removal efficiencies can be achieved at lower cost.

Strict emission limits are already implemented for many trace components like sulfur and mercury, as well as for carbon monoxide and nitrogen oxides. The U.S. Environmental

Protection Agency has not yet established regulations for carbon dioxide emissions. However, different strategies such as a carbon tax and cap-and-trade are currently discussed and implemented in order to reduce carbon dioxide emissions. Thus, highly efficient options for carbon dioxide removal are needed to ensure economical plant operation. Currently one of the most widely used and most advanced technologies is the Selexol^{TM} process. The Selexol^{TM} process was originally developed for desulfurization but has been extensively studied and tested for carbon dioxide removal and represents the state-of-the-art technology when it comes to carbon dioxide removal (for details see section 2.2). However, the Selexol^{TM} process is based on physical absorption and requires low temperatures in order to achieve reasonable carbon dioxide separation. As indicated before, the carbon dioxide removal unit is ideally placed between the gasifier and the gas turbine to take advantage of the higher partial pressure of CO_2 and lower stream flow rate. Both the gasifier and gas turbine operate at high temperatures while cooling the syngas after the gasifier and reheating it after the carbon dioxide removal process introduces a significant efficiency loss due to heat exchange and losses to the environment. Considering the large quantities of fuel being consumed in central power plants, even small efficiency gains can have a large impact on the economics and emissions. Identifying new technologies that can remove carbon dioxide at elevated temperatures and integrating them into the power plant has become a significant field of research interest. An increased efficiency in an IGCC plant not only reduces the operating costs, but also has an enormous impact on the overall plant cost. IGCC plants are still very expensive compared to existing commercial power plant technology and cost is the main reason why only a handful full-scale IGCC plants are in operation today.

Syngas is a versatile intermediate product. Besides electricity production, IGCC power plants have the capability of co-producing fuels and/or chemicals like gasoline, hydrogen and methanol from syngas. This could allow more flexibility in the plant operation as well as improve the economics of the cost of electricity and by-product costs as both scale with plant size.

A further aspect challenging future generation power plants is the limitation of water resources. As the global climate changes and the world population continues to grow, water will become less available and more expensive. Integrated gasification combined cycles offer clean and highly efficient electricity generation with significantly lower water consumption since the majority of the power is generated by gas turbines and thus, less cooling is required.

1.2 Goal and Objectives

In IGCC power plants, the challenge is to increase efficiency while reducing capital costs. In this study, a conventional Selexol^{TM} carbon dioxide removal unit is compared to a novel, newly developed warm gas carbon dioxide removal technology based upon mesoporous carbon modified with surface functional groups, a warm gas cleanup technology that utilizes the principle of selective carbon dioxide adsorption onto a surface without forming covalent bonds. After the surface sites are occupied with CO_2, the bed undergoes a recovery step and is reused. In this work, the synergistic effects between this new warm gas cleanup technology and transport integrated gasification (TRIG^{TM}) in an IGCC are investigated. The focus of this study is the influence of warm gas cleanup upon the plant performance and economics. Further investigations of the water gas shift reaction upon carbon capture are conducted to evaluate performance and economic benefits. Pathways to achieve the goal of the U.S. Department of Energy (DoE) of 90 % carbon capture [3] are delineated and analyzed. The goal of this research is to lower the environmental impact of electric power generation associated with IGCC power plants through the utilization of a novel, carbon-capture technology.

Successful achievement of this research goal requires a systematic approach. To achieve the research goal, the following six objectives are prescribed.

Objective 1: Establish a Design Basis and Calibration of Key Models

Objective 2: Develop a Dual-Stage Selexol^{TM} Scenario

Dioxide Removal Technology

Objective 3: Develop a PSA Warm Gas Cleanup Scenario

Objective 4: Study the Influences of the Water Gas Shift Reaction upon Carbon Capture

Objective 5: Evaluate Methods to reach the DoE Target of 90 % Carbon Capture

Objective 6: Techno-Economic Analysis

1.3 Thesis Outline

The first part of this thesis provides an introduction to the topic and gives an overview of technologies employed in integrated gasification combined cycle power plants. The current IGCC development status is analyzed and an assessment of commercially operated IGCC plants is carried out. Furthermore, a literature review of integrated gasification combined cycle power plants employing transport integrated gasification reactors was conducted and a summary of research results from literature on the integration of warm gas cleanup technologies into integrated gasification combined cycle power plants is presented.

The second part focuses on the approach and the above-mentioned objectives which will be restated as tasks with explanations of the work scope. The ensuing section states the design basis, introduces modeling approaches for the IGCC process units and describes the methodology for the techno-economic analysis. In the general process section, common process areas are introduced; case-specific process areas are described in the case description.

The first simulation is a state-of-the-art Selexol^{TM} CO_2-removal IGCC which functions as reference case. The kinetic model for the shift rector analysis is introduced in the specific section which is followed by the optimization of the shift reactor section of the IGCC plant. After the optimization scenarios, 3 Pathway scenarios for 90 % carbon capture are shown and discussed. The second last section provides a techno-economical evaluation of all studied cases. At the end a final conclusion is presented and recommendations for further research are provided.

Chapter 2

Background

This chapter provides an overview of IGCC technology and its major components. In the second part, a literature review is presented summarizing the IGCC development status, the progress in TRIG^{TM}-IGCC power plants and warm gas cleanup technology for the removal of carbon dioxide.

2.1 IGCC Technology Background

The first subdivision of this section will provide the reader with the basic concept of an IGCC power plant. Thereafter, the following section will provide further insights of key components of an IGCC power plant.

2.1.1 Thermodynamic Cycle

In order to understand the differences between an IGCC power plant and a conventional pulverized coal (PC) fired power plant, some background on PC plants is discussed first.

Conventional pulverized coal power plants operate on a Rankine-cycle. The working fluid, water, is pressurized employing pumps and heated in a boiler. The boiler is operated on coal and air and provides the heat-input for the generation of superheated steam. The hot steam is then expanded in a steam turbine which is connected to an electric generator to generate electricity. After the expansion process, the low-pressure steam is condensed in a heat exchanger and returned to the pump closing the cycle. Central power stations often include a reheat or even double reheat step to increase the efficiency of the plant. In this scenario the steam leaving the high pressure turbine is reheated before it is injected into the medium pressure steam turbine. However, details of reheat cycles will not be discussed here. A simple, ideal Rankine-cycle consists of four steps:

- 1) isentropic pressurization
- 2) isobaric heat addition
- 3) isentropic expansion
- 4) isobaric heat rejection

Many different variations and modifications of this simple cycle have been developed and realized. However, most of them can be divided into three major categories; subcritical PC plants, supercritical PC plants and ultra-supercritical PC plants. The most substantial differences are operating temperatures and pressures. Subcritical units typically operate at pressures below 22.1 MPa and main steam temperatures below 565 °C, supercritical plants operate in the range of $22.1 - 25$ MPa and a main steam temperature of $540 - 580$ °C. Ultra-supercritical power plants are exceeding pressures of 25 MPa and main steam temperature

of 580 °C [4]. Figure 2.1 shows the three simple cycles of the above-mentioned categories in a Temperature-Entropy-Diagram.

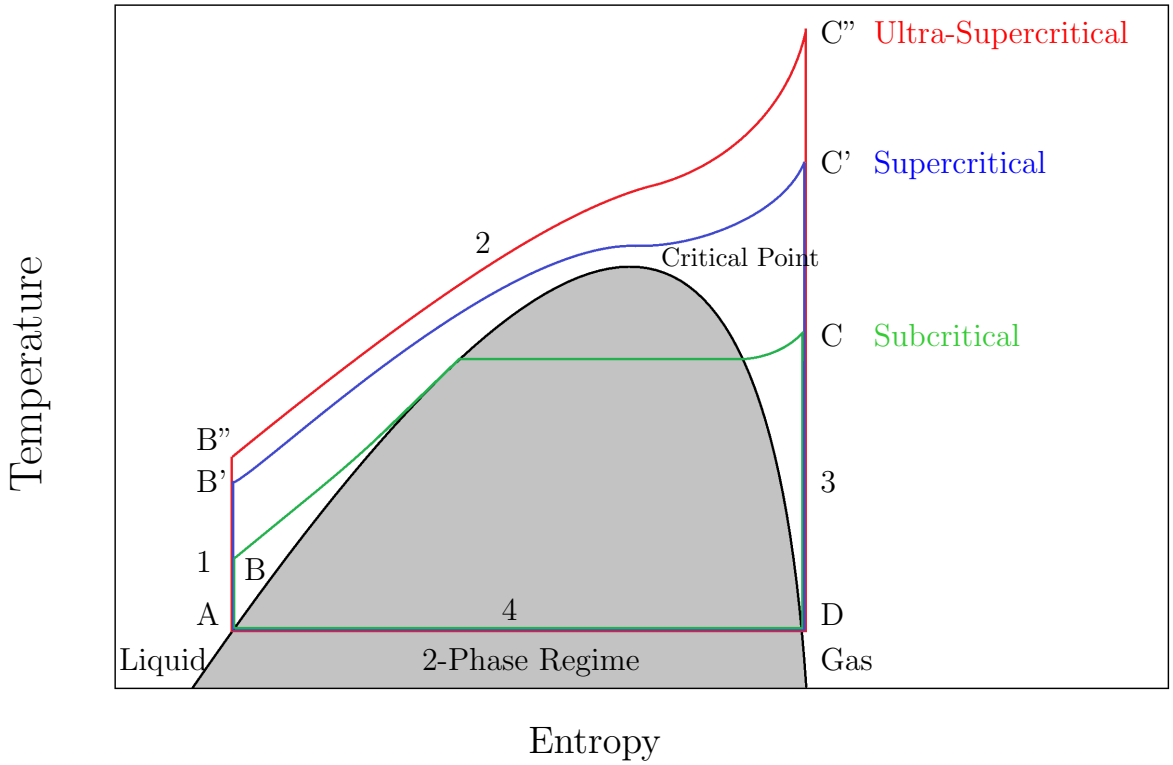

Figure 2.1: Illustration of the operating regimes of the three major categories of simple, ideal Rankine-cycles.

All of these ideal cycles operate upon the sequence of isentropic pressurization (1), isobaric heat addition (2), isentropic expansion (3) and isobaric heat rejection (4). The subcritical cycle is described by the states A-B-C-D and involves a constant temperature heat addition in the 2-phase regime. The supercritical plants (A-B'-C'-D and A-B"-C"-D) operate at super critical pressures and the pressurized water does not undergo a phase change. The higher turbine inlet temperature and higher turbine inlet pressure increase the efficiency of supercritical and ultra-supercritical plants. Furthermore, operating a plant at supercritical pressures reduces entropy losses associated with the heat transfer in the boiler which also benefits the plant efficiency. Efficiencies for subcritical boiler plants range from $33 - 39\,\% - \mathrm{HHV}$. Supercritical boiler plants typically reach efficien-

cies between $38 - 42\ \% - \text{HHV}$ and ultra-supercritical boiler plants operate in the range of $42 - 46\ \% - \text{HHV}$ [4].

An illustration of a simple pulverized coal power plant is depicted in Figure 2.2.

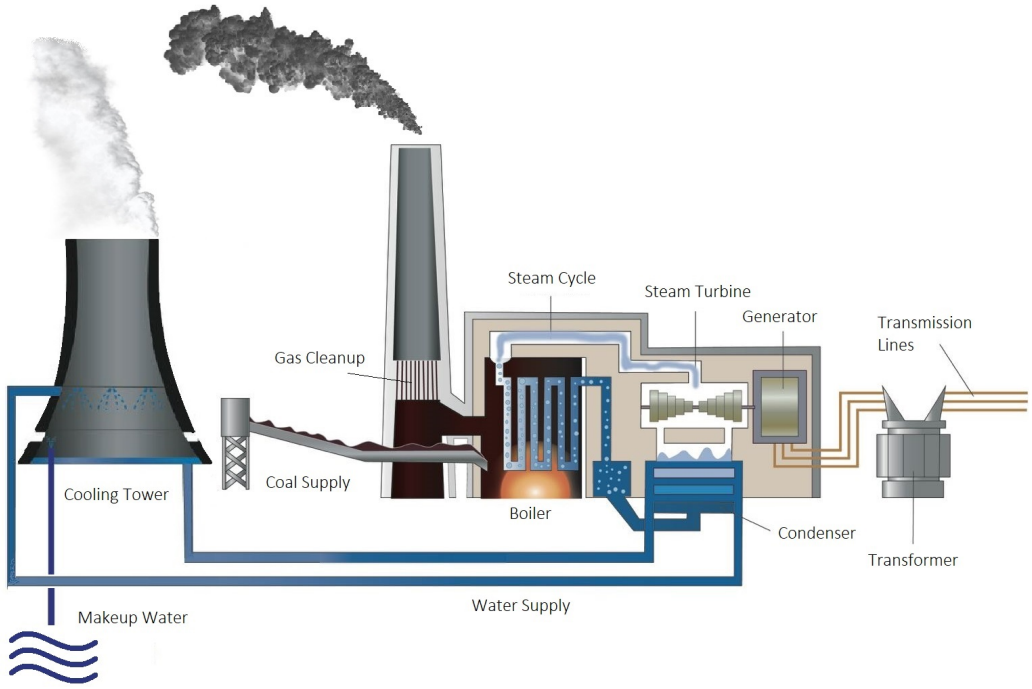

Figure 2.2: Design of a typical pulverized coal power plant.

In the coal supply chain, the delivered coal is first crushed, dried and milled before it can be fed into the boiler. The particle size of the milled coal is typically around 75 μm. Fine coal particles are desired to improve the combustion of the coal particles. The coal is entrained with primary air and injected into the boiler by a burner where it is mixed with a secondary air stream. The boiler consists of several burners and reaches operating temperatures of $500 - 600\ ^\circ\text{C}$. Ash is collected at the bottom of the boiler and the combustion products leave the boiler through the stack with typically post-combustion flue gas clean-up. The boiler features several different coils such as, an economizer to heat up pressurized water, evaporator, superheater and reheater. Many different boiler types have been developed over the last of couple of decades (e.g., grate boilers, fluidized bed boilers, and pulverized coal

boilers). However, all boiler types fulfill the same purpose of providing high quality heat at high coal conversion yields for steam generation. The high temperature and pressure steam leaving the boiler is expanded in the steam turbine which is coupled to the electricity generator and leaves the turbine as vapor. In order to complete the cycle, the vapor needs to be condensed. Pumping a liquid to high pressure is more efficient and economical than compressing as a vapor. The cooling load is typically provided by evaporative cooling in cooling towers which requires a source of water to make up for the loss of water which has been evaporated and transported into the atmosphere.

The biggest difference of an IGCC plant compared to a PC plant is that the coal in an IGCC plant is gasified instead of being combusted as a solid. The gasification process produces a combustible gas (syngas) which can be utilized in a gas turbine to generate electricity. Additionally, the exhaust of the gas turbine is sufficiently hot to raise high temperature steam and operate a bottoming Rankine-cycle like in a conventional PC-plant. Thus, an IGCC plant operates on a Brayton-cycle followed by a Rankine-cycle. The steps for the ideal cycles are as follows;

- 1) isentropic compression of the gas (air) in the turbine
- 2) isobaric heat addition in the turbine combustor
- 3) isentropic expansion in the turbine expander
- 4) isobaric heat rejection of the turbine exhaust
- 5) isentropic pressurization of the liquid water
- 6) isobaric heat addition through turbine exhaust
- 7) isentropic expansion in the steam turbine
- 8) isobaric heat rejection in the condenser

The working fluid for the Brayton-cycle is primarily air, whereas, the working fluid for the bottoming Rankine-cycle is water. In the Brayton-cycle air is compressed to a pressure that optimizes the combined cycle efficiency and fuel is supplied at this pressure from the gasifier. Thus, the gasifier operating pressure typically must be higher than the gas turbine combustion pressure in order to avoid the need for hot syngas compression. In addition, gas cleanup and/or cooling of the syngas can be accomplished at this high pressure as required by the cycle. The heat addition step in the gas turbine is an internal combustion process and ideally occurs at constant pressure. The depleted high-pressure product stream is then expanded in a turbine which is coupled to an electricity generator. In order to obtain a closed cycle, the gas has to be cooled to the initial compressor inlet temperature. However, since the Brayton-cycle contains an internal combustion process which consumes the oxygen in the air, the exhaust gas cannot be reused inside the cycle. This is why the Brayton-cycle is operated as an open cycle (continuously requiring fresh air). Nevertheless, cooling down the Brayton-cycle turbine exhaust to a certain degree in order to raise high pressure steam for a bottoming cycle is desirable as it improves the overall plant efficiency significantly. The bottoming Rankine-cycle operates as described above with the difference that the heat input is now provided by the gas turbine combustion and not a boiler. As a result of this, the maximum operating temperature of the Rankine-cycle or turbine inlet temperature of the Rankine-cycle is determined by the exhaust gas outlet temperature of the gas turbine. A schematic of the cycle arrangement in an IGCC power plant without steam reheat is shown in Figure 2.3.

As shown in Figure 2.3, the Brayton-cycle is not closed. Air is compressed isentropically from state A to state B, followed by the isobaric internal combustion process (B to C) and the isentropic expansion (C to D). The "cycle" ends at point E after most of the heat in the exhaust stream is transferred to the Rankine-cycle via heat exchangers. Thus, point D always has to be above point H and point E above point G to enable heat transfer with an acceptable temperature difference. Since the Brayton-cycle operates on air, it is not

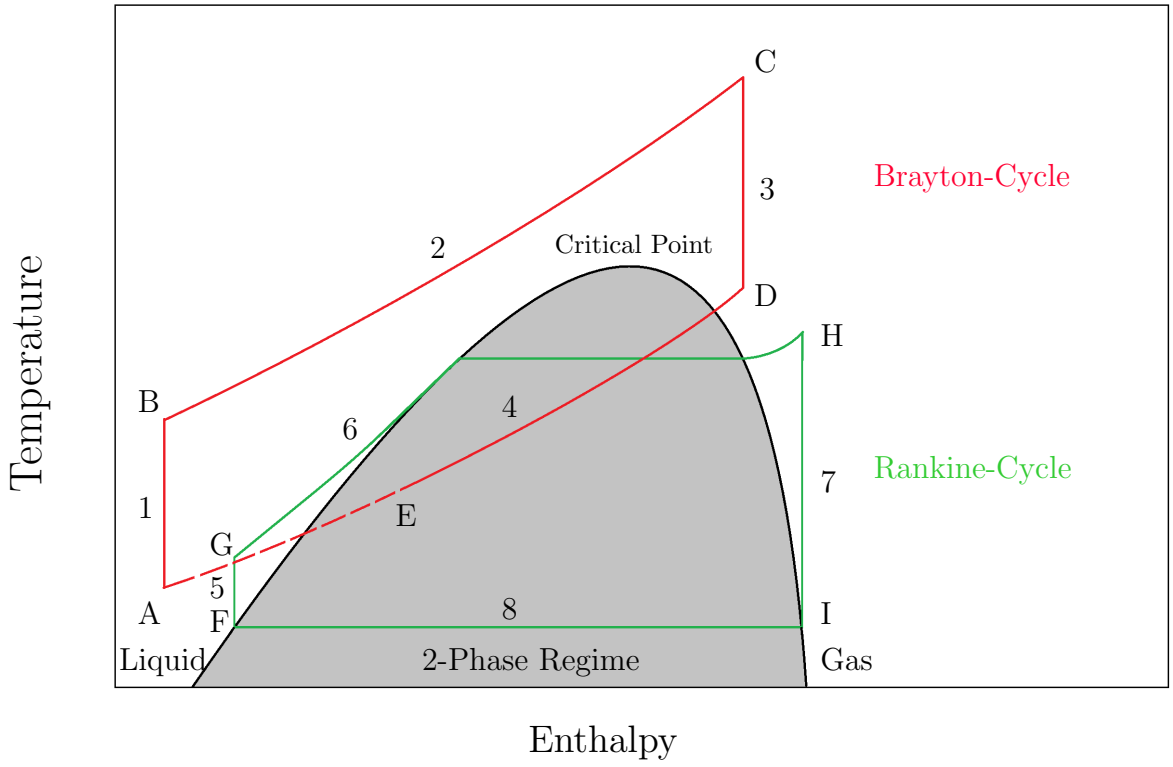

Figure 2.3: Illustration of the Brayton-cycle and Rankine-cycle integration strategy in an IGCC power plant.

affected by the vapor dome of water that is shown in the figure. The combination of two cycles allows IGCC power plants to reach efficiencies of greater 42 % – HHV [5] and, with further improvements (e.g., with warm gas sulfur removal technologies), efficiencies in the 60 % – HHV-range may be possible (without carbon capture and high temperature cleanup) [6].

A schematic of a simplified integrated gasification combined cycle power plant is depicted in Figure 2.4.

As it can be inferred from Figure 2.4 the IGCC plant design is more complex than the PC-plant design because of the conversion of coal to clean syngas and its two-cycle combination. The coal preparation in the IGCC plant is similar to the conventional boiler power plant. However, the coal preparation highly depends on the type of gasifier employed in the plant and can vary from slurry fed (E-Gas™ gasifier) to dry coal fed (Shell gasifier). In addition, an air separation unit (ASU) is required to provide oxygen for the oxygen-blown

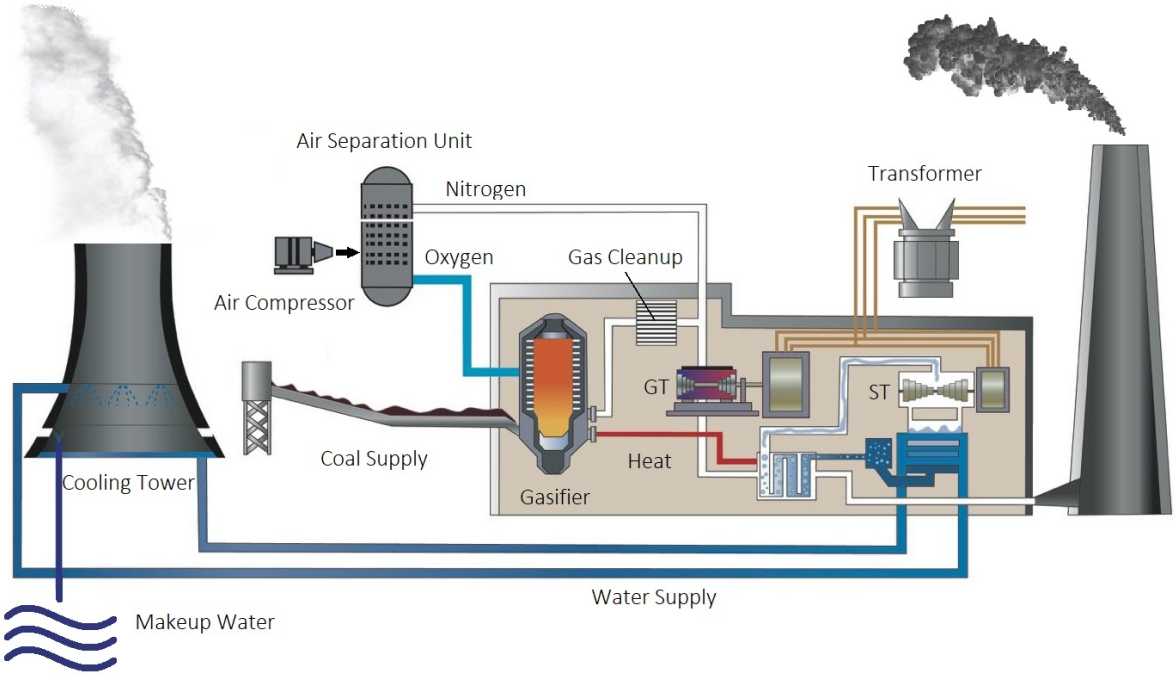

Figure 2.4: Design of a typical integrated gasification combined cycle power plant.

gasification process. Gasification takes place at high temperatures and requires a heat input which is provided by partial conversion of coal with oxygen. Pure oxygen has shown to be more efficient than air even though the ASU adds a large parasitic load to the plant balance. However, these losses are compensated through the higher efficiency of the gasifier and the gas cleanup processes when using pure oxygen (air contains 78 % nitrogen which dilutes the syngas in an air blown gasifier). Inside the gasifier the coal is being converted to syngas, containing mainly methane, carbon monoxide, carbon dioxide, hydrogen and water. Optional gas cleanup (e.g., removal of mercury, sulfur and/or carbon dioxide) is conducted before the combustion process since the compounds are present in much higher concentrations before being mixed with an oxidant and combusted, which makes the cleanup more efficient and reduces cost. After various cleanup steps, the syngas enters the combined power cycle which is described in Figure 2.3. Air is compressed in the gas turbine compressor, combusted with the syngas in the turbine combustor and expanded in the turbine expander. Waste heat from the turbine exhaust is recovered in a heat recovery steam generator (HRSG) unit which pro-

duces high pressure, high temperature steam for the bottoming Rankine-cycle. After the exhaust passed through the HRSG, the gas is released into the atmosphere. The operation of the Rankine-cycle follows the above description.

The advantages of the IGCC technology are high efficiency and low emissions. The integration of gasification allows the implementation of a high-pressure gas combustion process that can drive a gas expander while providing enough heat to operate a conventional steam cycle. This combination of a Brayton-cycle with a Rankine-cycle can reach very high efficiencies exceeding the limits of conventional PC-power plants. Furthermore, IGCC power plants can achieve significantly lower criteria pollutant emissions due to their suitability of pre-combustion gas cleanup. Before combustion, compounds containing heavy metals, sulfur and carbon dioxide are present in much higher concentration, which enables higher removal rates and lower emissions. However, current technologies mostly rely on absorption and/or adsorption processes that have to be operated at low temperatures. This results in a large thermodynamic penalty. In order to approach efficiencies of $60\,\% - \mathrm{HHV}$, new warm gas cleanup technologies have to be developed. Other advantages of the IGCC technology include its flexibility. An IGCC plant can be designed to co-produce chemicals like methanol, fuels or other chemicals because of syngas as an intermediate product. When fired with biomass, it can support the achievement of environmental targets and can produce renewable fuels. Further positive environmental impacts include its low water usage. In an IGCC power plant, most of the power is generated by the gas turbines which do not require any cooling water and only a small portion of power is generated by the Rankine-cycle. The disadvantages of IGCC power plants are their complexity which creates challenges regarding their controls and the high capital cost due to the additional equipment.

2.1.2 Key Components

The following section provides a more detailed description of major components found in IGCC power plants and explains their working principles.

Gasifier

The term gasification describes the conversion of solid carbonaceous feedstocks to a gaseous product stream with a net heating value. This is contrary to combustion where all the chemical energy of the fuel is released resulting in a product stream with a net heating value of zero.

Gasification has been around for a long time especially since larger scale gas production gained attraction at the end of the eighteenth century, promoted by the start of the industrial revolution. In 1812, with the foundation of the London Gas, Light and Coke Company gas production by pyrolysis became a commercial process and played an important role in the early stages of industrial development. The produced gas, called town gas, was comprised of mainly hydrogen and carbon monoxide and was used for illumination and heating purposes. Later in the 1920s, synthesis gas was produced by partial oxidation of coal and in combination with the water-gas-shift reaction the synthesis gas could be tuned, which made it useful for chemical applications like methanol and ammonia synthesis. Only 30 years later, in the 1950s, natural gas displaced the coal gasification technology and steam reforming became the predominant technology for syngas production. Only little development work on coal gasification technologies has been conducted since. During the oil crisis in the 1970s, some new programs were funded but with the new glut of oil in the 1980s these efforts were extinguished. Today, gasification is experiencing a renaissance with the emerging of the electricity market and the need for clean electricity generation from coal.

To understand coal gasification processes occurring in a gasifier, it is beneficial to

comprehend coal formation, classification and the resulting properties. Coal is formed over millions of years under high pressure and temperature from plant-based organic matter. Based on the development stage or age of the coal, it can be classified in accordance with its carbon content. The older the coal the higher the carbon content, and higher carbon content ultimately leads to a higher heating value. The evolution of coal starts with biomass which is first converted to lignite, sub-bituminous and bituminous coal before it eventually becomes anthracite. A summary of the different coals and their properties on an as-received basis, meaning without any processing at the plant site such as drying, is given in Table 2.1.

Table 2.1: Proximate Analyses of Coal Classes [7, 8]

wt-%	Lignite	Sub-Bituminous	Bituminous	Anthracite
Fixed Carbon	25-35	35-45	45-85	85-98
Volatiles	>45	20-45	20-9	<9
Moisture	30-70	10-45	2-16	2-16
Ash	2-30	2-30	2-15	2-10
Lower Heating Value $\frac{MJ}{Kg}$	26-28	28-32	32-36	36-27

This type of analysis is called proximate analysis. Several different bases for coal analysis are common: As-received, air-dry (without free moisture), dry (without any moisture), dry and ash free (daf), and dry and mineral matter free (dmmf). The volatile matter content is a crucial parameter in the proximate analysis with great significance for gasification applications. Volatile matter content is an indicator of the relative reactivity of the coal; the higher the volatile matter content the higher the reactivity, which is beneficial for the gasification process. Structural analysis of coal on an atomistic level is very complex and molecular structures differ a lot for different types of coal. However, the influence of the detailed petrographic composition of the organic compounds has no significant influence on the gasification behavior [7]. Complimentary to the proximate analysis is the ultimate analysis which provides information about the elemental composition of a coal. Examples of ultimate analyses for various coal types are shown in Table 2.2.

Table 2.2: Ultimate Analyses of various Coals [7]

Origin	Class	C	H	O	N	S
Germany, Rhein	Lignite	67.5	5	26.5	0.5	0.5
USA, Montana	Sub-Bituminous	76.4	5.6	14.9	1.7	1.4
China, Datung	Bituminous	84.4	4.4	9.5	0.9	0.8
Germany, Ruhr	Anthracite	91.8	3.6	2.5	1.4	0.7

The sulfur content in coal is important as it can form sulfuric acid in the atmosphere if not removed from the flue gas. Typical sulfur content in coals range from $0.5 - 6$ wt $-$ % and may be present in the form of organic sulfur as well as inorganic sulfur compounds [7]. Figure 2.5 illustrates the relationship between the proximate and ultimate analysis. Furthermore, it shows the origin of volatiles, ash and other coal components in form of an overlapping ring diagram illustrating the different subcategories and their relations to each other.

The innermost annulus represents the ultimate analysis and shows the elemental composition for a general coal. The circle in the middle of the diagram shows the different bases of analyses indicated by arrows whereby the whole circle represents the as-received basis. The second annulus from the inside shows the proximate analysis and the outer two annuli relate the analyses to the total moisture content, mineral matter content and organic substances content.

Beyond the components listed in the ultimate analysis, many other elements present in coal are especially important with respect to environmental and health concerns. Chlorides may be found in coal with chlorine concentrations of up to 2.5 wt $-$ %. These compounds can form HCl or NH_4Cl, which are not just concerning for health and environment but are also critical for plant operation. Furthermore, small amounts of phosphorous are present in many coals [7]. Phosphorous is less critical in coal gasification plants but can become problematic when using biomass feedstocks which can have significantly higher phosphorus concentrations. Additionally, coal contains traces of heavy metals like mercury and lead which need to be removed from the exhaust stream before being released into the environ-

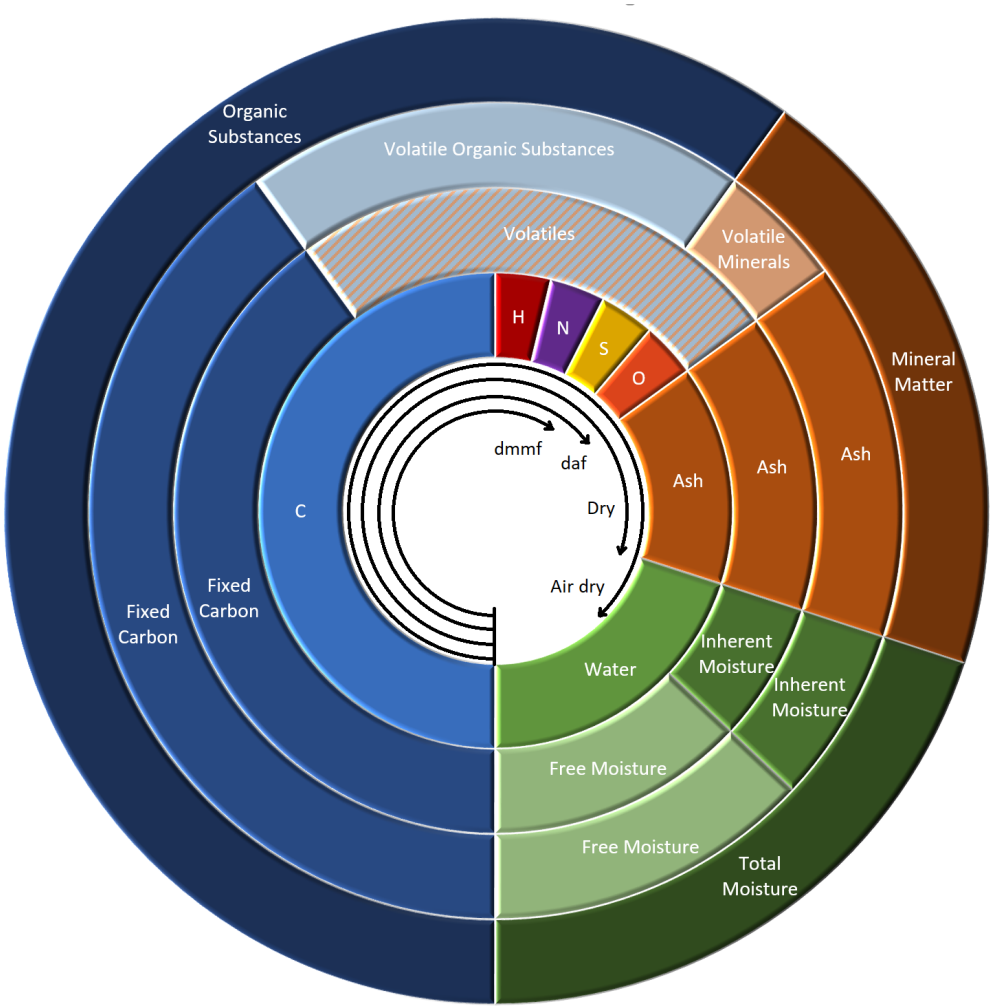

Figure 2.5: Illustration of the general coal composition.

ment.

Of great importance for the operation of a gasifier are the ash-softening and ash-melting temperatures. Depending upon the design of the gasifier, the ash either needs to remain as a liquid in the case of an entrained flow gasifier, or not soften (to avoid agglomeration) in the case of a fluidized bed gasifier. In many cases the ash determines the lower or upper temperature limit for the operation of a gasifier. Ash is produced from minerals in the coal and consists of compounds including, SiO_2, Al_2O_3, TiO_2, Fe_2O_3, CaO, MgO and many more. With respect to the ash melting point, most influential compounds are SiO_2, Al_2O_3, CaO and FeO. In general, SiO_2 and Al_2O_3 raise the ash meting temperature while CaO and FeO lower

the melting temperature [7]. Important are the conditions under which the softening and melting temperatures are determined. Gasifiers typically operate in reducing atmospheres in which the melting temperatures can differ from oxidizing conditions by more than 100 °C.

The gasification process can be divided into three different phases: dehydration, pyrolysis, and char conversion by oxygen, steam, carbon dioxide or hydrogen. Dehydration takes place at low temperatures around 100 °C. When the coal particle enters the hot gasifier, it starts heating up and moisture is removed. In many cases coal is already pre-dried to some degree when it enters the gasifier as pre-drying prevents agglomeration during the coal milling process. In the temperature regime $300 - 800$ °C, pyrolysis starts while the coal particle is further heating up. The overall pyrolysis process is endothermic where bonds of the solid carbonaceous material are broken up creating smaller compounds. The process can be described by the following equation [8].

$$\text{Coal} \longrightarrow CH_4 + C_mH_n + CO + CO_2 + H_2 + H_2O + \text{tars} + \text{char} + ... \tag{2.1}$$

An alternative description focusing on the major elements and components involved in pyrolysis is given by Equations 2.2 and 2.3 [8].

$$C_1H_xO_y \longrightarrow (1 - y)C + yCO + \frac{x}{2}H_2 \tag{2.2}$$

$$C_1H_xO_y \longrightarrow (1 - y - \frac{x}{8})C + yCO + \frac{x}{4}H_2 + \frac{x}{8}CH_4 \tag{2.3}$$

Despite the complexity of coal, it is reasonable for a first approximation to evaluate pyrolysis on a thermodynamic basis and only consider the elemental composition of coal (x and y are not necessarily stoichiometric, e.g. for a bituminous coal with 85 % C, 6 % H_2 and 9 % O_2, x and y are 0.874 and 0.0794 [8]). The heating rate, temperature, particle size and

steam partial pressure have an important influence on how devolatilization takes place [7]. If the heating rate is high, the pyrolysis step will overlap with the heterogeneous gasification reactions. The Heterogeneous gas-solid reaction between the carbon in the coal and the oxidizing feed gas and/or pyrolysis gas are characterized by the Boudouard reaction (Equation 2.4), the water gas reaction (Equation 2.5) and the methanation reaction (Equation 2.6).

$$\mathrm{C} + \mathrm{CO_2} \longrightarrow 2\mathrm{CO} \qquad +172\ \frac{\mathrm{kJ}}{\mathrm{mol}} \tag{2.4}$$

$$\mathrm{C} + \mathrm{H_2O} \longrightarrow \mathrm{CO} + \mathrm{H_2} \qquad +131\ \frac{\mathrm{kJ}}{\mathrm{mol}} \tag{2.5}$$

$$\mathrm{C} + \mathrm{H_2} \longrightarrow \mathrm{CH_4} \qquad -75\ \frac{\mathrm{kJ}}{\mathrm{mol}} \tag{2.6}$$

These reactions are limited by chamical reactions and transport mechanisms and govern the overall carbon conversion. Typically, the Boudouard reaction and water gas reaction are orders of magnitudes faster than the methanation reaction. In this case the methanation reaction does not need to be considered in equilibrium calculations. CH_4 is predominantly formed by the pyrolysis reactions. In the hydrogasification process, however, this reaction is the dominant chemical mechanism that forms CH_4.

Simultaneously, various gas phase reactions are proceeding. The two most important gas phase reactions are the water-gas-shift (WGS) reaction (Equation 2.7) and the steam methane reforming (SMR) reaction (Equation 2.8).

$$\mathrm{CO} + \mathrm{H_2O} \longrightarrow \mathrm{CO_2} + \mathrm{H_2} \qquad -41\ \frac{\mathrm{kJ}}{\mathrm{mol}} \tag{2.7}$$

$$\mathrm{CH_4} + \mathrm{H_2O} \longrightarrow \mathrm{CO} + 3\mathrm{H_2} \qquad +206\ \frac{\mathrm{kJ}}{\mathrm{mol}} \tag{2.8}$$

The gas phase reactions are fast at typical gasifier operating temperatures compared

to the heterogeneous gasification reactions. If the heating rate of the particle is slow, the pyrolysis will start at around 300 °C and will be completed before the gas phase reactions, WGS, SMR, hydrogenation and cracking reactions, reach substantial kinetic rates. This leads to high volatile concentrations, including higher hydrocarbons, tars and oils, in the close vicinity of the particle. This will ultimately result in a higher tar and oil content of the syngas. If the heating rate is high, gasification reactions proceed in parallel with pyrolysis preventing high concentrations of pyrolysis gas. This explains why entrained-flow reactors are able to produce very clean syngas compared to counter-flow moving bed reactors [7]. A schematic drawing of the gasification process of a coal particle is depicted in Figure 2.6.

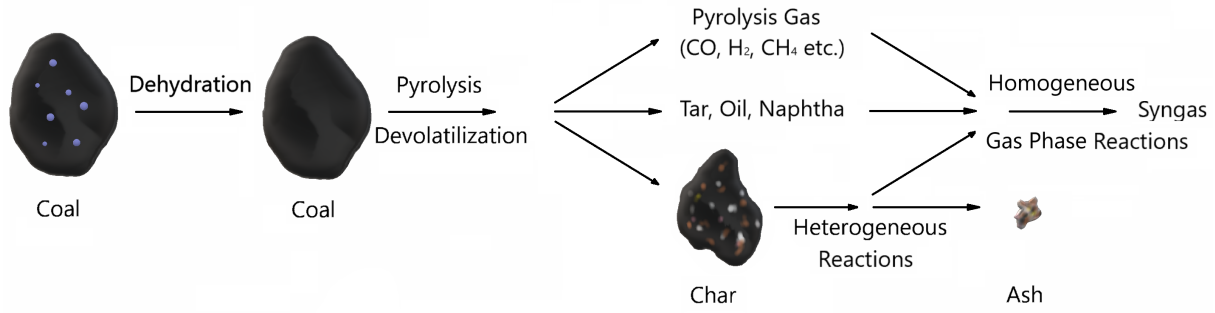

Figure 2.6: Illustration of the processes occurring during gasification.

Most of the gasification reactions are strongly endothermic and require a heat source. This energy can be provided externally or by the addition of an oxidant to the gasifier. Most modern gasifiers operate in an autothermal mode in which the heat required to drive the endothermic reactions is generated by partial oxidation and/or combustion. Having pure oxygen as an oxidant in lieu of air is a major advantage. Air contains substantial amounts of nitrogen which reduces the heating value of the syngas. Furthermore, the equipment size must be larger, which has an impact on the economics of the process. Introducing oxygen or air into the gasifier results in the following reactions.

$$C + \frac{1}{2}O_2 \longrightarrow CO \qquad -111\ \frac{kJ}{mol} \tag{2.9}$$

$$CO + \frac{1}{2}O_2 \longrightarrow CO_2 \qquad -283\ \frac{kJ}{mol} \tag{2.10}$$

$$H_2 + \frac{1}{2}O_2 \longrightarrow H_2O \qquad -242\ \frac{kJ}{mol} \tag{2.11}$$

$$CH_4 + \frac{1}{2}O_2 \longrightarrow CO + 2H_2 \qquad -36\ \frac{kJ}{mol} \tag{2.12}$$

$$CH_4 + 2O_2 \longrightarrow CO_2 + 2H_2O \qquad -890\ \frac{kJ}{mol} \tag{2.13}$$

Even today, most of the design work for gasification reactors is based on empirically collected data, due to complicated chemical kinetic effects of pyrolysis and heterogeneous char reactions. Before a gasification process can reach commercial scale, years of capital-intensive research are needed, collecting data from bench scale to pilot plant scale reactors with iterative re-engineering of the reactors. As mentioned by Higman and van Burgt modern gasification processes conserve $75 - 88$ % of the feedstock's original heating value in the syngas [7]. Most of the commercially available gasification processes can be classified into three major categories based upon their design and the transport of solid material in the process; moving bed gasifiers, fluidized bed gasifiers and entrained flow gasifiers.

Moving Bed Gasifier. In moving bed reactors, coal is continuously fed into the reactor from the top and moves slowly downwards as the particles are gasified. At the bottom of the reactor, only ash is left and removed from the gasifier. The oxidant can be introduced in co-, counter- or cross-flow, however, typically counter-flow is used as it offers advantages with respect to heat transfer. The bed can be divided into three zones: the combustion zone, the gasification zone, and the drying zone. For a counter-flow arrangement, the combustion zone is at the bottom of the gasifier where the char reacts with the oxidant to provide heat

for the gasification. This heat is carried with the depleted oxidant stream and promotes the gasification reactions in the second zone. Since the gasification reactions are endothermic, the temperature of the gas stream reduces as it travels further through the bed of coal. In the upper zone, moisture is removed from the coal and leads to a further reduction of the syngas' temperature. The problem with this type of gasifier is the high tar and oil content produced during pyrolysis. Due to the slow heating rate and counter-flow operation, the pyrolysis gas is not converted by the homogeneous gas phase reactions and leaves the reactor unchanged. Advantages of using moving bed gasifiers are the long residence times of the coal, which lead to high carbon conversion rates at low oxygen consumption rates. Upper operating limit for moving bed gasifiers is the slagging temperature. If the gasifier is operated above this temperature, ash clinkering will occur. Excessive clinkering will ultimately impair the gasifier operation. A schematic of a moving bed gasifier with its typical temperature profile is shown in Figure 2.7.

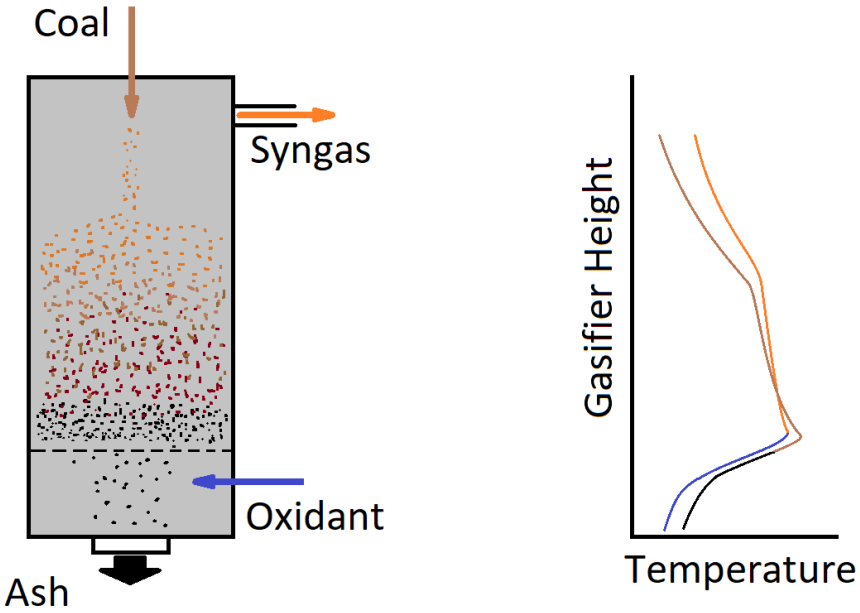

Figure 2.7: Operation mode of a moving bed gasifier with its corresponding temperature profile.

Moving bed gasifiers have been developed by Lurgi and BGL and are commercially available. Further information on this gasification technology and commercially available reactors can be found in [7].

Fluidized Bed Gasifier. The fluidized bed gasifier operates above the bed's fluidization point, either in a stationary mode or a circulating mode. The fluidization of the bed promotes heat and mass transfer and leads to almost constant temperatures and concentrations throughout the entire bed. In order to prevent agglomeration of the particles in the bed, the reactor temperature has to be maintained below the ash deformation temperature. Due to the higher gas velocities compared to a moving bed reactor, smaller particles are carried out of the reactor before they can react completely. Furthermore, the more intense mixing of the bed leads to char removal together with ash. All these effects, low operating temperature, gas flow entrained coal particles and coal removal with ash, contribute to a lower carbon conversion of fluidized bed reactors which are typically between $95 - 97$ % [8]. This effect can be countered by cyclone separators and particle recycling. A further disadvantage of fluidized bed gasifiers is the limited turndown rate. Relatively high gas velocities are needed to fluidize the bed. The syngas produced in fluidized bed gasifiers contains only small amounts of condensable by-products and is particularly suited for low rank coals and biomass with high ash content. A schematic of a stationary fluidized bed gasifier with its typical temperature profile is shown in Figure 2.8.

Circulating fluidized bed gasifiers operate at higher gas velocities and entrain the bed, which leads to even more intensive mixing. Larger particles that have been entrained by the gas are separated by a cyclone and recirculated. Overall this leads to higher carbon conversion rates compared to stationary fluidized bed reactors.
Commercially available fluidized bed gasifiers are offered as dry ash - Winkler, HTW and

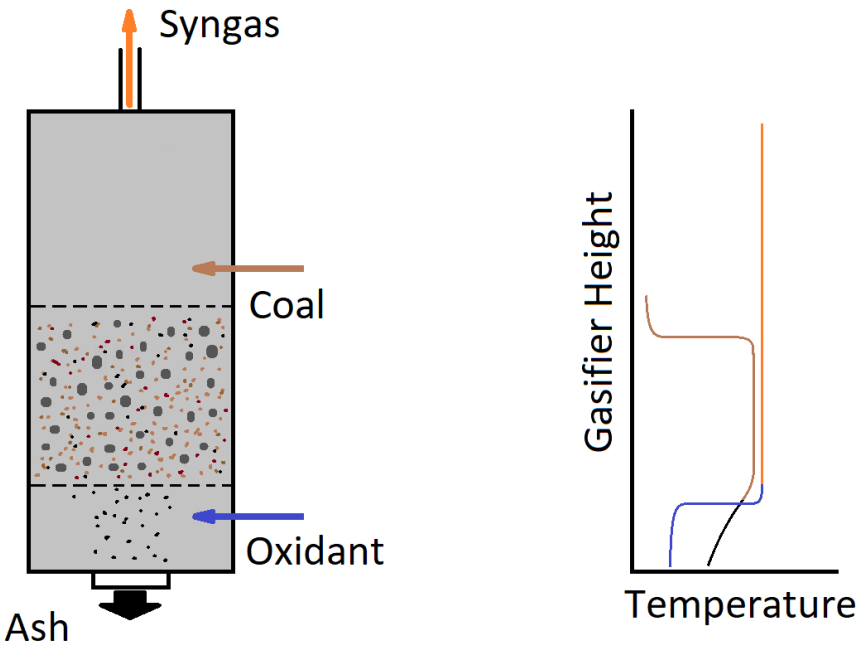

Figure 2.8: Operation mode of a stationary fluidized bed gasifier with its corresponding temperature profile.

CFB - and agglomerating - KRW and U-Gas - gasifiers. Details about the operation of these gasifiers can be found in [7].

Entrained Flow Gasifier. Entrained flow gasifiers are operated in a co-current flow with the coal entrained in the gas. As a result of this, the residence time of the coal particles is very short. In order to achieve high carbon conversion rates, typically >99 %, entrained flow gasifiers operate at very high temperatures and require a very fine ground coal feed, smaller 100 μm. The advantage of operating at temperatures greater 1400 °C is the very pure syngas which is free of tars and oils and low in methane content. For the operability of the gasifier at high temperatures it needs to operate above the ash slagging range. The liquid ash will stick to the reactor wall and run off. At the bottom of the reactor the ash is quenched and removed from the gasifier. In order to obtain these high operating temperatures large quantities of oxidant are needed. Because of its high temperatures, entrained flow gasifiers can be

operated on essentially any feedstock. However, high moisture or ash content feedstocks will further increase the oxidant demand which will eventually become critical with respect to the economical operation of the gasifier. A schematic of an entrained flow gasifier is shown in Figure 2.9.

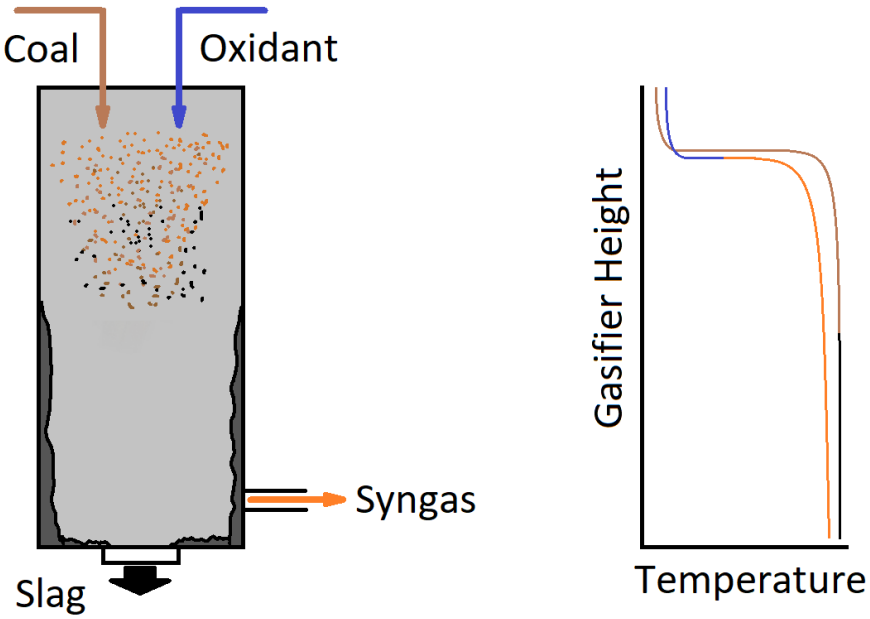

Figure 2.9: Operation mode of an entrained flow gasifier with its corresponding temperature profile.

Most of the currently employed gasifiers are entrained flow gasifiers, like the Shell gasifier, GE gasifier or E-Gas^{TM} gasifier. More information with respect to entrained flow gasifiers is available in [7].

A summary of the above-mentioned gasification processes is provided in Table 2.3. In general, low temperature gasifiers have a lower oxidant demand as less energy is required to heat up the feed. These gasifiers typically operate below the ash melting point and can be operated in moving bed or fluidized bed processes. In bed processes less feedstock preparation is needed; however, longer residence times and lower coal conversion should be expected. Higher operating temperatures lead to higher coal conversion and cleaner syngas.

Table 2.3: Summary of Gasification Technologies

Category	Moving Bed		Fluidized Bed		Entrained Flow
Ash Condition	Dry Ash	Slagging	Dry Ash	Agglomerating	Slagging
Process	Lurgi	BGL	Winkler, HTW CFB	KRW, U-Gas	Shell, GE E-Gas^{TM}
Feed Characteristics					
Size	$6-50$ mm	$6-50$ mm	$6-10$ mm	$6-10$ mm	<100 μm
Coal Rank	any	high	low	any	any
Operating Characteristics					
Reactor Temperature	$800-1200$ °C	$800-1200$ °C	$900-1050$ °C	$900-1050$ °C	>1400 °C
Outlet Gas Temperature	$425-650$ °C	$425-650$ °C	$900-1050$ °C	$900-1050$ °C	$1250-1600$ °C
Residence Time	$10-30$ min	$10-30$ min	$1-10$ min	$1-10$ min	<1 s
Oxidant Demand	low	low	moderate	moderate	high
Steam Demand	high	low	moderate	moderate	low
Cold Gas Efficiency	very high	very high	high	high	low
Carbon Conversion	high	high	low	low	very high
Syngas	contains hydrocarbons	contains hydrocarbons	some hydrocarbons	some hydrocarbons	pure gas

Adapted from [7, 8]

Air Separation Unit

The invention of the cryogenic air separation unit (ASU) by Carl von Linde in the 1920s was a major contribution for the development of advanced gasification technologies and many important gasification technologies have been commercialized in the following years. The advantage of using pure oxygen as oxidant over air is when the syngas is used for chemical applications where the nitrogen affects the downstream synthesis negatively. In the case of electricity generation from syngas, the pros and cons for using pure oxygen are not as evident. Using pure oxygen in IGCC applications has various impacts on equipment and chemistry. First, the downstream equipment size is reduced, which is beneficial with respect to the capital cost. Furthermore, it leads to a syngas with a higher heating value. As a result, oxygen blown gasifiers are favored in large scale applications with gasifiers that operate at high temperatures and have a high oxidant demand. In these applications nitrogen acts as ballast which degrades the chemical energy. Comparing the cold gas efficiencies of a pure

oxygen-blown to an air-blown gasifier, a decrease from 82 % to 61 % is observed [7]. In cases where carbon capture is desired, oxygen blown gasifiers are of particular advantage due to higher concentrations of carbon dioxide in the syngas which makes it easier to remove the carbon dioxide. An oxygen purity of 95 % has demonstrated to have the best economical value in IGCC applications. Higher purities of oxygen require an over proportional increase of distillation stages [9]. Air-blown operation of gasifiers becomes more attractive when considering low temperature gasification processes and small-scale applications.

Figure 2.10 shows a simplified flow sheet of a cryogenic air separation plant. Ambient air is compressed to about 6 bar and stepwise cooled against the rectification products, oxygen and nitrogen. After the first cooling stage, components, such as carbon dioxide and water, are removed from the air stream as they become solid at cryogenic temperatures. The clean air is further cooled in second heat exchanger with additional cooling provided by a nitrogen extraction stream from the high-pressure column which is expanded in a turbine. Using a turbine has three advantages over a throttling process: more cooling power due to the additional energy extraction in the form of work, the turbine can be coupled to a generator to generate electricity and increase the overall process efficiency. After the compressed air is partially liquefied in a third heat exchanger, the gas liquid mixture enters the high-pressure column. The column overhead produces pure nitrogen and the bottom product, a mixture of nitrogen and oxygen, is throttled and fed into a second low pressure column. The bottoms product of the second column acts as a condenser for the first column and the overhead of the first column acts as a re-boiler for the second column. Theoretically, the separation of nitrogen and oxygen is possible in one column but heat rejection at 79 K is not easily achieved. The two-pressure design allows the thermal coupling between the column and no condensers or re-boilers are needed.

The compression power required by an air separation unit is usually high and accounts for about $5 - 10$ % of the net power of an IGCC [9]. Capital cost of the air separation unit ranges between $10 - 15$ % of the total IGCC plant cost [7]. A way to reduce the power

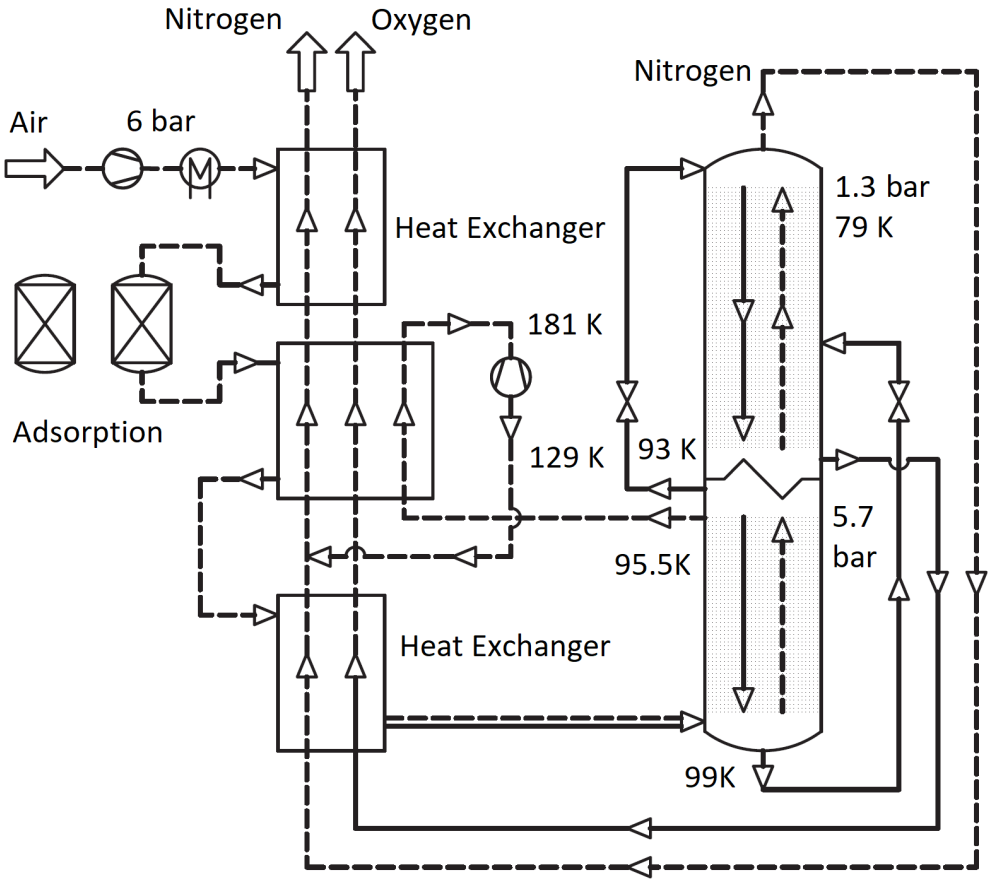

Figure 2.10: General flow sheet of an air separation unit [10].

consumption in an IGCC application is to integrate the gas turbine into the ASU and provide high pressure nitrogen to the gas turbine. The ASU is then operated at elevated pressures set by the gas turbine and less cooling is required (main reason for higher efficiency). The oxygen and nitrogen leaving the ASU (higher pressures compared to the conventional design) are then further compressed to the gasifier operating pressure in case of IGCC applications.

Gas Cleanup

The raw syngas composition leaving the gasifier can vary significantly depending on the gasification technology and the feedstock. As mentioned in the previous Section 2.1.2, moving bed gasifiers tend to produce syngas with higher hydrocarbon, oil and tar concentra-

tions than fluidized bed gasifiers or entrained flow gasifiers. However, syngas from moving bed gasifiers carries less particulates in the gas stream. Syngas trace components such as sulfur compounds and others depending on the gasified feedstock and to a lesser degree on the gasifier type. Different coals contain different amounts of trace components as it can be inferred from the ultimate analysis shown in Table 2.2. This has direct implications for the amount of trace components found in the syngas. Goal of the syngas treatment is to reduce concentrations of particular compounds down to levels that constitute no operational issues for the plant equipment, and danger to the environment and human health.

Gas cleanup technologies can be divided into state of the art cold gas cleanup systems and warm gas cleanup systems which are still under development. Warm gas cleanup systems are expected to boost the efficiency of IGCC power plants by several percent points. If the syngas is cleaned at higher temperatures, losses attributed to cooling, reheating and water vapor condensation can be reduced or completely avoided.

Gas Contaminants. Some of the most prominent gas impurities and related chemistry are discussed below. This list is not complete but provides an overview of the major challenges associated with certain compounds. The herein discussed compounds are typical for syngas produced from coal. By switching to a different feedstock like natural gas, biogas or biomass, the gas cleanup process needs to be reevaluated based upon the trace components (contaminants) present in the feedstock.

Sulfur Compounds. Sulfur is a poison for many catalysts used in chemical processing (e.g., water-gas-shift reaction promoting catalysts). If combusted in a gas turbine, these sulfur compounds are oxidized to sulfur dioxide which is the source for acid rain if emitted into the atmosphere. In high temperature gasification, 90 % of the sulfur components

leave the gasifier as hydrogen sulfide. The remaining sulfur is bound in carbonyl sulfide. Trace amounts of sulfur oxides and carbon disulfide are only present at low temperature gasification processes [8]. In order to remove more than 99 % of the sulfur from the syngas, carbonyl sulfide has to be converted to hydrogen sulfide in a hydrolysis reactor as it is not easily removed by most state-of-the-art acid gas removal systems like Selexol^{TM}.

Nitrogen Compounds. Two possible sources for raw syngas nitrogen, organic nitrogen bound in the fuel and molecular nitrogen, enter the gasifier as air or as transport medium for coal. During the gasification process small amounts of hydrogen cyanide and ammonia are formed which originates mostly from the organic nitrogen in the fuel. Nitrogen oxides are essentially not present due to the reducing environment in the gasifier. However, if combusted, both compounds (hydrogen cyanide and ammonia) form nitrogen oxides. Nitrogen oxides are toxic and a contributor to degraded air quality and climate change. Furthermore, the hydrogen cyanide in the raw syngas is known to degrade amines used in some sulfur removal processes. Thus, it is important to remove nitrogen compounds from the syngas before the sulfur is removed. A useful property of hydrogen cyanide and ammonia with respect to their removal is their high solubility in water. Syngas scrubbers and/or cooling the syngas below its dew point are an efficient and cost-effective way to remove nitrogen compounds from the syngas.

Chlorine Compounds. Chlorine compounds are mainly HCl and NH_4Cl which are formed from chlorine released from the fuel. HCl can react with metals, such as reactor walls, heat exchangers and piping. The resulting metal salts will start depositing in the syngas cooling section of the plant and pose a severe fouling risk. Similar consequences result from NH_4Cl which is a salt that solidifies at around 280 °C. Beyond fouling problems, chlorine

compounds constitute a poison for catalysts as used in low temperature shift reactors and thus, have to be removed before. Syngas scrubbers are an efficient and cost-effective way to remove these compounds from the syngas.

Particulate Matter. Particulate matter is not only a problem for human health but also for equipment downstream of the gasifier. Hot ash and carbon particles can stick to heat exchanger surfaces and cause problems with fouling. A syngas quench or cooler needs to ensure that the particles are solidified before removal to prevent fouling. Solid particles, however, can lead to abrasion in piping and other equipment wherefore they have to be removed at the very beginning of the syngas cleaning process.

Heavy Metals. Heavy metals like mercury, lead or arsenic are mostly encountered in coal feedstocks. Heavy metals have a significant deactivating effect on precious metal catalysts but more importantly, present a high risk for human health. Furthermore, metals present in coal can form metal carbonyls, such as $Ni(CO)_4$ and $Fe(CO)_5$ which are extremely dangerous for any form of living organisms.

Cold Gas Cleanup. A general process flow diagram for state-of-the-art syngas cleanup consists of several steps. Before any chemical cleaning can be conducted particulates have to be removed from the syngas. This process is followed by a wet scrubbing process for the removal of chlorine compounds. After the scrubbing process the carbonyl sulfide is converted to hydrogen sulfide in a hydrolysis reactor. The gas is then further cooled, hydrogen cyanide and ammonia are removed with the low temperature condensate and heavy metals are adsorbed in an activated carbon bed. Now the syngas can undergo desulfurization in an acid gas removal unit (AGR). AGR units are also able to capture carbon dioxide; however,

this has not yet been commercially realized in IGCC plants. In case of carbon capture, the hydrolysis reactor is replaced by a water-gas-shift (WGS) reactor. This way carbonyl sulfide can be hydrolyzed while CO is shifted to CO_2 which can be removed later in the acid gas removal unit.

Depending on the gasification technology, the raw syngas leaving the gasifier can have temperatures up to 1600 °C. Critical for such high syngas temperatures are the particulates that are entrained in the gas. In the temperature range between $900 - 1600$ °C, ash is present as a liquid and carries the potential of slag buildup in equipment. Thus, it is important to cool the hot syngas to temperatures below 900 °C as soon as the gas leaves the gasifier. Options for high temperature cooling are: radiant cooling (heat is transferred to water cooled walls by radiation), water quenching (injection of liquid water into the hot gas, or passing the hot gas through a pool of water), gas quench (injection/recycle of cooled syngas) and chemical quenching (syngas is cooled while the thermal energy is used to produce other valuable products). Further cooling to about 300 °C is achieved by convective heat exchangers while raising steam. At temperatures below 900 °C, the ash is solid and above 300 °C NH_4Cl is still in vapor form. This temperature range is typically used to remove ash and other particulates. Cyclones and filters or any combination of those are typically used in a temperature range between $500 - 300$ °C. Alkali compounds are solidified below 500 °C and, as mentioned before, NH_4Cl is still in vapor form at above 300 °C. In order to cool down the syngas below 300 °C NH_4Cl has to be removed. A common practice is the installation of a wet scrubbing process using water. If the temperature is sufficiently low, this simultaneously removes water soluble components such as NH_3, HCN, HCl and HF as well as remaining particulates which act as condensation nuclei during the cooling process. If no carbon capture is desired, the next cleaning step involves the hydrolysis of COS to H_2S over activated alumina or titanium oxide catalyst (≈ 200 °C). This step is only needed when an amine or Selexol™ process is chosen for sulfur removal. The Rectisol® process on the other hand also absorbs COS. If carbon capture is desired, a WGS reactor is required to shift

CO to CO_2. This is usually carried out in a high temperature WGS reactor for bulk shifting, which is favorable due to kinetics, in combination with a low temperature shift rector which thermodynamically favors the formation of CO_2. High temperature WGS reactors operate between $300 - 500$ °C versus low temperature shift reactors which are operated around 200 °C. The WGS catalyst also promotes the COS hydrolysis which makes the installation of a hydrolysis reactor redundant (only for sour shift catalyst). Subsequent to the hydrolysis or shifting, the syngas is cooled to around 40 °C and volatile metals such as Hg and As, are removed in an activated carbon bed. After all these treatments, the syngas is ready for acid gas removal. Acid gas removal is often used as a synonym for desulfurization but technically includes other acid gases like carbon dioxide, too. Many different technologies have been developed to remove acid gases from syngas: absorption (chemical) or adsorption (physical) by a liquid, absorption or adsorption by a solid and membrane separation. Depending on the concentration and partial pressure, some technologies are preferential to others. Zinc oxide is suitable for low sulfur content syngas (on a volume basis $\frac{\text{ml}}{\text{ml}}$) and can be used in low partial pressure regimes as well as high partial pressure regimes. For higher sulfur content, molecular sieves are the first choice. In the range of medium partial pressures ($0.1 - 5$ bar) chemical solvents like Amisol$^{\text{TM}}$, Sulfinol$^{\text{TM}}$, MEA and MDEA offer best removal efficiencies. In the regime of high partial pressures, physical sorbents work best and outperform chemical solvents. Examples for technologies operating on the principle of physical adsorption in liquids are Selexol$^{\text{TM}}$, Rectisol$^{\text{TM}}$ and Purisol$^{\text{TM}}$. The Rectisol$^{\text{TM}}$ process can achieve sulfur removal down to 0.1 ppmv [8] but requires cooling to at least -30 °C. Selexol$^{\text{TM}}$ and Purisol$^{\text{TM}}$ can operate at around $0 - 40$ °C while reducing the sulfur (H_2S) content down to 1 ppm [8] which is sufficient for IGCC applications.

In the following section, the dual stage Selexol$^{\text{TM}}$ process with sulfur removal and carbon dioxide removal is discussed in more detail. The Selexol$^{\text{TM}}$ process has been identified as the state of the art process for carbon capture in IGCC applications (for more details see Section 2.2) and will function as base case scenario for this study.

The solvent used in the Selexol^{TM} process consists of a mixture of dimethyl ethers of polyethylene glycols which preferentially absorbs hydrogen sulfide. The hydrogen sulfide and carbon dioxide laden syngas enters the sulfur removal column first, where it is stripped of the hydrogen sulfide with carbon dioxide laden solvent from the carbon dioxide absorber. The carbon dioxide and hydrogen sulfide rich solvent leaving the sulfur absorber is heated and flashed in a H_2S concentrator. Carbon dioxide is only weakly absorbed by the solvent and leaves the liquid phase together with some amount of hydrogen sulfide. Since this stream contains hydrogen sulfide as well as carbon dioxide, it is recycled back to the sulfur absorber. The residual liquid phase is now rich in hydrogen sulfide which has to be stripped off in a desorber column under heat input. The top of the desorber column produces an acid gas stream which can be utilized to produce elemental sulfur in a Claus plant. The bottom of the column produces the regenerated solvent which is sent to the CO_2 absorber. The feed for the CO_2 absorber is the desulfurized syngas from the sulfur absorber, which still contains carbon dioxide. The carbon dioxide is removed from the syngas with the fresh solvent and the leaving syngas is essentially free of hydrogen sulfide and significantly reduced in carbon dioxide content. The carbon dioxide laden solvent is partially used for the sulfur absorber while the remaining is flashed in two or more stages to produce a crude CO_2 stream for recycle and pure CO_2 stream(s). The decarbonized solvent still contains some of the CO_2 and is fed into the CO_2 absorber at an intermediate stage. A flow sheet of the Selexol^{TM} process is shown in Figure 2.11.

Warm Gas Cleanup. Warm gas cleanup offers several advantages over cold gas cleanup and has attracted research interest since the 1970s [7]. If the gas cleanup is conducted at higher temperatures, efficiency gains can be expected. Losses due to cooling and reheating are reduced and water does not have to be removed from the syngas stream. This water (vapor) can generate electricity when expanded and additional losses due to water treatment of the

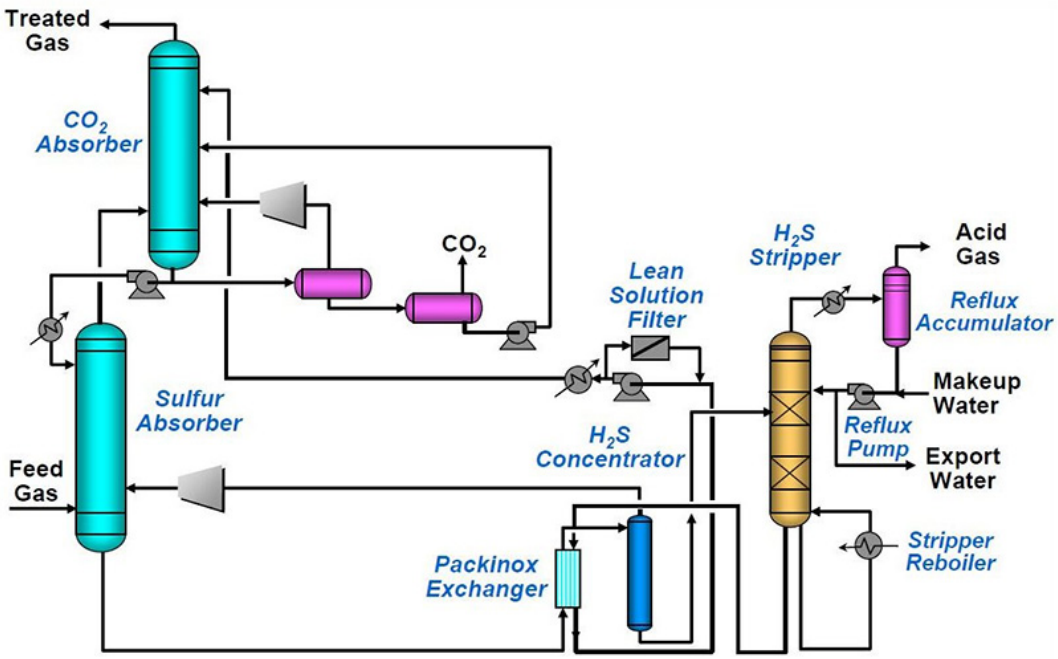

Figure 2.11: General flow sheet of the dual-stage Selexol^{TM} process [11].

condensate can be diminished. In general, it is desired to clean and feed the syngas into the gas turbine at the highest possible temperature in order to improve the efficiency. However, limitations are evident independent from the cleanup technology. In IGCC applications, the temperature limit is set by the highest possible operating temperature of the gas turbine fuel control system. Under consideration of alkali corrosion, metallurgy and refractory-lining this temperature is around $500 - 550$ °C [8]. Gas turbine vendor guaranties given are typically for much lower temperature ranges. Many different approaches and technologies for warm gas cleanup have been developed and studied. The next paragraph introduces some of these ideas. A complete summary of this research area would go beyond the scope of this study.

Alkali cleaning in cold gas cleanup systems is achieved by solidification in the gas phase when the syngas is cooled below 550 °C and consecutive separation from the syngas by filters. Alternative cleaning methods involve physisorption and chemisorption on activated bauxite or activated alumina. For the removal of hydrogen chloride, sodium and potassium compounds such as nahcolite have been identified as effective reagent with operating temperatures up to 600 °C [8]. Sprayed into the syngas, solid sodium chloride is formed which

can be captured in the particle removal section together with other solids. The high temperature removal of mercury remains one of the main challenges and is the Achilles tendon of warm gas cleanup. Mercury can also be captured after combustion; however, this introduces penalties compared to pre-combustion cleanup. At elevated temperatures of around 200 °C mostly activated carbon and metal based materials like ZnO and Pb are investigated. One of the most promising technologies for warm gas cleanup >260 °C are palladium based adsorbents which are described in [12]. Hot gas desulfurization between $350 - 750$ °C can be achieved via metal oxides like ZnO or Zn_2TiO_4. RTI and Eastman are commercializing a high temperature desulfurization process based on ZnO and demonstrated the process on a pilot plant scale in 2005 [13]. In this process, the ZnO reacts with H_2S forming ZnS and water. Later the ZnS is regenerated with air under the formation of SO_2. Many different technologies are currently under development for warm gas CO_2 capture. When looking into high temperature CO_2 removal, one needs to distinguish between temperature above 300 °C and below 300 °C. If carbon is intended to be captured above 300 °C, the capture process has to be integrated into a process that promotes the WGS reaction. The thermodynamic equilibrium favors CO_2 at low temperature. Thus, at high temperatures, the CO_2 present is insufficient to achieve high carbon capture. As a result, the CO_2 needs to be removed from the reactive phase to prevent it from participating in the equilibrium. In gasifiers, CO_2 can be trapped with CaO which shifts the equilibrium to the product side. This reduces CO concentrations and simultaneously increases hydrogen concentrations. A similar concept is used in WGS reactors with internal carbon capture, however, operating temperatures will be lower than in gasifiers. Also, high temperature CO_2-membranes with internal WGS have been proposed. Below 250 °C separate carbon capture technologies can be used. These technologies are further in development and closer to commercialization. Stand-alone carbon capture technologies require CH_4 reforming and CO shifting, which is thermodynamically favored at low temperature, before the syngas enters the CO_2 removal unit. The physical principles for warm gas carbon capture are similar to those for cold gas carbon capture;

however, it is much more difficult to find materials with the same properties at elevated temperatures, especially for adsorption based processes.

Gas Turbine

Historically gas turbines have been developed for natural gas and liquid hydrocarbon fuels but have been advanced to combust syngas and even hydrogen. Gas turbines operate on a Brayton-cycle with air as working fluid. The cycle has been already discussed in Section 2.1.1. In large gas turbines suitable for IGCC applications, compression is conducted in an axial compressor which is mounted on the same shaft as the expander. Thus, no motor is needed to drive the compressor and losses are minimized. The compressed air is then heated in the combustor by injecting fuel into the combustion chamber which immediately reacts with the oxygen to release energy in form of heat. The high-pressure, high-temperature gas is expanded in a turbine. For aero-derivative engines this turbine is divided into two parts. The first expander provides the power required for compression. The second expansion step drives an electricity generator. In aero-engines the second expander is not present and the remaining energy in the gas stream is used to generate thrust. Gas turbines for large scale power generation compressor, expander and generator are mounted on a single shaft. A general flow diagram of a gas turbine is shown in Figure 2.12.

The compression work in a Brayton-cycle is significantly larger than in a Rankine-cycle due to the high specific volume of gases. In large machines compression consumes about 50 % of the generated power. Thus, it can make sense to use intercoolers to reduce the workload and increase efficiency. However, intercooling lowers the combustor temperature, which has to be compensated with a higher fuel input. Another important factor influencing the turbine efficiency is the turbine inlet temperature (TIT); the higher the TIT the higher the gas turbine efficiency, limited only by material constraints. If, for example, methane is

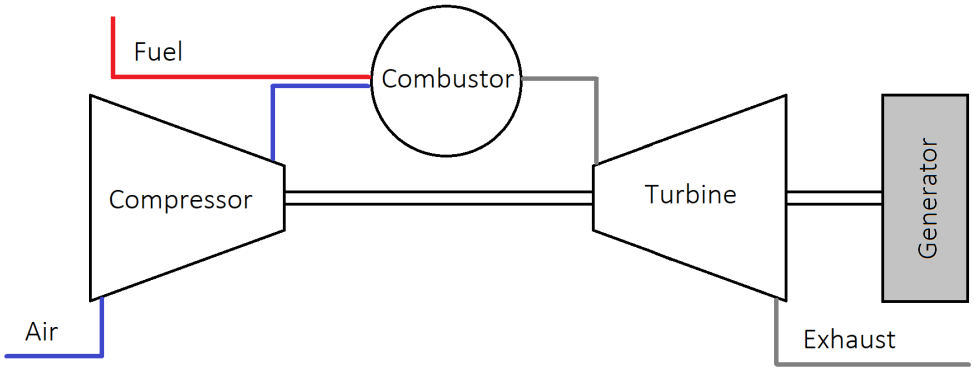

Figure 2.12: General flow sheet of a gas turbine.

combusted with air in a stoichiometric mixture, temperatures around 1940 °C are possible [9]. In order to reduce the TIT to a temperature in the range $1300 - 1400$ °C (state-of-the-art TIT), excess air is used. State-of-the-art TITs are only achievable due to the usage of advanced materials and internal blade cooling by air extracted from the compressor or even steam. Syngas, which is a mixture of mostly CO and H_2, has very different combustion characteristics than natural gas. Hydrogen is very reactive and increases the flame diffusion speed. A consequence of this property is the high risk of flash back when using dry low-NO_x burners. Hence, conventional combustors have to be used and NO_x control is accomplished by lowering the flame temperature by diluent injection [8]. NO_x control is of special importance in syngas applications since syngas combustion has a lower air requirement which increases the adiabatic flame temperature. In IGCC applications, it is common practice to use syngas humidification and/or nitrogen injection from the ASU as diluent. However, large amounts of diluent can be problematic for the operation of the gas turbine. The heating value of the gas turbine fuel syngas lies between $8 - 11$ $\frac{\text{MJ}}{\text{kg}}$ for oxygen blown gasifiers and between $4 - 6$ $\frac{\text{MJ}}{\text{kg}}$ for air-blown gasifiers [8]. This is significantly lower than the heating value of natural gas. The higher mass flow through the turbine generates more power which may be beyond the shaft limitations, and will increase the pressure ratio in the compressor. This will result in a higher turbine inlet or compressor outlet pressure which can lead to compressor surge [8, 9]. Countermeasures to prevent compressor surge are: increasing turbine cross-sectional

area, addition of a compression stage, closing compressor guide vanes or bleeding off air from the compressor. The latter is an attractive solution for IGCCs with ASU because it does not require expensive modification of the gas turbine and the compressed air from the gas turbine can be used in the ASU where high pressure air is needed. Closing the inlet guide vanes is the most popular option to reduce the mass flow. Alternative concepts for syngas or even hydrogen combustion are Brayton reheat cycles as described in [9].

Heat Recovery Steam Generator

A heat recovery steam generator (HRSG) is a unit that utilizes the waste heat from the gas turbine to raise steam for the bottoming Rankine-cycle. The HRSG consists of several heat exchangers for preheating of boiler feed water (economizer), evaporating (evaporator coils), superheating (superheater coils) and reheating of steam leaving the high-pressure turbine (reheater coils). Since the HRSG utilizes the waste heat from the expanded gas turbine exhaust, the HRSG heat exchangers are designed to have a very low pressure drop on the gas turbine exhaust side. The heat exchangers operate in cross-flow with the gas turbine exhaust flowing through a rectangular duct engineered with horizontal or vertical tubes. Various design options for HRSGs are based on the available heat. Some small units completely evaporate the boiler feed water in a single pass but commonly recirculation of boiler feed water between steam drum and evaporator coils is practiced. In large scale applications three steam drums producing high-pressure, intermedium-pressure and low-pressure steam are used. The vacuum condensate from the steam turbine is pumped to low pressure and preheated in the economizer before it enters the low-pressure steam drum which also functions as deaerator. The low-pressure steam drum separates steam and liquid. The steam leaving the low-pressure drum is superheated in a low-pressure superheater and sent to the low-pressure steam turbine. The liquid from the steam drum is split into two streams for high-pressure steam production and intermedium-pressure steam production. After pressur-

ization, both streams are preheated in economizers before they enter their respective steam drum. The high-pressure steam leaving the high-pressure steam drum is then further heated in several superheater coils to increase the efficiency of the expansion process in the high-pressure turbine. The intermedium-pressure steam exiting the high-pressure steam turbine is combined with the steam from the intermedium-pressure superheater which is fed by the intermedium-pressure steam drum. The intermedium-pressure steam is superheated in re-heaters and is then utilized in the intermedium-pressure steam turbine followed by expansion in the low-pressure turbine. The steam drums are continuously purged to avoid buildup of solids. The high-pressure blowdown is reused in the intermediate steam drum and the blow-down from the intermediate-pressure steam drum is flashed and the steam is used in the low-pressure steam drum [9]. If a special need for steam or if small quantities of low pressure fuel are available, duct firing is a common practice to increase the heat content of the exhaust gas. A flow sheet of a triple pressure HRSG is shown in Figure 2.13.

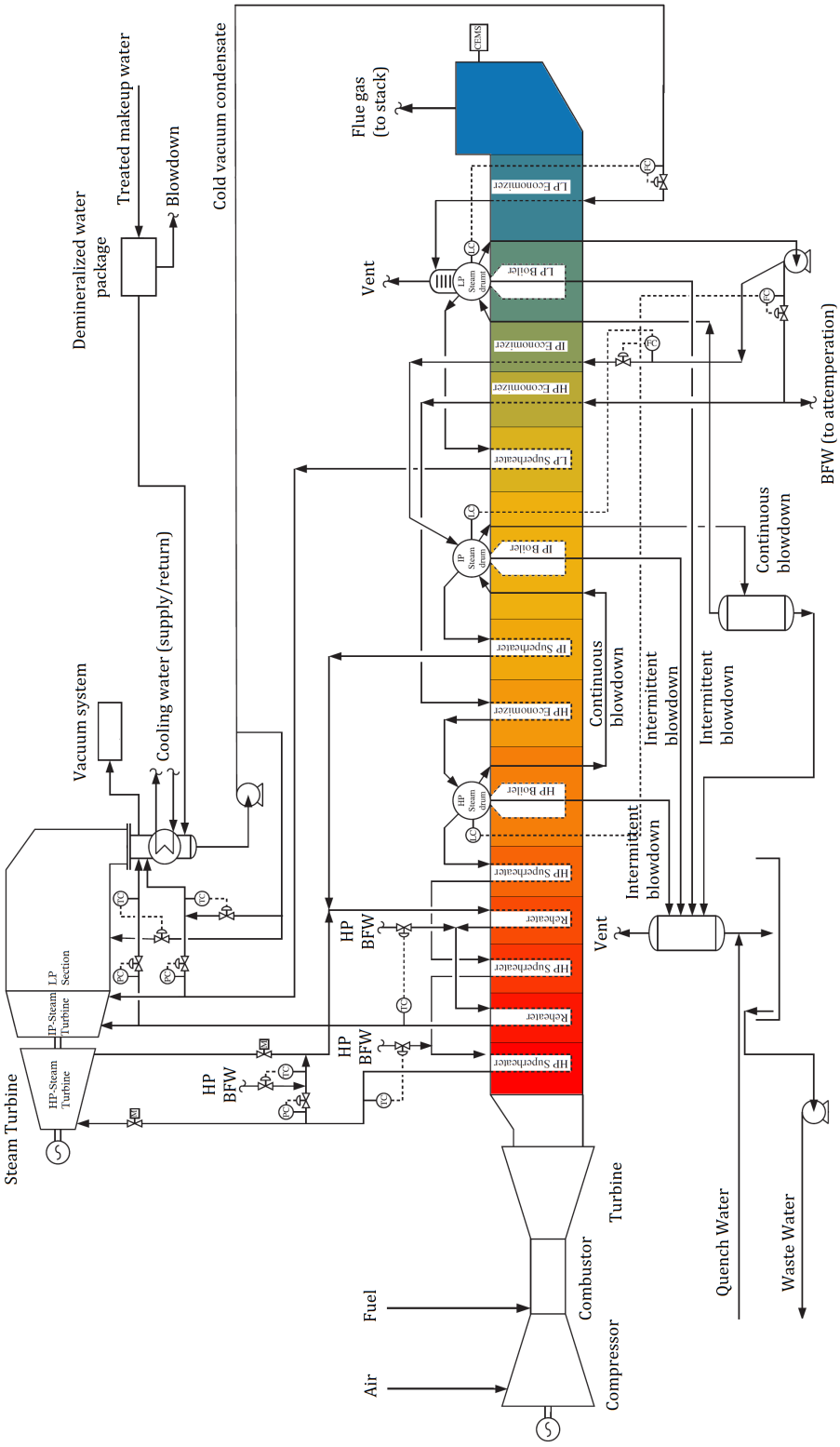

Figure 2.13: General flow sheet of a triple pressure heat recovery steam generator unit [9].

2.2 IGCC Technology Status and Literature Review

With the growing challenges of climate change and air quality, the research interest in IGCC has grown significantly over the last couple decades. At the current state, several demonstration plants have been built and successfully operated. Beyond this, numerous commercial scale IGCC plants are in operation today. The pioneer plant of IGCC technology was built in 1984 and operated for 4 years at Southern California Edison's Cool Water station. The plant was designed to generate a power output of 100 MW and was able to demonstrate low emissions and integrated controls. A seconded, less integrated, demonstration IGCC plant was built in Louisiana and operated by Dow Chemical Co. between 1987 and 1995 [14]. Over the last two decades, IGCC plants have been developed further and large scale IGCC plants reached commercial scales. Many of these projects started out as demonstration plants but have transitioned into regular operation. Years of operation have collected important data and shown that IGCC power plants are able to operate highly efficient while maintaining low emissions. Some of these established commercial IGCC power plants are: Buggenum IGCC, Nakoso IGCC, Puertollano IGCC, Tampa Electric Polk Power IGCC, Vresova IGCC, Wabash River IGCC and Wakamatsu EAGLE IGCC. Before diving into current research topics, the above listed, current state-of-the-art, IGCC plants will be examined in more detail. These plants employ a variety of different gasifiers and technologies which provide important lessons and information for future research for the improvement of next generation IGCC power plants.

The Buggenum IGCC is located in the Netherlands and was the world's first IGCC to enter commercial operation in 1998. The plant is designed around a dry coal fed oxygen blown Shell gasifier. The ASU is fully integrated with the gas turbine compressor and the coal pre-conditioning system provides dry coal powder in the size of 100 μm. A portion of the cooled syngas, which is used to raise steam, is burned to provide heat for the coal dry-

ing process. The gasification process takes place at 24.8 bar and a temperature of 1600 °C, which results in very high carbon conversion rates of greater 99 %. The oxidant is provided by the ASU and consists of 95 % oxygen. The design of the Shell gasifier allows steam generation inside a gasifier membrane, which simultaneously acts as reactor wall cooler. The slag produced during the gasification process is removed by a quench bath at the bottom of the gasifier. After the raw syngas leaves the gasifier, it is further processed. Fly ash removal is achieved by a cyclone and candle filters. Halide cleanup is obtained by wet scrubbing and sulfur removal and recovery is conducted using carbonyl sulfide/hydrocyanic acid hydrolysis in combination with a Sulfinol® wash and Claus plant to produce elemental sulfur. The power island consists of a Siemens V94.2 gas turbine modified for syngas operation, which is able to generate a power output of 156 MW. Additionally, nitrogen from the ASU is mixed with the syngas to NO_x emissions. Furthermore, the nitrogen diluent improves the emission reduction of nitrous oxides which is further controlled by syngas humidification. The waste heat of the gas turbine exhaust is used in a steam cycle which generates additional 284 MW of power. The total net electricity generation of the Buggenum IGCC adds up to 253 MW at an efficiency of 43 % − HHV with an availability of 75 % after 7 years of operation [15, 16]. In order to meet future regulatory compliances regarding carbon dioxide emission, co-gasification of biomass and bio-waste have been successfully demonstrated [17]. The biggest advantages of the Buggenum IGCC power plant are its low NO_x emissions of lower than 10 ppm combined with its high sulfur removal efficiency of greater than 99 % and virtually zero air emission of ash, chlorides and volatile heavy metals. Furthermore, due to the recycle of waste water and re-use in the system, there is no discharge of waste water [16].

The Nakoso IGCC has a gross capacity of 252 MW and started with its demonstration in September 2007. After completing numerous tests, the plant entered the commercial phase in 2013. The gasification process employed in the IGCC plant is based on a technology developed by Mitsubishi Heavy Industries (MHI) and uses a pressurized, upflow, two-stage,

slagging entrained bed gasifier using enriched air as oxidant. By using air as oxidant, only a small ASU ($75 - 80$ % smaller compared to oxygen blown gasifier) is needed to provide nitrogen as transport gas for the gasifier. The co-produced oxygen is used to enrich the air's oxygen content. Reasons for employing an air-blown gasifier are the high parasitic losses and high capital cost associated with the ASU. Furthermore, the operator hopes to gain benefits in continuous operation and higher plant capacity factors at lower maintenance cost. Similar like the Shell gasifier, the MHI gasifier requires dry, milled coal as feed which is fed into the gasifier at two different stages. The first stage operates in combustion mode and produces carbon monoxide, carbon dioxide and water vapor together with heat from coal and air. The operating temperature of the combustor is sufficiently high to produce molten slag which falls to the bottom of the gasifier where it is quenched in a bath and transported out of the gasifier through lock hoppers. The hot gas products are transported to the second stage where additional coal is fed into the gasifier without air. In the second stage, also called the reductor stage, the heat is used to drive the endothermic gasification reactions. This leads to a lower operating temperature of the reductor stage and any slag that is carried over to the second stage is solidified. The syngas leaving the reductor is about 1200 °C and is used to raise steam. Particulates in the cooled raw syngas are removed by a cyclone and are being recycled to the first stage of the gasifier to achieve carbon conversion rates of greater 99.8 %. A porous filter removes remaining particulates before the syngas is further cooled to enable acid gas removal and sulfur recovery which are low temperature processes. First, all carbonyl sulfide is converted before entering the acid gas removal unit which is a commercial methyl-diethanol-amine (MDEA) unit. The removed sulfur components are then converted to saleable gypsum in a limestone-gypsum unit. The cleaned syngas is reheated and converted into electricity in the power island. A Mitsubishi M701DA gas turbine generates 142 MW. This turbine type was selected because of its track record of combined cycle usage and burning other low heating value fuels. The waste heat is recovered in a HRSG and additional 110 MW of electricity are generated by the steam turbine. The net efficiency

during the demonstration phase was 41 % − HHV and a significant reduction of emissions has been demonstrated: with measured concentrations of SO_x at 1.0 ppm (planned: 8 ppm), NO_x at 3.4 ppm (planned: 5 ppm) and PM $< 0.1 \frac{mg}{m_N^3}$ (planned: 3.3 $\frac{mg}{m_N^3}$). The advantages of the Nakoso plant are its high reliability and the ability to process various coal types such as high rank coals like bituminous coal and low rank, high moisture coals like sub-bituminous coal [15, 16, 18].

The Puertollano IGCC started operation of the demonstration phase in 1992 and entered the commercial stage in 1998. The plant operates on a 50:50 mixture by weight of coal and petroleum coke. The power output is 300 MW at an efficiency of 42.1 %. The PRENFLO^{TM} single stage entrained flow gasifier used operates at a pressure of 25 bar and a temperature of 1600 °C. The PRENFLO^{TM} gasifier uses an integrated waste heat boiler and a compressed recirculated quench gas resulting in comparatively low moisture raw syngas at moderately high exit temperatures and carbon conversion rates of greater 98 %. The raw syngas enters the waste heat boiler at around 800 °C where it is cooled in two stages to 400 °C and to 235 °C while raising high pressure steam and intermediate pressure steam. Most of the produced ash is collected at the bottom of the gasifier in the form of liquid slag which contains less than 1 % residual carbon. The coal preparation includes the addition of limestone to the feed mixture to reduce the melting temperature of the ash. In further processing, the feed is milled to a particle size of 50 μm and dried to a moisture content of 2 wt − % before it enters the gasifier through lock hoppers which use nitrogen from the ASU as carrier gas. The fully integrated ASU provides oxygen for the gasification process at a purity of 85 %. The cooled raw syngas is filtered through ceramic candle filters to remove remaining particulates. The syngas is then scrubbed with liquid water at a temperature of 165 °C in order to remove ammonia and halides. After this step, carbonyl sulfide is hydrolyzed to remove the sulfur in form of hydrogen sulfide in the desulfurizer. Desulfurization is achieved in a MDEA wet scrubbing column and the acid gas is sent to a Claus plant

producing elemental sulfur with air and oxygen intake from the ASU. The Claus tail gas is recycled to the carbonyl sulfide hydrolysis reactor. After desulfurization, the syngas is humidified and diluted with nitrogen. Nitrogen dilution of the syngas is necessary to adjust the heating value but dangerous because of the oxygen content in the nitrogen stream and thus has to be executed immediately before it is combusted in order to prevent autoignition of the mixture. This dilution process together with low NO_x burners in the Siemens V94.3 gas turbine enables NO_x emissions of less than 60 ppm (15 % O_2). The gas turbine exhaust heat is recovered in a HRSG to raise further steam for the Rankine-cycle [15, 16].

The Puertollano IGCC successfully demonstrated the operation of IGCC technology using a mixture of low quality coal with high ash content along with refinery residues while achieving high emission standards. Sulfur dioxide emissions are reduced by 99 % and also carbon dioxide emissions are reduced to 85 % of conventional PC power plants.

The gasification technology has proven to be flexible in handling various feed types from high ash coals to biomass while maintaining a consistent syngas composition. However, during operation, several problems in the gasifier and other equipment were encountered. The gasifier showed problems with water leakage in the membrane tubes as well as gas leakage which could be fixed by modifying the gasifier design. Fouling problems in the waste heat boiler were resolved by lowering the inlet temperature to the cooler and increasing the quench flow. Furthermore, optimization of the gas turbine was required to prevent overheating and humming which improved the lifetime and stability of various components. The ceramic filters and the COS hydrolysis catalyst exhibited significantly lower lifetimes than expected which could be resolved by redesigning the filter element support and switching from an alumina based catalyst to a titanium oxide based catalyst.

The Tampa Electric Polk Power IGCC has a capacity of 250 MW and started its four-year demonstration phase in 1996 before entering the commercial phase in 2000. The plant is built around a GE gasifier (formerly known as Texaco gasifier) and operates at an efficiency

of 38 % – HHV [19]. The operating pressure of the gasifier is greater than 20 bar and the gasifier reaches temperatures between 1325 – 1430 °C. The GE gasifier is a single stage, downward-feed, entrained flow reactor and operates on a coal-water-slurry, which contains about 65 wt – % solids, and oxygen at 95 % oxygen purity. The slurry is injected from the top into the gasifier through custom nozzles where the coal reacts exothermically with oxygen to produce syngas and slag. The feed water acts as temperature moderator and hydrogen source for the coal gasification process which produces syngas containing mostly hydrogen and carbon monoxide. The raw syngas is then cooled by a radiant cooler which produces high pressure steam. The slag is quenched at the bottom of the gasifier using liquid water. After the radiant cooler the syngas passes through a convective heat exchanger, raising more high-pressure steam. Leaving the convective heat exchanger, the syngas has a temperature of approximately 430 °C and enters a wet scrubber that removes particulates and halogen compounds. The unburned carbon is recycled back to the gasifier which achieves single-pass carbon conversion efficiencies of greater 95 %. The ASU is not fully integrated with the gas turbine and has a separate air compressor. This allows a more dynamic operation and shorter start-up times. High efficiencies are typically more important in Europe where the feedstock prices are higher than in the U.S. In the U.S., fuel prices are lower and availability has a bigger influence on the plant design [14]. The achieved availability for the gasification unit was 83.5 % and for the combined cycle 94 %. The coal preparation for the GE gasifier is very different compared to the previously discussed cases since it is a slurry-fed gasifier. In this case the coal (alternatively petroleum coke) is crushed and mixed with recycled water before it is milled to slurry using wet-rod mills. The produced syngas is cleaned in a wet scrubbing process and the carbonyl sulfide in the syngas is converted into hydrogen sulfide in a subsequent hydrolysis reactor in order to be removed from the gas. Thereafter, the syngas is further cooled to 40 °C before it enters the cold gas cleanup section consisting of a MDEA absorber for sulfur removal. The H_2S is stripped off the MDEA-solution via steam and sent to a sulfuric acid plant. The clean syngas is reheated, saturated with water and mixed with

nitrogen from the ASU before it is combusted in a GE MS 7001FA gas turbine generating 192 MW. The exhaust heat of the gas turbine engine (approx. 570 °C) is used to generate more steam which is converted into electricity using a double flow reheat steam turbine that generates additional 123 MW [15, 16].

Criteria pollutants in the Tampa Electric Polk Power IGCC are reduced to very low levels; SO_2 emissions are below 0.15 $\frac{\text{lb}}{\text{MMBTU}}$ (goal: 0.21 $\frac{\text{lb}}{\text{MMBTU}}$) and NO_x emissions are below 0.27 $\frac{\text{lb}}{\text{MMBTU}}$ (goal: 0.15 $\frac{\text{lb}}{\text{MMBTU}}$). Particulate matter emissions of lower 17 $\frac{\text{lb}}{\text{hr}}$ have been achieved consistently [19].

After the start-up in 1996, serious problems with ash leaking into the clean syngas in the syngas reheater located in the high temperature heat recovery system occurred, which lead to serious damage of the gas turbine. Removal of this heat exchanger and modifications to the particulate removal system were necessary. Other problems with the gasifier were resolved by a reduction of the gasifier operating temperature in order to extend the lifetime of the gasifier liner. Further modification to improve start-up times and corrosion in the coal/slurry piping system had to be made. The experimentation of using different coals with higher sulfur content lead to the commissioning of a COS hydrolysis reactor in 1999 because of the unacceptable high SO_2 emission levels. An ongoing issue is the failure of thermocouples in the high temperature section caused by the expansion of dissimilar materials.

The Vresova IGCC is one of the largest coal fired IGCC power plants with a gross capacity of 400 MW. In times of the Soviet Union, the plant produced town gas but was converted into an IGCC power plant after the fall of the iron curtain. The plant started in 1996 with 26 custom water jacket-cooled moving bed gasifiers arranged in a counter flow scheme with gasification occurring in several stages. The gasifier operates on a steam oxygen mixture which is injected into a several centimeter-high ash layer at bottom of the gasifier. The hot ash preheats the oxidant and accomplishes an even distribution of the gas over the whole cross section. In the second stage, the oxygen reacts with the coal particles and gener-

ates the heat input for the following gasification sections. The top sections in the gasifier are the carbonization, where most of the tar is formed, and the coal drying zones. The gasified coal is brown coal that is fed into the gasifier with a particle size between $3 - 25$ mm. The raw syngas leaves the gasifier at about 27 bar and a temperature of 200 °C and is further cooled to 30 °C by a water-hydrocarbon wash before entering a Rectisol® unit for acid gas removal. Additional to the cooling, the wash removes fly ash and particulates present in the raw syngas. The condensate from the cooling process is separated into a water-phenol-rich product stream by a gravitational separation technology which is then dephenolized in a butyl acetate extraction process. Furthermore, ammonia is stripped off the dephenolized water and phenol and ammonia are sold to consumers as high purity products. The water undergoes further treatment and can be reused within the plant.

In addition to the above-mentioned byproducts, crude naphtha is recovered in the Rectisol® process and sulfuric acid is produced from the acid gas. Due to the economic situation it is more profitable to generate electricity than selling the liquid hydrocarbon products. For this reason, a Siemens SFG-500 gasifier was installed in 2008 to convert tars and other liquid hydrocarbons from the moving bed reactors into syngas. The Siemens gasifier operates at 28 bar, 1400 °C and produces a similar raw gas composition as the moving bed gasifiers but with the difference of essentially zero methane and other hydrocarbons. Interestingly, the plant had a second Rectisol® stage when it was operated to produce town gas which captured carbon dioxide from the town gas stream before it was distributed and reduced the carbon dioxide content to 5 %. This section is now bypassed and the high-pressure carbon dioxide is used to produce power through expansion in the gas turbines. Downstream of the Rectisol® process the syngas has a pressure of $21 - 25$ bar and is essentially free of sulfur ($13\ \frac{\text{mg}}{\text{m}^3}$) and nitrogenous substances. The power block consists of two GE 9E-frame gas turbines with steam injection to reduce the firing temperature. The exhaust gas is used in a two-pressure HRSG to raise steam for a steam turbine which is supplied by ABB. The total emissions of the IGCC are $0.2\ \frac{\text{mg}}{\text{Nm}^3}$ SO_2 and 45 ppm NO_x (at 15 % oxygen). The overall

efficiency of the IGCC plant is 50.5 % [16, 15, 20].

The Wabash River IGCC started its demonstration phase in 1995 and entered commercial operation in 1999 with overall availabilities around 70 %. It employs two gasifiers, although only one is needed to process the coal input to generate a net power output of 262 MW. The thermal efficiency of the IGCC is approximately $40\,\% - \mathrm{HHV}$. The established gasification technology is commercially available under the name E-Gas$^{\mathrm{TM}}$ gasifier and is slurry fed technology similar to the GE gasifier. The slurry concentration typically ranges from $50 - 70$ % depending on moisture content and coal quality. Unique about the gasifier design is its two-stage upflow construction. 75 % of the slurry is fed together with 95 % pure oxygen into the first stage at the bottom of the gasifier. The exothermic partial reaction of coal with oxygen at pressures of 28 bar generates a temperature of 1370 °C. This temperature is hot enough to prevent the formation of hydrocarbons. Furthermore, the ash will be melted, run down the wall and leave the gasifier through a tap hole at the bottom. The hot syngas travels from the first stage upwards to the second stage where the remaining 25 % of the slurry is injected. The second stage is operated at about 870 °C which can be varied according to the desired syngas composition. These lower temperatures allow the formation of methane and char which requires recycling to the first stage. The syngas leaves the gasifier at about 870 °C and is cooled to 590 °C by raising saturated steam at 110 bar in fire-tube coolers. Particles entrained in the syngas are now filtered by candle filters and recycled to the first stage of the gasifier. After particulate removal, the syngas is further cooled to 38 °C and chlorides are removed in a wet scrubbing process. Condensate from the cooling process contains ammonia, hydrogen sulfide and carbon dioxide and has to be sent to a water treatment site. The carbonyl sulfide hydrolysis reactor shifts the sulfur towards hydrogen sulfide which is removed to 99.99 % in an acid gas removal unit using a MDEA system. The acid gas is used to produce elemental sulfur in a Claus plant. Before the syngas is sent to the power block, it is humidified to control $\mathrm{NO_x}$ emissions. However, the combus-

tion temperature of the GE MS7001FA gas turbine in this particular case still reaches about 1220 °C which is significantly higher than expected. The gas turbine output is 192 MW. Waste heat from the gas turbine is recovered in a HRSG to produce more steam and utilized in a bottoming Rankine-cycle which generates additional 104 MW. The SO_2 emission are 0.1 $\frac{\text{lb}}{\text{MMBtu}}$, NO_x emissions are 1.09 $\frac{\text{lb}}{\text{MWh}}$ with no measurable particulate matter emissions. These values are well below the emission limits including the NO_x values despite the high turbine firing temperature [15, 16, 21].

The Wakamatsu EAGLE IGCC started demonstration in 2002 and was developed by the Japanese Electric Power Development Company and Japan's New Energy and Industrial Technology Organization under the acronym EAGLE (Energy Application for Gas, Liquid and Electricity) with the goal of developing a multi-purpose oxygen-blown entrained flow gasifier. The EAGLE gasifier operates on dry coal at a rate of 150 $\frac{\text{t}}{\text{d}}$ which is transported into the gasifier using nitrogen from an ASU. Furthermore, the ASU provides the oxygen at a 95 % purity for the gasification. The gasifier consists of two stages. The bottom stage injection system introduces coal with large amounts of oxygen providing the heat for the endothermic reaction in the second stage where only small amounts of oxygen together with coal are introduced. Unique about this gasifier is the tangential injection of coal and oxygen which creates a spiral flow similar to a cyclone. This enables a longer residence time of coal in the gasifier and higher gasification efficiency. Furthermore, it is claimed to help with slag removal by creating a pressure differential between the center and the wall which helps to draw the slag to the bottom of the gasifier where it is removed. The first stage at the bottom operates at higher temperatures in slagging conditions. The second stage is operated at non-slagging conditions. However, the coal to oxygen ratio can be adjusted to optimize between high gasification efficiency and stable slag discharge. Unreacted carbon and ash are removed downstream in cyclones and filters and are returned to the gasifier. The gasifier walls are protected by a membrane, similar to the Shell or Siemens gasifier, which produces

high pressure steam. After gasification, the syngas is cooled to low temperatures for wet scrubbing, ammonia and chlorine removal followed by a carbonyl sulfide hydrolysis reactor, using a titanium oxide catalyst, and a MDEA acid gas removal unit. The removed sulfur is processed to gypsum and can be sold. After the cleanup, the syngas is reheated, humidified and combusted in an 8 MW gas turbine. The exhaust heat is recovered in a HRSG; however, the pilot plant does not include a steam cycle. The demonstration phase was finished in 2013 and a 167 MW is in construction which will include a carbon dioxide removal unit. The CO_2 removal technology has been intensively tested at the Wakamatsu pilot plant. Mostly physical absorption technologies have been tested in various configurations. In order to achieve high carbon capture efficiencies, a shift reactor has to be added to the plant design which converts the CO in the syngas to CO_2. In this context, variations of sweet and sour shift and the position of desulfurization have been studied settling on an advanced sour shift process. The new plant at Osaki will be one of the first IGCC power plants with carbon capture and will be an important milestone towards clean and sustainable electricity [15, 22, 23].

However, carbon capture in power plants remains a major area of research. The National Energy Technology Laboratory (NETL) and the U.S. Department of Energy (DoE) studied the effect of carbon capture on plant performance and economics for high rank and low rank coals [5, 24, 25]. In total 6 IGCC cases for low rank coal, using Montana Powder River Basin Coal (PRB) and North Dakota Lignite Coal, were investigated in combination with Shell-gasifiers, TRIG$^{\text{TM}}$-gasifiers, Siemens-gasifiers and E-Gas$^{\text{TM}}$-gasifiers. High rank coal cases using Illinois No. 6 Coal were studied for the GE-gasifier, E-Gas$^{\text{TM}}$-gasifier and the Shell-gasifier. Results clearly show that IGCC power plants can operate more efficiently than PC power plants (sub-critical, supercritical and ultra-supercritical). IGCC plants in these two studies were able to reach efficiencies between $36.7 - 42.1\,\% - \text{HHV}$ while PC plants ranged from $36.8 - 39.3\,\% - \text{HHV}$. However, PC plants showed to have better economics. Considering carbon capture, this economic advantage of PC power plants vanishes and IGCC

power plants become not just more efficient but also more economical. Efficiencies for the IGCC cases with carbon capture span from $30.0 - 32.6\ \% - \text{HHV}$. PC power plants with carbon capture reaching efficiencies from $26.2 - 28.4\ \% - \text{HHV}$. The efficiency advantage of IGCC versus PC power plants results from the carbon capture strategy. IGCC plants allow pre-combustion cleanup where carbon dioxide is present at high concentration and pressure versus post-combustion cleanup which is much more challenging and energy intensive due to the high dilution of carbon dioxide with air. All IGCC cases use a dual-stage Selexol$^{\text{TM}}$ process for removing carbon dioxide from the syngas and all cases have a very similar integration of the dual-stage Selexol$^{\text{TM}}$ unit into the plant design. After the syngas leaves the gasifier, the hot gas is cooled, scrubbed and shifted (sour shift) before it enters a mercury removal unit. The clean, low temperature syngas enters the Selexol$^{\text{TM}}$ unit where acid gas as well as carbon dioxide is removed. After the syngas leaves the Selexol$^{\text{TM}}$ unit, it is reheated, diluted with water vapor and/or nitrogen from the ASU and combusted in a gas turbine.

Also, in [26], conventional PC power plants with post-combustion carbon capture and oxy-combustion with carbon capture have been compared to IGCC power plants with separate carbon dioxide and acid gas removal and combined removal using the Selexol$^{\text{TM}}$ process. The authors found that the IGCC technology showed the highest efficiencies and the lowest penalties for carbon capture. From an efficiency point of view, the co-capture of acid gas and carbon dioxide is more favorable, although, the CO_2 stream contains a higher concentration of hydrogen sulfide. Majoumerd and Assadi [27] compared an IGCC with a dual-stage Selexol$^{\text{TM}}$ to a natural gas combined cycle plant with a monoethanolamine (MEA) post-combustion cleanup unit and a supercritical PC with a state-of-the-art post-combustion cleanup. The results show that the IGCC plant has a better performance than the supercritical PC plant in both cases with and without carbon capture and that for the carbon capture case the cost of electricity for the IGCC is lower than for the PC plant. However, the IGCC was not able compete with the natural gas combined cycle plant. A study conducted by Padurean et al. [28] found that in pre-combustion capture scenarios, the Selexol$^{\text{TM}}$ pro-

cess is more energy efficient than Rectisol^{TM}, Purisol^{TM} and MDEA processes due to its lower heat consumption for solvent regeneration and a simpler process configuration. The Selexol^{TM} process with 90 % carbon capture reaches an efficiency of 36.1 %. Ahmed et al. [29] concluded that the implementation of a sour shift in combination with carbon dioxide removal is more efficient than sweet CO-shifting due to the fact that both, sulfur removal and carbon capture, were low temperature processes. Based on this result, three cold gas cleanup cases were investigated: pre-combustion cleanup of shifted syngas with air as gas turbine oxidant, pre-combustion cleanup of shifted syngas with 99.5 %-pure oxygen as gas turbine oxidant and post-combustion cleanup with 99.5 %-pure oxygen as gas turbine oxidant. The post-combustion cleanup showed to have the highest efficiency with 37.2 % over the air fired gas turbine with 36.2 %. Furthermore, the post-combustion cleanup case showed the best economics due to the redundancy of the shift reactor and despite the significant increase in the ASU. Combustion of syngas with pure oxygen in a gas turbine will create extremely high firing temperatures which is desired from a thermodynamic perspective but it introduces many new challenges with respect to engineering, materials as well as emission. Pure oxygen fired gas turbines are very far from commercial scale and the results represent a more futuristic scenario. Based on the Selexol^{TM} case, similar efficiencies of 36.4 % were found for pre-combustion cleanup cases with carbon capture of 90 % for Selexol^{TM} and MDEA in [30]. Furthermore, the commercially available Selexol^{TM} and MDEA processes were compared to a non-commercial potassium carbonate acid gas and carbon dioxide removal process (UNO Mk1, in demonstration). This process operates at temperatures around $393 - 493$ K, compared to Selexol^{TM} $253 - 313$ K and MDEA $313 - 337$ K, which has advantages with respect to the plant's heat integration. This results in significantly higher efficiencies ranging from $37.3 - 39.3$ %. Schlather and Turk presented a study in [31] which was commissioned by Eastman Chemical Company together with RTI International and was conducted by Nexant. The study investigated the influence of using warm gas cleanup technologies without carbon capture operating at temperatures greater than 200 °C. The efficiency gains due to

warm gas cleanup were 3.6 % − points and similar efficiency gains can be expected for IGCC plants with warm gas carbon capture versus cold gas carbon capture.

This illustrates why over the last couple of years, major efforts and research have been conducted to identify technologies that can separate carbon dioxide from syngas at medium and high temperatures. Many different approaches have been taken into consideration and technologies like H_2 membranes [32, 33, 34], CO_2 membranes [33, 34], chemical looping [35, 36], cryogenic separation [37, 38], temperature swing adsorption (TSA) units [39, 40] and pressure swing adsorption (PSA) units for carbon capture have been developed. In [41] the U.S. Department of Energy studied several future technologies for advancing power generation in IGCC. Next to progress in turbine technology and air separation technology, the study includes scenarios of elevated temperature Selexol^{TM} carbon cleanup and H_2-membrane separation showing efficiency benefits of 0.8 % − points and 3.7 % − points.

Although, many promising technologies are being developed, only the sorbent-based technologies, like PSA, are expected to reach commercial availability within the next few years [42]. One of the earlier studies on IGCC power plants using a PSA for warm gas cleanup for carbon dioxide removal from syngas was conducted by Ito and Makino [43]. They compared IGCC power plants with post-combustion chemical carbon dioxide absorption with an air and oxygen blown gasifier to a pre-combustion PSA warm gas cleanup IGCC power plant. The PSA technology in the study is based on zeolites and operates at 423 K. The results show a significant increase in plant efficiency due to warm gas cleanup. Even at lower temperatures around $338 - 358$ K, Riboldi and Bolland [44] showed that their PSA process has a better performance than the dual-stage Selexol^{TM} base case. Another warm gas CO_2 capture PSA technology has been investigated by Liu and Green [45]. The study looked at a PSA technology that can operate with a syngas inlet temperature of 180 °C and compared the results to a duel-stage Selexol^{TM} process. The results showed only a small advantage of the warm gas cleanup PSA technology. However, due to the particular desulfurization technology chosen for the study, 2.3 % of the hydrogen was lost in the process.

Choosing a different desulfurization technology will further boost the efficiency. Couling et al. [46] conducted density functional theory calculations to identify metal hydroxides for warm gas carbon dioxide adsorption. A comparison with a conventional Selexol^{TM} process showed efficiency losses of around 0.5 %. However, the plant integration was not very efficient. Using a different sulfur removal unit that does not consume hydrogen and raising the regeneration steam by electricity and not by heat add huge penalties to their IGCC design. In another study Couling et al. [33] investigated membranes and a PSA adsorbent process for warm gas cleanup. The study includes the investigation of various H_2 and CO_2 membranes as well as a hypothetical adsorption process. Focus of the work is the detailed modeling of the diffusion and/or adsorption processes and the identification of important design parameters. The results show efficiency gains of up to 1.5 % for the adsorption process and evaluate warm gas cleanup processes based on adsorption as advantageous over membrane technologies. In [47] Zhu et al. integrated an elevated temperature PSA (226 °C) for 90 % carbon capture into a 540 MW IGCC plant design. In order to be competitive with the Selexol^{TM} process, a hydrogen recovery rate of at least 93.5 % is necessary. High hydrogen recovery rates are desirable to increase the power output of the turbine and reduces the power dissipation in the CO_2 compression section due to H_2 impurities in the CO_2 stream. Further work by Zhu et al. [48] intensively studied the CO_2 separation's auxiliary load with respect to hydrogen recovery and CO_2 capture in the above-mentioned elevated temperature PSA IGCC plant and compared the results to a Selexol^{TM} scenario. Chen et al. [49, 50] integrated a warm gas cleanup PSA process into an IGCC plant together with an ion transport membrane for oxygen production and showed that efficiencies of $36.7 - 38.3\ \% - \text{HHV}$ while capturing 90 % of the carbon are achievable. Chi et al. [36] studied an oxygen-blown TRIG^{TM} gasifier IGCC with various warm and hot gas cleanup technologies and compared the results to a conventional MDEA CO_2 capture process plant. Significant improvements on the net plant efficiency and carbon capture efficiency could be realized. Warm gas cleanup with Na_2CO_3-MgO at 400 °C improved the plant efficiency by $2.8\ \% - \text{points} - \text{LHV}$ and

increased the carbon capture efficiency about 4.8 % − points. Even greater improvements on both, net efficiency and carbon capture efficiency, were obtained with CaO as adsorbent operating at a temperature of 650 °C. Sorbent regeneration is achieved by burning some of the syngas in a regenerator with oxygen. Two additional cases investigated the integration of the carbon capture step into the water-gas-shift reactor which lead to improvements of the net plant efficiency of up to 4.2 % − points − LHV. Carbon capture within the WGS unit shifts the equilibrium to the CO_2 side and can operate at lower steam to carbon ratios without compromising CO conversion.

In general, less research has been conducted in the field of TRIG^{TM} gasifier IGCCs. In the DoE study [24] the TRIG^{TM} gasifier has been compared to the Shell gasifier, Siemens gasifier and E-Gas^{TM} gasifier with and without cold gas carbon capture using PRB coal. The study revealed that with the TRIG^{TM} gasifier, utilizing PRB coal in combination with a cold gas Selexol^{TM} unit, the DoE goal of 90 % carbon capture is not achievable due to the high methane content in the syngas which is a result of the lower gasification temperature. Zhuang et al. [51] studied an air blown TRIG^{TM} gasifier IGCC showing the superior performance of the TRIG gasifer compared to ultra-supercritical power plants utilizing low rank coals. Six TRIG^{TM} IGCC cases have been developed by Bonsu et al. [52] and Rogers et al. [53] which compare pre-combustion, post-combustion, air-blown, oxygen-blown, no carbon capture and with carbon capture scenarios. The air blown cases reach higher efficiencies than the corresponding oxygen-blown cases and lower cost of electricity. Results further show that post-combustion gas cleanup, without carbon capture, is more efficient than pre-combustion cleanup. For the carbon capture cases, the oxygen-blown gasifier achieved higher plant efficiencies than the air-blown case but ultimately resulted in higher cost of electricity because of the higher capital investment. The air-blown case missed the DoE target of 90 % carbon capture by only 0.2 % − points. The oxygen-blown gasifier case was able to capture 91.9 % of the produced carbon dioxide. These numbers are different to the maximum capture efficiency presented in [24]. Next to the different CO_2 capture technologies used in these studies,

Selexol^{TM} versus MDEA, a major difference is the methane content in the produced syngas. Methane is not affected by WGS reaction nor by the gas cleanup and will convert to CO_2 in the combustion turbine. Thus, it is very important for the TRIG^{TM} gasifier to estimate the methane content of the syngas correctly. Arthur et al. [54] investigated different approaches to predict the syngas composition of the TRIG^{TM} gasifier. The pseudo-equilibrium approach showed better agreement with experimental data than the free Gibbs and kinetic approach. Further information on TRIG^{TM} to substitute natural gas and syngas composition can be found in [55].

2.3 Summary

Based on the literature review, a study of an IGCC utilizing sub-bituminous coals with a CO_2-PSA warm gas cleanup technology has not yet been conducted. Most studies utilize bituminous coals in combination with high temperature entrained flow gasifiers. Little work has been done in the field of lignite and biomass gasification in IGCCs with CO_2-PSA warm gas cleanup. The area of sub-bituminous coal gasification in IGCCs employing a CO_2-PSA warm gas cleanup technology remains unexplored. Sub-bituminous coals have a higher water content than bituminous coals and are more reactive. Thus, it is most efficient to use gasification technologies that are engineered particularly for low rank coal utilization such as the TRIG^{TM} gasifier. TRIG^{TM} gasification IGCCs have been studied in the context of no carbon capture and classical cold gas carbon capture as well as in the temperature range $450 - 600$ °C using chemical looping for carbon capture. PSA-based carbon capture at elevated temperatures in combination with the TRIG^{TM} gasifier have not been addressed in literature. Problematic for the highly efficient, low rank coal TRIG^{TM} gasification process is the methane content in the syngas which can limit the carbon capture. Strategies to

increase the carbon capture for these systems have not been proposed, yet. This work aims to fill this space in literature and provide a detailed analysis of TRIG^{TM} gasification IGCCs with CO_2-PSA warm gas decarbonization utilizing sub-bituminous coal; and to provide a comprehensive understanding of strategies for increasing the carbon capture of high methane syngas which will lay the foundation for future work in this area.

Chapter 3

Approach

In the approach, tasks are developed for each of the stated objectives and the work scope is delineated.

Task 1: Establish a Design Basis and Calibration of Key Models

First, a design basis needs to be established which defines the used feedstock and site characteristics. This basis will be the same for all simulations to ensure comparability between the different scenarios. Furthermore, the design basis defines critical operating parameters which influence the plant performance, e.g. purity and pressure of the carbon dioxide product stream. The second part of this task deals with the modeling of key components of the simulation. Models need to be developed and validated to ensure the reliability of the simulation results. The simulations will be carried out in ASPEN Plus, a well-established commercially available chemical processing software. Important therefore is, the selection of the right property method to describe the compounds' behavior.

Task 2: Design a Reference Case with a State-of-the-Art Carbon Dioxide Removal Technology

For purposes of comparing the IGCC performance, a reference case with a state-of-the-art carbon capture technology needs to be designed. As previously pointed out in Section 2.2, the state-of-the-art-carbon capture technology is the Selexol^{TM} process. This task is responsible to identify an IGCC case with a Selexol^{TM} carbon capture unit from a reliable source in literature and its implementation in ASPEN Plus. It needs to be ensured that simulation results are reproducible and in good agreement with the literature source.

Task 3: Integrate PSA Warm Gas Cleanup Technology

The development of the warm gas cleanup scenario is based upon the TRIG^{TM}-IGCC base case with cold gas cleanup. However, the Selexol^{TM} carbon capture process will be replaced by a CO_2-PSA process. Performance data of this process are obtained from TDA Research, Inc. The implementation of the PSA process into the flow sheet will require a reevaluation of many system components, especially the heat integration. The Selexol^{TM} process removes carbon dioxide as well as hydrogen sulfide. Next to the implementation of the CO_2-PSA process a high temperature desulfurization process needs to be identified. Other cold gas cleanup technologies, such as the mercury removal unit, will be replaced by adequate warm gas cleanup technologies, too.

Task 4: Study the Influences of the Water Gas Shift Reaction upon Carbon Capture

Aspen Plus simulations of the water gas shift reactors are purely thermodynamic. Task 4 involves the development of a kinetic model for a more detailed evaluation of the water gas shift reaction. The kinetic model will be used to predict pressure drop, temperature profile, species profiles, apparent reaction rate, intrinsic reaction rate, catalyst effectiveness and required steam to carbon ratio. The CO_2-PSA base case developed in Task 3 will be optimized to improve the IGCC plant performance. Different flow sheet configuration will be evaluated and optimized for maximization of power output and efficiency.

Task 5: Evaluate Methods to reach the DoE Target of 90 % Carbon Capture

Task 5 involves the development of new strategies and integration schemes to enable carbon capture of at least 90 %. Reasons for limited carbon capture will be analyzed and strategies to efficiently overcome these limiting factors will be elaborated. Crucial for high carbon capture is the amount of methane in the syngas. In order to reduce the methane content in the syngas before entering the CO_2-PSA different options will be identified. This includes the investigation of recycle options and the employment of additional technologies such as reformers and hydrogen PSAs which are commonly not found in IGCC power plants (i.e. without H_2 co-production).

Task 6: Techno-Economic Analysis

Performance numbers based upon thermodynamics like efficiency are very important. However, the techno-economic analysis is of even greater importance. Cost of electricity and costs associated with carbon capture, cost of capture and avoided cost, are very important

to evaluate the profitability of a plant. For the cost analysis scaling parameters and scaling exponents will be derived from literature data. A financing structure of the plant will be elaborated to estimate the cost of electricity. A cost analysis for both technologies, Selexol™ and PSA (including 90 % capture scenarios), will be conducted and key values will be compared.

Chapter 4

Design and Results

The simulations of the IGCC configurations presented in this study were carried out in the simulation software ASPEN Plus® V9. ASPEN Plus® is an established, commercially available chemical processing design software with built-in data bases for a large selection of chemical compounds. ASPEN Plus® handles equilibrium calculations as well as mass and energy balances. Based upon these capabilities steady state simulations were conducted which served as foundation of the coast analysis. Performance of single process units are estimated upon publicly available reports and publications.

4.1 Establish Design Basis and Calibrate Key Models

The design basis offers a common ground upon which the different scenarios are able to be compared with each other. Feed and site characteristics will remain unchanged throughout this study. The same holds true for the models used for simulating key components like the gasifier. However, some of the models will be interchanged from one scenario to another

(e.g., the Selexol^{TM} unit will be replaced by a warm gas PSA unit).

4.1.1 Feed Characteristics

The TRIG^{TM} gasifier is a low temperature, circulating bed gasifier which is specifically designed for low rank coals like sub-bituminous coals or lignite. Because of its non-slagging ash removal system, it can handle coals with high ash content and high ash fusion temperature. The coal used in this study is a mine mouth Powder River Basin (PRB) coal from Montana Rosebud, area D [24]. A detailed analysis of the coal is given in the following tables 4.1 and 4.2.

Table 4.1: Proximate Analysis of PRB-Coal

Proximate Analysis	Dry Basis, %	As Received, %
Moisture	0.00	25.77
Ash	11.04	8.19
Volatile Matter	40.87	30.34
Fixed Carbon	48.09	35.70
Total	100.00	100.00

Table 4.2: Ultimate Analysis of PRB-Coal

Ultimate Analysis	Dry Basis, %	As Received, %
Carbon	67.45	50.07
Hydrogen	4.56	3.38
Nitrogen	0.96	0.71
Sulfur	0.98	0.73
Chlorine	0.01	0.01
Ash	11.03	8.19
Moisture	0.00	25.77
Oxygen[1]	15.01	11.14
Total	100.00	100.00

[1]by difference

The higher heating value (HHV) on a dry basis is $26,787\ \frac{kJ}{kg}$ and $19,920\ \frac{kJ}{kg}$ on an as-

received basis. The lower heating value (LHV) is given as $25,810\ \frac{\text{kJ}}{\text{kg}}$ on a dry basis and $19,195\ \frac{\text{kJ}}{\text{kg}}$ on an as-received basis [24]. Ash composition is not specified in this study and handled as solid waste leaving the gasifier. However, details on the ash composition can be found in [24].

4.1.2 Site Characteristics

Low rank coals are not considered valuable enough to be shipped over long distances. Thus, the plant site has to be located close to the mine mouth. The plant in this study is assumed to be built in Montana which leads to the ambient conditions presented in Table 4.3 [24].

Table 4.3: Plant Site Characteristics

Elevation, m	1,036
Barometric Pressure, MPa	0.09
Design Ambient Temperature, Dry Bulb, °C	5.6
Design Ambient Temperature, Wet Bulb, °C	2.8
Design Ambient Relative Humidity, %	62

The values in Table 4.3 are annual average values and will serve as input for the steady state simulations of the plant in ASPEN Plus®.

The air composition at the plant site is shown in Table 4.4.

Table 4.4: Plant Site Air Composition

Component	Mole-%
Oxygen	20.81
Nitrogen	77.59
Argon	0.93
Carbon dioxide	0.03
Water	0.64

Montana is located in the western United States and limited water supply for cooling has to be taken into account. Hence, for cooling a combination of a dry air-cooled condenser and a mechanical draft, evaporative cooling tower is used in the process design. Considering an ambient wet bulb temperature of 2.8 °C and using an 11 °F temperature approach, a cooling water temperature of 9 °C is obtained [24]. The cooling tower range is assumed to be 11 °C. Evaporative losses in the cooling tower account for 0.8 % of the water circulation flow rate per 5.5 °C of range [56]. Drift losses are assumed to be 0.001 % of the recirculation flow rate [56]. Blow down losses are based on a medium level water quality and the assumption that drift losses are very small compared to other losses. Therefore, the following equation can be used to calculate the blowdown [56]:

$$Blowdown = \frac{Evaporative\,Losses}{Cycles\,of\,Concentration - 1} \tag{4.1}$$

$Cycles\,of\,Concentration$ is a function of the water quality and describes the ratio of the concentration of dissolved solids in the blowdown water compared to the make-up water, a medium value of 4 is assumed in this study[24]. Raw water makeup is obtained to 50 % from publicly owned treatment works and 50 % from groundwater. Raw water makeup is considered as water withdrawal that is used in the plant for any purpose. The net-water consumption is determined by the difference between water withdrawal and process water returned to the water source. In order to reduce the water footprint, water is internally recycled, e.g. boiler feed water or condensate is used to offset water demand [24].

The dry cooling initial temperature difference is 26 °C, which is in the typical design range of air cooled exchangers ($22 - 31$ °C). Dry cooling is assumed to have an auxiliary load factor of 3.5 compared to an equivalent wet cooling system [24].

Carbon dioxide is stored in a 171 m thick saline formation at a depth of 1239 m. The pressure of the formation is 84 bar, which is representative for an average storage site. The

injection rate per well is determined to be 9360 $\frac{t}{d}$. For the transport of about 80 km, the carbon dioxide needs to be compressed to a pressure of 153 bar before it leaves the plant to reach the storage facility at a high enough pressure [57]. The CO_2 is injected into the pipeline as super critical fluid and maintained at supercritical pressure at all times to prevent transients similar to water hammer [58]. A high purity of CO_2 is required to avoid corrosion. Limits of trace components are listed in Table 4.5 [57].

Table 4.5: CO_2 Pipeline Specifications

Parameter	Unit	Value
Inlet Pressure	bar	153
Inlet Temperature	°C	35
N_2	ppm	<300
O_2	ppm	<40
Ar	ppm	<10
H_2O	ppm	<150

The IGCC plant site itself is assumed to be of level topography and accessible by rail and highway. The size of the site is estimated to be 300 acres which includes a buffer zone and fencing [24].

4.1.3 Common Process Areas

The following section provides an overview of modeling approaches of various IGCC key components and their performance estimation. Common process areas are defined as processes that are found in the state-of-the-art cold gas cleanup scenario as well as the warm gas cleanup scenarios.

TRIG^{TM} Gasifier and Coal Preparation

The TRIG^{TM} gasifier has been developed specifically for low rank coals. Most existing coal gasification technologies show good performance on high rank coals but suffer significant losses when utilizing low rank coals. The TRIG^{TM} gasifier design is based on fluidized catalytic crackers as used in the petroleum industry and is a circulating bed reactor. The gasifier consists of a mixing zone, riser, presalter cyclone, standpipe cyclone, loop seal and J-leg. A schematic of the gasifier is shown in Figure 4.1.

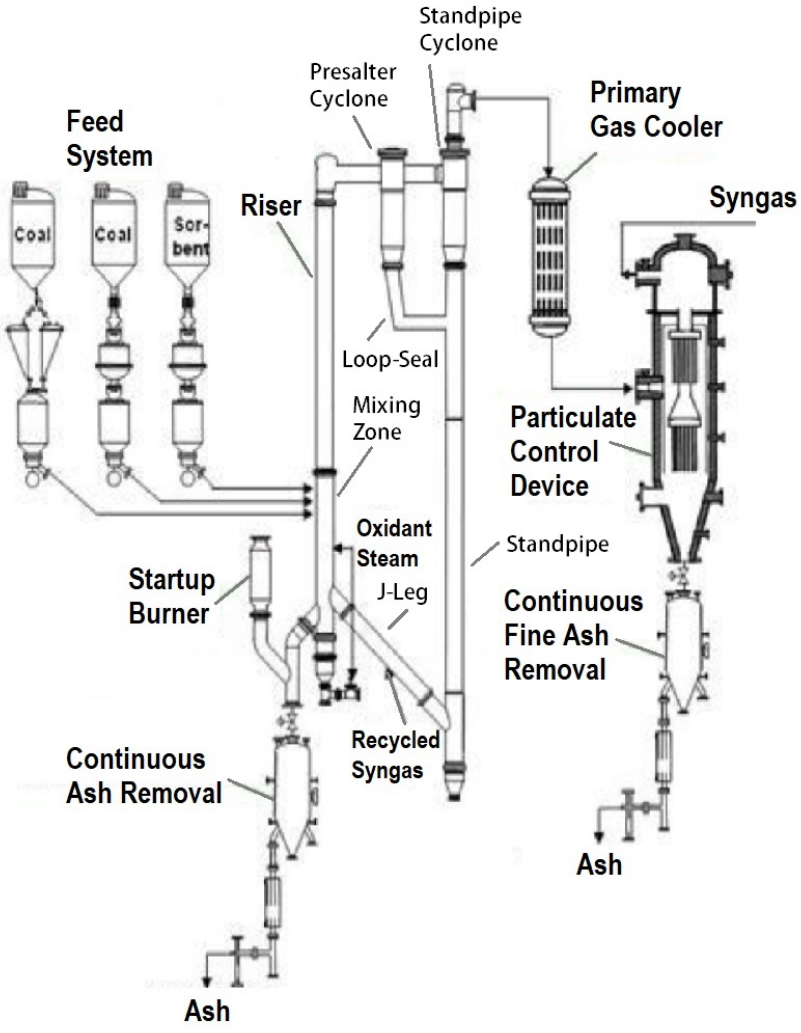

Figure 4.1: Design of the TRIG^{TM} gasifier [59].

The oxidant, air or pure oxygen, is fed into the gasifier at the bottom and/or middle section of the mixing zone where it is mixed with the recirculated coal particles. The exothermic oxidation reactions generate the heat for the endothermic gasification processes. The gasifier typically operates between $871 - 982\,^{\circ}\mathrm{C}$ [24]. These temperatures are relatively low compared to other gasification technologies which allows the usage of less expensive materials for construction. Because of its low operating temperature, the TRIG$^{\mathrm{TM}}$ gasifier is able to efficiently handle high moisture, high melting point, high ash content coals. The ash is removed at the bottom of the stand pipe and mixing zone in form of dry ash. Coal is added in the upper section of the mixing zone as dry feed. The high recirculation rates obtained in the TRIG$^{\mathrm{TM}}$ gasifier allow the feeding of larger particle sizes of up to 2 cm [24]. More flexibility and overall larger particle sizes save money in the coal preparation section of the plant. The high velocities and recirculation rates create a highly turbulent flow regime. As a result, intensive mixing of coal particles and gas is achieved in the riser. The enhanced heat and mass transport promote rapid gasification and reduce the formation of hydrocarbons, oils and tars. In order to obtain high carbon conversion efficiencies, cyclones are employed to recycle unreacted carbon. The unreacted carbon and ash particles are collected in the stand pipe where ash is removed first and the unreacted coal is fluidized with recycled syngas before it is transported back to the mixing zone. This design makes the TRIG$^{\mathrm{TM}}$ gasifier unique and highly suitable for low rank coals. The more reactive low rank coals can be easily gasified at lower temperatures which leads to a higher thermal efficiency of the gasifier. A lower operating temperature also diminishes the penalty of high moisture and ash content compared to high temperature reactors. Furthermore, the lower operating temperature promotes the formation of methane which has a higher heating value and boosts the cold gas efficiency. When considering pre-combustion carbon capture, however, this can limit the carbon capture efficiency.

In order to simulate coal in ASPEN Plus®, a non-conventional stream class is defined and the coal's characteristics are based on its proximate and ultimate analysis. Structural

effects of the organic compounds are not of major importance in gasification [7] and are not considered. Before the coal is fed into the gasifier, it is dried to a moisture content of 18 wt $-$ % in a roll mill incorporated flash dryer which operates at a superheat of 13.9 °C. The drying air – nitrogen enriched air to keep the oxygen level below 11.3 vol $-$ % due to safety concerns – is heated to 232 °C (which is safely below the devolatilization and autoignition temperature of PRB coal, 432 ± 4 °C [60] and 357 °C [61]) and dries the coal particles in a drying column. Subsequently, the coal is separated from the gas stream by cyclones and a bag house. The moisture rich gas is moved by an induced draft fan to the cooling section where the moisture is condensed. The gas is then recycled to the heater which is supplied with intermediate steam [24, 52, 62, 63].

The gasifier performance is calibrated based upon the syngas composition used in [24]. The operating pressure is 42 bar and the operating temperature is 982 °C. The resulting carbon conversion efficiency under these conditions is 98 %. Oxidant for the operation of the gasifier is supplied by an ASU, which delivers oxygen at a purity of 95 vol $-$ %. The specific oxidant consumption, ratio of oxidant to dry coal, used in this study is 0.661 on a mass basis.

The model chosen to simulate the gasification process is a pseudo-equilibrium temperature approach. This empirical approach has been shown to predict the TRIG$^{\text{TM}}$ performance most accurately [54]. Based upon the elements present in the above-mentioned coal, the following set of chemical equations is used to predict the syngas composition:

$$\mathrm{C} + \frac{1}{2}\mathrm{O_2} \rightleftharpoons \mathrm{CO} \tag{4.2}$$

$$\mathrm{C} + \mathrm{H_2O} \rightleftharpoons \mathrm{CO} + \mathrm{H_2} \tag{4.3}$$

$$\mathrm{C} + 2\,\mathrm{H_2} \rightleftharpoons \mathrm{CH_4} \tag{4.4}$$

$$2\,\mathrm{C} + \mathrm{H_2} + \mathrm{N_2} \rightleftharpoons 2\,\mathrm{HCN} \tag{4.5}$$

$$S + H_2 \rightleftharpoons H_2S \tag{4.6}$$

$$Cl_2 + H_2 \rightleftharpoons 2\,HCl \tag{4.7}$$

$$H_2S + CO_2 \rightleftharpoons COS + H_2O \tag{4.8}$$

$$N_2 + 3\,H_2 \rightleftharpoons 2\,NH_3 \tag{4.9}$$

$$H_2 + CO_2 \rightleftharpoons H_2O + CO \tag{4.10}$$

$$C_2H_6 + H_2 \rightleftharpoons 2\,CH_4 \tag{4.11}$$

$$C_3H_8 + 2\,H_2 \rightleftharpoons 3\,CH_4 \tag{4.12}$$

$$C_4H_{10} + 3\,H_2 \rightleftharpoons 4\,CH_4 \tag{4.13}$$

In order to obtain the same syngas composition as in [24], the equilibrium temperature for each individual equation is adjusted until the composition matches the reported in [24]. The resulting pseudo-equilibrium temperatures do not have a physical meaning as they account for kinetic effects within the gasifier. Not all reactions inside the gasifier will reach thermodynamic equilibrium due to limitations in heat and mass transfer as well as residence time. The determined pseudo-equilibrium temperatures are only used to determine the syngas composition; the outlet syngas temperature is set by the operating temperature. Differences in energy resulting from chemical reaction enthalpies and heat content of the leaving syngas prescribe the thermal losses to the environment. When establishing the gasifier model, it is important to include the syngas recycle stream which has an influence on the pseudo-equilibrium temperatures. Before the recycle steam is fed back into the gasifier, it is cooled to 343 °C while raising high pressure steam. Subsequently, the syngas stream passes through a particulate control device, which is purged periodically with a fraction of the recycle stream. A fraction of the syngas stream leaving the particulate control device is used as the recycle stream and is compressed to the required pressure of 45.9 bar.

Air Separation Unit

The flow sheet and operating principle of an air separation unit have been discussed previously in Section 2.1.2. For this study, air is not extracted from the gas turbine compressor for use in the ASU. The simulations use an elevated pressure ASU with a main compressor discharge pressures of 13.1 bar. For IGCC applications where high-pressure oxygen for the gasifier and high-pressure nitrogen as GT diluent are needed, power requirements and equipment size can be reduced by using an elevated pressure ASU. Injecting nitrogen into the gas turbine has a number of benefits: increased mass flow, increased power output at lower firing temperature and lower NO_x emissions. For this purpose, the syngas's heating value is ideally reduced to $4.2 - 4.8\ \frac{\mathrm{MJ}}{\mathrm{Nm^3}}$. To meet this target, the syngas is additionally humidified before being injected into the GT.

The ASU uses an air compressor that is powered by an electric motor and the air supplied to the compressor is filtered prior to compression. The air compressor is a centrifugal compressor with intercooling to reduce the power requirement. Then, the air is passed through an adsorbent based pre-purifier, which removes water, carbon dioxide and hydrocarbons from the air. Regeneration is achieved by purging with hot nitrogen. A small stream of air is withdrawn for supplemental instrument air. Booster compressors compress two split streams to provide the cooling duty required for the cryogenic separation. Then the air is fed into the cold box. Inside the cold box, the air is rectified with oxygen as bottom product and high-pressure nitrogen as overhead product. The liquid oxygen is supplied to the low-pressure column and further rectified producing 95 %-pure oxygen and low pressure nitrogen. The oxygen leaving the bold box as liquid is pumped to a pressure of 8.6 bar before leaving the ASU and is vaporized against high pressure feed air. After leaving the ASU, nitrogen and oxygen are further compressed to gasifier or GT supply pressure. The separation performance of the cold box is calibrated with the results from [24].

In the case of warm gas cleanup where the treated syngas has a much higher moisture

content, less nitrogen is required for injection into the gas turbine. This will affect the ratio of nitrogen to oxygen produced by the ASU and thus the performance. An effective way of modeling this change in the nitrogen to oxygen ratio is to comprise the ASU of an elevated pressure section and a low-pressure section [64]. The elevated pressure ASU is sized based upon the nitrogen demand and the low-pressure ASU is sized based on the oxygen demand that cannot be provided by the elevated pressure ASU. This design was common practice before gas supplier companies combined both processes into a single ASU. Nevertheless, the performance of ASUs can be approximated very well using this method [65]. The main compressor discharge pressures in this design are 13.1 bar and 4.6 bar, respectively. The oxygen leaves the low-pressure ASU at a pressure of 1.0 bar and a purity of 95 %.

Water-Gas-Shift Reactors

In order to enable pre-combustion carbon capture, the carbon needs to be captured in the form of carbon dioxide. Carbon dioxide has no enthalpy of combustion and is the desired form for carbon removal. However, the syngas leaving the gasifier contains large amounts of carbon monoxide (note: in some cases also methane). This carbon monoxide needs to be converted to carbon dioxide which is accomplished by the water-gas-shift reaction (WGS).

$$\mathrm{CO} + \mathrm{H_2O} \rightleftharpoons \mathrm{CO_2} + \mathrm{H_2} \tag{4.14}$$

In order to prevent the deposition of elemental carbon on the catalysis, a certain steam to carbon ratio needs to be maintained. Furthermore, the addition of steam helps to shift the equilibrium of the WGS reaction to the right side. The formation of whisker carbon is determined by evaluation of the thermodynamic equilibrium between carbon, hydrogen and

oxygen. Furthermore, the formation of Fischer-Tropsch liquids and/or methanol is critical for the operation of shift reactors. Details on equilibrium calculation and avoidance of Fischer-Tropsch liquids will be discussed in Section 4.4.2.

There are two possible locations for the water-gas-shift reactor: upstream of the AGR (sour shift) or downstream of the AGR (sweet shift). Sweet shifting requires less stringent specifications on the metallurgy but has other disadvantages. In the case of classical cold gas cleanup, sweet shifting involves more heating and cooling steps since the water-gas-shift reaction operates at $200 - 400$ °C and sulfur removal and carbon removal are low temperature processes. Another important aspect is that the raw syngas leaving the scrubber contains water which already accounts for some of the water required to achieve the necessary steam to carbon monoxide ratio. If the WGS reactor is located downstream of the AGR, this water vapor would be condensed and would have to be re-injected, which causes additional losses. Beyond that, the sour shift catalysis supports hydrolysis reactions, e.g. of COS, which makes the hydrolysis reactor redundant in the case of sour shifting.

$$\mathrm{COS} + \mathrm{H_2O} \rightleftharpoons \mathrm{CO_2} + \mathrm{H_2S} \tag{4.15}$$

$$\mathrm{HCN} + \mathrm{H_2O} \rightleftharpoons \mathrm{NH_3} + \mathrm{CO} \tag{4.16}$$

As a result of the above-mentioned reasons, a sour gas shift reactor is used in this study. Due to the exothermic character of the water-gas-shift reaction, the reactor is comprised of several stages with intercooling. The released heat is used to raise intermediate pressure steam and superheated shift steam. In the WGS reaction, higher reaction temperatures are favorable from a kinetic point of view and reduce reactor size, however, thermodynamics favor low temperatures to shift the equilibrium to CO_2. The lifetime of shift catalysts ranges from 2-4 years depending on the trace components present in the syngas. Origin of this necessary replacement at the end of the catalyst's lifetime is the deactivation of the catalyst

which impacts the kinetics and conversion. The shift reactors in the ASPEN® simulation use an equilibrium temperature approach of 13.9 °C to account for catalyst deactivation and middle of run conditions.

Mercury Removal

The mercury content of PRB coal is 0.081 ppm on a dry basis [24]. Mercury constitutes a hazard for human health and needs to be removed from the flue gas. For the removal a carbon bed is used, which is able to remove about 95 % of the mercury. In the Selexol™ scenario the mercury removal is conducted at low temperature which is important for the removal efficiency of carbon beds. The bed is replaced after 24 months. Switching the bed is not due to reaching full capacity. Instead, it is due to buildup in pressure drop, water and other contaminates. With an estimated lifetime of 24 months, the bed is assumed to reach mercury loadings of around $0.64\ \text{wt} - \%$ which is significantly below its maximum capacity which can be as high as $30\ \text{wt} - \%$ [66]. For the warm gas cleanup, a high temperature bed material is used. RTI is offering high temperature mercury removal beds for temperatures >200 °C together with their warm gas desulfurization process. The bed material is not disclosed to the general public. It is likely that the Hg removal process is based on a chemisorption process involving heavy metal beds. The lifetime of those high temperature sorbents such as lead, is much shorter and the bed has to be replace every 3 months. Furthermore, RTI is developing sorbents for temperatures in the range $260 - 315\ °\text{C}$ [67], however, the bed materials are kept confidential. It is possible that RTI's materials of interest are similar to the high temperature palladium based sorbents previously described [12].

Power Island

The gas turbine generator used in this study is an advanced F-class turbine. Advanced F-class turbines are axial machines that operate at constant speed with variable inlet guide vanes and advanced compressor aerodynamic engineering. It applies advanced cooling technology combined with high temperature alloys, which allows it to reach higher combustion temperatures compared to other conventional gas turbines. Turbines for high hydrogen content syngas are assumed to be offered commercially in near future and problems like flame stability, flashback and NO_x emissions will be solved. The turbine is modeled as a non-intercooled axial compressor, combustor and a turbine-expander. For the model it is assumed that the gas turbine has a fixed geometry and that the model has the same geometry as in the calibration case. The performance of the turbine compressor, combustor and expander are calibrated with the data provided in [24] which are obtained from vendors and are specifically for the operation on syngas. In order to correct for differences in the gas composition, the firing temperature is adjusted to maintain the same blade metal temperature as in the reference case [65].

$$TIT = TIT_{\mathrm{R}} + \frac{644.23}{1.8}\left(y_{\mathrm{H_2O,\,CO_2\,R}} - y_{\mathrm{H_2O,\,CO_2}}\right) \tag{4.17}$$

TIT is the turbine inlet temperature in degrees Celsius and $\Delta y_{\mathrm{H_2O,\,CO_2}}$ is the mole fraction of water and carbon dioxide at the combustor outlet. Equation 4.17 corrects the firing temperature based on the amount of water and carbon dioxide content in the syngas. Water and carbon dioxide have high heat capacities which impact the heat transfer in the expander. The pressure ratio is corrected by Equation 4.18 [65].

$$p = k \cdot \dot{m}\sqrt{\frac{TIT}{\overline{M}}} \tag{4.18}$$

p is the pressure, k is a constant and obtained from the calibration, $\dot{m}$ is the mass flow, $\overline{M}$ is the average molecular weight and TIT is the turbine inlet temperature in Kelvin. For the turbine operation it is important to determine the limit of operation. This limit is either set by the shaft work or the air inlet flow which change with ambient pressure and temperature. Under ISO condition the generator terminal can generate a maximum electrical power output of 232 MW. The maximum mass flow through the turbine compressor at Montana at the average air condition is $2,897,000\ \frac{\text{kg}}{\text{h}}$.

The heat recovery steam generator unit produces HP, IP, and LP steam. High pressure steam boiler feed water is pressurized to 136 bar and heated to 538 °C. A reheat cycle together with the IP coils produce steam at 28 bar and 535 °C before it enters the lower pressure steam sections. The steam leaving the LP steam turbine is condensed at 35 °C partly by a water cooled condenser and partly by an air-cooled condenser.

4.1.4 Techno-Economic Analysis

The design of large scale plants with the size of several hundreds of megawatts like the herein studied IGCC plants underlay limitations in the equipment capacity. Thus, it is necessary to split equipment that reaches a critical capacity into several trains. In this study, single train design is used with exception where capacity limitations require a second train. Redundancies are not considered in the techno-economic analysis with the exception that Pumps are always spared: either 2 x 100 % in case of single operating train or 3 x 50 % in case of two 50 % operating trains. The design capacities of the IGCC subsystems in this study are assumed as follows: two ASUs (2 x 50 %), two trains of coal preparation (2 x 50 %), two trains of TRIG$^{\text{TM}}$ gasification systems (2 x 50 %), two trains of syngas cleanup systems (2 x 50 %), two trains of Selexol$^{\text{TM}}$ or CO_2-PSA (2 x 50 %), one train of Claus unit or sulfuric acid unit (1 x 100 %), two gas turbine/HRSG tandems (2 x 50 %), one steam

turbine (1 x 100 %).

Gas turbines constitute one of the largest and most expensive equipment in an IGCC power plant and are typically purchased off the shelf. Other equipment like the gasifier will be adjusted in size to provide enough syngas to operate the gas turbine at full load conditions.

The plant costs are based on total plant costs (TPC) estimated for the year 2011. The TPC includes: cost of process equipment, on-site facilities and infrastructure that support the plant, direct and indirect labor and engineering services, procurement and construction (EPC). EPC includes the detailed equipment design, contractor permitting and project/construction management costs. In order to obtain cost estimates for the investigated IGCC concepts, comparable process equipment is scaled to the required capacity using Equation 4.19.

$$SC = RC \cdot \left(\frac{SP}{RP}\right)^{u} \cdot (1 + AER)^{SY-RY} \cdot \left(\frac{TS}{TR}\right)^{0.9} \tag{4.19}$$

SC represents the scaled cost, RC represents the reference cost, SP is the scaled parameter and RP is the reference parameter used to scale the equipment. u is the scaling exponent, AER the annual escalation rate, SY the scaled year and RY the reference year. TS is the number of trains/purchased number of equipment of the scaled plant and TR is the number of trains/purchased number of equipment in the reference case. The exponent 0.9 accounts for the cost reduction when more than one of the same pieces of equipment is purchased and installed. The expected accuracy of this methodology for cost estimation is expected to be in the range of -15 % to $+30$ %.

A summary of the parameters used in this study is provided in Table 4.6. Values have been derived from [5, 24, 65, 68, 69, 70]. Transport cost, storage cost and monitoring cost (TS&M) for CO_2 sequestration are not included in the TPC but will be accounted for

separately.

Operating and maintenance costs are expenses associated with the daily operation of the power plant and include: operating labor, maintenance material and labor, administrative and support labor, consumables, fuel, waste disposal and byproduct sales. Operating and maintenance cost can by separated into fix and variable costs. Fix costs are comprised of annual operating labor, maintenance labor, administrative and support labor as well as property tax and insurance. For the operation of the plant 2 skilled operators, 10 regular operators, 1 foreman and 3 technicians are needed who are assumed to be paid an average hourly salary of 39.70 $\frac{\$}{\mathrm{h}}$. The operating labor burden is estimated at 30 % and the overhead charge rate is assumed to be 25 % at a plant capacity factor of 1.0. The maintenance labor is approximated as 35 % of the total maintenance cost which is determined on basis of individual cost relationships to each of the initial unit cost. Administrative and support labor are expressed as 25 % of operating and maintenance labor. Property tax and insurance costs are considered to be 2 % of the TPC.

Variable operating and maintenance costs are impacted by the plant's availability. Variable costs include: maintenance cost as well as consumables like fuel, water, catalysts, sorbents but also byproducts (byproducts generate credit). Catalysts, sorbents and other process solutions require an initial fill before the plant can operate which has to be considered in the cost analysis. Consumables are evaluated on their consumption rate which varies for different types of catalysts and sorbets. Furthermore, costs associated with their disposal after reaching their end of life are accounted for. Base values for major operating costs are provided in Table 4.7.

Costs for CO_2 transport, storage and monitoring are treated separately. For CO_2 storage in an average saline formation, the cost of CO_2 transport, storage and monitoring are 22.00 $\frac{\$}{\mathrm{t}}$ [71].

The global economic assumptions for the financing structure are an income tax rate of

Table 4.6: Reference Data for Cost Estimation

Process Unit	Scaling Parameter	Unit	Parameter Value	Cost in $1000	Type of Cost	Year	Scaling Exponent	Annual Escalation Rate	Number of Trains
Air Separation Unit	Mole-Flow Oxygen	kmol/h	4,019	154,470	TPC	2007	0.70	4.93%	2
Fuel Receiving, Preparation & Feeding	Mass-Flow As-Received Coal	kg/h	262,152	168,004	TPC	2007	0.66	4.65%	2
Gasifier, Syngas Cooler & Auxiliaries	Mass-Flow Dried Coal	kg/h	194,595	273,739	TPC	2007	0.77	5.37%	2
Gasification Foundations	Mass-Flow Dried Coal	kg/h	194,595	19,877	TPC	2007	0.50	3.99%	2
Ash Handling Systems	Mass-Flow Dried Coal	kg/h	194,595	38,573	TPC	2007	0.55	4.67%	2
Flare Stack System	Mass-Flow Dried Coal	kg/h	194,595	1,881	TPC	2007	0.50	5.02%	2
Adiabatic Shift Reactor (including heat exchanger)	Catalyst Volume	m^3	177.0	16,159	TPC	2007	0.80	4.67%	1
Isothermal Shift Reactor	Catalyst Volume	m^3	57.1	6,156	TPC	2010	0.80	4.67%	1
LTGC + Syngas Humidification	Mole-Flow Unshifted and Humidified Syngas	kmol/h	29,511	16,705	TPC	2007	0.77	4.67%	2
Warm Gas Desulfurization	Mole-Flow Total Sulfur in Feed	kmol/h	89	10,550	TPC	1999	0.79	5.02%	1
Sulfuric Acid Plant	Mole-Flow Total Sulfur in Feed	kmol/h	89	23,050	TPC	1999	0.67	5.02%	1
Blowback Gas Systems	Mass-Flow Dried Coal	kg/h	194,595	2,795	TPC	2007	0.30	5.02%	2
Fuel Gas Piping	Mole-Flow of Decarbonized and Humidified Syngas	kmol/h	17,944	1,529	TPC	2007	0.72	5.54%	2
Gas Cleanup Foundations	Mole-Flow Unshifted and Humidified Syngas	kmol/h	29,511	1,622	TPC	2007	0.79	3.93%	2
Mercury & Trace Contaminant Removal (Cold Gas)	Mole-Flow Unshifted and Humidified Syngas	kmol/h	29,511	2,827	TPC	2007	0.77	4.65%	2
Mercury & Trace Contaminant Removal (Warm Gas)	Mass-Flow Mercury in Feed	kg/h	210	3,397	TPC	2011	0.77	5.02%	2
Selexol^{TM} Unit	Removal of CO_2,H_2S and COS from Syngas	kmol/h	9,168	180,134	TPC	2007	0.79	4.65%	2
CO_2 Compression, Dehydration & Pumping (Selexol)	Compressor Power	kW	288,290	34,805	TPC	2007	0.88	14.82%	4
Claus unit & TG Recycle	Mass-Flow Sulfur	kg/h	1,903	16,578	TPC	2007	0.67	4.59%	1
Carbon Dioxide PSA	Mass-Flow CO_2 Captured	US tons/h	422	142,640	TPC	2011	0.77	5.02%	2
Carbon Dioxide Purification & Heat Recovery	Mole-Flow Raw CO_2 Captured	kmol/h	21,491	27,887	TPC	2007	0.88	5.02%	2
CO_2 Compression, Dehydration & Pumping (CO_2-PSA)	Compressor Power	kW	27,564	51,076	TPC	2007	0.88	5.02%	2
Hydrogen PSA	Mole-Flow Hydrogen Product	kmol/h	3,665	7,500	TPC	2002	0.70	5.02%	1
Adiabatic Reformer	Catalyst Volume	m^3	8.5	4,078.0	TPC	2006	0.75	5.02%	1
Gas Turbine, Generator & Auxiliaries	Gas Turbine Power Output	kW	426,400	132,015	TPC	2007	0.00	4.76%	2
HRSG, Ducting & Stack	Mole Flow GT Exhaust x ($T_{HRSG\,in}$-$T_{HRSG\,out}$)	kmol K	54,565,710	55,023	TPC	2007	0.70	-0.70%	2
Steam Turbine, Generator & Auxiliaries	Steam Turbine Power Output	kW	194,900	46,715	TPC	2007	0.70	11.13%	1
Steam Surface Condenser	Heat Duty	GJ/h	496	3,659	TPC	2007	0.71	-6.34%	1
Steam Aircooled Condenser	Heat Duty	GJ/h	496	33,414	TPC	2008	0.71	5.02%	1
Feedwater System	Demineralized Water	gal/min	1,138	6,462	TPC	2007	0.71	4.65%	2
Water Makeup & Pretreating	Raw Water Withdrawal	gal/min	2,517	1,059	TPC	2007	0.71	4.82%	1
Other Feedwater Subsystems	Steam Turbine Power Output	kW	194,900	3,196	TPC	2007	0.71	5.02%	1
Service Water Systems	Mass-Flow As-Received Coal	kg/h	262,152	3,727	TPC	2007	0.71	4.68%	1
Other Boiler Plant Systems	Steam Turbine Power Output	kW	194,900	4,237	TPC	2007	0.73	5.03%	1
Fuel Oil System & Natural Gas	Gas Turbine Power Output	kW	426,400	1,781	TPC	2007	0.24	4.65%	1
Waste Water Treatment	Mass-Flow Dried Coal	kg/h	194,595	1,436	TPC	2007	0.71	4.33%	1
Misc. Power Plant Equipment	Gross Power Generated at Terminals	kW	621,300	2,387	TPC	2007	0.24	4.34%	1
Cooling Water System	Cooling Tower Heat Duty	GJ/h	884	22,187	TPC	2007	0.72	1.58%	1
Accessory Electric Plant	Gross Power Generated at Terminals	kW	621,300	81,309	TPC	2007	0.45	4.55%	1
Instrumentationo & Controls	Number of Gasifier Trains	-	2	26,110	TPC	2007	0.13	4.51%	2
Improvement to Site	Mass-Flow As-Received Coal	kg/h	262,152	18,659	TPC	2007	0.08	3.99%	1
Buildings & Structures	Mass-Flow As-Received Coal	kg/h	262,152	16,423	TPC	2007	0.10	4.57%	1

Values and coefficients recalculated from economic data in [5, 24, 65, 68, 69, 70]

Table 4.7: Operation Cost Basis

Compound	Unit	Cost in $ per Unit	Year
Feed			
Coal	US ton	19.63	2011
Water	gal	1.67	2011
Product (Credit)			
Sulfur	US ton	99.00	2011
Sulfuric Acid	US ton	95.70	2011
Catalyst			
Desulfurization, ZnO	US ton	25,230	2011
Sour Shift, Mo/Co-based	m^3	17,620	2007
LT Sweet Shift, CuO/ZnO/Promoter	m^3	16,900	2016
HT Sweet Shift, Fe/Cr/Cu	m^3	6,690	2015
IT Sweet Shift, CuO/ZnO/Cr	m^3	12,120	2016
Reforming, Ni/Ca-Al_2O_3	m^3	17,520	2014
Sulfuric Acid Plant, V_2O_5	ft^3	84.32	2011
Claus Catalyst	ft^3	203.20	2011
Catalytic CO_2 Combustor	ft^3	3,770	2011
Carbon Capture Sorbent	lb	1.67	2011
Trace Contaminant Sorbent	kg	14.75	2011
Activated Carbon Bed	lb	1.63	2011
Selexol^{TM} Solution	gal	36.79	2011
MU & WT Chemicals	lb	0.27	2011
Waste Disposal			
Activated Carbon Bed	lb	0.65	2011
Slag	US ton	25.11	2011
Desulfurization, ZnO	US ton	25.11	2011
Sulfuric Acid Plant, V_2O_5	ft^3	20.37	2002
Carbon Capture Sorbent	lb	0.65	2011

Data from vendors and recalculated from [5, 24, 65, 68]

36 % comprised of an effective federal tax of 34 % and 6 % state tax. Capital depreciation has a declining balance of 150 % over the course of 20 years. Investment tax credits are not considered in the financial analysis as well as tax holidays are assumed to be 0 years. Debt financing is of non-recourse type which secures debt is limited to the real assets of the project. Debt is repaid over a period of 15 years with no grace period and/or debt reserve funds. Expenditure period for coal power plants is typically 5 years and an operational period of 30 years is assumed which results in an economic analysis period of 35 years. Capital cost escalation during expenditure is assumed to be 3.6 %. The total capital of

overnight capital during the 5-year expenditure period is distributed as follows: 10 %, 30 %, 25 %, 20 % and 15 %. 100 % of the total overnight capital is depreciated. Cost-of-electricity (COE), operating and maintenance costs as well as fuel costs are assumed to have an annual inflation rate of 3.0 %.

Treating an IGCC project as a high-risk project will require an equity of 55 %. With a current dollar cost of 5.5 % (debt) and 12 % (equity), this results in a weighted capital cost of 8.13 % after tax. According to [24], this financing structure can be approximated with a capital charge factor (CCF) of 0.1243.

The first year COE can be approximated using the following Equation 4.20

$$COE = \frac{(CCF)(TOC) + OC_{\text{fix}} + (CF)(OC_{\text{var}})}{(CF)(MWH)} \tag{4.20}$$

COE is the cost of electricity in the first year, CCF is the capital charge factor, TOC is the total overnight capital, OC_{fix} total fixed annual operating cost, OC_{var} total variable annual operating cost, CF the capacity factor of the plant and MWH annual net-megawatt-hours generated at 100 % capacity factor.

Measures for the additional expenses of carbon capture are expressed in Cost of CO_2 Capture and Avoided Cost.

$$Cost\,of\,Capture = \frac{COE_{\text{with CC}} - COE_{\text{without CC}}}{CO_2\,Captured} \tag{4.21}$$

$$Avoided\,Cost = \frac{COE_{\text{with CC}} - COE_{\text{without CC}}}{CO_2\,Emissions_{\text{without CC}} - CO_2\,Emissions_{\text{with CC}}} \tag{4.22}$$

The difference between these equations lies in the origin of the carbon emissions. Car-

bon capture requires energy input and thus increases the carbon emissions per unit output of the plant with carbon capture. As a result, Avoided Cost is more commonly found as basis for comparing carbon capture since it accounts for the effect of increased emissions. Reference costs for the calculation of the Cost of Capture and Avoided Cost are taken from [24, 25].

4.2 Development of a Dual-Stage Selexol^{TM} Scenario

The Selexol^{TM} case is the base case scenario and will function as a state-of-the-art reference case for the warm gas cleanup scenario.

Unique processes in this case are the Selexol^{TM} acid gas removal unit and the Claus unit for production of elemental sulfur. Modeling approaches of these units will be briefly discussed below.

4.2.1 Acid Gas Removal

This study uses a state-of-the-art dual-stage Selexol^{TM} process for the removal of acid gas. The flow diagram and fundamental operating principles have been discussed in Section 2.1.2. Since the syngas pressure is very high, the solvent used in the Selexol^{TM} process works on the principle of physical absorption (Henry's Law) which has a much higher capacity than chemical solvents at these pressures. As a result, the absorption of gases is highly dependent on the gas temperature. The lower the temperature, the higher the capacity of the solvent. The gas inlet temperature in this study is chosen to be 35 °C at a pressure of 30.5 bar. In the first column H_2S is removed selectively and regenerated along with some CO_2 and sent to the Claus unit. The second column removes the remaining CO_2 which is

flashed off the solvent in three stages. The first stage is recycled to the absorber column and the following two stages produce pure CO_2 for sequestration. With the multi-stage flash design, CO_2 compression work can be reduced to make the process more efficient. In general, the Selexol^{TM} process is capable of removing 99.77 % of the H_2S and 97.5 % of the CO_2 [24] but with the high CO_2 to H_2S ratio in the PRB coal derived syngas it is necessary to slip a significant amount of CO_2 to maintain a high enough H_2S concentration in the acid gas stream. An advantage of the Selexol^{TM} process is that only very little amounts of hydrogen are dissolved in the syngas. The exact amount of hydrogen loss during acid gas removal depends on the operating condition. In this study, the design resulted in a hydrogen recovery rate of 99.4 %. The environmental target for sulfur dioxide emissions from coal power plants are 0.0128 $\frac{\mathrm{lb_{SO_2}}}{\mathrm{MMBtu}}$ which corresponds to a sulfur concentration of 30 ppm in the syngas. The performance of the Selexol^{TM} process was calibrated with the data available in [24].

4.2.2 Claus Unit

The Claus process produces elemental sulfur as a salable byproduct from hydrogen sulfide. In the Claus process, a third of the hydrogen sulfide is first converted to sulfur dioxide which is then converted to elemental sulfur by the Claus reaction.

$$H_2S + \frac{3}{2}O_2 \rightleftharpoons H_2O + SO_2 \tag{4.23}$$

$$2\,H_2S + SO_2 \rightleftharpoons 2\,H_2O + 3\,S \tag{4.24}$$

Elemental sulfur exists in the gas phase as S_2, S_6 and S_8 with S_2 predominant at higher temperatures and S_8 predominant at lower temperatures. The Claus unit can operate on

air or pure oxygen. In this work, 95 % pure oxygen is used as oxidant. Main reason for using pure oxygen is that the tail gas of the Claus unit can be recycled to the Selexol^{TM} unit without introducing nitrogen into the syngas. Another advantage of using oxygen instead of air is that it reduces the cost of the Claus unit and since an ASU is needed regardless in this setup, burning oxygen is more economical. However, using oxygen has no significant impact on the sulfur recovery efficiency. A flow diagram of the 3-stage Claus unit implemented into the simulation is shown in Figure 4.2.

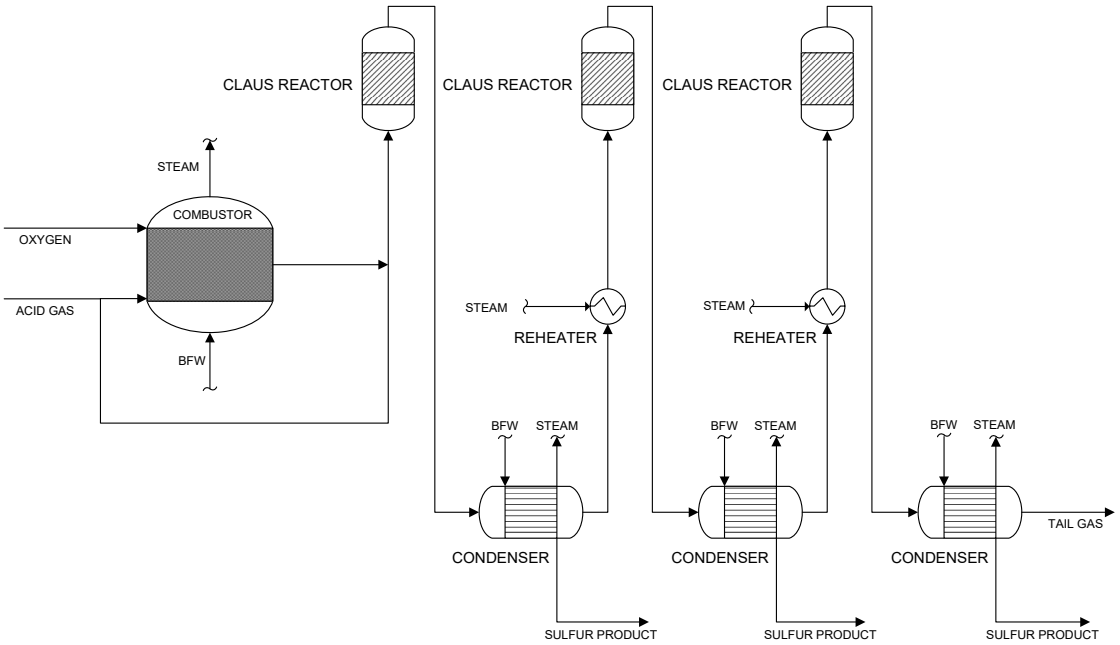

Figure 4.2: Flow sheet of the three stage Claus unit.

In the combustor, one third of the acid gas is combusted with oxygen according to Equation 4.23. The reaction is highly exothermic and takes place at around 1370 °C. Some of the released heat is used to raise intermediate pressure steam. The SO_2 rich stream is mixed with the bypassed acid gas stream and reacts in the first Claus reactor according to reaction 4.24. In the following condenser, sulfur is condensed while raising more steam. The Claus reaction is assumed to reach equilibrium condition (due to sufficient residence time)

and the gas leaving the condenser is reheated and further converted in a second and third Claus reactor to maximize the sulfur yield. The remaining tail gas is sent to the tail gas treatment unit.

Tail gas treatment is required to meet the stringent environmental regulations if vented to the atmosphere. The Claus process can recover about 95 % of the sulfur. With tail gas treatment, sulfur recovery rates of up to 99.8 % can be achieved. Tail gas from the Claus unit contains various sulfur species like COS, CS_4, H_2S, SO_2 and elemental sulfur. In addition, there might be H_2, CO and CO_2 present in the tail gas. In order to remove these compounds, they have to be catalytically converted to H_2S. H_2S can be captured with a solvent or condensing water. In this case, the "clean" tail gas, which contains H_2S, can be recycled back to the acid gas removal unit.

4.2.3 Simulation Results

This section contains the evaluation of the IGCC plant design using the Selexol^{TM} process for carbon capture. A block flow diagram of the overall IGCC design is provided in Figure 4.3 showing the major process streams. The corresponding stream summary with information about stream temperature, pressure, flow rate, vapor fraction and composition of the streams indicated in the flow sheet is given in Table 4.8.

The net power generated by this plant is $451,634\,\text{kW}$ which requires a coal input of $262,678\,\frac{\text{kg}}{\text{hr}}$. Significant amounts of heat ($32,463\,\text{kW}_\text{t}$) in the form of intermediate pressure steam are required to reduce the moisture content in the coal from initially $25.77\,\text{wt}-\%$ to $18\,\text{wt}-\%$. Coal drying is a substantial parasitic loss, however, it is necessary to enable milling and feeding. Furthermore, drying the coal before it enters the gasifier is more efficient as lower quality heat can be used compared to the heat available inside the gasifier.

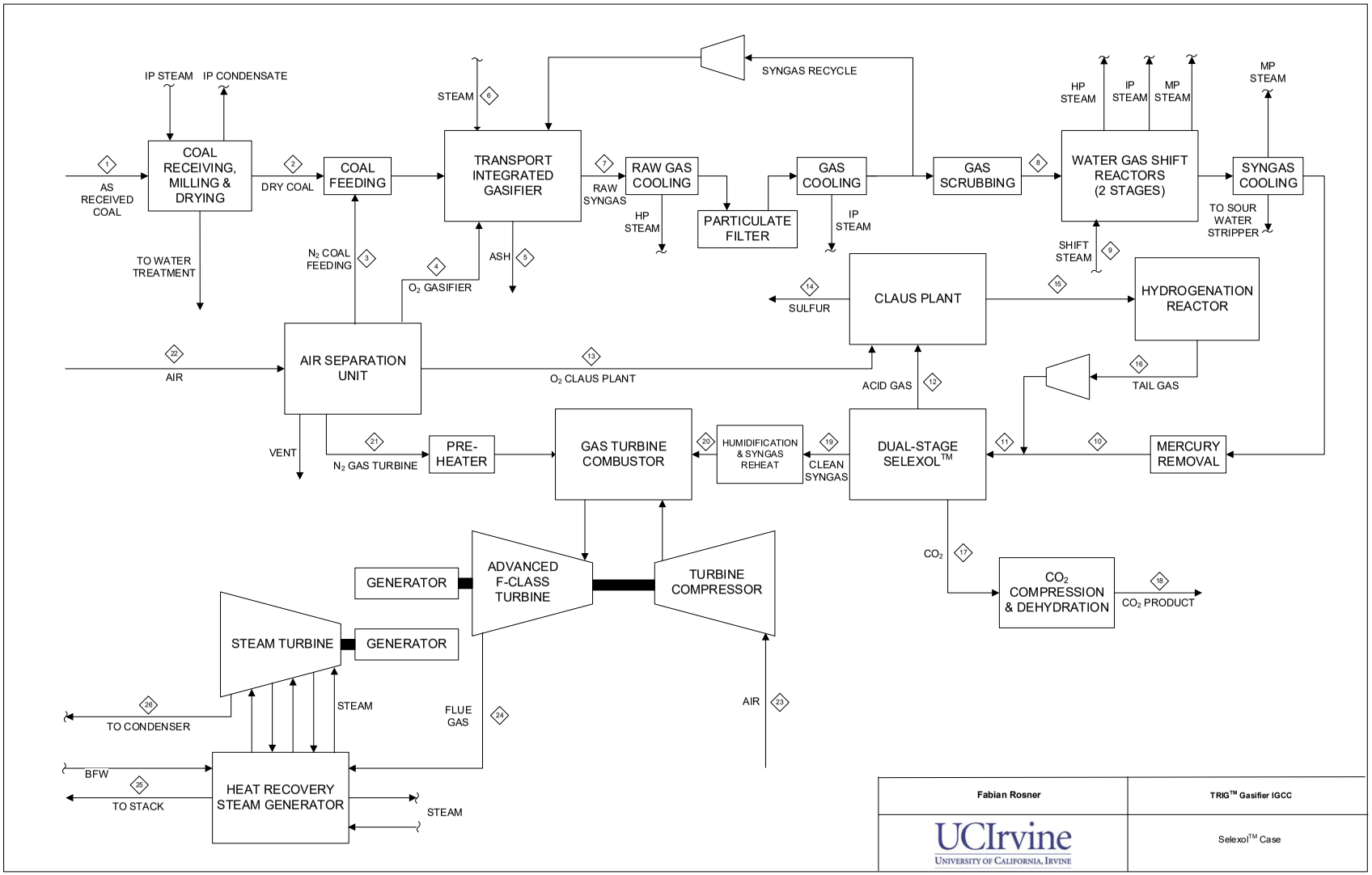

Figure 4.3: Flow sheet of the cold gas cleanup Selexol^{TM} case.

Table 4.8: Stream Summary of the Cold Gas Cleanup Selexol^{TM} Case at Fully Loaded Gas Turbine

Stream Number	Unit	1	2	3	4	5	6	7	8	9	10	11	12	13
Temperature	°C	5.6	71.1	105.9	64.7	982.2	397.9	982.2	161.0	329.6	37.8	34.7	48.3	232.2
Pressure	bar	0.9	0.9	56.2	50.3	3.4	51.0	41.7	38.3	51.0	32.0	31.7	1.6	7.9
Mole Flowrate	kmol/h	-	-	1695	4240	-	3564	25433	20016	14848	22892	23427	383	124
Mass Flowrate	kg/h	-	-	47558	136642	-	64203	546028	427262	267486	479071	492891	13786	3989
Solid Flowrate	kg/h	262678	237788	-	-	24137	-	-	-	-	-	-	-	-
Mass Vapor Fraction	-	0	0	1	1	0	1	1	1	1	1	1	1	1
Composition	mol-basis													
O_2	-	0.00000	0.00000	0.00540	0.95001	0.00000	0.00000	0.00000	0.00000	0.00000	0.00000	0.00000	0.00000	0.95001
N_2	-	0.00000	0.00000	0.99230	0.01406	0.00000	0.00000	0.00473	0.00456	0.00000	0.00399	0.00559	0.00068	0.01406
Ar	-	0.00000	0.00000	0.00230	0.03594	0.00000	0.00000	0.00789	0.00761	0.00000	0.00666	0.00685	0.00184	0.03594
H_2	-	0.00000	0.00000	0.00000	0.00000	0.00000	0.00000	0.27141	0.26179	0.00000	0.51400	0.50966	0.09968	0.00000
CO	-	0.00000	0.00000	0.00000	0.00000	0.00000	0.00000	0.34265	0.33051	0.00000	0.00389	0.00543	0.00163	0.00000
CO_2	-	0.00000	0.00000	0.00000	0.00000	0.00000	0.00000	0.16160	0.15587	0.00000	0.42155	0.42059	0.57839	0.00000
H_2O	-	0.00000	0.00000	0.00000	0.00000	0.00000	1.00000	0.15360	0.18363	1.00000	0.00092	0.00096	0.01900	0.00000
CH_4	-	0.00000	0.00000	0.00000	0.00000	0.00000	0.00000	0.05136	0.04954	0.00000	0.04332	0.04338	0.02174	0.00000
H_2S	-	0.00000	0.00000	0.00000	0.00000	0.00000	0.00000	0.00289	0.00278	0.00000	0.00260	0.00451	0.27551	0.00000
NH_3	-	0.00000	0.00000	0.00000	0.00000	0.00000	0.00000	0.00364	0.00351	0.00000	0.00307	0.00300	0.00000	0.00000
COS	-	0.00000	0.00000	0.00000	0.00000	0.00000	0.00000	0.00020	0.00019	0.00000	trace	trace	0.00152	0.00000
HCl	-	0.00000	0.00000	0.00000	0.00000	0.00000	0.00000	trace	0.00000	0.00000	0.00000	0.00000	0.00000	0.00000
SO_2	-	0.00000	0.00000	0.00000	0.00000	0.00000	0.00000	0.00000	0.00000	0.00000	0.00000	trace	trace	0.00000
Total	-	0	0	1	1	0	1	0.99997	1	1	1	0.99998	1	1

Stream Number	Unit	14	15	16	17	18	19	20	21	22	23	24	25	26
Temperature	°C	173.7	174.6	19.4	15.5	33.8	31.0	193.3	104.2	5.6	5.6	563.3	151.7	32.4
Pressure	bar	1.1	1.1	0.8	10.0	152.7	27.0	24.3	26.2	0.9	0.9	0.9	0.9	0.05
Mole Flowrate	kmol/h	30	610	546	9002	8987	13971	17498	15965	21196	100248	126138	126138	23663
Mass Flowrate	kg/h	1907	17573	14018	393645	393379	84264	151043	448019	612442	2896627	3448130	3448130	426292
Solid Flowrate	kg/h	-	-	-	-	-	-	-	-	-	-	-	-	-
Mass Vapor Fraction	-	1	1	1	1	0	1	1	1	1	1	1	1	0.91309
Composition	mol-basis													
O_2	-	0.00000	trace	0.00000	0.00000	0.00000	0.00000	0.00000	0.00540	0.20810	0.20810	0.10403	0.10403	0.00000
N_2	-	0.00000	0.06088	0.07258	0.00000	0.00000	0.00935	0.00732	0.99230	0.77590	0.77590	0.72992	0.72992	0.00000
Ar	-	0.00000	0.00845	0.01507	0.00010	0.00010	0.01138	0.00891	0.00230	0.00930	0.00930	0.00889	0.00889	0.00000
H_2	-	0.00000	0.06067	0.31723	0.00411	0.00412	0.84919	0.66491	0.00000	0.00000	0.00000	0.00000	0.00000	0.00000
CO	-	0.00000	0.13181	0.06997	0.00014	0.00014	0.00898	0.00703	0.00000	0.00000	0.00000	0.00000	0.00000	0.00000
CO_2	-	0.00000	0.23775	0.37161	0.99176	0.99339	0.05036	0.03943	0.00000	0.00030	0.00030	0.01436	0.01436	0.00000
H_2O	-	0.00000	0.41468	0.02284	0.00164	0.00000	trace	0.21704	0.00000	0.00640	0.00640	0.14279	0.14279	1.00000
CH_4	-	0.00000	0.00913	0.04517	0.00225	0.00225	0.07070	0.05536	0.00000	0.00000	0.00000	0.00000	0.00000	0.00000
H_2S	-	0.00000	0.00068	0.08454	0.00000	0.00000	trace	trace	0.00000	0.00000	0.00000	0.00000	0.00000	0.00000
NH_3	-	0.00000	0.00000	0.00000	0.00000	0.00000	0.00000	0.00000	0.00000	0.00000	0.00000	0.00000	0.00000	0.00000
COS	-	0.00000	0.00064	0.00100	0.00000	0.00000	0.00000	0.00000	0.00000	0.00000	0.00000	0.00000	0.00000	0.00000
HCl	-	0.00000	0.00000	0.00000	0.00000	0.00000	0.00000	0.00000	0.00000	0.00000	0.00000	0.00000	0.00000	0.00000
SO_2	-	0.00000	0.07532	trace	0.00000	0.00000	0.00000	0.00000	0.00000	0.00000	0.00000	trace	trace	0.00000
Total	-	0	1	1	1	1	0.99995	0.99999	1	1	1	1	1	1

The thermal input to the gasifier in the form of coal based on the higher heating value is $1,451,388\,\mathrm{kW_t}$ which is converted at 982 °C to syngas with a higher heating value of $10,744\,\frac{\mathrm{kJ}}{\mathrm{kg}}$. This amounts to 85.2 % of the chemical energy bound in the coal being contained in the gaseous chemical compounds formed (based on HHV). After the raw gas cooling, the syngas temperature is lowered to 343 °C for bulk particulate removal by filters. Further cooling and scrubbing removes fine particulates as well as water soluble contaminants such as chlorides. The gas leaves the scrubber at its dew point. Wet scrubbing is advantageous to dry cleanup when syngas shifting is needed. It is a comparatively simple process to remove fine particulates and other contaminates while pre-humidifying the syngas for shifting. Before the syngas can enter the first shift reactor, the steam to carbon monoxide ratio is adjusted to S/CO=2.80 to avoid carbon deposition. In order to prevent pore condensation of water inside the catalyst pellets, the inlet temperature is set to 15 °C superheat. Details regarding the setup of the shift reactors will be discussed in Section 4.4. After shifting 98.7 % of the initial carbon monoxide is converted to carbon dioxide, the stream leaving the second shift reactor has a dew point temperature of 184 °C. Cooling the stream close to room temperature results in large amounts of high pressure water vapor being condensed and not available for expansion in the gas turbine anymore. Furthermore, cooling the syngas down to almost room temperature requires large amounts of cooling water. Raw water withdrawal is already problematic in many areas and will gain importance in the future with respect to a growing world population and changes in climate. In the dual-stage Selexol$^{\mathrm{TM}}$ unit, the hydrogen sulfide concentration is reduced to about 8 ppm while about $5\,\mathrm{mol}-\%$ of carbon dioxide remains in the decarbonized syngas. High purity carbon dioxide is obtained in two pressure stages which is then dehumidified, to meet the pipeline specifications, and further compressed to 152.7 bar. In order to minimize the compression work, 3-stage intercooled compressors are used; however, the work associated with CO_2 compression remains substantial. In addition to the penalty of $28,732\,\mathrm{kW}$ of electrical power input for CO_2 compression and $16,421\,\mathrm{kW}$ for the Selexol$^{\mathrm{TM}}$ unit, removing the high pressure carbon dioxide from the

syngas lowers the mass flow through the expander of the gas turbine and thus the power output. These are the major reasons why carbon dioxide removal has such a strong impact on the plant efficiency.

The U.S. Department of Energy targets a carbon removal efficiency of 90 % [3]. However, this target was not achievable in this case due to the high methane content in the syngas produced by the TRIG^{TM} gasifier. About 9.2 mol − % of the total carbon in the syngas is in the form of methane. Methane passes through the shift reactors and the Selexol^{TM} unit unreacted and is converted to carbon dioxide in the gas turbine combustor. Although 98.7 % of the CO was shifted to CO_2, only 83.4 % of the total carbon could be removed from the syngas. An additional factor for this low carbon removal rate is the low CO_2-yield achieved in the Selexol^{TM} process, which leaves about 5 % of CO_2 in the decarbonized syngas. Similar carbon capture for high methane content syngas has been found in [24]. In order to have a fair comparison between this case and following cases, a carbon removal rate of 83.4 % will be used as benchmark for the warm gas cleanup cases.

Before the decarbonized syngas is fed into the gas turbine, it is humidified and preheated. Addition of water vapor helps to control NO_x emissions and is more effective than using nitrogen on a mole per mole basis. The extent of humidification however, is limited by the amount of low temperature heat available for the humidifier and syngas humidification alone is not sufficient to control the combustion process and supplementary nitrogen injection into the gas turbine is needed. The two advanced F class gas turbines generate 424, 753 kW of power at the generator terminals. The heat in the flue gas is recovered in a HRSG and utilized in a steam Rankine cycle. The multi-stage steam turbine generates an additional 192, 173 kW of power at the terminals. The steam leaving the steam turbine has a mass vapor fraction of 0.91. Condensation of the remaining steam is achieved by combined dry and wet cooling. The total amount of cooling duty for steam condensation is 265, 216 kW_t. This amount is significantly less than cooling duties in conventional PC power plants since only 31.2 % of the generated power is generated by the Rankine cycle. The total duty of the cool-

ing tower is $338,995\ \mathrm{kW_t}$ which evaporates about $7.0\ \frac{\mathrm{m^3}}{\mathrm{min}}$. The total net water withdrawal of the plant accumulates to $14.45\ \frac{\mathrm{m^3}}{\mathrm{min}}$. The overall plant efficiency is $31.11\ \mathrm{HHV} - \%$ which is in good agreement with other results found in literature for IGCC plants with Selexol$^{\mathrm{TM}}$ carbon capture technology [5, 24, 33, 41, 45, 46, 48, 72]. A summary of the performance data of the Selexol$^{\mathrm{TM}}$ process based IGCC with carbon capture can be found in Table 4.9.

Table 4.9: Performance Summary of the Cold Gas Cleanup Selexol™ Case

Gross Power Generation	Unit	
Gas Turbine	kW	424,753
Steam Turbine	kW	192,173
Total	kW	616,926
Auxiliary Load	Unit	
Coal Handling	kW	511
Coal Milling	kW	731
Coal Dryer Circulation Blower	kW	2,564
Ash Handling & Dewatering	kW	633
Air Separation Unit Auxiliaries	kW	1,016
Air Separation Unit Main Compressor	kW	54,543
Oxygen Compressor	kW	7,436
Nitrogen Compressor	kW	29,008
Syngas Recycle Compressor	kW	1,553
Tail Gas Recycle Compressor	kW	2,175
Carbon Dioxide Compressor	kW	28,732
Boiler Feed Water & Demin. Pumps	kW	5,445
Vacuum Condensate Pump	kW	356
Process Condensate & SWS System	kW	52
Humidifier & BFW Circulation Pumps	kW	216
Cooling Water Circulation Pumps	kW	2,830
Cooling Tower Fans	kW	1,556
Air Cooled Condenser Fans	kW	2,040
Scrubber Pumps	kW	611
Selexol™ Unit	kW	16,421
Gas Turbine Auxiliaries	kW	996
Steam Turbine Auxiliaries	kW	99
Claus & Tail Gas Treating Auxiliaries	kW	251
Miscellaneous Balance of Plant	kW	3,006
Transformer Losses	kW	2,512
Total	kW	165,292
Net Power Generation	Unit	
Net Power Output	kW	451,634
Plant Performance	Unit	
Net Efficiency	%-HHV	31.11
Net Heat Rate	kJ/kWh	11572.0
Consumables	Unit	
As-Received Coal	kg/h	262,678
Thermal Input	kW-HHV	1,451,388
Raw Water Usage	m^3/min	14.45
Carbon Capture	Unit	
Carbon Recovery	%	83.40

4.3 Development of a PSA Warm Gas Cleanup Scenario

Processes unique to this case are the warm gas sulfur removal unit, the sulfuric acid plant and the warm gas carbon dioxide removal PSA. Modeling approaches of these units will be briefly discussed below, followed by the simulation results.

4.3.1 Sulfur Removal

For warm gas desulfurization, a circulating bed adsorption process developed by RTI is used. RTI, who is industrializing this process, has completed large scale pre-commercial testing with over 3500 hours of total syngas operation at the Polk County IGCC. RTI's test facility uses a 20 % split stream of the raw gas produced at the Polk County IGCC which is equivalent to a 50 MW plant scale. The syngas, cleaned in the test facility, is shifted in sweet-shift reactors and 90 % of carbon is removed in a downstream aMDEA® process. The sulfur dioxide produced in the regeneration loop of RTI's desulfurization unit is used to produce sulfuric acid. The technology is now ready for demonstration and deployment at full commercial scale.

RTI's desulfurization process consists of an adsorber and regenerator which are illustrated in Figure 4.4.

In the adsorber, the raw syngas is mixed with the regenerated zinc oxide sorbent which is entrained in the gas flow and carried through the riser. This enables sulfur components like H_2S and COS to react with the sorbent to form ZnS. The riser typically operates in a temperature range from $315 - 535$ °C. A great advantage of this process is the simultaneous removal of H_2S and COS. Most commercial processes can only remove one or the other and a conversion reactor is needed before the sulfur can be removed. The chemical reactions of

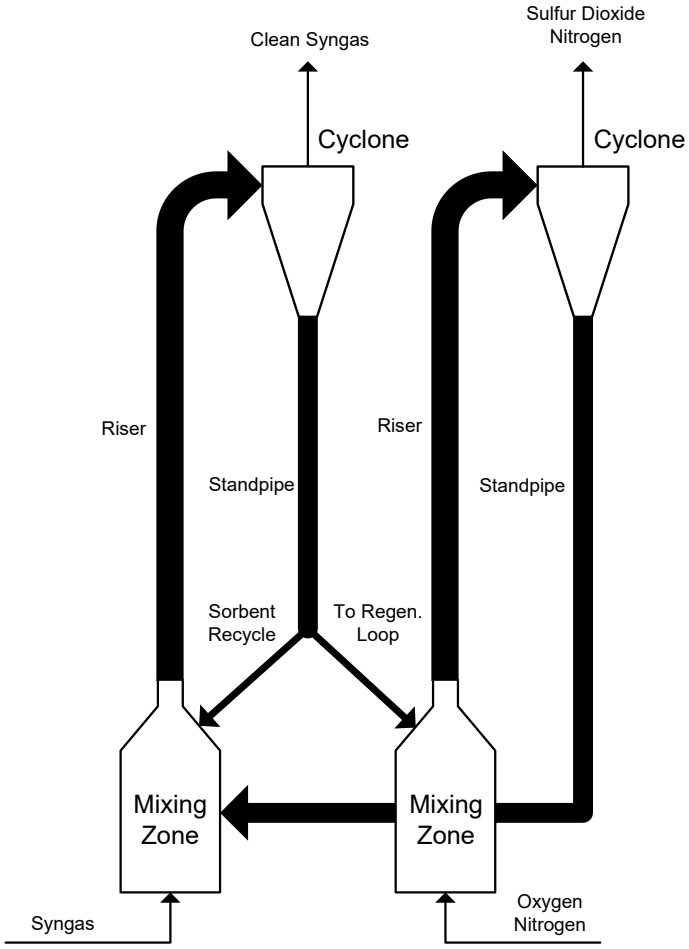

Figure 4.4: Process diagram of the warm gas sulfur removal unit.

H_2S and COS with zinc oxide are described in equations 4.25 and 4.26.

$$ZnO + H_2S \rightleftharpoons ZnS + H_2O \tag{4.25}$$

$$ZnO + COS \rightleftharpoons ZnS + CO_2 \tag{4.26}$$

The performance of sulfur removal from the syngas by equations 4.25 and 4.26 is estimated based upon the equilibrium data of the process generated by RTI [73].

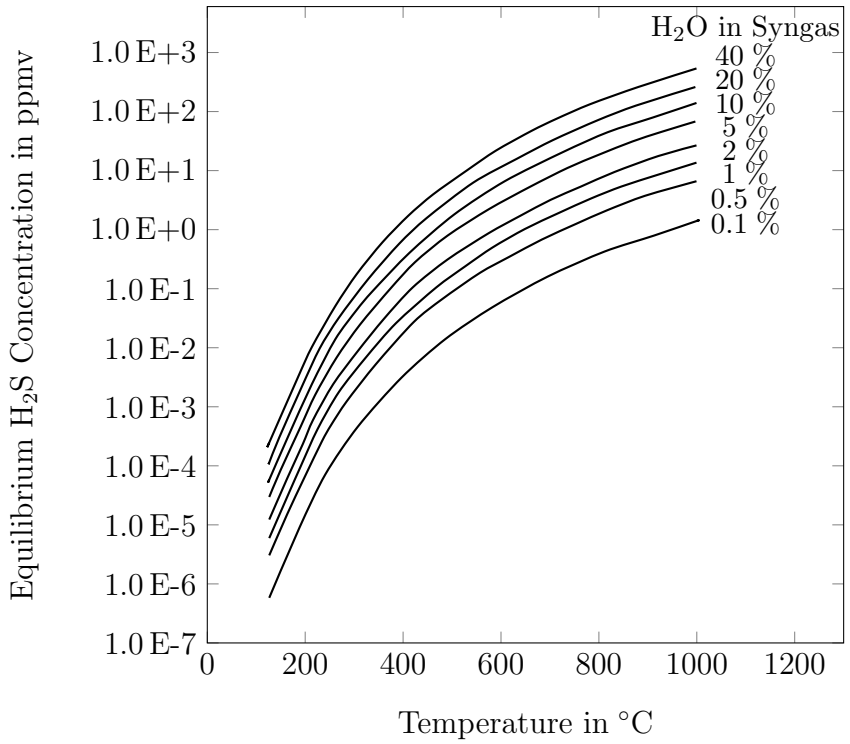

Figure 4.5: Warm gas sulfur removal equilibrium concentrations of hydrogen sulfide as function of temperature and syngas water content.

The used sorbent is separated from the clean syngas via a cyclone and accumulated in a standpipe. Some of the used sorbent is recycled into the adsorber. The other portion is regenerated in a regeneration loop. In the regeneration loop, a mixture of oxygen and nitrogen is used to oxidize the ZnS at $650 - 815$ °C.

$$\mathrm{ZnS} + \frac{3}{2}\mathrm{O_2} \rightleftharpoons \mathrm{ZnO} + \mathrm{SO_2} \tag{4.27}$$

After separation of the regenerated sorbent, the sorbent is collected in a second standpipe and ready for reuse. The sulfur dioxide rich off gas can be used in a direct sulfur recovery process, sulfuric acid unit or modified Claus unit. The overall process can operate at pressures between $7 - 82$ bar and achieves sulfur removal rates of greater than 99.9 % [31].

4.3.2 Sulfuric Acid Unit

Contrary to the Selexol^{TM} scenario, the warm gas cleanup scenario uses a sulfuric acid unit instead of a Claus unit. The RTI process described above for desulfurization regenerates the sulfur in the form of SO_2 (Selexol^{TM} recovers H_2S) which is more suitable for the synthesis of sulfuric acid than elemental sulfur.

In a sulfuric acid unit, the sulfur dioxide is catalytically converted to sulfur trioxide over a vanadium oxide based catalyst using air.

$$SO_2 + \frac{1}{2}O_2 \rightleftharpoons SO_3 \tag{4.28}$$

This reaction is strongly exothermic. In order to have the conversion efficiency approaching 99 %, the reactor is split into several layers with intercooling. Before the last stage, some of the sulfur trioxide rich gas is fed into a pre-absorber to remove sulfur trioxide from participating in the equilibrium resulting in a higher sulfur dioxide conversion. The approximately $400 - 430$ °C hot sulfur trioxide stream is then introduced into the main absorber where the gas is scrubbed with sulfuric acid.

$$SO_3 + H_2SO_4 \rightleftharpoons H_2S_2O_7 \tag{4.29}$$

Absorbing sulfur trioxide directly into water is not possible due to the highly exothermic character of the reaction. Thus, water is added later to form sulfuric acid under more controllable conditions.

$$H_2S_2O_7 + H_2O \rightleftharpoons 2\,H_2SO_4 \tag{4.30}$$

The tail gas leaves the sulfuric acid unit through the stack and the raw sulfuric acid can be sold as it is or further purified as required. A flow sheet of the described sulfuric acid unit is shown in Figure 4.6

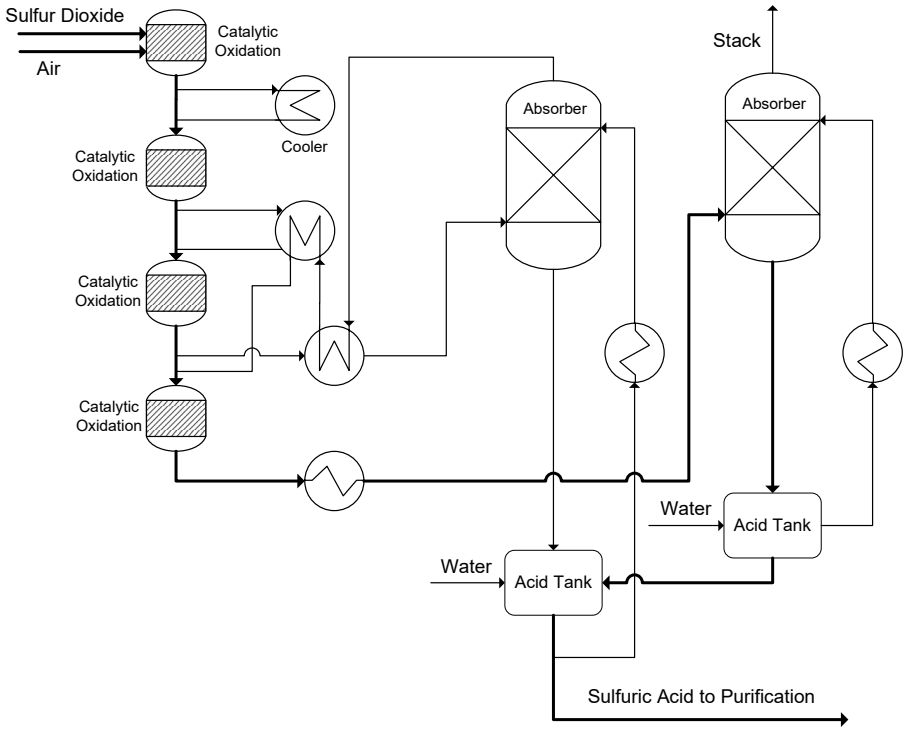

Figure 4.6: Flow sheet of the sulfuric acid unit.

4.3.3 CO_2 Pressure Swing Adsorption

The warm gas carbon dioxide removal technology simulated in this study is based upon a pressure swing technology developed by TDA Research, Inc. [64, 74]. Performance data used in this study were provided from TDA and were collected under realistic operating conditions at their demonstration site. TDA's sorbent selectively removes carbon dioxide

from syngas via physical adsorption without forming covalent bonds. The sorbent consists of mesoporous carbon modified with surface functional groups. The heat of adsorption, 4.9 $\frac{\text{kcal}}{\text{mol}}$, is similar to the heat of absorption in the Selexol$^{\text{TM}}$ process, ≈ 4.0 $\frac{\text{kcal}}{\text{mol}}$ [74]. This reduces the energy requirement for regeneration substantially compared to amine solvents and other chemical sorbents. In order to maximize regeneration efficiency, a combination of temperature swing, pressure swing and concentration swing is used. Especially, the regeneration at low pressure has a significant impact on the regeneration behavior and the required amount of purge steam. Since the adsorption is carried out in a fixed bed (batch process), several adsorption vessels are needed to enable continuous operation. Each adsorber will have to go through several operation and regeneration stages. If the number of adsorbers is equal to the number of process stages, a continuous operation is possible with one adsorber operation at each process stage. Also the time period for each step plays an important role. If a step process is short, two or more processes can be executed during the same operational stage. For continuous operation TDA developed an 8 bed/8 stage cycle which in total involves 10 steps.

1. Carbon Dioxide Adsorption (ADS
2. Pressure Equalization to approx. 29.0 bar (EQ1D)
3. Pressure Equalization to approx. 23.4 bar (EQ2D)
4. Pressure Equalization to approx. 17.9 bar (EQ3D)
5. Blowdown to approx. 9.9 bar (CoDEP)
6. Regeneration at approx. 9.7 bar (Purge)
7. Pressure Equalization to approx. 17.2 bar (EQ3R)
8. Pressure Equalization to approx. 22.8 bar (EQ2R)

9. Pressure Equalization to approx. 28.3 bar (EQ1R)

10. Pressure Equalization to approx. 33.2 bar (PRESS)

An illustration of the sequencing of the single steps is given in Figure 4.7.

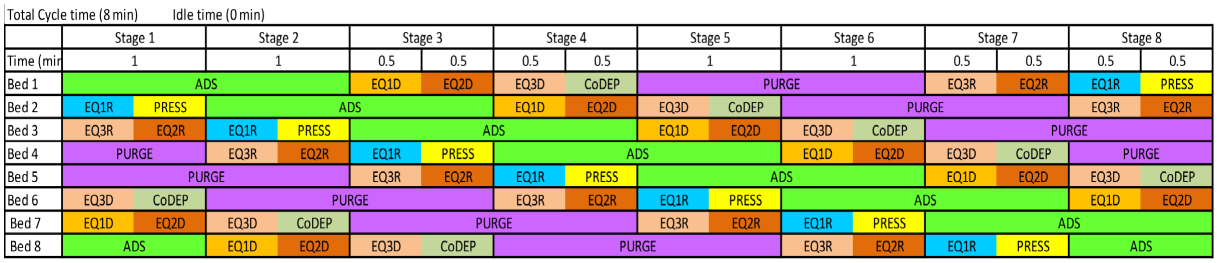

Figure 4.7: Process stages of TDA's pre-combustion carbon dioxide capture system using solid sorbents [75].

An illustration of the bed cycling is provided in Figure 4.8. It shows the interplay between the 8 different adsorbers during various stage of operation. All steps in each stage are engineered to be completed at the same time and smooth transition into the next stage of operation.

The data provided in Figure 4.7 and Figure 4.8 are as of 22nd August 2017 and might be subject to modification as TDA is constantly working to improve its process. Several test campaigns for proof-of-concept demonstrations have been completed at facilities at the Wabash River IGCC and the National Carbon Capture Center in Wilsonville, AL. Throughout the demonstration, the sorbent reliably removed carbon dioxide from the syngas while the sorbent was able to maintain its activity and capacity. TDA's sorbent based PSA technology is able to reduce the carbon dioxide content in the syngas from around 27.7 % to less than 0.6 %. Furthermore, large scale sorbent production has been accomplished as well as long-term testing with over 20,000 cycles. Pilot scale testing and commercial demonstration readiness are believed to be achieved in 2018 which makes this technology a promising candidate for carbon removal in near future.

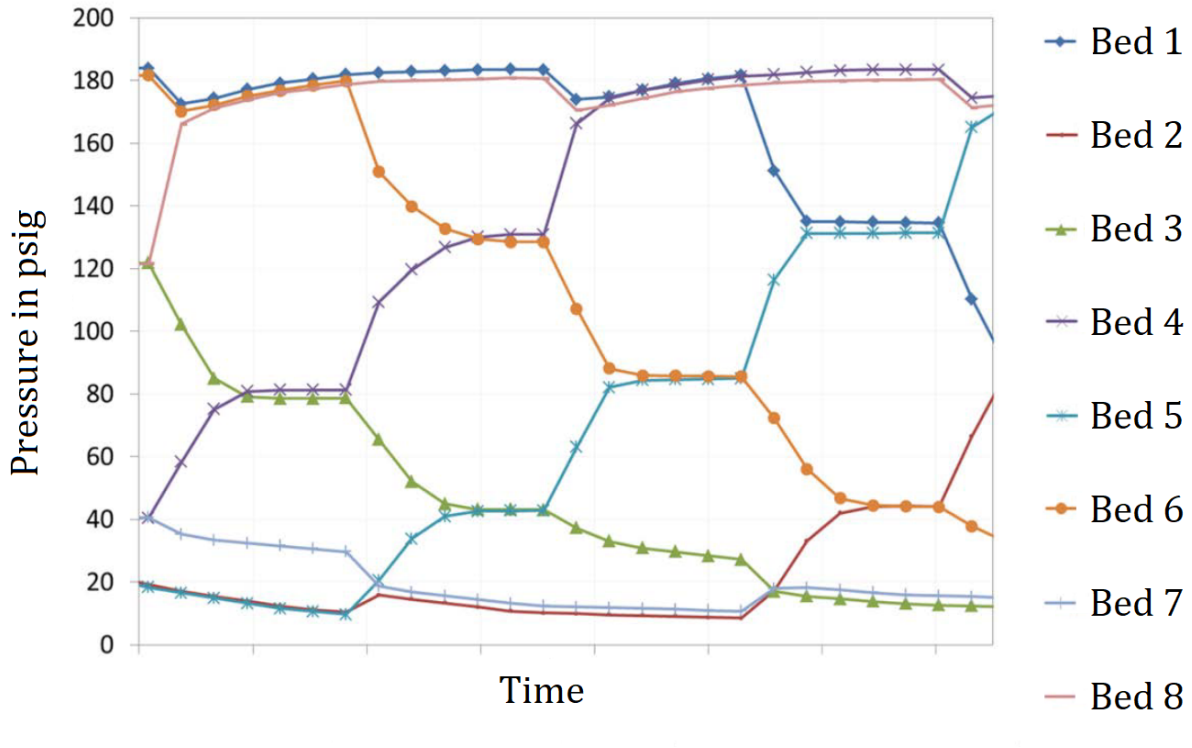

Figure 4.8: Flow sheet of TDA's pre-combustion carbon dioxide capture system using solid sorbents [75].

4.3.4 Simulation Results

The integration of the warm gas clean-up PSA into the IGCC has effects upon processes downstream of the first water-gas-shift reactor. The high temperature sulfur removal unit operates best in the range between $315 - 535$ °C. By placing the sulfur removal unit between the two shift reactors (after the high temperature shift reactor), the exothermic water-gas-shift reaction can be used to heat the syngas to a temperature of about 393 °C without external heat input. This temperature is sufficient to operate RTI's desulfurization technology in its designed temperature range. After desulfurization, the syngas is cooled and fed into the second shift reactor. The second shift reactor is operated at a lower temperature to maximize CO-shifting. In this scenario, the operation temperature of the second shift reactor is kept at 204 °C to have identical conditions as in the cold gas clean-up scenario. However, the catalyst used in the second shift reactor is a sweet shift catalyst (sulfur has

been removed) based on $Cu/ZnO/Al_2O_3$ which is more active at lower temperatures than the Fe/Cr-based sweet shift catalysts. The sulfur captured in the process described above is oxidized using vitiated air and further converted to sulfuric acid in a sulfuric acid unit. The shifted syngas is cooled to 199 °C before it passes through the mercury removal unit and enters the CO_2-PSA. The dew point temperature of the syngas at this point is 181.6 °C. This allows the syngas to carry the added shift steam and water vapor from the scrubber all the way to the gas turbine and makes the syngas humidification unit redundant. On a dry basis both cases, the Selexol^{TM} case as well as the warm gas PSA case, have an almost identical syngas composition entering the CO_2 removal unit. Inside the CO_2 removal unit, CO_2 is adsorbed onto the adsorbent material. Regeneration of the bed material is achieved by purging the vessel with medium pressure steam. Because the carbon removal yield of the PSA process is much higher than the Selexol^{TM} process, some of the syngas is bypassed to obtain an overall carbon capture of 83.4 % to maintain consistency between the two cases. The raw CO_2 leaving the PSA needs to be conditioned before it can be injected into a pipeline and stored underground. Water is condensed out by cooling the raw CO_2 down to 20 °C. Together with the condensate, NH_3 and HCN will be removed from the CO_2 stream. However, the stream still contains some syngas components like H_2,CO and CH_4, which are introduced during the transitioning from syngas depressurization (at 9.9 bar) to steam purge operation. These combustible components are oxidized in a combustor using oxygen from the ASU. The generated heat is used to preheat the CO_2 stream feeding into the combustor and to raise high pressure steam for the Rankine cycle. Oxygen as oxidant is preferred over air in this case, because an air separation plant is needed nevertheless and introducing nitrogen into the carbon dioxide product stream should be avoided. Using oxygen increases the adiabatic flame temperature and provides heat at a higher quality which allows raising high pressure steam.

The entire raw CO_2 conditioning section is fundamentally different to the Selexol^{TM} case which produces a very pure raw CO_2 stream that only requires compression and dehy-

dration. The CO_2 outlet pressures of the Selexol^{TM} process are 1.2 bar and 10.3 bar with a stream mass flow ratio of 1.15:1. The outlet pressure of the PSA unit is 9.7 bar, which means that over 34 % of the total CO_2 compression power in the Selexol^{TM} case is needed to raise the pressure to the same outlet pressure of the PSA case. The specific compression energy per kg carbon dioxide in the Selexol^{TM} case is 262.94 $\frac{kJ}{kg_{CO_2}}$ whereas the compression energy per kg carbon dioxide in the PSA case is only 204.45 $\frac{kJ}{kg_{CO_2}}$. Carbon dioxide compression is one of the largest parasitic losses in the entire plant and plays a key role in increasing the plant efficiency. Comparing the relative parasitic power consumption of CO_2 compression, the Selexol^{TM} case consumes about 4.66 % of the generated power versus only 3.69 % for the PSA scenario. The Selexol^{TM} unit itself has a specific auxiliary load of 150.28 $\frac{kJ}{kg_{CO_2}}$. However, the Selexol^{TM} process operates in two stages which allows for simultaneous syngas decarbonization and desulfurization. Thus, for the comparison with the PSA cleanup technology, the auxiliary load of RTI's desulfurization unit has to be included in this analysis. The specific auxiliary load of RTI's desulfurization unit is 15.90 $\frac{kJ}{kg_{CO_2}}$. The PSA unit has essentially no electrical power consumption as it operates upon the principle of pressure swing, temperature swing and concentration swing. Nevertheless, it requires an energy input in the form of medium pressure steam. The steam supplied to the PSA has a temperature of 382 °C and 10.34 bar. The condenser in the bottoming Rankine cycle operates at 32 °C and 0.05 bar. In order to convert the steam to energy, the same conversion efficiency as used in the steam turbines in the simulation has been assumed. The resulting energy input for the PSA in terms of lost electrical output is then 264.23 $\frac{kJ}{kg_{CO_2}}$. Together with the auxiliary load of the desulfurization unit, this totals in 280.13 $\frac{kJ}{kg_{CO_2}}$ for the PSA unit. The Selexol^{TM} unit also requires steam input. Steam to the Selexol^{TM} unit is supplied at 342 °C and 7.3 bar. Converting this to electrical power, another 94.00 $\frac{kJ}{kg_{CO_2}}$ of energy are utilized in the Selexol^{TM} process. For desulfurization, decarbonization and compression, the specific auxiliary load for the Selexol^{TM} and PSA cases are 507.22 $\frac{kJ}{kg_{CO_2}}$ and 484.58 $\frac{kJ}{kg_{CO_2}}$. Although the power requirement for the PSA unit is only 4.5 % lower per unit of captured

carbon dioxide, the overall efficiency of the PSA case is 34.20 % and thus 9.9 % higher than the Selexol^{TM} case. Another reason for this substantial increase in efficiency is the decrease in compression power in the air separation unit. Due to the lower nitrogen requirement of the gas turbine, less air has to be compressed and that is why the main air compression power dropped from 54,543 kW to 36,595 kW considering gas turbine air inlet flow limitations. Similar to the main air compressor, the nitrogen compression power decreased from 28,732 kW to 10,500 kW. The power input for the oxygen compressor, however, rose at the same time from 7,436 kW to 12,921 kW. The oxygen demand inside the plant stayed almost constant even though an additional oxygen consumer in the PSA case scenario was created. This amount of oxygen is so small that it is offset by the reduced oxygen demand of the sulfuric acid unit versus the Claus unit. The increased oxygen compression power is caused by the shift in the production ratio of oxygen to nitrogen. If there is no need for high pressure nitrogen, it is more economical to produce the oxygen at ambient pressure. Later, this low pressure oxygen needs to be compressed to the gasifier inlet pressure at a much higher pressure ratio which drives up the power requirement of the oxygen compression. Nevertheless, this increase in compression power is small compared to the savings in air and nitrogen compression power. Translating this reduction of power to a per unit of captured carbon basis, the energy savings in the ASU are 263.53 $\frac{\text{kJ}}{\text{kg}_{\text{CO}_2}}$. This effect of the warm gas cleanup upon the ASU further boosts the energy savings of the CO_2-PSA technology. In addition, the significant amount of syngas humidification required in the Selexol^{TM} case leads to a large parasitic loss and is not needed in the warm gas cleanup case. With 216 kW the auxiliary load is low but its utilization of 56.2 MW_t of power in the form of heat, which reduces the steam generation, is significant. Further differences in the auxiliary loads of the sulfuric acid unit and the Claus unit can be identified. Both units operate near ambient pressure; the reason why the electricity is generated in the PSA case is that the Selexol^{TM} unit uses the pressure differential to recover the sulfur species from the solvent, whereas the RTI desulfurization unit recovers the sulfur at high pressure and uses the pressure differential

to generate electricity through expansion of the sulfur dioxide rich stream.

The power output of a gas turbine can be limited by its shaft work or by its air inlet flow. Shaft work limitation limits the power generation to an absolute maximum value which is determined by the turbine/generator shaft. Air inlet flow limitation means that the air mass flow that can be compressed by the gas turbine compressor limits the power output. Gas turbines operate at a constant suction volume. At lower temperatures and lower altitude, the air density is higher and more mass is compressed. Thus, it is more likely to be limited by the shaft work. At higher temperatures and or elevation, less air can be compressed. As a result, air inlet flow limitation is more likely. Both, the Selexol^{TM} and the PSA cases are limited by the compressor air flow, which determines the scale of the other plant equipment. With respect to the economic analysis, it is important to scale the plant with the gas turbine. Gas turbines are non-customized off-the-shelf items. Since they represent the largest single item cost of the plant, the rest of the plant is scaled to full load gas turbine operation.

The total gross power generation of the warm gas cleanup case is $584,936$ kW scaled to full load gas turbine operation with $401,657$ kW (68.7 %) generated by the gas turbine generator and $183,279$ kW (31.3 %) generated by the steam turbine generator. The gross electricity generation in the warm gas cleanup case is significantly less than that for the Selexol^{TM} case with a total gross power of $616,926$ kW ($424,753$ kW (68.8 %) by GT, $192,173$ kW (31.2 %) by ST). One reason for this is the increased efficiency of the warm gas cleanup scenario. Higher efficiency leads to a reduced coal mass flow. The coal mass flow of the warm gas cleanup scenario is reduced to $253,356$ $\frac{\text{kg}}{\text{h}}$, which is a reduction of 3.4 % compared to the Selexol^{TM} case. This reduction is directly proportional to the thermal input and leads to a reduction in the power output. However, comparing the Selexol^{TM} and warm gas cleanup cases on basis of constant coal feed rate a reduction in the total gross power output is observed, as well.

The power output of the warm gas cleanup scenario with a coal feed rate of $262,678$ $\frac{\text{kg}}{\text{hr}}$

is 606,458 kW, which is about 98.3 % of the Selexol^{TM} case. The reason for this is the higher water content of the syngas in the warm gas cleanup scenario. The syngas composition leaving the CO_2-PSA and the Selexol^{TM} unit are identical within a margin of $0.5\,\% - \text{points}$ on a dry basis. On a wet basis, the PSA case contains $49.9\,\text{mol} - \%$ of water, whereas the syngas leaving the Selexol^{TM} unit is essentially free of water. After humidification, the water content in the syngas in the Selexol^{TM} case rises to $21.7\,\text{mol} - \%$. The amount of required nitrogen diluent in the Selexol^{TM} case was established in [24]. For the warm gas cleanup scenario, the nitrogen diluent was adjusted to achieve the same level of NO_x emissions. Water has a higher specific heat capacity and is much more efficient in suppression NO_x formation than nitrogen on a mole per mole basis. This leads to the lower nitrogen requirement in the warm gas clean up scenario and ultimately results in a smaller GT fuel mass flow rate in the warm gas cleanup scenario. The major diluent in the cold gas clean up scenario is nitrogen ($45.0\,\text{mol} - \%$) with $11.9\,\text{mol} - \%$ water. In the warm gas cleanup scenario, the syngas injected into the gas turbine has a nitrogen content of $12.5\,\text{mol} - \%$ and a water content of $42.7\,\text{mol} - \%$. This also impacts the heating value of the syngas, which is $7,990\ \frac{\text{kJ}}{\text{kg}}$ in the Selexol case and $11,444\ \frac{\text{kJ}}{\text{kg}}$ in the warm gas cleanup case. The higher fuel mass flow required in the Selexol^{TM} case (including diluent) increases the mass flow through the turbine expander and subsequently the power output. Additionally, the higher water content in the syngas leads to a reduction of the turbine firing temperature of 23 °C in the CO_2-PSA case which is equivalent to a reduction of the gas turbine power output by 3.1 MW and the steam turbine power output by 3.9 MW on a constant coal flow basis just because of the reduced firing temperature.

Although the gross power generation in the warm gas cleanup scenario decreased, an increase in the net power generation can be observed. The net power generation of the Selexol^{TM} case is 451,634 kW. The warm gas cleanup scenario scaled to full turbine load reaches a net generation of 478,819 kW. The net power generated in the warm gas cleanup scenario at constant coal feed rate is 496,436 kW. This increase in the net power generation

is mainly due to the reduction of the auxiliary load from 165,292 kW to 106,118 kW (fully loaded GT)/110,022 kW (constant coal flow rate), due primarily to the reduction of compression work associated with the ASU and CO_2 compression as discussed above.

The water consumption in the warm gas cleanup scenario rose from 14.45 $\frac{m^3}{min}$ to 14.64 $\frac{m^3}{min}$ if scaled to full turbine load or 15.18 $\frac{m^3}{min}$ if compared on a constant coal feed rate basis. The following discussion is based on a constant feed flow rate. Although the majority of the power in an IGCC power plant is generated by the gas turbine, a significant amount of power is still generated in the Rankine cycle. Comparing the power output of the Rankine cycle of the two cases, it can be seen that the power output in the warm gas cleanup case was reduced by 2150 kW at a constant coal feed rate. This ultimately leads to a reduction of the steam condenser cooling load (from 264,685 kW_t to 247,417 kW_t) required by the Rankine cycle and a reduction in the water usage. However, this trend is not reflected in the total water consumption of the plant. The two main outlets for water are the cooling tower and the HRSG exhaust. The cooling tower duty was reduced from 338,316 kW_t to 262,562 kW_t, which is due to the reduced cooling load of the Rankine cycle, reduction of cooling load during gas compression in the ASU and CO_2 compression as well as elimination of syngas cooling before and within the Selexol^{TM} process. Evaporative water loss through the cooling tower was lowered from 7.0 $\frac{m^3}{min}$ to 5.4 $\frac{m^3}{min}$. Together with the evaporative losses in the cooling tower, the cooling tower blowdown is reduced by 0.5 $\frac{m^3}{min}$. However, the HRSG exhaust in the warm gas cleanup scenario exhibits a much higher water concentration than the cold gas cleanup case where the major diluent is nitrogen. The stack in the cold gas cleanup case emits liquid water equivalents of 5.4 m^3 per minute. The warm gas cleanup scenario emits a water equivalent of 8.2 m^3 of liquid water per minute. A detailed summary of all major streams containing water entering and leaving the plant is given in Table 4.10.

Comparison of the water usage within the plant on a constant coal flow rate is easier when comparing single items. However, comparison of the total water consumption should be done on a normalized basis with respect to the final product, electricity (net power).

Table 4.10: Water Usage of CO_2-PSA Warm Gas Cleanup Base Case at Constant Coal Flow Rate

	Unit	Cold Gas Cleanup	Warm Gas Cleanup
Coal Flow Rate	kg/h	262,678	262,678
Water Inlet			
Coal Moisture	m^3/min	1.132	1.132
Combustion Product	m^3/min	1.326	1.326
Raw Water Makeup	m^3/min	14.449	15.178
Air ASU	m^3/min	0.041	0.040
Air GT	m^3/min	0.193	0.200
Air H_2SO_4 Unit	m^3/min	0.000	0.001
Total	m^3/min	17.141	17.877
Water Outlet			
HRSG Stack	m^3/min	5.424	8.218
Steam Cycle Vent	m^3/min	0.203	0.114
Waste Water Blowdown	m^3/min	0.011	0.011
Demin Blowdown	m^3/min	1.968	2.071
Cooling Tower Makeup	m^3/min	9.360	7.249
Ash Handling	m^3/min	0.173	0.173
Product Stream H_2SO_4 Unit	m^3/min	0.000	0.026
H_2SO_4 Unit Stack	m^3/min	0.000	0.015
CO_2 Dryer Vent	m^3/min	0.004	0.005
ASU Dryer Vent	m^3/min	0.021	0.018
Total	m^3/min	17.164	17.900
Water Balance	Unit		
Balance Difference	%	0.133	0.128

The warm gas cleanup case consumes more water but also generates more electricity. These effects can be levelized by using the specific water consumption of the plant. The cold gas cleanup case has a specific water consumption rate per net generated power of 1.9197 $\frac{m^3_{water}}{MWh_{Net}}$. On a normalized basis, the warm gas cleanup scenario has a specific water consumption of 1.8345 $\frac{m^3_{water}}{MWh_{Net}}$ which is 4.44 % lower than the cold gas cleanup case.

A flow sheet of the warm gas cleanup scenario is provided in Figure 4.9. The corresponding stream summary for the fully loaded turbine case is shown in Table 4.11 and a stream summary of the case with constant coal feed rate is provided in the appendix Table A.1. A total plant performance summary comparing the warm gas cleanup case with fully loaded turbine and constant coal feed flow rate is given in Table 4.12.

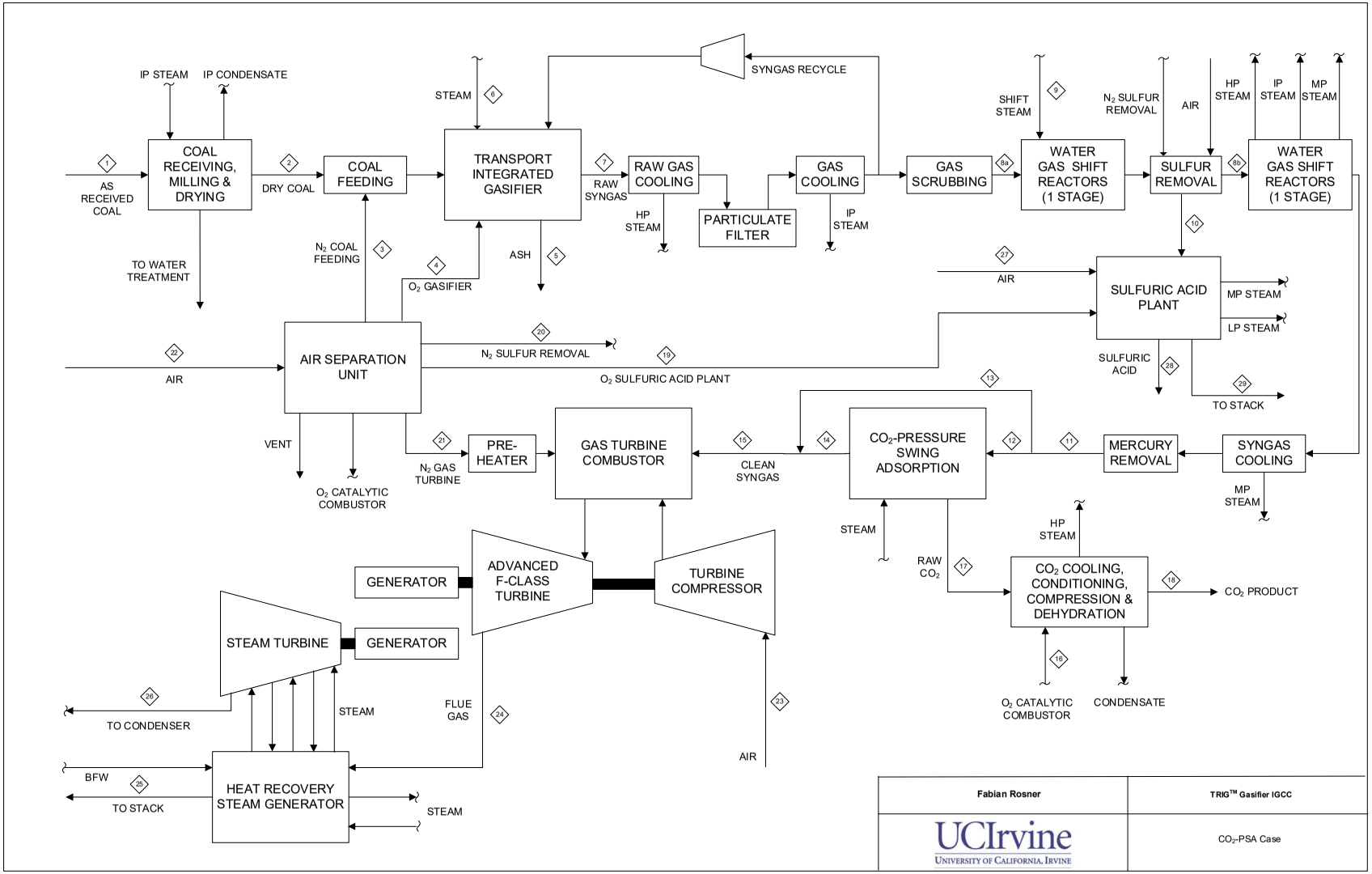

Figure 4.9: Flow sheet of the CO_2-PSA warm gas cleanup base case.

Table 4.11: Stream Summary of the CO_2-PSA Warm Gas Cleanup Base Case at Fully Loaded Gas Turbine

Stream Number	Unit	1	2	3	4	5	6	7	8a	8b	9	10	11	12	13	14
Temperature	°C	5.6	71.1	105.9	80.5	982.2	397.9	982.2	161.7	408.5	328.9	760.0	199.0	199.0	199.0	203.0
Pressure	bar	0.9	0.9	56.2	50.3	3.4	51.0	41.7	38.3	35.7	51.0	34.3	32.8	32.8	32.8	32.4
Mole Flowrate	kmol/h	-	-	1635	4093	-	3437	24532	19382	33621	14239	499	33604	31623	1981	23757
Mass Flowrate	kg/h	-	-	45870	131792	-	61924	526650	413457	669058	256524	16126	668756	629334	39422	265131
Solid Flowrate	kg/h	253356	229349	-	-	23281	-	-	-	-	-	-	-	-	-	-
Mass Vapor Fraction	-	0	0	1	1	0	1	1	1	1	1	1	1	1	1	1
Composition	mol-basis															
O_2	-	0.00000	0.00000	0.00540	0.95023	0.00000	0.00000	0.00000	0.00000	0.00000	0.00000	0.01093	0.00000	0.00000	0.00000	0.00000
N_2	-	0.00000	0.00000	0.99230	0.01647	0.00000	0.00000	0.00518	0.00497	0.00287	0.00000	0.86405	0.00287	0.00287	0.00287	0.00378
Ar	-	0.00000	0.00000	0.00230	0.03330	0.00000	0.00000	0.00732	0.00703	0.00405	0.00000	0.00858	0.00406	0.00406	0.00406	0.00535
H_2	-	0.00000	0.00000	0.00000	0.00000	0.00000	0.00000	0.27127	0.26064	0.31941	0.00000	0.00000	0.33764	0.33764	0.33764	0.44517
CO	-	0.00000	0.00000	0.00000	0.00000	0.00000	0.00000	0.34256	0.32914	0.02059	0.00000	0.00000	0.00253	0.00253	0.00253	0.00334
CO_2	-	0.00000	0.00000	0.00000	0.00000	0.00000	0.00000	0.16179	0.15545	0.25888	0.00000	0.00026	0.27708	0.27708	0.27708	0.00587
H_2O	-	0.00000	0.00000	0.00000	0.00000	0.00000	1.00000	0.15374	0.18694	0.36372	1.00000	0.00122	0.34585	0.34585	0.34585	0.49906
CH_4	-	0.00000	0.00000	0.00000	0.00000	0.00000	0.00000	0.05122	0.04921	0.02837	0.00000	0.00000	0.02839	0.02839	0.02839	0.03743
H_2S	-	0.00000	0.00000	0.00000	0.00000	0.00000	0.00000	0.00289	0.00277	trace	0.00000	0.00000	trace	trace	trace	trace
NH_3	-	0.00000	0.00000	0.00000	0.00000	0.00000	0.00000	0.00381	0.00365	0.00211	0.00000	0.00000	0.00158	0.00158	0.00158	0.00000
COS	-	0.00000	0.00000	0.00000	0.00000	0.00000	0.00000	0.00020	0.00019	trace	0.00000	0.00000	trace	trace	trace	trace
HCl	-	0.00000	0.00000	0.00000	0.00000	0.00000	0.00000	trace	0.00000	0.00000	0.00000	0.00000	0.00000	0.00000	0.00000	0.00000
SO_2	-	0.00000	0.00000	0.00000	0.00000	0.00000	0.00000	0.00000	0.00000	0.00000	0.00000	0.11497	0.00000	0.00000	0.00000	0.00000
Total	-	0	0	1	1	0	1	0.99997	1	1	1	1	1	1	1	1
Stream Number	Unit	15	16	17	18	19	20	21	22	23	24	25	26	27	28	29
Temperature	°C	202.6	145.3	187.3	35.0	32.2	69.0	105.9	5.6	5.6	562.6	151.9	32.4	5.6	20.0	43.3
Pressure	bar	32.4	20.5	9.7	152.7	8.6	41.2	26.2	0.9	0.9	0.9	0.9	0.05	0.9	0.9	0.9
Mole Flowrate	kmol/h	25738	72	14829	8638	35	93	4675	19876	100248	123927	123927	21362	273	82	755
Mass Flowrate	kg/h	304553	2316	489639	380094	1120	2599	131186	574296	2896627	3302357	3302357	384833	7891	6069	20896
Solid Flowrate	kg/h	-	-	-	-	-	-	-	-	-	-	-	-	-	-	-
Mass Vapor Fraction	-	1	1	1	1	1	1	1	1	1	1	1	0.91096	1	0	1
Composition	mol-basis															
O_2	-	0.00000	0.95001	0.00000	trace	0.95001	0.00540	0.00540	0.20810	0.20810	0.10753	0.10753	0.00000	0.20810	0.00000	0.04020
N_2	-	0.00371	0.01406	trace	0.00022	0.01406	0.99230	0.99230	0.77590	0.77590	0.65729	0.65729	0.00000	0.77590	0.00000	0.88466
Ar	-	0.00525	0.03594	trace	0.00044	0.03594	0.00230	0.00230	0.00930	0.00930	0.00868	0.00868	0.00000	0.00930	0.00000	0.01069
H_2	-	0.43689	0.00000	0.00685	trace	0.00000	0.00000	0.00000	0.00000	0.00000	0.00000	0.00000	0.00000	0.00000	0.00000	0.00000
CO	-	0.00328	0.00000	trace	trace	0.00000	0.00000	0.00000	0.00000	0.00000	0.00000	0.00000	0.00000	0.00000	0.00000	0.00000
CO_2	-	0.02675	0.00000	0.58148	0.99934	0.00000	0.00000	0.00000	0.00030	0.00030	0.01411	0.01411	0.00000	0.00030	0.00000	0.00033
H_2O	-	0.48727	0.00000	0.40754	0.00000	0.00000	0.00000	0.00000	0.00640	0.00640	0.21237	0.21237	1.00000	0.00640	0.30349	0.06397
CH_4	-	0.03673	0.00000	0.00058	trace	0.00000	0.00000	0.00000	0.00000	0.00000	0.00000	0.00000	0.00000	0.00000	0.00000	0.00000
H_2S	-	trace	0.00000	trace	trace	0.00000	0.00000	0.00000	0.00000	0.00000	0.00000	0.00000	0.00000	0.00000	0.00000	0.00000
NH_3	-	0.00012	0.00000	0.00337	0.00000	0.00000	0.00000	0.00000	0.00000	0.00000	trace	trace	0.00000	0.00000	0.00000	0.00000
COS	-	trace	0.00000	trace	0.00000	0.00000	0.00000	0.00000	0.00000	0.00000	0.00000	0.00000	0.00000	0.00000	0.00000	0.00000
HCl	-	0.00000	0.00000	0.00000	0.00000	0.00000	0.00000	0.00000	0.00000	0.00000	0.00000	0.00000	0.00000	0.00000	0.00000	0.00000
SO_2	-	0.00000	0.00000	0.00000	trace	0.00000	0.00000	0.00000	0.00000	0.00000	trace	trace	0.00000	0.00000	0.00000	0.00015
Total	-	1	1	0.99981	0.99999	1	1	1	1	1	0.99997	0.99997	1	1	0.30349	1

Table 4.12: Performance Summary of the of the CO_2-PSA Warm Gas Cleanup Base Case

Gross Power Generation	Unit	GT Air Flow Limited	Constant Coal Flow
Gas Turbine	kW	401,657	416,436
Steam Turbine	kW	183,279	190,023
Total	kW	584,936	606,458
Auxiliary Load	Unit		
Coal Handling	kW	493	511
Coal Milling	kW	706	731
Coal Dryer Circulation Blower	kW	2,474	2,565
Ash Handling & Dewatering	kW	609	631
Air Separation Unit Auxiliaries	kW	339	352
Air Separation Unit Main Compressor	kW	36,595	37,942
Oxygen Compressor	kW	12,921	13,396
Nitrogen Compressor	kW	10,500	10,886
Syngas Recycle Compressor	kW	1,498	1,553
Carbon Dioxide Purification & Compressor	kW	21,586	22,381
Boiler Feed Water & Demin. Pumps	kW	5,387	5,585
Vacuum Condensate Pump	kW	342	355
Process Condensate & SWS System	kW	80	83
BFW Circulation Pumps	kW	88	92
Cooling Water Circulation Pumps	kW	2,116	2,194
Cooling Tower Fans	kW	1,163	1,206
Air Cooled Condenser Fans	kW	1,841	1,909
Scrubber Pumps	kW	590	611
Desulfurization Unit	kW	1,679	1,741
Gas Turbine Auxiliaries	kW	942	977
Steam Turbine Auxiliaries	kW	94	97
Sulfuric Acid Plant	kW	(1,207)	(1,251)
Miscellaneous Balance of Plant	kW	2,899	3,006
Transformer Losses	kW	2,382	2,470
Total	kW	106,118	110,022
Net Power Generation	Unit		
Net Power Output	kW	478,819	496,436
Plant Performance	Unit		
Net Efficiency	%-HHV	34.20	34.20
Net Heat Rate	kJ/kWh	10525.0	10527.6
Consumables	Unit		
As-Received Coal	kg/h	253,356	262,678
Thermal Input	kW-HHV	1,399,878	1,451,385
Raw Water Usage	m^3/min	14.64	15.18
Carbon Capture	Unit		
Carbon Recovery	%	83.40	83.40

4.4 Optimization of the Water-Gas-Shift Section

In the optimization of carbon capture and thus, plant efficiency, the water-gas-shift reaction plays a key role. The water-gas-shift reaction, as describes in Equation 4.14, is mildly exothermic at standard conditions and favors the formation of carbon dioxide at lower temperatures. However, kinetics are proceeding faster at higher temperatures and reactant partial pressures but increasing shift steam injection into the syngas lowers the output of the steam turbine and can lead to an overall decrease in the plant efficiency. Another major concern is the formation of solid carbon inside the shift reactor. Solid carbon formation can lead to deactivation of the catalyst or even clogging of the catalyst bed in the worst case. In order to optimize the water-gas-shift section and ensure its safe operation, two tools have been developed: an equilibrium code for carbon formation and a chemical kinetic model of the shift reactor.

4.4.1 Whisker Carbon Equilibrium

Predicting whether a gas mixture will form solid carbon under certain conditions of temperature, pressure and chemical composition is not an exact science and requires experimental validation. However, taking thermodynamic equilibrium into consideration, it is possible to identify safe regions where the formation of solid carbon is impossible.

From a thermodynamic equilibrium stand point, carbon monoxide decomposes to solid carbon if the temperature is too low. Methane on the other hand cracks if the temperature is too high. Based on this information, it is impossible to predict whether the gas mixture is stable, unless it is in equilibrium with other components of the gas phase. Major components in syngas are methane, carbon monoxide, carbon dioxide, hydrogen and water. For simplicity, these compounds will be the only compounds considered for determining the

equilibrium. Based upon these compounds there are three heterogeneous reactions involving solid carbon.

$$\mathrm{CH_4} \rightleftharpoons 2\,\mathrm{H_2} + \mathrm{C} \tag{4.31}$$

$$\mathrm{CO_2} + \mathrm{C} \rightleftharpoons 2\,\mathrm{CO} \tag{4.32}$$

$$\mathrm{H_2O} + \mathrm{C} \rightleftharpoons \mathrm{CO} + \mathrm{H_2} \tag{4.33}$$

The reaction 4.31 is known as reverse hydrogasification. Equation 4.32 is the Boudouard reaction and reaction 4.33 is the water gas reaction. The respective equilibrium constants can be formulated as follows:

$$K_1 = \frac{p_{\mathrm{H_2}}^2}{p_{\mathrm{CH_4}}} \tag{4.34}$$

$$K_2 = \frac{p_{\mathrm{CO}}^2}{p_{\mathrm{CO_2}}} \tag{4.35}$$

$$K_3 = \frac{p_{\mathrm{H_2}} p_{\mathrm{CO}}}{p_{\mathrm{H_2O}}} \tag{4.36}$$

The partial pressures are expressed in atmospheres and the activity of solids is unity. Gas phase reactions and equilibria can be obtained by various combinations of the above stated reaction equations and equilibrium constants. The water-gas-shift reaction for example can be expressed as a combination of reaction 4.32 and 4.33. Expressions for the equilibrium constants for graphite are given in [76],

$$K_1 = e^{15.6525 - \frac{19069.9}{T}} \tag{4.37}$$

$$K_2 = e^{23.8898 - \frac{37243.6}{T}} \tag{4.38}$$

$$K_3 = e^{19.8794 - \frac{29286.6}{T}} \tag{4.39}$$

where the equilibrium constants K are in psia and the temperature T is in Rankine. In order to account for the possibility of formation of amorphous carbon, the following modifications are used [76]:

$$K_1' = K_1/a_1 \tag{4.40}$$

$$K_2' = K_2 \cdot a_2 \tag{4.41}$$

$$K_3' = K_3 \cdot a_3 \tag{4.42}$$

where,

$$a_1 = 1.0 + e^{\frac{400.3 - T}{78.2}} \tag{4.43}$$

$$a_2 = 1.0 + e^{\frac{570.3 - T}{117}} \tag{4.44}$$

$$a_3 = \sqrt{a_1 \cdot a_2} \tag{4.45}$$

the temperature T is in Rankine and a is dimensionless. For determining the equilibrium curve for a certain temperature consider a binary sub-system, the ratio involving the partial pressures according to the equilibrium constant (Equations 4.34-4.36) can be determined by the equilibrium constant (Equations 4.37-4.45). Since the equilibrium curve is the point where carbon deposition is just about to occur, the following equation can be formulated:

$$p_{H_2} + p_{CH_4} = p_{HC} \tag{4.46}$$

p_{HC} is the binary hydrogen and carbon which requires an initial guess. Combining Equations 4.46 and 4.34 results in a quadratic equation. The solution of the positive root (negative root has no physical meaning) is of the form:

$$p_{H_2} = -\frac{K_1}{2} + \sqrt{\frac{K_1^2}{4} + K_1 p_{HC}} \tag{4.47}$$

p_{CH_4} is then calculated from the difference using the result from 4.47 and the initial guess from p_{HC}. The same approach is taken for the binary oxygen-carbon. The results of both binaries are used to determine the partial pressure of water using the equilibrium constant K_3. After all partial pressures are obtained from the initial guess, the system pressure is normalized to the real pressure and iterated until the error is small enough. This method is used for several points until enough points are obtained to draw an equilibrium line. Details on the algorithm and iteration scheme can be found in [76]. The results can be displayed in a ternary diagram as seen in Figure 4.10.

The area above the equilibrium is the unstable gas region where carbon deposition can occur. Below the equilibrium line, the gas mixture is thermodynamically stable and carbon deposition is impossible. For the operation of water-gas-shift reactors, as well as reformers, this area constitutes safe reaction conditions. For the water-gas-shift reactors and reformers in this work, the solid carbon equilibrium criterion will be used for determining the steam requirement. Thereby, it is important to maintain a small safety margin and not operate the reactors exactly on the equilibrium curve.

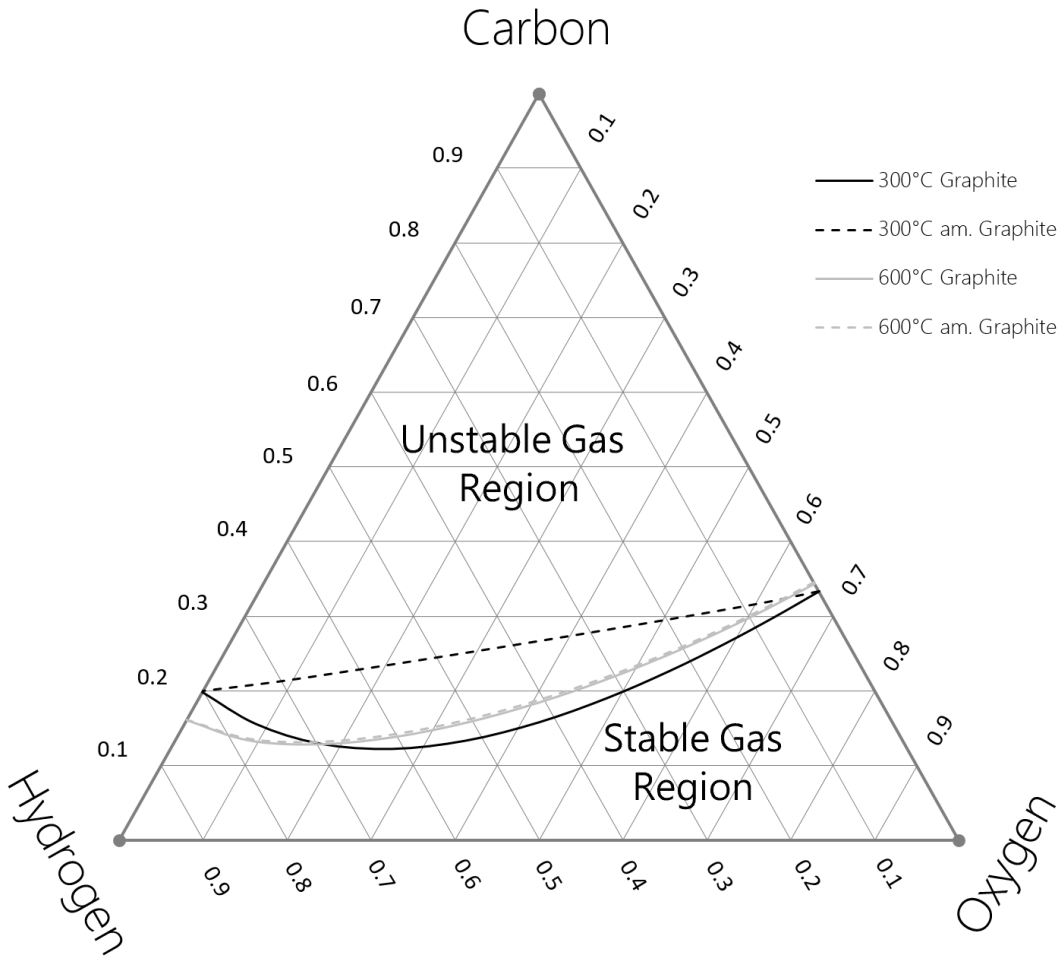

Figure 4.10: Ternary equilibrium curves for whisker carbon formation at 300 °C and 600 °C.

4.4.2 Shift Reactor Model

A chemical kinetic shift reactor model has been developed in order to determine reactor size and pressure drop of the catalyst bed. Low temperatures slow down the reaction kinetics and lead to a significant increase of catalyst material and consequently to a higher pressure drop. With carbon capture approaching 90 %, almost all the CO has to be shifted to CO_2. Thermodynamic equilibrium favors CO_2 at low temperatures which makes it important to evaluate the catalyst volume and pressure drop across the catalyst bed.

Assumptions for the shift reactor model are:

I) Peng-Robinson Equation of State

II) Shift Reaction is the only Reaction to Occur

III) Equal Catalyst Distribution

IV) Plug Flow through Reactor and Catalyst Bed

V) Isothermal Catalyst Pellets

Real gas behavior is approximated with the Peng-Robinson equation of state which is well suited for hydrocarbon gas systems and petrochemical applications. The shift reaction is the only reaction considered in this analysis since COS and HCN are only present in trace amounts. Since the catalyst pellet dimension is small versus the rector dimension it can be assumed that the catalyst is equally distributed inside the reactor. Industrial scale shift reactors have large diameters and high flow velocity which can be approximated by plug flow conditions. The catalyst pellet is assumed to be isothermal since the pellets are small. The validity of assumption s IV and V will be further discussed at the end of this section.

The model is a finite volume model which requires molar flow, temperature and pressure

as input, as well as the reactor dimensions. Gas properties are obtained from ASPEN Properties® using the Peng-Robinson equation of state. The volumetric flow rate $\dot{V}$ for every volume element q is calculated by

$$\dot{V}_q = \frac{\overline{M}_q \sum_0^i \dot{n}_q}{\rho_q} \tag{4.48}$$

where $\overline{M}$ is the average molecular weight of the gas mixture, $\dot{n}$ is the molar flow rate and ρ the gas density of the mixture. The gas velocity v and superficial gas velocity u are determined by

$$v_q = \frac{\dot{V}_q}{(\frac{D}{2})^2 \cdot \pi \varepsilon_{\text{bed}}} \tag{4.49}$$

and

$$u_q = \frac{\dot{V}_q}{(\frac{D}{2})^2 \cdot \pi} \tag{4.50}$$

with D the inner reactor diameter, π the circle constant and ε_{bed} the catalyst bed void fraction. The calculation of the pressure drop is accomplished by applying the Ergun equation.

$$\Delta p_q = \frac{150\mu_q(1-\varepsilon_{\text{bed}})^2 u_q}{\varepsilon_{\text{bed}}^3 d_{\text{p}}^2}\Delta x + \frac{1.75(1-\varepsilon_{\text{bed}})\rho_q u_q^2}{\varepsilon_{\text{bed}}^3 d_{\text{p}}}\Delta x \tag{4.51}$$

where μ is the dynamic viscosity, Δx the height of the reactor volume element and d_{p} is

the catalyst pellet's diameter. For a cylindrical catalyst pellet, the diameter is approximated with the equivalent diameter

$$d_{\mathrm{p}} = \sqrt[3]{\frac{3}{4} R_{\mathrm{pellet}}^2 \cdot L} \tag{4.52}$$

R_{pellet} is the pellet radius and L is the length of the cylindrical pellet. The pressure of the following volume element is given by

$$p_{q+1} = p_q + \Delta p_q \tag{4.53}$$

An additional pressure drop is associated with the inlet and outlet of the reactor. The pressure drop at the reactor inlet $\Delta p_{\mathrm{inlet}}$ is approximated as sudden expansion. Equation 4.54 approximates the pressure drop of the inlet within an error margin of 5 % for turbulent flow and 33 % for laminar flow [77]. The gas velocity in pipes is typically around $5 - 46\ \frac{\mathrm{m}}{\mathrm{s}}$ [9] and thus almost always turbulent.

$$\Delta p_{\mathrm{inlet}} = \left(1 - \frac{C_{\mathrm{pipe}}}{C_{\mathrm{reactor}}}\right)^2 \frac{\rho}{2} u_{\mathrm{pipe}}^2 \tag{4.54}$$

C_{pipe} is the cross-sectional area of the pipe which is determined by the volume flow and the gas velocity. C_{reactor} is the cross sectional area of the reactor, ρ the density of the gas mixture and u_{pipe} the gas velocity in the pipe. The gas velocity, u_{pipe}, is limited to $46\ \frac{\mathrm{m}}{\mathrm{s}}$ in industrial applications to avoid noise, vibrations and damaging wear and tears of pipes and fittings [9]. The outlet pressure drop is approximated with a sudden contraction and is calculated by the following equation [77].

$$\Delta p_{\text{outlet}} = \zeta \frac{\rho}{2} u_{\text{pipe}}^2 \tag{4.55}$$

ζ is the friction coefficient and is estimated with 0.5 in this study [77]. The total pressure drop composes of the inlet pressure drop, pressure drop across the catalyst bed and the outlet pressure drop.

In case of an adiabatic reactor, the reaction kinetics have to be known to determine the temperature increase, due to the exothermic character of the water-gas-shift reaction. The difference in enthalpy of formation between reactants and products leads to an increase of sensible heat in the stream. Kinetic rate expressions are often given in the form of power laws. The generalized power law for the water-gas-shift reaction can be described as follows

$$r = k_0 \, e^{\frac{-E_{\text{A}}}{R_{\text{g}} T}} \, p_{\text{CO}}^m \, p_{\text{H}_2\text{O}}^n \, p_{\text{CO}_2}^o \, p_{\text{H}_2}^p \cdot \left(1 - \frac{1}{K} \cdot \frac{p_{\text{CO}_2} \, p_{\text{H}_2}}{p_{\text{CO}} \, p_{\text{H}_2\text{O}}}\right) \tag{4.56}$$

k_0 is the reaction constant, E_{A} the activation energy, R_{g} the universal gas constant, T the temperature, p_j the partial pressure of component j. The exponents m, n, o and p are constants and K is the equilibrium constant of the water-gas-shift reaction. According to Moe [78], the equilibrium constant can be calculated using the following equation, which is fairly accurate in the range from $200 - 550$ °C.

$$K = e^{\left(\frac{4577.8}{T + T_{\text{m}}} - 4.33\right)} \tag{4.57}$$

The temperature in this equation is in Kelvin. The equilibrium is only considered to be a function of temperature. The influence of pressure on the equilibrium constant due to

non-ideality is typically very small and is irrelevant over pressure ranges less than several hundreds of bars. The relation developed by Moe has been modified by the term T_{m} which accounts for the temperature approach for middle of run condition which makes K a pseudo "equilibrium" constant.

The rate equation has two temperature dependent driving factors. A thermal potential factor $F = e^{\frac{-E_{\mathrm{A}}}{R_{\mathrm{g}}\,T}}$ which depends on temperature in a Arrhenius fashion and a chemical potential factor $G = \left(1 - \frac{1}{K} \cdot \frac{p_{\mathrm{CO_2}}\,p_{\mathrm{H_2}}}{p_{\mathrm{CO}}\,p_{\mathrm{H_2O}}}\right)$ which is related to temperature in an exponential manner. In order to optimize the reaction temperature with respect to its two driving forces a new dimensionless quantity Ro for rate optimization can be defined.

$$\mathrm{Ro} = \frac{\frac{F'(T)}{F(T)}}{\frac{G'(T)}{G(T)}} = \frac{\frac{E_{\mathrm{A}}\,e^{\frac{-E_{\mathrm{A}}}{R_{\mathrm{g}}\,T}}}{R_{\mathrm{g}}\,T^2}}{-\frac{347{,}657.8\,e^{\frac{4577.8}{T+T_{\mathrm{m}}}}}{(T+T_{\mathrm{m}})^2}\,\frac{p_{\mathrm{CO_2}}\,p_{\mathrm{H_2}}}{p_{\mathrm{CO}}\,p_{\mathrm{H_2O}}}} \tag{4.58}$$

where $F'(T)$ is the derivative of F with respect to T and $G'(T)$ is the derivative of G with respect to T.

The interpretation of Ro is

Ro > 1 F and G drive the reaction in the same direction, impact of T on F is stronger than on G and an increase in T accelerates the reaction rate

Ro $= 1$ F and G drive the reaction in the same direction, impact of T on F is equal to G and an increase in T accelerates the reaction rate

$1 >$ Ro > 0 F and G drive the reaction in the same direction, impact of T on F is weaker than on G and an increase in T accelerates the reaction rate

$0 > \text{Ro} > -1$ F and G drive the reaction in the opposite direction, impact of T on F is weaker than on G and an increase in T decelerates the reaction rate

$\text{Ro} = -1$ F and G drive the reaction in the opposite direction, impact of T on F is equal to G, the reaction rate is at its optimum.

$\text{Ro} < -1$ F and G drive the reaction in the opposite direction, impact of T on F is stronger than on G and an increase in T accelerates the reaction rate

Typically, kinetic rate expressions are determined under conditions without external and/or internal transport limitations, also known as intrinsic rate. This is achieved by grinding the catalyst pellet into small particles in order to expose the internal surface area entirely to the gas flow. Intrinsic rate equations have the advantage that they can be applied to many different types of problems. On the other hand, when designing a reactor, diffusion inside the catalyst pellet needs to be considered.

Considering one-dimensional mass transfer inside the catalyst, e.g., a slab or inner region of a flat cylinder, the mass balance is governed by species diffusion and chemical reaction as illustrated in Figure 4.11.

where $\dot{n}_{\text{CO}}$ is the flux of carbon monoxide at the top and the bottom of the volume element and r^{v}_{CO} is the volumetric reaction rate. In order to balance the species

$$\text{Rate of Input CO} - \text{Rate of Output CO} - \text{Rate of Consumption CO} = 0 \tag{4.59}$$

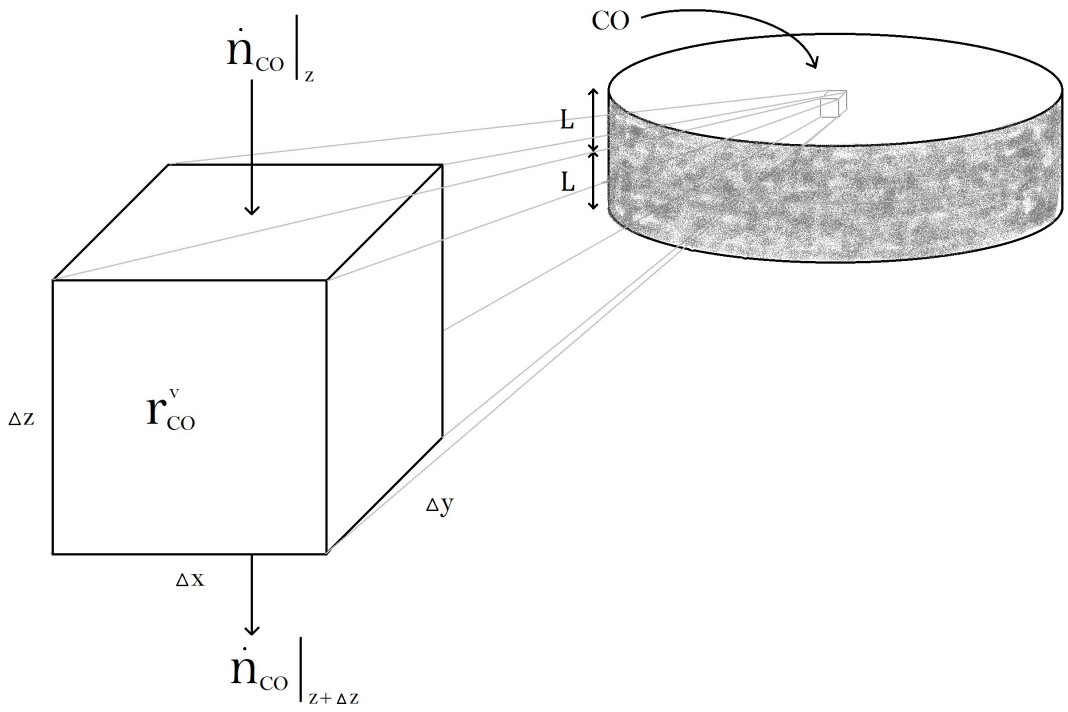

Figure 4.11: Finite volume element of a catalyst pellet.

$$\Delta x \Delta y \, \dot{n}_{\mathrm{CO}}|_z - \Delta x \Delta y \, \dot{n}_{\mathrm{CO}}|_{z+\Delta z} - r^{\mathrm{g}}_{\mathrm{CO}} \rho_{\mathrm{pellet}} \Delta x \Delta y \Delta z = 0 \tag{4.60}$$

$r^{\mathrm{g}}_{\mathrm{CO}}$ is the gravimetric reaction rate which is more commonly found in literate than the volumetric reaction rate and ρ_{pellet} is the density of the catalyst pellet. Applying Fick's Law 4.61 and the Taylor expansion 4.62

$$\dot{n}_{\mathrm{CO}} = -D_{\mathrm{eff}} \frac{\mathrm{d}c_{\mathrm{CO}}}{\mathrm{d}z} \tag{4.61}$$

$$\dot{n}_{\mathrm{CO}}|_{z+\Delta z} = \dot{n}_{\mathrm{CO}}|_z + \frac{\mathrm{d}\dot{n}_{\mathrm{CO}}}{\mathrm{d}z} \Delta z \tag{4.62}$$

to Equation 4.60, results in Equation 4.63

$$-\frac{\mathrm{d}}{\mathrm{d}z}\left(-D_{\mathrm{eff}}\frac{\mathrm{d}c_{CO}}{\mathrm{d}z}\right)-r^{\mathrm{g}}_{\mathrm{CO}}\,\rho_{\mathrm{pellet}}=0 \tag{4.63}$$

c_{CO} is the carbon monoxide concentration and D_{eff} is the effective diffusivity in the catalyst pellet and is the only transport mechanism inside the pellet. Realizing that the effective diffusivity is independent from the z-direction, the equation can be simplified and the differential equation of the catalyst pellet is given by

$$D_{\mathrm{eff}}\frac{\mathrm{d}^2c_{\mathrm{CO}}}{\mathrm{d}z^2}-r^{\mathrm{g}}_{\mathrm{CO}}\,\rho_{\mathrm{pellet}}=0 \tag{4.64}$$

The boundary conditions are:

$$c_{\mathrm{CO}}|_{z=L}=c_{\mathrm{CO_{surface}}} \tag{4.65}$$

$$\left.\frac{\mathrm{d}c_{\mathrm{CO}}}{\mathrm{d}z}\right|_{z=0}=0 \tag{4.66}$$

The concentration at distance L (characteristic length) is the surface concentration. Due to axis symmetry the change of concentration in the middle of the slab or flat cylinder (z=0) is zero.

If the pore size of the catalyst pellet is very small, molecules will increasingly interact with the walls. If diffusion is governed by wall interaction and not by molecule-molecule interaction, a regime of pure Knudsen diffusion is reached. In the transition between bulk diffusion and Knudsen diffusion both mechanisms have to be considered. The effective diffusivity is determined by [79]

$$D_{\text{eff}} = \min \left\{ \frac{\varepsilon_{\text{pellet}}}{\tau_{\text{pellet}}} \left(\frac{1}{D_{i,\text{Mix}}} + \frac{1}{D_{\text{K},i}} \right)^{-1} \right\}_{i=\text{CO, CO}_2\text{, H}_2\text{O, H}_2} \tag{4.67}$$

$\varepsilon_{\text{pellet}}$ is the porosity of the catalyst pellet, τ_{pellet} is the tortuosity of the catalyst pellet, $D_{i,\text{Mix}}$ is the diffusivity of component i in the gas mixture and $D_{\text{K},i}$ is the Knudsen diffusivity of component i. D_{eff} is evaluated for all in the reaction participating components i, in every volume element of the reactor and the slowest diffusivity is used in the calculation as it constitutes the rate limiting step. In the case of diffusion limitation of a reactant; the supply of reactants limits the reaction rate. In the case of product diffusion limitation; the removal of product species limits the reaction as under steady state condition the reactant cannot be supplied at a higher rate as the products are removed. Knudsen diffusion can be calculated by [80]

$$D_{\text{K},i} = \frac{d_{\text{pore}}}{3} \sqrt{\frac{8 R_{\text{g}} T}{\pi M_i}} \tag{4.68}$$

d_{pore} is the pore diameter of the catalyst pellet, R_{g} the universal gas constant and M_i is the molecular weight of component i.

The Knudsen number is a good measure to estimate the importance of Knudsen diffusion.

$$\text{Kn} = \frac{k_{\text{B}}\, T}{\sqrt{2}\, \pi\, d_{\text{k}}^2\, p\, d_{\text{pore}}} \tag{4.69}$$

k_{B} is the Boltzmann constant, d_{k} the kinetic diameter of the molecule and d_{pore} is the pore diameter. If the Knudsen number is much greater than unity, laws of kinetic gas theory

apply. For Kn, values much smaller than unity continuum theories can be applied. In this work Knudsen diffusion is considered for conditions of Kn > 0.01.

The diffusivity of a particular component i in a gas mixture can be estimated by [81]

$$D_{i,\mathrm{Mix}} = \frac{1 - y_i}{\sum_{j,j\neq i} \frac{y_j}{D_{i,j}}} \tag{4.70}$$

where y is the mole fraction of component i or j and $D_{i,j}$ the binary diffusivity of components i and j. Binary diffusivity, in $\frac{\mathrm{cm}^2}{\mathrm{s}}$ is estimated using the Fuller equation [82].

$$D_{i,j} = \frac{0.00143\, T^{1.75}}{p\, \overline{M}_{i,j}^{\frac{1}{2}} \left[\left(\sum\nolimits_{\mathrm{v}}\right)_i^{\frac{1}{3}} + \left(\sum\nolimits_{\mathrm{v}}\right)_j^{\frac{1}{3}} \right]^2} \tag{4.71}$$

The temperature T is in Kelvin and the pressure p is in bar. The average molecular weight is in $\frac{\mathrm{g}}{\mathrm{mol}}$ and is calculated as follows:

$$\overline{M}_{i,j} = 2 \left[\left(\frac{1}{M_i} \right) + \left(\frac{1}{M_j} \right) \right]^{-1} \tag{4.72}$$

The diffusion volumes $\left(\sum\nolimits_{\mathrm{v}}\right)_i$ are given in Table 4.13.

Table 4.13: Diffusion Volumes of the Fuller Equation [82]

Component	Diffusion Volume
Carbon monoxide	18.0
Carbon dioxide	26.9
Water	13.1
Hydrogen	6.1

Inserting Equation 4.56 into 4.64 and converting the partial pressure into concentrations using the ideal gas law the following equation is obtained.

$$D_{\text{eff}} \frac{\mathrm{d}^2 c_{\text{CO}}}{\mathrm{d}z^2} - k_0 \, e^{\frac{-E_{\text{A}}}{R_{\text{g}} T}} \, R_{\text{g}}^{(m+n+o+p)} \, T^{(m+n+o+p)} \, c_{\text{CO}}^{m} \, c_{\text{H}_2\text{O}}^{n} \, c_{\text{CO}_2}^{o} \, c_{\text{H}_2}^{p} \left(1 - \frac{1}{K} \cdot \frac{c_{\text{CO}_2} \, c_{\text{H}_2}}{c_{\text{CO}} \, c_{\text{H}_2\text{O}}} \right) \rho_{\text{pellet}} = 0 \tag{4.73}$$

Under isothermal, isobaric conditions, the concentration of carbon containing species involved in the water-gas-shift reaction remains constant, as well as the concentration of hydrogen containing species. Furthermore, the concentration difference between carbon monoxide and water remains constant due to equimolar product consumption.

$$c_{\text{C}} = c_{\text{CO}} + c_{\text{CO}_2} \tag{4.74}$$

$$c_{\text{H}} = c_{\text{H}_2\text{O}} + c_{\text{H}_2} \tag{4.75}$$

$$c_{\text{D}} = c_{\text{CO}} - c_{\text{H}_2\text{O}} \tag{4.76}$$

Thus, the differential equation can be expressed as function of the carbon monoxide concentration only.

$$\begin{aligned} &D_{\text{eff}} \frac{\mathrm{d}^2 c_{\text{CO}}}{\mathrm{d}z^2} - k_0 \, e^{\frac{-E_{\text{A}}}{R_{\text{g}} T}} \, R_{\text{g}}^{(m+n+o+p)} \, T^{(m+n+o+p)} \, c_{\text{CO}}^{m} \, (c_{\text{CO}} - c_{\text{D}})^{n} \, (c_{\text{C}} - c_{\text{CO}})^{o} \\ &(c_{\text{H}} - (c_{\text{CO}} - c_{\text{D}}))^{p} \left(1 - \frac{1}{K} \cdot \frac{(c_{\text{C}} - c_{\text{CO}}) \, (c_{\text{H}} - (c_{\text{CO}} - c_{\text{D}}))}{c_{\text{CO}} \, (c_{\text{CO}} - c_{\text{D}})} \right) \rho_{\text{pellet}} = 0 \end{aligned} \tag{4.77}$$

In order to simplify the integration of the differential equation, a part of the expression of the reaction rate can be regressed over the range of the bulk concentration of each of

the individual cells in the reactor domain and expressed in the form of an exponential relation. This relation can be represented by the factor a and the exponent b. The regression is necessary for every single volume element of the reactor model since the reaction rate is not only dependent on the carbon monoxide concentration but also on parameters like temperature and pressure. Thus, a matrix of differential equations of the from

$$D_{\text{eff}}\frac{\mathrm{d}^2 c_{\text{CO}}}{\mathrm{d}z^2} - k_0\, e^{\frac{-E_{\text{A}}}{R_{\text{g}}\,T}}\, a c_{\text{CO}}^{b}\, \rho_{\text{pellet}} = D_{\text{eff}}\frac{\mathrm{d}^2 c_{\text{CO}}}{\mathrm{d}z^2} - k\, c_{\text{CO}}^{b}\, \rho_{\text{pellet}} = 0 \tag{4.78}$$

is obtained. Non-dimensionalization of the equation above with $c^* = c_{\text{CO}}/c_{\text{CO}_{\text{surface}}}$ and $z^* = z/L$ leads to,

$$\frac{\mathrm{d}^2 c^*}{\mathrm{d}z^{*2}} - \frac{k\, c_{\text{CO}_{\text{surface}}}^{b-1}\, \rho_{\text{pellet}}\, L^2}{D_{\text{eff}}}\, c^{*b} = 0 \tag{4.79}$$

After transformation of the boundary conditions the following new boundary conditions are obtained,

$$c^*|_{z^*=1} = 1 \tag{4.80}$$

$$\left.\frac{\mathrm{d}c^*}{\mathrm{d}z^*}\right|_{z^*=0} = 0 \tag{4.81}$$

The dimensionless quantity in Equation 4.79 is commonly known as Thiele Modulus and will be referred to as Φ_{b}.

$$\Phi_{\mathrm{b}}^2 = \frac{k\, c_{\mathrm{CO_{surface}}}^{b-1}\, \rho_{\mathrm{pellet}}\, L^2}{D_{\mathrm{eff}}} \tag{4.82}$$

The Thiele Modulus is a measure of the ratio between surface reaction rate and diffusion rate inside the catalyst pellet. If the Thiele Modulus is large, internal diffusion is usually limiting the reaction. If the Thiele Modulus is small, the reaction kinetics are usually the rate limiting factor. By using the generalized Thiele Modulus for irreversible reactions (no rate constant for reversible reaction included in the kinetic expression) of the form

$$\Phi_{\mathrm{g}}^2 = \frac{V^2}{S^2}\frac{b+1}{2}\frac{k\, c_{\mathrm{CO_{surface}}}^{b-1}\, \rho_{\mathrm{pellet}}}{D_{\mathrm{eff}}} \tag{4.83}$$

the value of $1/\Phi_{\mathrm{g}}$ for large Thiele Moduli coincides for different reaction orders and all reaction orders can be approximates with the analytical results for first order reaction kinetics [83] (note: the Thiele Modulus keeps the real reaction order). V is the volume of the catalyst pellet and S is the surface area of the catalyst pellet.

The first order differential equation is then:

$$\frac{\mathrm{d}^2 c^*}{\mathrm{d}z^{*2}} - \Phi_{\mathrm{g}}^2\, c^* = 0 \tag{4.84}$$

The solution for this differential equation with the boundary conditions 4.80 and 4.81 is [79]:

$$c_{\mathrm{CO}} = c_{\mathrm{CO_{surface}}} \frac{\cosh\left[\Phi_{\mathrm{g}}\left(1 - \frac{z}{L}\right]\right)}{\cosh\left[\Phi_{\mathrm{g}}\right]} \tag{4.85}$$

In order to get the real reaction rate of the catalyst pellet with internal diffusion limitation, the reaction rate needs to be integrated over the catalyst volume. Since the carbon monoxide concentration changes from the surface of the pellet to the center of the pellet, the reaction rate is a function of the location. By defining the effectiveness factor of the catalyst this factor can be used in every volume element to determine the true reaction rate.

$$\eta = \frac{r_{\text{apperent}}}{r_{\text{intrinsic}}} = \frac{1}{V} \frac{\int_0^V r(c_{\text{CO}}) \mathrm{d}V}{r(c_{\text{CO}_{\text{surface}}})} \tag{4.86}$$

After integration, the following relation for a slab geometry is obtained [79].

$$\eta = \frac{\tanh(\Phi_{\text{g}})}{\Phi_{\text{g}}} \tag{4.87}$$

With the appropriate Thiele Modulus, expression 4.87 can be used to approximate any catalyst pellet shape [79]. The catalyst effectiveness is calculated for every volume element.

A measure for the limitation of the reaction rate through internal mass transfer is the Weisz-Prater criterion which relates the apparent reaction rate to the diffusion rate [84].

$$\Psi = \eta \, \Phi_{\text{g}}^2 = \frac{-r_{\text{intrinsic}}^{\text{g}} \, \rho_{\text{pellet}} \, V^2}{D_{\text{eff}} \, c_{\text{surface}} \, S^2} \frac{b+1}{2} < 0.15 \tag{4.88}$$

If Ψ is smaller than 0.15 intra-particle diffusion limitations can be neglected.

In order to determine the reaction rate, the surface concentrations of the species have to be determined under consideration of external mass transport phenomena. For steady state operation the molar flux from the bulk flow to the surface of the catalyst pellet has to

equal the reaction rate. Since the molar flux is area specific, the reaction rate of the catalyst is normalized to the external surface area of the catalyst pellet.

$$r^{\mathrm{a}}_{\mathrm{apparent}} = r^{\mathrm{g}}_{\mathrm{apparent}} a_{\mathrm{c}} \tag{4.89}$$

with a_{c} the specific external surface area of the catalyst pellet.

$$a_{\mathrm{c}} = \frac{S_{\mathrm{pellet}}}{\rho_{\mathrm{pellet}} V_{\mathrm{pellet}}} \tag{4.90}$$

Thus, under steady state conditions and after applying Fick's Law the following equation has to hold true.

$$r^{\mathrm{a}}_{\mathrm{CO,apparent}} = \dot{n}_{\mathrm{CO}} = \beta \left(c_{\mathrm{CO,bulk}} - c_{\mathrm{CO,surface}} \right) \tag{4.91}$$

where β is the mass transfer coefficient. The mass transfer coefficient can be determined via a correlation, e.g. using the Colburn **j** factor. The relationship between the Colburn factor and various dimensionless numbers is:

$$J_{\mathrm{M}} = \frac{\mathrm{Sh}}{\mathrm{Sc}^{\frac{1}{3}} \mathrm{Re}} = \frac{\left(\frac{\beta \, d_{\mathrm{p}}}{D_{i,\mathrm{Mix}}} \right)}{\left(\frac{\nu}{D_{i,\mathrm{Mix}}} \right)^{\frac{1}{3}} \left(\frac{u \, \rho \, d_{\mathrm{p}}}{\mu} \right)} \tag{4.92}$$

u is the superficial velocity, ρ is the bulk density of the mixture and μ is the dynamic viscosity of the gas mixture. The Dwidevi-Upadhyay correlation relates the Colburn factor

to the Reynolds number and is valid for fixed beds with Reynolds numbers greater 10. The accuracy of the Dwidevi-Upadhyay correlation is 17.95 % [85].

$$\varepsilon_{\mathrm{bed}} J_{\mathrm{M}} = \frac{0.765}{\mathrm{Re}^{0.82}} + \frac{0.365}{\mathrm{Re}^{0.386}} \tag{4.93}$$

Thus, the concentration gradient from the bulk to the catalyst pellet can be calculated. Reactant species will experience a concentration decrease from the bulk medium to the catalyst surface and product species will increase from the bulk medium to the catalyst surface. A measure for the significance of external mass transport limitation is the Carberry number Ca.

$$\mathrm{Ca} = \frac{r^{\mathrm{g}}_{\mathrm{apparent}} \, |b|}{a_{\mathrm{c}} \, \beta \, c_{\mathrm{bulk}}} < 0.05 \tag{4.94}$$

The Carberry number relates the reaction rate to the external mass transfer rate and if Ca is smaller than 0.05 external mass transport limitations can be neglected [86].

After determining the actual reaction rate under consideration of external and internal mass transport the change in carbon monoxide concentration per volume element can be calculated by

$$\Delta c^{\mathrm{r}}_{\mathrm{CO},q} = r^{\mathrm{g}}_{\mathrm{actual},q} \, \rho_{\mathrm{reactor}} \, \tau_q \, \frac{F_{\mathrm{actual}}}{F_{\mathrm{reference}}} \tag{4.95}$$

with $\Delta c^{\mathrm{r}}_{\mathrm{CO},q}$ the concentration change in volume element q per reactor volume, ρ_{reactor} the catalyst density per reactor volume and τ_q being the residence time in the reactor volume element q. F is a pressure correction factor that accounts for differences between the pressure

at which the power law kinetics were experimentally established and the actual operating pressure of the reactor. Power law kinetic rate expressions tend to over-predict the reaction rates at high pressure operation if measured at atmospheric pressure. A correction factor that can be applied up to a pressure of 55 atm is given in Equation 4.96 [87]:

$$F = p^{0.5-\frac{p}{500}} \tag{4.96}$$

p is the pressure in atmospheres. For the reference case, this would be the pressure at which the reaction kinetics were measured and for the actual case this is the operating pressure of the reactor.

Due to the equimolarity of the water-gas-shift reaction, the subsequent volume element on a per reactor volume basis has the following new concentrations:

$$c^{\mathrm{r}}_{\mathrm{CO},q+1} = c^{\mathrm{r}}_{\mathrm{CO},q} - \Delta c^{\mathrm{r}}_{\mathrm{CO},q} \tag{4.97}$$

$$c^{\mathrm{r}}_{\mathrm{H_2O},q+1} = c^{\mathrm{r}}_{\mathrm{H_2O},q} - \Delta c^{\mathrm{r}}_{\mathrm{CO},q} \tag{4.98}$$

$$c^{\mathrm{r}}_{\mathrm{CO_2},q+1} = c^{\mathrm{r}}_{\mathrm{CO_2},q} + \Delta c^{\mathrm{r}}_{\mathrm{CO},q} \tag{4.99}$$

$$c^{\mathrm{r}}_{\mathrm{H_2},q+1} = c^{\mathrm{r}}_{\mathrm{H_2},q} + \Delta c^{\mathrm{r}}_{\mathrm{CO},q} \tag{4.100}$$

The released energy per volume element $\dot{Q}_q$ is calculated based on the amount of shifted carbon monoxide and is described in Equation 4.101.

$$\dot{Q}_q = \Delta h_q \cdot r^{\mathrm{g}}_{\mathrm{actual},q}\, \rho_{\mathrm{reactor}}\, V_q\, \frac{F_{\mathrm{actual}}}{F_{\mathrm{reference}}} \tag{4.101}$$

with V the volume of element q and Δh_q the reaction enthalpy at cell condition q. The reaction enthalpy, as function of temperature, can be approximated over a range from $150 - 600$ °C by the function presented in Equation 4.102.

$$\Delta h = -\frac{0.0000133486 \cdot T^3 - 0.0280557823 \cdot T^2 + 9.2234616980 \cdot T + 41310.0882555674}{1000} \tag{4.102}$$

The temperature input is in Kelvin and the enthalpy output is in $\frac{\text{kJ}}{\text{mol}}$.

In case of an adiabatic reactor the energy release from the chemical reaction per cell is used to increase the temperature from one element to the next element. The temperature increase per cell which is determined by Equation 4.103 is related to the molar flow and the heat capacity of the gas mixture.

$$\Delta T_q = \frac{\dot{Q}_q}{c_{\text{p},q} \cdot \dot{N}_q} \tag{4.103}$$

with c_p the specific heat capacity of the gas mixture and $\dot{N}$ the total molar flow. In case of an ideal isothermal reactor $\Delta T_q = 0$ and $\dot{Q}_q$ has to be met by a cooling load. For an isoflux (constant heat flux) reactor $\dot{Q}_q$ is lowered by the cooling flux before the temperature change is determined.

For the modeling of a real isothermal reactor the energy release per volume element is given by

$$\dot{Q}_q = \Delta h_q \cdot r^\text{g}_{\text{actual},q}\, \rho_\text{reactor}\, V_q\, \frac{F_\text{actual}}{F_\text{reference}} + \alpha_\text{exchanger}\, A_\text{exchanger}\, (T_q - T_\text{coolant}) \tag{4.104}$$

$A_\text{exchanger}$ is the surface area of the heat exchanger and $\alpha_\text{exchanger}$ is the heat transfer

coefficient on the outside of the tubes. In this model only the outside heat transfer coefficient of the heat exchanger is considered since it constitutes largest resistance. The resistance of the tube is small due to its relatively thin wall thickness and high thermal conductivity (manufactured from metal) and the heat transfer coefficient on the inside of the tube is very large as a result of boiling/steam generation.

The heat transfer coefficient $\alpha_{\text{exchanger}}$ is approximated with a reactor wall correlation developed by Li and Finlayson [88]. Heat transfer correlations for horizontal tubes submerged in packed beds were not available. However, depending on the reactor design, reactor wall heat transfer coefficients are a good approximation for isothermal reactors that use U-shaped tubes which are installed parallel to the flow direction.

$$\alpha_{\text{exchanger}} = 0.17 \left(\frac{u \, \rho \, d_{\text{p}}}{\mu} \right)^{0.79} \frac{\lambda}{d_{\text{p}}} \tag{4.105}$$

After determining $\dot{Q}_q$ and ΔT_q for the reactor type of interest, the temperature of the subsequent volume element is given by

$$T_{q+1} = T_q + \Delta T_q \tag{4.106}$$

Important for the validity of the model are the correctness of initial assumptions. Especially errors caused by the assumptions of plug flow or isothermal catalyst pellets can have a significant impact on the simulation results. Pure plug flow requires two criteria that have to be met: uniform velocity profile and no axial dispersion. Certain real catalyst bed operating conditions approximate plug flow.

Non-uniform velocity distribution is a result of wall effects inside the reactor. Chu and Ng [89] showed that wall effects can be neglected if

$$\frac{D}{d_\mathrm{p}} > 25 \tag{4.107}$$

and a uniform velocity distribution inside the reactor is obtained.

In order to eliminate axial dispersion, the following criterion has to be considered during the reactor design [90]:

$$\frac{L_\mathrm{bed}}{d_\mathrm{p}} > \frac{20\,b}{\mathrm{Pe}_\mathrm{disp}} \ln \frac{1}{1-X} \tag{4.108}$$

where $\mathrm{Pe}_\mathrm{disp}$ is the dispersion Peclet number or Bodenstein number, Bo, which is more commonly found in European literature and X is the conversion. The dispersion Peclet number is defined as

$$\mathrm{Pe}_\mathrm{disp} = \frac{u\,L_\mathrm{bed}}{D_\mathrm{ax}} \tag{4.109}$$

The axial dispersion D_ax is determined by the Gunn correlation which has shown to be accurate for low and high Reynolds numbers and various particle sizes [91, 92].

$$D_\mathrm{ax} = \frac{\max\left\{D_{i,\mathrm{Mix}}\right\}_{i=\mathrm{CO,\,CO_2,\,H_2O,\,H_2}}}{\tau_\mathrm{bed}} + \frac{1}{2}\,\frac{u\,d_\mathrm{p}}{\varepsilon_\mathrm{bed}} \tag{4.110}$$

The axial diffusivity consists of a momentum and diffusion term whereby the maximum diffusion rate among the species i is selected. The tortuosity of the catalyst bed, τ_bed can be

approximated by [93].

$$\tau_{\text{bed}} = 1.23 \frac{(1-\varepsilon_{\text{bed}})^{\frac{4}{3}}}{\varepsilon_{\text{bed}} \left(\frac{[36\pi\, V^2]^{\frac{1}{3}}}{S} \right)^2} \tag{4.111}$$

The temperature difference between the bulk medium and the catalyst pellet's surface can be described by

$$\Delta T_{\text{interphase}} = \frac{\Delta h_q \cdot r^{\text{g}}_{\text{actual},q}\, \rho_{\text{reactor}}\, V_q\, \frac{F_{\text{actual}}}{F_{\text{reference}}}}{\rho_{\text{bed}}\, V_q\, a_{\text{c}}\, \alpha_{\text{pellet}}} \tag{4.112}$$

where α_{pellet} is the heat transfer coefficient between the catalyst pellet and the bulk fluid. Although internal heat transfer is not explicitly modeled, criteria for the importance of intra- as well as extra-particular heat transfer can be analyzed by similar dimensionless quantities as for mass transfer to evaluate the assumption of the isothermal catalyst pellets. For this purpose, Mears developed two moduli: Γ for intra-particle heat transfer limitation and Ω for extra-particle heat transfer limitation [84, 86, 94].

$$\Gamma = \left| \frac{-\Delta h\, E_{\text{A}}\, r^{\text{g}}_{\text{apparent}}\, \rho_{\text{pellet}}\, V^2}{R_{\text{g}}\, T^2\, \lambda_{\text{pellet}}\, S^2} \right| < 0.10 \tag{4.113}$$

$$\Omega = \left| \frac{-\Delta h\, E_{\text{A}}\, r^{\text{g}}_{\text{apparent}}}{R_{\text{g}}\, T^2\, \alpha_{\text{pellet}}\, a_{\text{c}}} \right| < 0.05 \tag{4.114}$$

where λ_{pellet} is the thermal conductivity of the catalyst pellet. Γ and Ω assume Arrhenius type temperature dependence of the reaction rate identical to the kinetic rate expression. If Γ is smaller than 0.10 the particle can be assumed as isothermal. If Ω is smaller than 0.05

the temperature difference between the bulk medium and the catalyst surface is negligible.

A comparison shows that the interphase heat transfer becomes limiting before the intraparticle heat transfer providing Biot numbers of smaller than 10.

$$\mathrm{Bi} = \frac{\alpha_{\mathrm{pellet}}\, V}{\lambda_{\mathrm{pellet}} S} < 10 \tag{4.115}$$

this condition is typically met in reactors and heat transfer limitations only have to be considered for fast, highly exothermic reactions [94]. The Biot number itself is not a good measure for the applicability of an isothermal catalyst pellet. The Biot number does relate the external heat transfer rate to the internal heat transfer rate and provides a measure of the uniformity of the temperature in a body, however, the dependence of the reaction kinetics on the temperature play an important role as well. This dependence is not captured in the Biot number but by the Mears moduli Γ and Ω.

To determine the value of the heat transfer coefficient α_{pellet} from the Colburn factor J_{H}, the following correlation is used [95].

$$J_{\mathrm{H}} = \begin{cases} 0.61\,\mathrm{Re}^{-0.41}\,\chi & \mathrm{Re} > 50 \\ 0.91\,\mathrm{Re}^{-0.51}\,\chi & \mathrm{Re} < 50 \end{cases} \tag{4.116}$$

where χ is a shape factor and is 0.91 for cylindrically shaped pellets. Equation 4.116 is needed and cannot be inferred from Equation 4.93 since the fully dimensionless analogy between heat and mass transfer is only valid in the fully turbulent regime with $\mathrm{Re} > 10{,}000$ [96]. Thus, $J_{\mathrm{M}} \neq J_{\mathrm{H}}$ for most cases since the characteristic length of the flow through the catalyst bed (space between the catalyst pellets) is very small. The relation between the Colburn factor and the heat transfer coefficient is

$$J_{\mathrm{H}} = \frac{\mathrm{Nu}}{\mathrm{Pr}^{\frac{1}{3}}\mathrm{Re}} = \frac{\left(\frac{\alpha_{\mathrm{pellet}}\,V}{\lambda\,S\,(1-\varepsilon)}\right)}{\left(\frac{c_{\mathrm{p}}\mu}{\lambda}\right)^{\frac{1}{3}}\left(\frac{v\,\rho\,V}{\mu\,S\,(1-\varepsilon)}\right)} \tag{4.117}$$

4.4.3 Catalyst Selection

In the Selexol$^{\mathrm{TM}}$ case, the shift reactors are located upstream of the sulfur removal unit. Thus, a sulfur tolerant sour shift catalyst is required. The catalyst used in this study is a sulfided molybdenum based catalyst supported on alumina. The intrinsic rate equation was established at an operating pressure of 5 bar with $1\,\% - \mathrm{vol}$ of H_2S in the feed gas. Molybdenum based sour shift catalysts require a certain amount of sulfur in the feed gas to maintain their sulfided state which is the active component of the catalyst. Typically, the reaction kinetics improve with higher sulfur content. The intrinsic rate equation of the sour shift catalyst was determined in [97] and is shown below.

$$r = 3.616\mathrm{E}-5\ \frac{\mathrm{mol\,kPa}^{0\,84}}{\mathrm{g_{cat}\,s}}\ e^{\frac{-22.05\ \frac{\mathrm{kJ}}{\mathrm{mol}}}{R\,T}}\ p_{\mathrm{CO}}^{0.70}\,p_{\mathrm{H_2O}}^{0.14}\,p_{\mathrm{CO_2}}^{0}\,p_{\mathrm{H_2}}^{0}\cdot\left(1-\frac{1}{K}\cdot\frac{p_{\mathrm{CO_2}}\,p_{\mathrm{H_2}}}{p_{\mathrm{CO}}\,p_{\mathrm{H_2O}}}\right) \tag{4.118}$$

Sour shift catalysts are used for high temperature shifting as well as low temperature shifting, however, the activity of sour shift catalyst suffers significantly at low temperatures. The catalyst investigated in [97] is a commercially available catalyst but no physical data on the catalyst are available. A summary of the properties of the physical sour shift catalyst used in this study is provided in table 4.14.

The solid density is based upon the composition of the sour shift catalyst disclosed in BASF's patent [101] and the bed void volume has been calculated based on the bed bulk density disclosed in the same document which is given as 1050 $\frac{\mathrm{kg}}{\mathrm{m}^3}$. Catalyst pore data are

Table 4.14: Physical Catalyst Properties - Sour Shift Catalyst

Specification	Unit	Value	Source
Pellet Radius	m	0.0015	[98]
Pellet Height	m	0.0065	[98]
Solid Density	$\frac{\text{kg}}{\text{m}^3}$	4753	
Bed Void Volume	-	0.45	
Porosity	-	0.60	[99]
Tortuosity	-	3	[65]
Pore Diameter	nm	50	
Thermal Conductivity	$\frac{\text{W}}{\text{m K}}$	1.7	[100]

difficult to obtain and the pore diameter changes with aging of the catalyst. For this simulation a medium pore diameter of 50 nm is chosen based on literature values which range from $14 - 79$ nm [99, 102]. The thermal conductivity is estimated with a value from a copper based catalyst due to the limited availability of data. However, shift catalysts are typically supported on an alumina support which makes the conductivity of the pellet insensitive to the actual catalytic compound.

Sweet shifting is divided into adiabatic high temperature shifting, low temperature shifting, medium temperature shifting and isothermal shifting. For high temperature shifting, temperature resistant Fe/Cr-based catalysts are used. In this study, the following intrinsic rate equation of a commercially available high temperature shift catalyst was used [103].

$$r = 300\ \frac{\text{mol}\,\text{kPa}^{1\,33}}{\text{g}_{\text{cat}}\,\text{s}}\ e^{\frac{-102\ \frac{\text{kJ}}{\text{mol}}}{RT}}\ p_{\text{CO}}^{1.37}\ p_{\text{H}_2\text{O}}^{0.23}\ p_{\text{CO}_2}^{-0.16}\ p_{\text{H}_2}^{-0.11} \cdot \left(1 - \frac{1}{K} \cdot \frac{p_{\text{CO}_2}\ p_{\text{H}_2}}{p_{\text{CO}}\ p_{\text{H}_2\text{O}}}\right) \tag{4.119}$$

Critical for the operation of iron based shift catalysts is the formation of Fischer-Tropsch liquids. In order to avoid formation of Fischer-Tropsch liquids, the following criterion is applied [104].

$$R_{FT} = \frac{y_{CO} + y_{H_2}}{y_{CO} + y_{H_2O}} \cdot \frac{\mathrm{P}}{26\ \mathrm{bar}} < 1.9 \tag{4.120}$$

The gas analysis y in this equation is expressed in vol-%. Physical properties and other specifications from the supplier of the catalyst described above are not available and the following values from literature have been assumed.

Table 4.15: Physical Catalyst Properties - High Temperature Sweet Shift Catalyst

Specification	Unit	Value	Source
Pellet Radius	m	0.0027	[105]
Pellet Height	m	0.0036	[105]
Solid Density	$\frac{\mathrm{kg}}{\mathrm{m}^3}$	4650	[106]
Bed Void Volume	-	0.36	
Porosity	-	0.59	[106]
Tortuosity	-	3	[65]
Pore Diameter	nm	50	
Thermal Conductivity	$\frac{\mathrm{W}}{\mathrm{m\ K}}$	1.7	[100]

The bed void volume is calculated based on the bed bulk density provided in [105] which is given as 1220 $\frac{\mathrm{kg}}{\mathrm{m}^3}$.

For the low temperature sweet shift catalyst, the commercially available SHIFTMAX 240 catalyst from Süd Chemie is used. The low temperature shift catalyst is based on Cu/Zn supported on alumina. Critical for low temperature sweet shift reactors is the formation of methanol; especially at temperatures below 200 °C, the equilibrium concentration of methanol becomes important. Thermodynamic equilibrium concentrations of methanol produced from the syngas leaving the TRIG$^{\mathrm{TM}}$ gasifier are shown in Figure 4.12.

The plot, Figure 4.12, shows that with increasing steam to carbon ratio, the formation of methanol can be suppressed. However, for very low temperatures, e.g. $175 - 200$ °C, the dew point of the gas mixture is reached before the methanol formation can be pushed below

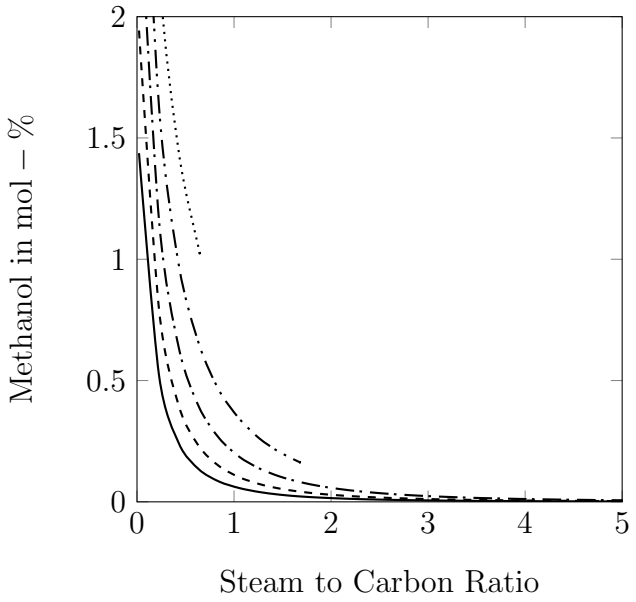

Figure 4.12: Methanol equilibrium concentrations derived from TRIG^{TM} syngas for various temperatures as function of steam to carbon ratio. 175 °C(·····), 200 °C (−··), 225 °C (−·-), 250 °C(- - -), 275 °C (——).

0.1 %. Due to operation concerns the syngas entering the reactor should contain enough super heat to avoid pore condensation. In this study a 15 °C super heat approach has been chosen. The SHIFTMAX 240 catalyst is identical in performance to the SHIFTMAX 230 catalyst but contains a promoter to suppress the formation of methanol by 95 % [107]. As a result of this, the formation of methanol with the SHIFTMAX 240 catalyst is insignificant and can be neglected.

Kinetic rate equations of the SHIFTMAX 240 catalyst were not available. However, since SHIFTMAX 240 and SHFITMAX 230 have identical performance [107], the intrinsic rate equation of the SHIFTMAX 230 catalyst is used instead. The intrinsic rate equation is given in Equation 4.121 [108].

$$r = 0.008009 \, \frac{\mathrm{mol\,kPa^2}}{\mathrm{g_{cat}\,s}} \, e^{\frac{-47.7 \, \frac{\mathrm{kJ}}{\mathrm{mol}}}{R\,T}} \, p^1_{\mathrm{CO}} \, p^1_{\mathrm{H_2O}} \, p^0_{\mathrm{CO_2}} \, p^0_{\mathrm{H_2}} \cdot \left(1 - \frac{1}{K} \cdot \frac{p_{\mathrm{CO_2}} \, p_{\mathrm{H_2}}}{p_{\mathrm{CO}} \, p_{\mathrm{H_2O}}}\right) \tag{4.121}$$

The physical properties of the SHIFTMAX 240 catalyst used in this investigation are

in the range of typical shift catalyst properties and are summarized in Table 4.16.

Table 4.16: Physical Catalyst Properties - Low Temperature Sweet Shift Catalyst

Specification	Unit	Value	Source
Pellet Radius	m	0.0024	[107]
Pellet Height	m	0.0032	[107]
Solid Density	$\frac{kg}{m^3}$	4133	[65]
Bed Void Volume	-	0.40	[65]
Porosity	-	0.25	[65]
Tortuosity	-	3	[65]
Pore Diameter	nm	50	[109]
Thermal Conductivity	$\frac{W}{m\ K}$	1.7	[100]

The pore diameter is an estimated value between fresh catalyst and used catalyst [109].

4.4.4 Analysis of the Water-Gas-Shift Section

The plant optimization with respect to the water-gas-shift reactors is conducted in the following section. First a detailed analysis of the Selexol™ and warm gas cleanup scenario is carried out, followed by two optimization scenarios.

Analysis of the Selexol™ Scenario

For all simulations including the above presented Selexol™ case and CO_2-PSA case, the sizing and determination of the steam requirement have been executed using the approach described in Section 4.4.1 and Section 4.4.2.

The Selexol™ case uses a dual-stage Selexol™ process downstream of the water-gas-shift reactors which removes the sour gases, hydrogen sulfide and carbon dioxide. The water-gas-shift reactors serve two purposes: shifting of CO to CO_2 and converting sulfur species to

hydrogen sulfide. Since the shift reactors operate in the presence of sulfur species, a sour shift catalyst is required that can withstand poisoning by sulfur. Furthermore, it has to support the hydrolysis reaction of sulfur components like COS. The sour shift catalyst introduced in Section 4.4.3 consisting of molybdenum sulfide has these features. Important for the design of the shift reactor section is the steam to carbon monoxide ratio and the operating temperature. A certain minimum amount of steam is required to avoid carbon deposition onto the catalyst. The operating temperature has an effect on the thermodynamic equilibrium, as well as the kinetics. The temperature has to be low enough to drive the reaction towards carbon dioxide but has to be high enough to drive the reaction at a reasonable rate. A slow reaction rate increases the required catalyst volume, vessel size and pressure drop, which ultimately increases capital and operating cost. CO-shifting is typically done in two or three stages in adiabatic reactor with intercooling. Isothermal reactors are more expensive than adiabatic reactors, but intercoolers can be eliminated. However isothermal reactors are only applicable for sweet shift applications due to their complicated catalyst loading process (sour shift requires more frequent replacement of the catalyst bed than sweet shifting). Most commonly, the first reactor is operated at high temperatures for bulk shifting at high reaction rates, followed by medium or low temperature reactors for yield optimization.

The temperature profile along the 1$^{\text{st}}$ shift reactor of the Selexol$^{\text{TM}}$ case is shown in Figure 4.13.

The humidified syngas enters the 1$^{\text{st}}$ shift reactor safely above the dew point with a temperature of 224 °C. Inside the reactor, the temperature monotonically increases until it reaches a value of 395 °C after passing through 80 % of the catalyst bed. After passing the 80 %-mark, there is no further increase in temperature and the profile remains constant. Since the water-gas-shift reaction is exothermic and the reactor walls are assumed to be adiabatic, this indicates that the reaction came to halt and equilibrium is established. For the design of the reactor, a system sizing factor of 1.25 is chosen to accommodate the reaction. As criterion for equilibrium a reaction rate of smaller than 0.1 $\frac{\text{mol}}{\text{m}^3\,\text{s}}$ is chosen. Employing

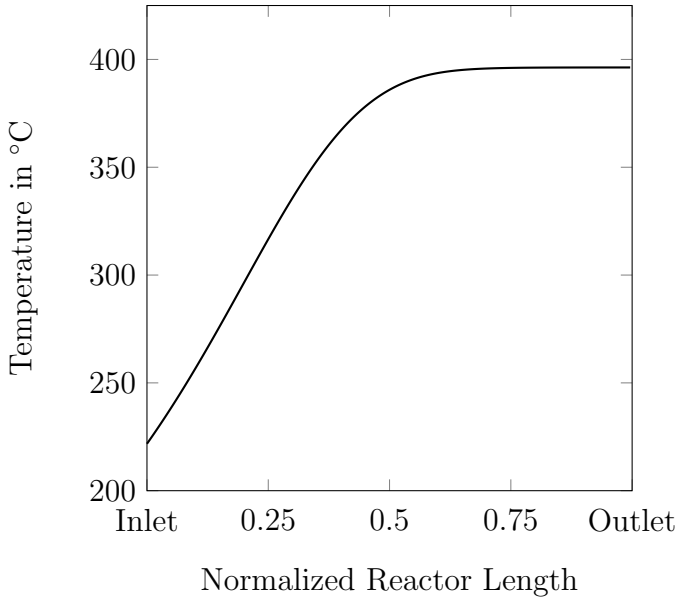

Figure 4.13: Temperature profile of the 1st shift reactor of the Selexol™ cold gas cleanup scenario using a sour shift catalyst with a system sizing factor of 1.25.

a sizing factor guarantees the completion of the reaction and leaves a buffer for possible contamination of the catalyst due to unexpected irregularities during operation. Catalyst poisoning is most critical for the first reactor which will act like a contaminant trap for the following reactors. Typically, this is realized in the form of a guard bed at the inlet of the reactor which can be replaced more easily. For the reactor design, an equilibrium approach temperature of 13.9 °C was used in order to account for middle of run condition. On closer examination of the temperature profile, it can be seen that the temperature slop right after the inlet slightly increases until it reaches a reactor length of 0.2. After that, the temperature's slope remains almost constant before it starts leveling off very quickly at a reactor length of 0.35. From the middle of the reactor to the outlet, the temperature remains constant at a value of 395 °C. As it can be inferred from Equations 4.119 and 4.121, the reaction rate is influenced by the temperature as well as the species concentrations of reactants and products. The over proportional increase in reactor temperature at reactor inlet hints at a stronger influence of the reaction temperature upon the reaction rate than the species concentration for the first section of the reactor. However, after a certain time (distance

in plug flow reactor), the concentration of reactants becomes so low that the reaction slows down.

The species profiles for water, hydrogen, carbon dioxide and carbon monoxide along the axis of the reactor are shown in Figure 4.14.

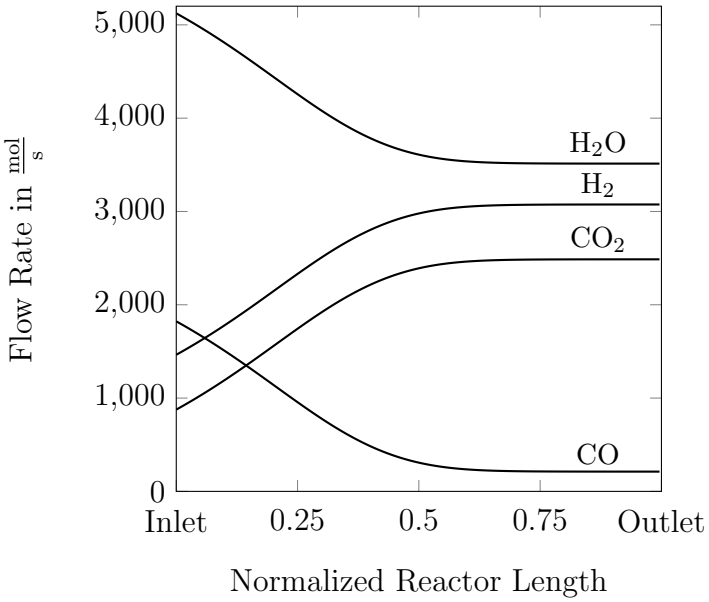

Figure 4.14: Species profiles of the 1st shift reactor of the Selexol™ cold gas cleanup scenario using a sour shift catalyst with a system sizing factor of 1.25.

The ordinate shows the flow rate of water, hydrogen, carbon dioxide and carbon monoxide in $\frac{\text{mol}}{\text{s}}$. Along the axis reactants, water and carbon monoxide, decrease and products, hydrogen and carbon dioxide, increase. Due to the equimolar nature of the water-gas-shift reaction, the absolute slopes of reactants and products are identical at a given location inside the reactor. From the species profiles, it is evident that after the syngas has passed through the first 80 % of the reactor, equilibrium is essentially established and no further change in the molar flow rates is observed. At the reactor inlet, the slopes of the species molar flows are almost linear but have a little curvature similar to the temperature profile. Then at a reactor length of 0.35, the slopes decrease until the molar flows stay constant. Main driver of the reaction rate next to the reaction temperature is the partial pressure of carbon monoxide.

In Equation 4.118, the exponent applied to the carbon monoxide partial pressure is 0.80. This is much higher than any of the other exponents which indicates a stronger influence of the carbon monoxide partial pressure on the reaction rate than any other component.

The inlet mole-fraction of carbon monoxide is 0.190. At the outlet, the mole-fraction is reduced to 0.021. This corresponds to a CO-conversion of 89.1 %. Since the carbon dioxide yield of the Selexol^{TM} process is not very high and the decarbonized syngas will contain about $5\,\mathrm{mol}-\%$ of CO_2, it is necessary to nearly completely shift CO to CO_2 in order to maximize carbon capture. However, further shifting is not possible without intercooling since the thermodynamic equilibrium is dictated by the temperature.

A plot of catalyst effectiveness, intrinsic and apparent reaction rate is shown in Figure 4.15.

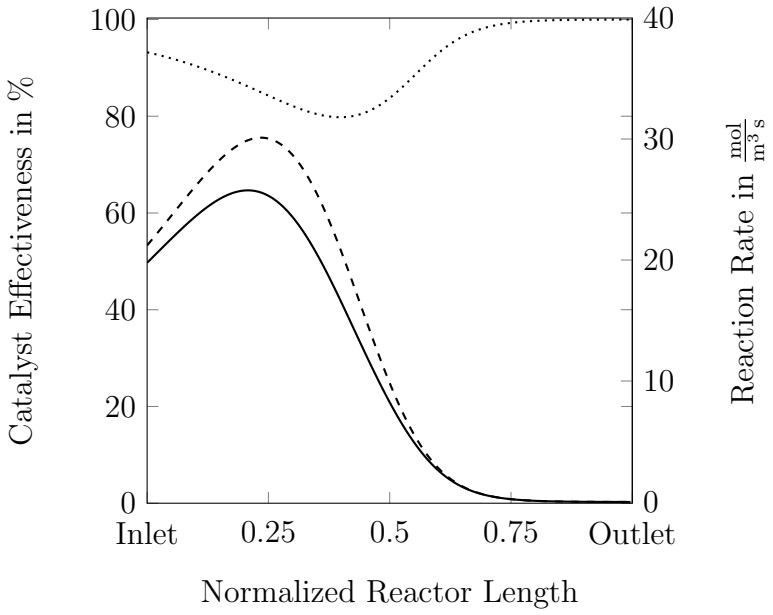

Figure 4.15: Catalyst effectiveness (·····), intrinsic reaction rate (- - -) and apparent reaction rate (——) of the 1st shift reactor of the Selexol^{TM} cold gas cleanup scenario using a sour shift catalyst with a system sizing factor of 1.25.

The catalyst effectiveness is represented by the dotted line and refers to the scale on the left ordinate. Apparent and intrinsic reaction rates are shown as solid and dashed lines and

refer to the scale on the right ordinate. The intrinsic reaction rate is the maximum reaction rate without pore diffusion limitations. It is the rate at which the reaction would occur if all the internal surface would be exposed to the gas. At the beginning, the intrinsic reaction rate starts at a moderate value of 21 $\frac{\text{mol}}{\text{m}^3\,\text{s}}$ and increases. Until a reactor length of 0.2, the reaction rate rapidly increases until it reaches its maximum value of 30 $\frac{\text{mol}}{\text{m}^3\,\text{s}}$. It drops to essentially 0 $\frac{\text{mol}}{\text{m}^3\,\text{s}}$ after reaching the 80 %-mark of the reactor. The apparent reaction rate has a similar trend, however, starting at a reaction rate of 20 $\frac{\text{mol}}{\text{m}^3\,\text{s}}$. The following increase in reaction rate is smaller than that for the intrinsic reaction rate. At the maximum value, the apparent reaction rate differs from the maximum intrinsic reaction rate by 4 $\frac{\text{mol}}{\text{m}^3\,\text{s}}$. Furthermore, the maximum of the apparent reaction rate is slightly shifted to the left side. Subsequent to passing the maximum reaction rate, the value drops and the reaction comes to halt at a reactor length of 0.80. The reaction rate increase of the apparent and intrinsic reaction rate in the first section of the reactor follows an exponential growth. This acceleration in the kinetics is due to the increase in temperature which dominates the reaction rate at the reactor inlet while the CO concentration is sufficiently high. Along the axis of the reactor, the CO concentration is decreasing until the concentration is so low that it leads to a slowdown of the reaction rate. Additionally, the temperature increase influences the chemical equilibrium and the chemical potential difference, another important driver of the reaction. At higher temperatures, the equilibrium shifts to the reactant side for exothermic reactions. This reduces the chemical potential difference and ultimately slows the reaction down. The difference in the reaction rates between the apparent and intrinsic reaction rates is due to pore diffusion inside the catalyst pellet. Diffusion limits the internal surface penetration with reactants and slows down the process of product removal from the reaction site. An increase in temperature has only a small impact on the effective diffusivity which leads to the conclusion that the observed increase in apparent reaction rate is mostly due to the increase in intrinsic reaction rate. This means that when increasing the temperature, more reaction will occur closer to the pore entrance. Thus, less reactants can diffuse all the way into the

pore, which reduces the active reaction surface significantly and widens the gap between the apparent and intrinsic reaction rate.

A measure of this phenomenon is the catalyst effectiveness, which is the ratio between the intrinsic and apparent reaction rate. At the reactor inlet, the catalyst effectiveness lies just above 93 %. Accordingly, to the above described phenomenon, the catalyst effectiveness decreases down to 80 % before it recovers and rises all the way to 100.0 %. This rapid increase and full utilization of the catalyst is due to the establishment of chemical equilibrium. In this situation, the chemical reaction rate is infinitesimally slow but the diffusion into the pore is at its maximum rate. Reactants can diffuse all the way into the pore before they can react and can fully utilize the internal surface area.

The catalyst bed for this reactor has a total volume of 145.4 m^3, which results in a pressure drop of 1.17 bar. Together with the pressure drop for reactor inlet and reactor outlet, the total pressure drop of the 1^{st} shift reactor is 1.24 bar. The shift reactor section is operated in two trains each reactor with a diameter of 3.66 m.

Important measures for the performance of a reactor are the Weisz-Prater modulus and the Carberry number. Both parameters are plotted in Figure 4.16.

The Prater-Weisz modulus (solid line) relates the reaction rate to the pore diffusion rate and is plotted versus the left ordinate. The initial value of the modulus is 0.22 which initially increases exponentially, followed by a short linear section and levels off to reach a maximum value of 0.64 at a reactor length of 0.4. After that the modulus decreased rapidly and asymptotically approaches a value of zero. The exponential increase at the beginning can be traced back to the exponential temperature dependence of the reaction rate and shows that the increase in reaction rate is faster than the increase in diffusion rate due to an increase in temperature at the reactor inlet section. The linear section of the Weisz-Prater modulus coincides with the maximum intrinsic reaction rate. Here the increase in temperature is the strongest but the reaction rate is beginning to slow down which brings the reactant consumption rate to the same order as the diffusion rate. Later, the reaction

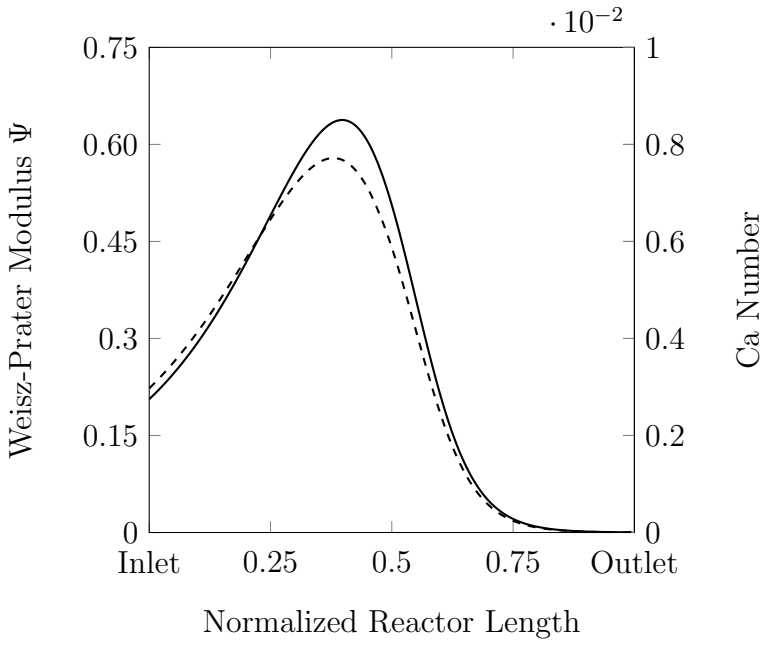

Figure 4.16: Prater-Weisz modulus (——) and Carberry number (- - -) of the 1st shift reactor of the Selexol™ cold gas cleanup scenario using a sour shift catalyst with a system sizing factor of 1.25.

rate slows down further because of the low reactant concentration, however, the temperature keeps increasing and so does the diffusion rate.This leads to a further increase of the modulus until the decrease of the reaction rate is so strong that it dominates the behavior of the Weisz-Prater modulus. According to Equation 4.88 the effect of internal diffusion is not limiting if the value of the Weisz-Prater modulus is smaller than 0.15. As it can be seen from Figure 4.16 the internal diffusion limitation is present in the reactor up to a normalized length of 0.63.

The Carberry number (dashed line) is a measure for the limitation of external mass transport limitation and relates the reaction rate to the external mass transport rate. The shape of the Carberry number curve is similar to the Weisz-Prater modulus since the same physical principles apply as the ones described above. However, there is a slight left shift of the maximum compared to the Weisz-Prater modulus. This is because the relevant reaction rate for the Weisz-Prater modulus is the intrinsic reaction rate but for an external mass transport limitation criterion the apparent reaction rate is of interest. The initial value of

the Carberry number at reactor inlet is 0.003 and the maximum value is 0.008. Both values are below the threshold of 0.05 (Equation 4.94) and, thus external mass transport does not limit the reaction kinetics.

To evaluate the limitations of heat transfer upon the reaction kinetics the Mears moduli for internal and external heat transfer are plotted in Figure 4.17.

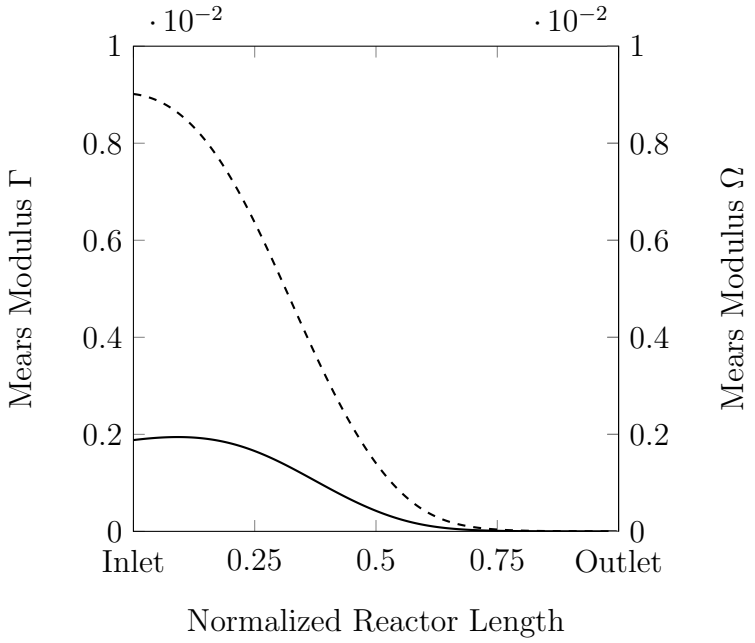

Figure 4.17: Mears Modulus for internal heat transfer Γ (——) and Mears Modulus for external heat transfer Ω (- - -) of the 1st shift reactor of the Selexol™ cold gas cleanup scenario using a sour shift catalyst with a system sizing factor of 1.25.

The Mears modulus Γ (solid line) is plotted versus the left ordinate and is a measure for the importance of internal heat transfer. The initial value of the Mears modulus for internal heat transfer is 0.0018. The initial increase is slow and the maximum value is 0.0020 which is reached at a reactor length of 0.09. After the maximum, the modulus asymptotically approaches 0. The internal heat transfer is most critical before the maximum reaction rate is reached and is already declining when the reaction rate arrives at its highest value. Reason for this behavior is the reaction enthalpy that decreases with increasing temperature and Arrhenius number that relates the activation energy to the thermal potential. Applying the

criterion from Equation 4.113 shows that internal heat transfer does not play an important role in this scenario and the model assumption of an isothermal catalyst particle is justified.

The Mears modulus Ω (dashed line) is an indicator for the relevance of extra particle heat transfer limitation and is plotted versus the right ordinate in Figure 4.17. The modulus Ω starts with its highest value of 0.009 and a low negative slope. The slope decreases towards the middle of the reactor and Ω levels off asymptotically as it approaches a value of zero. The mechanisms that impact the reaction rate, e.g. activation energy, thermal potential and enthalpy of reaction are identical to the Γ modulus, however, in Ω they are related to the heat transfer coefficient instead of the conductivity. The shape of the two moduli is generally very similar. Nevertheless, Ω has a local maximum and Γ does not. In the calculation of Ω the conductivity is assumed to be constant, while in the calculation of Γ the heat transfer coefficient is a function of the location in the reactor. Since the gas in the reactor is heating up and expands, the volume flow is increased leading to a higher Colburn factor and higher heat transfer coefficients which leads to the elimination of the maximum and a decrease of the Γ modulus from the inlet of the reactor. As the highest value of Γ lies below the critical value of 0.05 external heat transfer is not limiting the reaction.

Another useful measure in reactor engineering is the proposed rate optimization number, Ro, that compares the influence of temperature on the thermal driving force and the chemical driving force. The rate optimization number is plotted in Figure 4.18.

The rate optimization number starts with a very high negative value of -460 and increases almost logarithmically up to a value of -0.0001. Thereby, it intersects with the -1 value at around 0.45. This shows that for most of the time the chemical reaction is operated far away from its optimum rate. Values below -1 show that the reaction rate could proceed much faster if more thermal energy would be available. Values above -1 show that the reaction kinetics could be accelerated if the chemical driving force would be increased by lowering the temperature. A wide range of Ro values indicates that large amounts of catalyst could potentially be saved by optimizing the reactor design. This is a very different finding

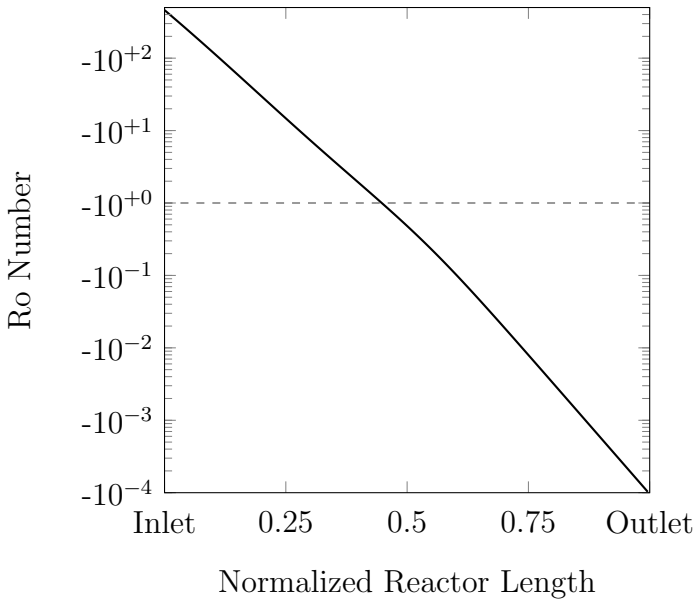

Figure 4.18: Rate optimization number of the 1st shift reactor of the Selexol™ cold gas cleanup scenario using a sour shift catalyst with a system sizing factor of 1.25.

compared to the catalyst effectiveness. In this reactor the catalyst effectiveness is quite high with values greater than 80 %. However, the catalyst effectiveness only evaluates how much of the catalyst is actually being used. If improving the reaction kinetics according to the Ro number, it is very likely that the catalyst effectiveness will go down while the total amount of catalyst needed to accommodate the reaction will be reduced. The impact of optimizing the reactor design with the Ro number and details on the Ro number will be discussed at a later point in section 4.4.5.

The inlet temperature of the 2nd shift reactor is set to be 15 °C above the dew point temperature. This is 204 °C and the lowest acceptable inlet temperature. Lower temperatures are desirable with respect to the thermodynamic equilibrium but also lead to a slowdown of the reaction kinetics. Thus, low temperatures in the water-gas-shift reaction can result in unreasonable catalyst bed sizes and pressure drops, which have to be evaluated in this analysis. The system sizing factor for the 2nd shift reactor was set to 1.1 to ensure completion of the reaction. Poisoning is not as much of a concern for the reason that potential trace

contaminants will be trapped in the first reactor.

The temperature profile of the 2nd shift reactor is shown in Figure 4.19.

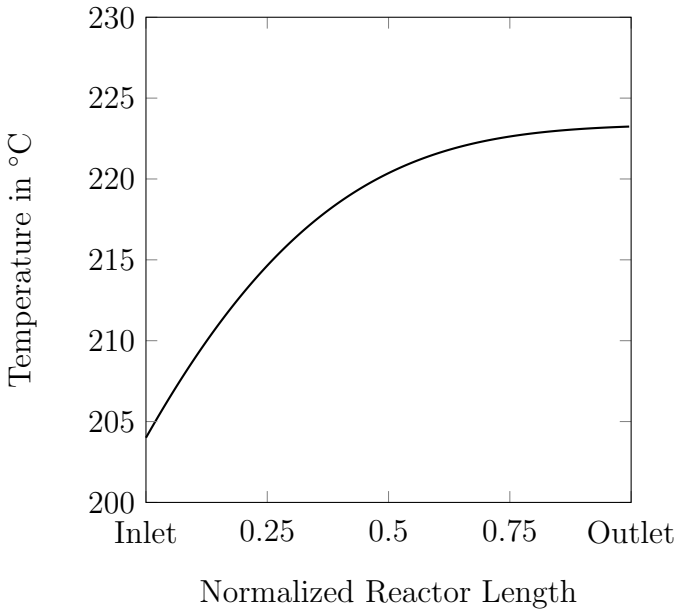

Figure 4.19: Temperature profile of the 2nd shift reactor of the Selexol™ cold gas cleanup scenario using a sour shift catalyst with a system sizing factor of 1.1.

The temperature range of the low temperature shift reactor is much smaller than in the high temperature shift reactor. The temperature increases from 204 °C at the inlet to 222 °C at the outlet. Identically to the 1st shift reactor, a 13.9 °C equilibrium temperature approach is used. Although both reactors feature the same reaction, the temperature profile within the reactors is very different. The temperature increase at reactor inlet for the high temperature shift reactor is 2.22 $\frac{°C}{m^3}$ and accelerates in the first section, whereas the temperature increase at the reactor inlet for the second reactor is 0.31 $\frac{°C}{m^3}$ and stagnates from the very beginning. After a normalized reactor length of 0.25, the reaction starts to slow down significantly and levels off at around 0.90. This indicates that the heat provided by the reaction is not enough to accelerate the reaction kinetics. The CO concentration at the reactor inlet is already so low that it starts to impact the reaction rate from the very beginning and the slope of the temperature profile decreases along the reactor axis until it

eventually reaches a value of zero meaning the temperature reaches a constant value.

When the syngas enters the 2nd shift reactor, 89.1 % of the CO is already converted to CO_2. After the 2nd shift reactor, the CO conversion is increased to 98.7 %. The progression of CO conversion along the reactor axis can be seen in Figure 4.20 together with the other species profiles of the 2nd shift reactor.

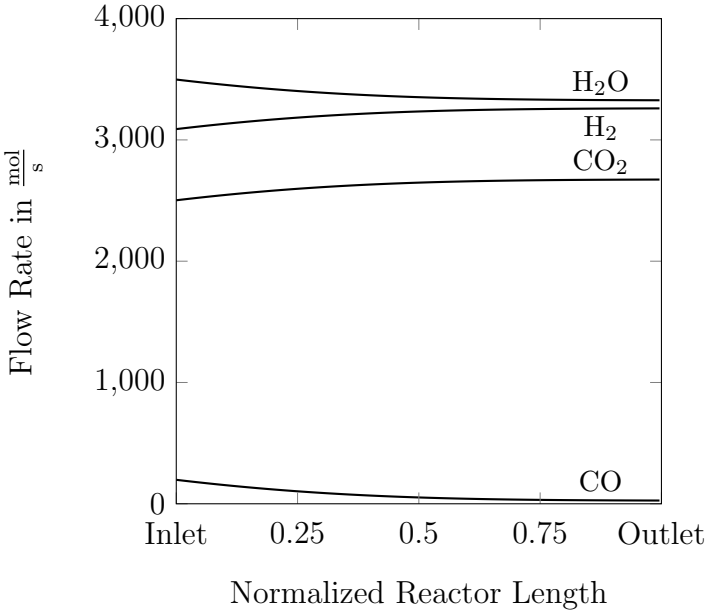

Figure 4.20: Species profiles of the 2nd shift reactor of the Selexol™ cold gas cleanup scenario using a sour shift catalyst with a system sizing factor of 1.1.

As described before, the reactant and product species lines run parallel to each other and the absolute slopes of the reactant and product curves are identical due to equimolar shifting. Carbon monoxide values at reactor inlet are more than an order of magnitude lower than the other species participating on the water-gas-shift reaction. The reactants, water and carbon monoxide, experience the strongest decrease at the reactor inlet and slowly level off. Inverse behavior is found for the product species, hydrogen and carbon dioxide. The highest slope is at the reactor inlet and it levels off as the reaction approaches equilibrium. This very slow change in species concentration is because of the fact that the chemical potential difference is already very small at the reactor inlet due to low CO concentration.

Figure 4.21 shows the catalyst effectiveness, apparent and intrinsic reaction rates.

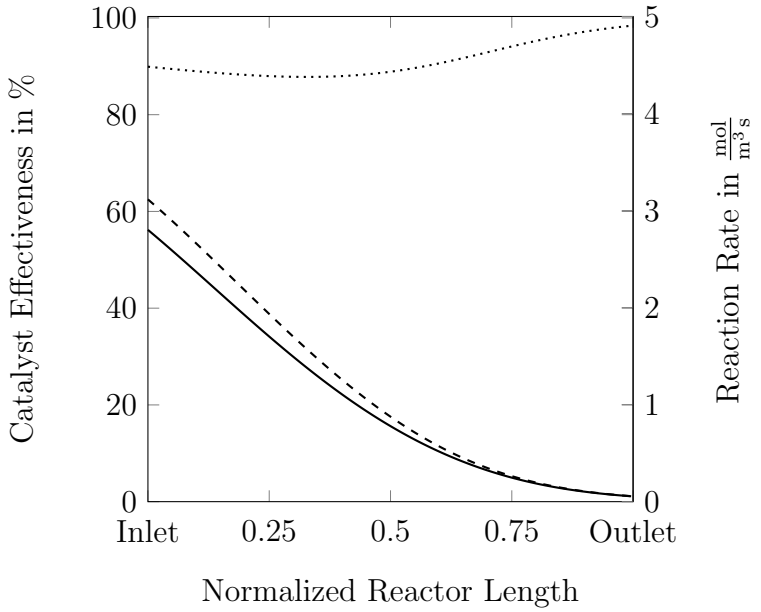

Figure 4.21: Catalyst effectiveness (·····), intrinsic ration rate (- - -) and apparent reaction rate (——) of the 2nd shift reactor of the Selexol™ cold gas cleanup scenario using a sour shift catalyst with a system sizing factor of 1.1.

As indicated before, the reaction kinetics of the low temperature shift reactor are much slower than those in the high temperature reactor. The maximum apparent reaction rate of the second reactor at 2.80 $\frac{\text{mol}}{\text{m}^3\,\text{s}}$, is 89 % lower than the maximum reaction rate of the first reactor. Differences in the intrinsic reaction rate are smaller and around 90 %. The intrinsic reaction rate has an initial value of 3.12 $\frac{\text{mol}}{\text{m}^3\,\text{s}}$ and decreases to a value of 0.06 $\frac{\text{mol}}{\text{m}^3\,\text{s}}$ towards the reactor outlet. A reaction rate of 0.1 $\frac{\text{mol}}{\text{m}^3\,\text{s}}$ is considered as equilibrium. Applying a sizing factor of 1.1 allows the reaction to proceed beyond this limit. The slope of the intrinsic rate decreases linearly until a reactor length of 0.25 and starts leveling off after passing the 0.25 mark. The almost linear behavior is due to the exothermic nature of the water-gas-shift reaction, which leads to a temperature increase and an acceleration in the kinetics. However, this effect is competing with the reduction in reaction rate as a result of the lowering CO concentration. At the beginning, both effects are apparent but as the reaction proceeds, the

impact of the lower CO concentration begins dominating the reaction rate. This can be also seen in the apparent reaction rate. As the reaction approaches equilibrium, the difference between the intrinsic and apparent reaction rate vanishes because internal mass transport becomes less of a limitation.

The catalyst effectiveness of the low temperature shift reactor is overall higher than the high temperature shift reactor. At inlet conditions, the effectiveness is 90 %, and drops to 88 % and then rises to 98 %. The higher overall effectiveness compared to the 1st shift reactor is due to the slower reaction rate, which allows species transport farther into the pore and a higher utilization of the internal surface area. The minimum effectiveness value is located at a reactor length of 0.33, this is where the ratio of apparent reaction rate to intrinsic reaction rate is the smallest.

The catalyst bed in the 2nd shift reactor occupies a volume of 168.6 m^3. The pressure drop associated with this bed is 1.11 bar. Although the bed volume is the larger, the pressure drop of the low temperature shift reactor is smaller. The reactor's lower inlet temperature reduces the volume flow through the bed, which is correlated to the pressure drop resulting in a lower pressure drop. Considering reactor inlet and outlet pressure drops a total pressure drop of 1.20 bar is obtained. The shift reactor section is operated in two trains each of the two low temperature shift reactors with a diameter of 3.66 m.

The dimensionless quantities describing internal and external mass transport phenomena of the catalyst particle are plotted in Figure 4.22.

The Weisz-Prater Modulus at the reactor inlet has a value of 0.31 and reaches a maximum value of 0.38 at a reactor length of 0.33 where the minimum catalyst effectiveness is reached. The curvature of the curve is positive until a reactor length of 0.68 and decreases to a value of 0.05 at reactor outlet. This means that even at slow reaction rates severe limitations due to internal mass transport exist within the catalyst pellet. At the reactor inlet the Weisz-Prater modulus of the second shift reactor is even greater than at the inlet of the first reactor which has a much higher reaction rate. This is due to the reduced diffusion

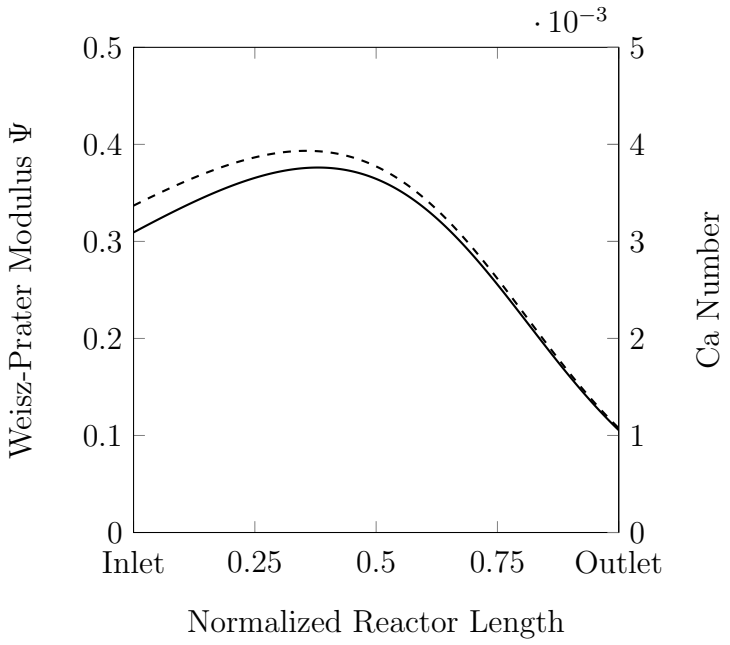

Figure 4.22: Prater-Weisz modulus (——) and Carberry number (- - -) of the 2nd shift reactor of the Selexol™ cold gas cleanup scenario using a sour shift catalyst with a system sizing factor of 1.1.

rate (note: the diffusivity increases, although the temperature is lower; the composition of the gas mixture in the second reactor is different leading to a smaller concentration gradient causing the diffusion rate to drop).

The Carberry number is initially 0.003 and reaches a maximum value of 0.004 when the minimum catalyst effectiveness is reached. Overall the shape of the curve is very similar to the first shift reactor but the Carberry number is in general lower than in the first reactor. This means that the reaction rate in the second reactor decrease more than the heat transfer coefficient in the second reactor due to the lower volume flow. Nevertheless, in both reactors the external mass transfer resistance is so small that it can be neglected.

The dimensionless quantities for internal and external heat transport are shown in Figure 4.23.

Also for the second shift reactor the assumption of an isothermal catalyst particle is justified. The Mears modulus Γ is smaller than 0.1 at all locations. The initial value is

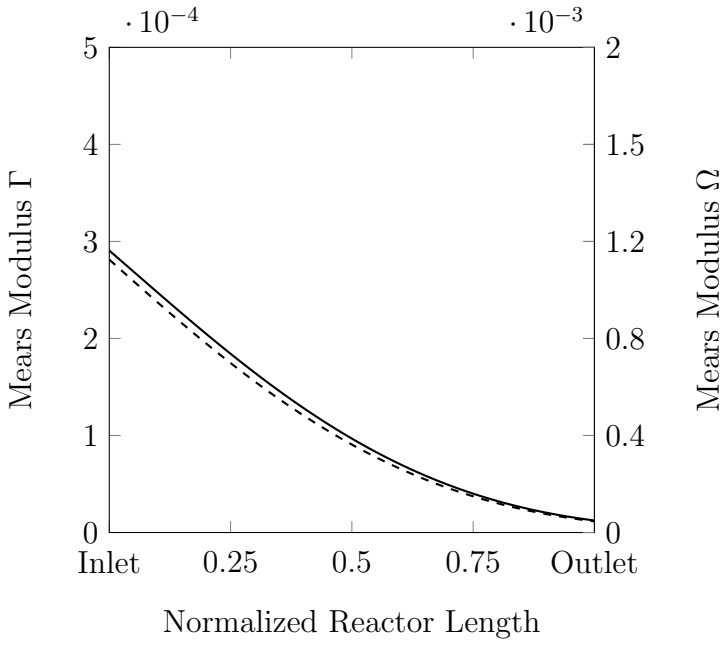

Figure 4.23: Mears Modulus for internal heat transfer Γ (——) and Mears Modulus for external heat transfer Ω (- - -) of the 2nd shift reactor of the Selexol™ cold gas cleanup scenario using a sour shift catalyst with a system sizing factor of 1.1.

0.0003 and decays to a value of 5x10^{-6} at reactor outlet. These values are much smaller than for the first shift reaction due to the slower reaction kinetics while the conductivity is considered to be the same.

The Mears modulus Ω has an initial value of 0.001 and decreases to 2x10^{-5}. This means that external heat transfer in the second reactor is not important for the reaction kinetic. Compared to the first reactor the modulus for external heat transfer is smaller which is also due to the reaction rate and heat transfer coefficient. The external heat transfer coefficient in the second reactor is actually higher compared to the first shift reactor due to the differences in density, viscosity and heat capacity although the actual gas velocity in the catalyst bed is lower because of the lower inlet temperature.

In Figure 4.24, the rate optimization number for the second shift reactor is shown.

The range in which the reactor operates is much smaller than the first reactor and goes from -7.5 to -0.04 which means that it operates closer to its optimum reaction rate.

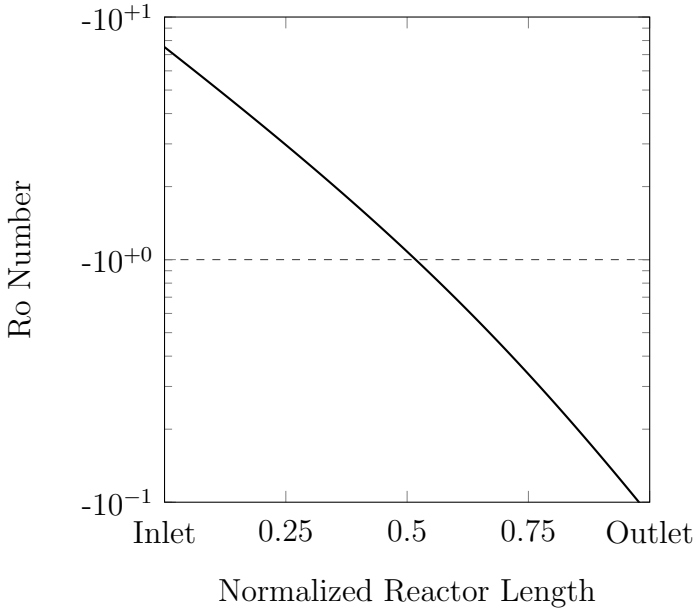

Figure 4.24: Rate optimization number of the 2nd shift reactor of the Selexol™ cold gas cleanup scenario using a sour shift catalyst with a system sizing factor of 1.1.

At a reactor length of approximately 0.5 the reactor operates at is optimum reaction rate. Below a reactor length of 0.5 the reactor temperature is too low and above a reactor length of 0.5 the reactor temperature is too high to achieve the optimum reaction rate. However, since the reactor is operated adiabatically the reactor inlet temperature is determined by the conversion target. If internal cooling can be achieved an improvement of the reaction rate is feasible while maintaining the same conversion.

Critical for the operation of the water-gas-shift reactors is the equilibrium evaluation between carbon, hydrogen and oxygen species in order to avoid carbon deposition onto the catalyst. Figures 4.25 and 4.26 show the equilibrium curves for the high temperature and low temperature water-gas-shift reactors at inlet and outlet conditions for the formation of graphite and amorphous graphite.

The ternary diagrams are based upon atomic balances and can depict any composi-

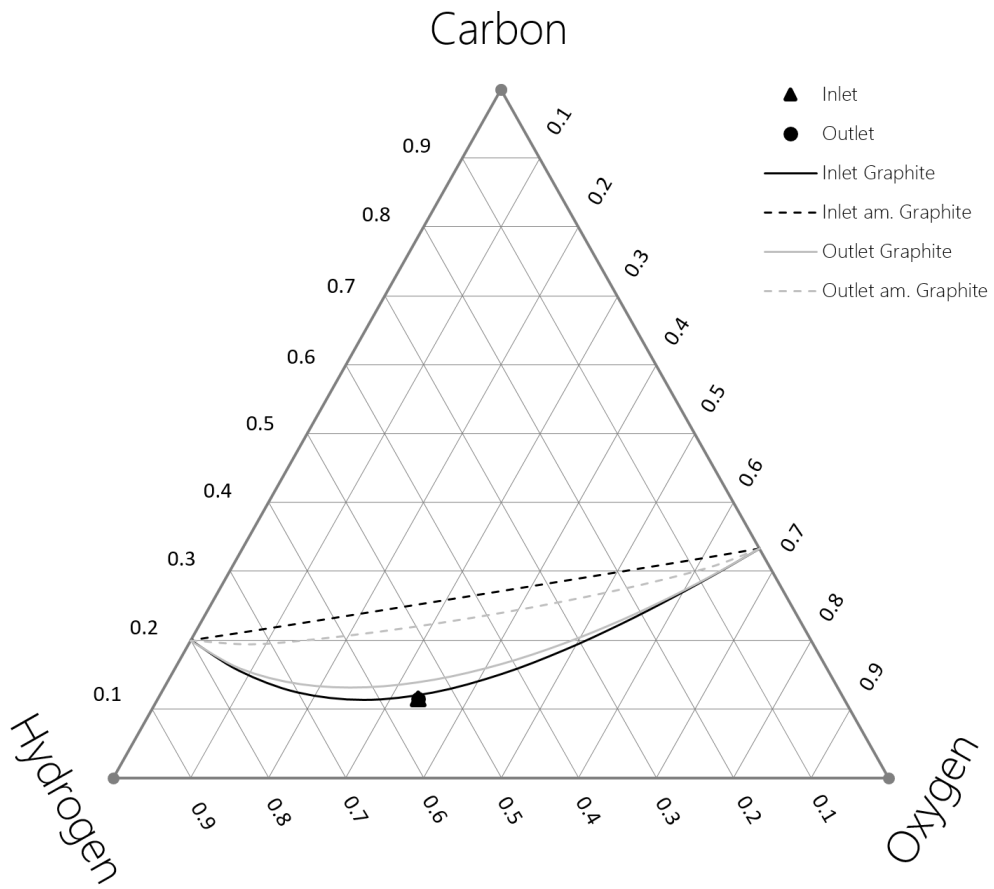

Figure 4.25: Evaluation of the carbon, hydrogen and oxygen equilibrium at inlet and outlet conditions of the 1st water-gas-shift reactor of the Selexol™ cold gas cleanup case.

tion of the syngas. The solid line shows the equilibrium curve for graphite, the dashed line for amorphous graphite. Black lines represent the reactor inlet conditions and gray lines represent the outlet conditions. The triangle and circle show the reactor inlet and outlet composition. Gas compositions above the equilibrium composition are unstable and can lead to carbon deposition. In this case, the formation of graphite is more critical than the formation of amorphous graphite and will function as the design limit. With the addition of water (67 % H, 33 % O), the atomic composition of the syngas can be changed. Adding water moves the final composition closer to the state of water. This way the initial gas composition can be moved across the critical equilibrium line. In this study, a 1 % surplus (with respect to total molar flow) of water is added to ensure that the inlet gas composition

is not too close to the critical equilibrium composition. The carbon equilibrium is mostly dependent upon temperature. Solid carbon is favored at lower temperatures, CO_2 and CO are favored at higher temperatures. Thus, in most cases the inlet condition of the second shift reactor represents the limiting case.

The equilibrium curves for the low temperature water-gas-shift reactor is shown in Figure 4.26.

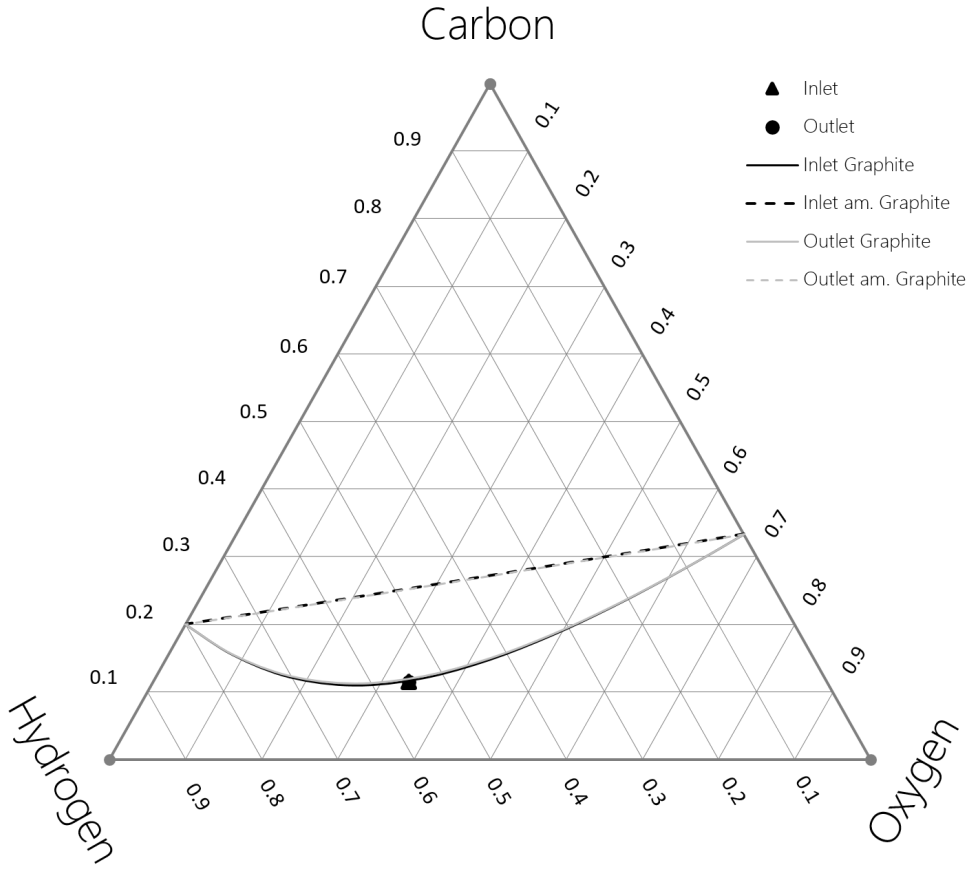

Figure 4.26: Evaluation of the carbon, hydrogen and oxygen equilibrium at inlet and outlet conditions of the 2nd water-gas-shift reactor of the Selexol™ cold gas cleanup case.

Since the second water-gas-shift reactor has a much smaller temperature difference between inlet and outlet, the equilibrium curves for both states almost coincide. Inlet and outlet gas compositions are almost the same since no chemical components are added inside the reactor during the reaction. For the syngas composition obtained from the TRIG™

gasifier, a steam to carbon monoxide ratio of 2.80 ensures safe operation of the first and second shift reactor.

The analysis of this case shows that the DoE target of 90 % carbon capture cannot be achieved in this case. One reason is the high methane content in the syngas, which cannot be converted by shift reactors. Secondly, the shift reactors are already converting 98.7 % of the CO to CO_2. Further shifting would result in significant additional cost because this would require a third reactor with an enormous amount of catalyst. Ultimately this would lead to a huge pressure drop as well. Alternatively, the amount of steam added could be increased. However, this would impair the plant efficiency. Lastly, the Selexol^{TM} process does not have the necessary CO_2 capture yield to achieve carbon capture greater 83.4 %. Thus, it is not possible to improve the carbon capture with an optimization of the water-gas-shift section in the Selexol^{TM} case. Nevertheless, it is possible to improve the plant efficiency, however, only at the expense of the carbon capture.

Analysis of the Warm Gas Cleanup Scenario

The high temperature shift reactor of the warm gas cleanup scenario is almost identical to the cold gas cleanup case and will not be discussed in detail. The temperature profile and temperature increase are the same for both reactors. The same is true for the intrinsic reaction rate, apparent reaction rate, catalyst effectiveness, mass transfer quantities, heat transfer quantities and rate optimization number, which show exactly the same behavior as discussed in the first part of Section 4.4.4. Small differences between the cold gas cleanup and warm gas cleanup cases are present in the species profiles of the high temperature water-gas-shift reactor. Due to the smaller coal flow, the total molar flow of syngas entering the shift reactor is smaller. However, this does not affect the general shape of the profiles. It only leads to a shift to lower molar flows. For completion, the results of the analysis of high

temperature shift reactor of the warm gas cleanup scenario are given in appendices C.1 - C.6. The analysis of the equilibrium is provided in B.1. As a result of the reduced molar flow, the required catalyst volume is reduced to 140.5 m^3. The pressure drop remains the same, 1.24 bar. It is assumed that only the diameter of the reactor is resized which leads to the same internal velocities and pressure drop.

The low temperature shift reactor in the warm gas cleanup scenario differs from the low temperature shift reactor in the Selexol^{TM} case. In the warm gas cleanup case, sulfur is removed from the syngas after the first shift reactor and the reactor uses the alumina supported Cu/Zn alloy sweet shift low-temperature catalyst described in Section 4.4.3. The reactor inlet temperature is identical to the low temperature shift reactor in the cold gas cleanup scenario. On the way through the reactor, the syngas is heated from 204 °C to 222 °C. The profile of the temperature inside the reactor is shown in Figure 4.27.

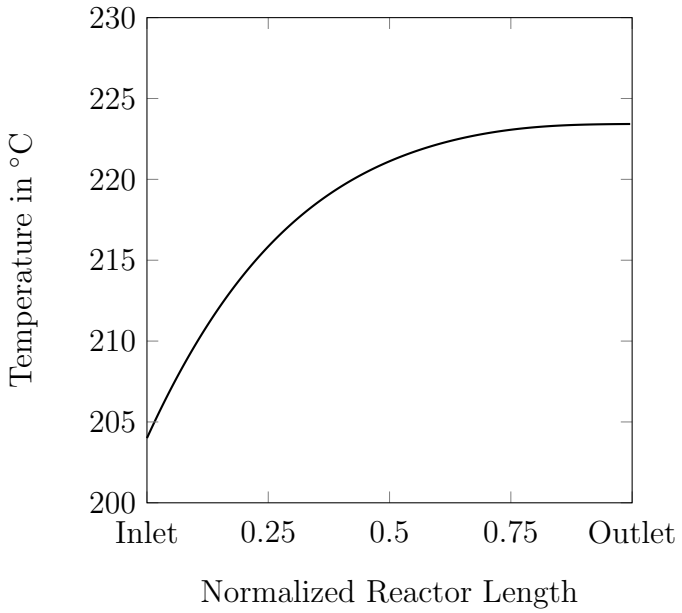

Figure 4.27: Temperature profile of the 2nd shift reactor of the CO_2-PSA warm gas cleanup base scenario using a low temperature, sweet shift catalyst with a system sizing factor of 1.1.

The temperature increase is the strongest at reactor inlet and the slope levels off as

it approaches the reactor exit. In general, the trend is very similar to the low temperature reactor of the Selexol^{TM} case. Small differences can be identified in the initial slope at reactor inlet and the bending of the curve. The bending in the warm gas cleanup case is more gradual and wider compared to the cold gas case. This is due to the lower activation energy of the sweet shift catalyst and its higher dependency on the CO partial pressure. Also for the low temperature sweet shift catalyst, a 13.9 °C equilibrium temperature approach and a system sizing factor of 1.1 is used. The linear increase at reactor inlet and the subsequent bending of the curve have the same origin as discussed for the low temperature shift reactor in the cold gas cleanup scenario.

The species profiles of the species participating in the water-gas-shift reaction are illustrated in Figure 4.28.

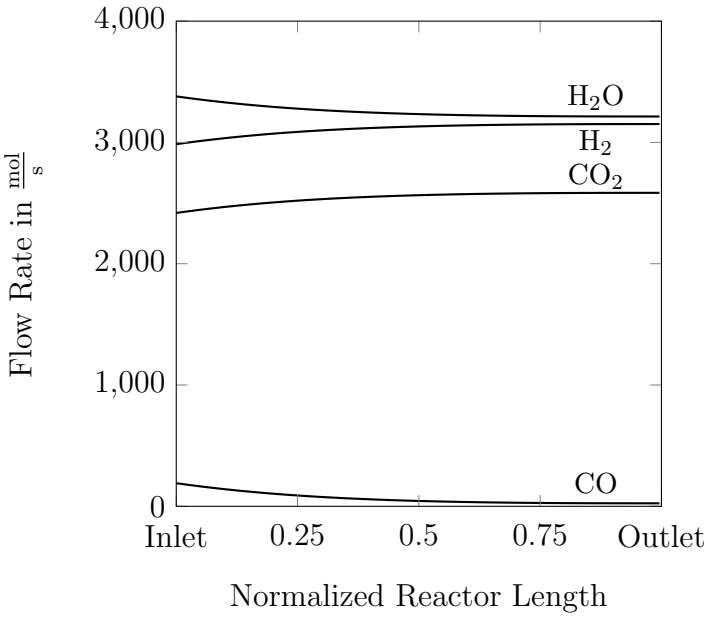

Figure 4.28: Species profiles of the 2nd shift reactor of the CO_2-PSA warm gas cleanup base scenario using a low temperature, sweet shift catalyst with a system sizing factor of 1.1.

Changes in the species flows are only small in the second shift reactor. The species flow profiles are almost identical to the low temperature shift reactor in the cold gas cleanup case. The decay of reactant species and the increase in product species concentrations are more

gradual than those in the cold gas clean up case but the final gas composition is essentially the same. The total CO conversion after the second shift reactor in the warm gas cleanup case is 98.7 %, which matches the performance of the cold gas cleanup case. In total, the syngas molar flow is smaller due to the higher efficiency of the warm gas cleanup scenario and limitations in the gas turbine inlet air flow. However, this does not affect the reactor performance, and it only affects the reactor size.

The evaluation of the reaction rates and the catalyst effectiveness are shown in Figure 4.29.

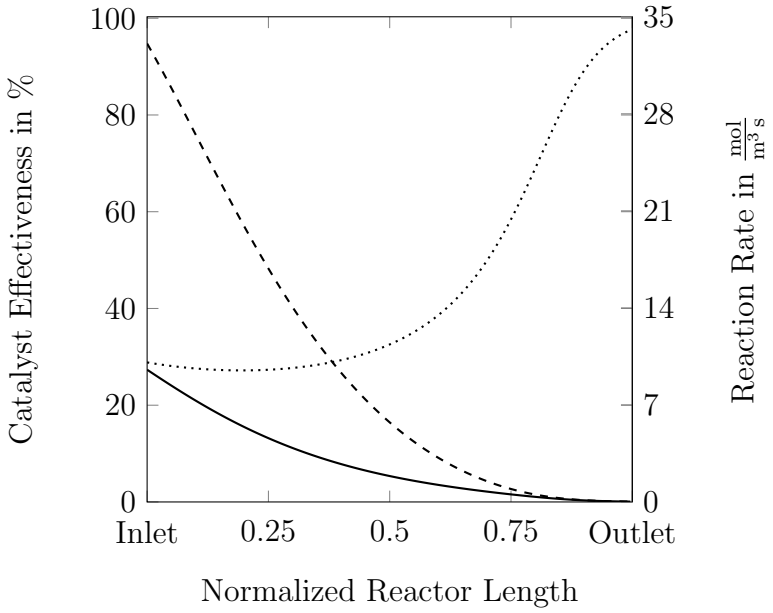

Figure 4.29: Catalyst effectiveness (·····), intrinsic ration rate (- - -) and apparent reaction rate (——) of the 2nd shift reactor of the CO_2-PSA warm gas cleanup base scenario using a low temperature, sweet shift catalyst with a system sizing factor of 1.1.

The reaction kinetics of the sweet shift catalyst are much faster than the reaction kinetics of the sour shift catalyst. The intrinsic reaction rate has its maximum value of 33 $\frac{\text{mol}}{\text{m}^3\,\text{s}}$ at the reactor inlet and then decays quickly until it zeros out when the reactor outlet is reached. The decay at the beginning is relatively linear and eventually starts bending at a reactor location of 0.20. The same behavior is observed for the intrinsic rate, however, its

maximum value starts at 10 $\frac{\text{mol}}{\text{m}^3\,\text{s}}$. The almost linear decay of the reaction rate at the beginning shows that the influence of temperature is countered by the reduction in CO in the first section of the reactor. The rates of the sweet shift catalyst are 10.6 times (intrinsic) and 3.4 times (apparent) larger than that for the sour shift catalyst. The improved kinetics are the major reason why sweet shift catalyst are preferred over sour shift catalyst. However, sweet shift catalysts are very prone to sulfur poisoning and can be only used after desulfurization of the syngas. The catalyst effectiveness of the sweet shift catalyst is lower than the sour shift catalyst. One reason is that the characteristic length of the sweet shift catalyst pellet is longer, but the observed effect is mostly due to the higher reaction rate that moves the reaction closer to the pore inlet and less of the internal surface area is effectively used. The catalyst effectiveness remains relatively constant in the first half of the reactor and then increases as the reaction approaches equilibrium. Since the effectiveness factor is the result of the ratio between apparent and intrinsic reaction rate, the constant course in the first reactor half can be explained with the linear behavior of both reaction rates. Later, the intrinsic and apparent reaction rates level off and cause the effectiveness factor to increase. On a physical basis, this can be explained with accessibility of the internal surface area by diffusion as described above.

The total pressure drop of the sweet shift reactor is 1.51 bar, whereby 1.42 bar of the total pressure drop are caused by the fluid dynamics inside the catalyst bed, which occupies a volume of 59.0 m^3. This is a significant reduction compared to the sour shift catalyst and can potentially lead to a cost reduction of the power plant. The sweet shift reactors have a diameter of 3.15 m.

Plots of the Weisz-Prater modulus, Ca number, Mears modulus for internal heat transfer, Mears modulus for external heat transfer and the Ro number are shown in appendix C.7 - C.9. The maximum values of the Weisz-Prater modulus and the Ca number are 3.7 and 0.01 which indicates limitations by internal diffusion but no limitations due to external mass transfer. Maximum values for the Mears moduli for internal and external heat transfer are:

0.003 and 0.004. This justifies the assumption of an isothermal catalyst particle and shows that the impact of external heat transfer is extremely small.

The equilibrium graph, Figure 4.30, of the low temperature sweet shift reactor is identical to the sour shift reactor since the steam to carbon monoxide ratio of 2.80 is used and the reactor inlet temperatures are the same.

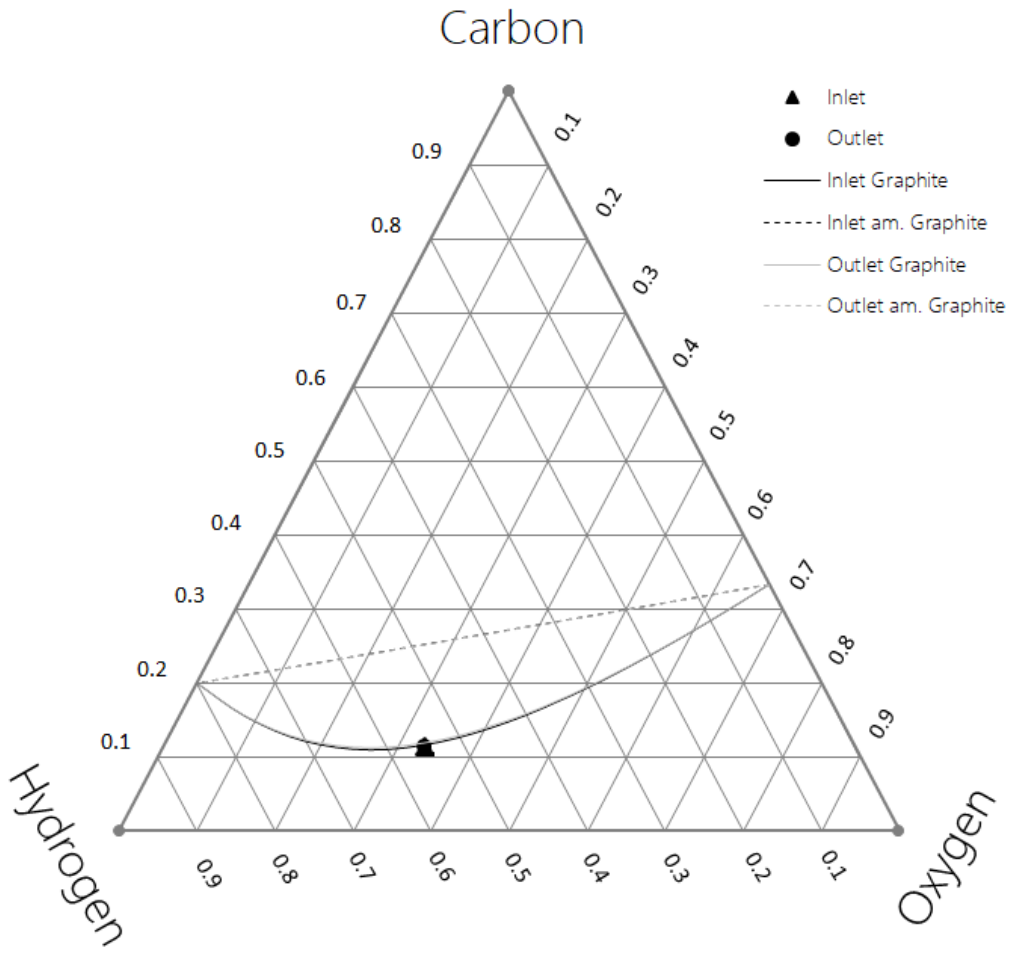

Figure 4.30: Evaluation of the carbon, hydrogen and oxygen equilibrium at inlet and outlet conditions of the 2nd water-gas-shift reactor of the CO_2-PSA warm gas cleanup base case.

However, because the warm gas cleanup case uses a carbon capture technology with a higher yield, the interpretation is a different one. Sending all the syngas through the CO_2-

PSA would result in a carbon capture of 88.6 % at a plant efficiency of 33.9 %. As a result of this, a certain fraction of the syngas is bypassed in order to compare the two technologies upon the same basis. A higher carbon capture would increase the steam requirement for sorbent regeneration and add a penalty to the plant performance.

An alternative option to bypassing some of the syngas around the CO_2-PSA is to limit conversion of the shift reactors. Adjusting the conversion accordingly to the CO_2 yield of the CO_2-PSA can potentially reduce the steam requirements and boost the plant efficiency. Another advantage of shifting only the minimal required amount of CO is an increase in the heating value of the syngas. Chemical energy has a higher value than thermal energy. If CO is shifted in the shift reactor, its released energy has to be captured in the form of heat, which can be utilized in the Rankine cycle. However, if CO is combusted directly in the gas turbine the energy yield is higher leading to an increased efficiency. This option will be explored in the following section.

4.4.5 Optimization of the Water-Gas-Shift Section

Important for adjusting the CO conversion of the shift unit is the outlet temperature of the last shift reactor. Thermodynamic equilibrium predicts lower CO conversion at higher temperatures. Raising the inlet temperature of the shift reactor will ultimately increase the outlet temperature and simultaneously change the steam requirement necessary to avoid carbon deposition. As shown in Figure 4.10, the carbon equilibrium line is strongly dependent upon temperature. Gas compositions with a very high H:O ratio can lead to an increase of the steam requirement. However, for most compositions, a higher operating temperature leads to a decrease in steam requirement. The atomic composition of the syngas before the addition of shift steam is H:C:O = 0.44:0.22:0.34. The composition has a well-balanced H:O ratio and finds itself in the central part of the diagram. This opens the possibility of reducing

the shift steam requirement and increasing the overall plant performance.

Optimization I – 2 Adiabatic High Temperature Shift Reactors.

The first optimization uses a very similar plant configuration as the un-optimized warm gas cleanup base scenario. Instead of preheating and humidifying the syngas simultaneously by using just steam, an additional heat exchanger is necessary to raise the temperature to 315 °C before it enters the first shift reactor. The heat input for this additional heat is provided by the high pressure boiler feed water. Subsequent to the syngas preheater, shift steam is added. After shifting the syngas is desulfurized and cooled to the same inlet temperature as the first reactor before it enters the second shift reactor. As result of this increased temperature, the second reactor uses the Fe/Cr based high temperature shift catalyst. A flow sheet of the plant design is shown in Figure 4.31. A summary of the major streams indicated in the flow sheet are provided in Table 4.17. Additionally, a stream summary with constant coal mass flow is provided in the appendix Table A.2.

Setting both reactor inlet temperatures to the same value is most effective. The smaller the temperature rise in the last reactor, the higher the inlet temperature can be while maintaining the same CO conversion. If the inlet temperature for the first reactor is lower, the higher the conversion in the first reactor will be. This leads to less conversion in the second reactor and a smaller temperature increase. As a result, both reactor inlet temperatures have to be the same to maximize conversion in the first reactor and minimize the steam requirement. For this setup, a temperature of 315 °C was determined to deliver the right amount CO_2 to achieve the same carbon capture as in the Selexol^{TM} case, 83.4 %. Concurrently with the temperature determination, the steam requirement was iteratively calculated by using the whisker carbon equilibrium algorithm. By using a reactor inlet temperature of 315 °C, the steam to carbon monoxide ratio is reduced from 2.80 to 2.16 while still operating

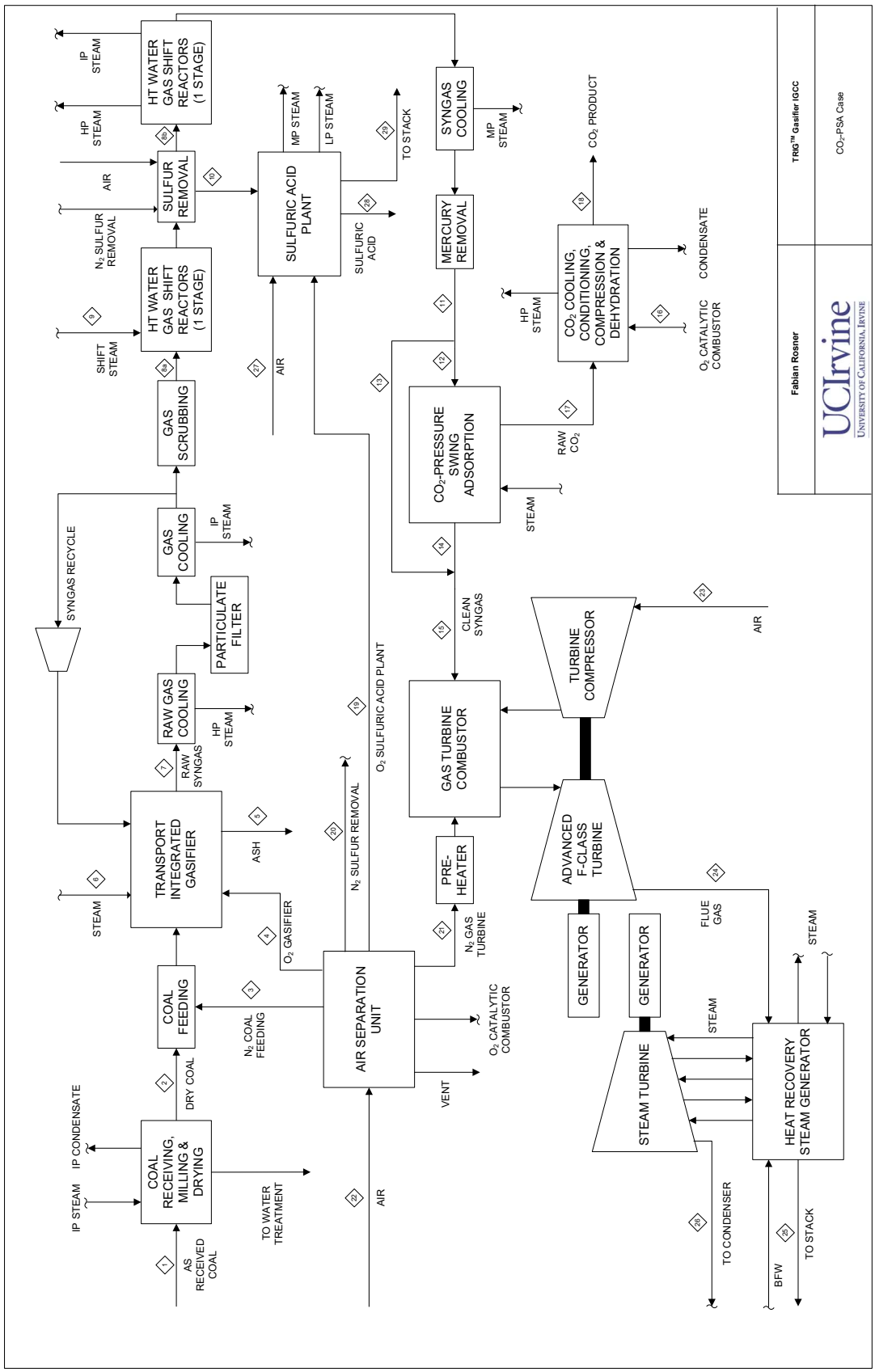

Figure 4.31: Flow sheet of the Optimization I CO_2-PSA warm gas cleanup case with 2 high temperature shift reactors.

Table 4.17: Stream Summary of the Optimization I CO_2-PSA Warm Gas Cleanup Case at Fully Loaded Gas Turbine

Stream Number	Unit	1	2	3	4	5	6	7	8a	8b	9	10	11	12	13	14
Temperature	°C	5.6	71.1	105.9	74.2	982.2	397.9	982.2	161.7	492.9	382.0	760.0	199.0	199.0	0.0	203.0
Pressure	bar	0.9	0.9	56.2	50.3	3.4	51.0	41.7	38.3	35.3	51.0	33.9	32.7	32.7	0.0	32.4
Molar Flowrate	kmol/h	-	-	1635	4093	-	3439	24541	19389	29551	10162	498	29534	29534	0	21863
Mass Flowrate	kg/h	-	-	45887	131841	-	61947	526844	413611	595766	183075	16070	595470	595470	0	234905
Solid Flowrate	kg/h	253450	229434	-	-	23289	-	-	-	-	-	-	-	-	-	-
Mass Vapor Fraction	-	0	0	1	1	0	1	1	1	1	1	1	1	1	0	1
Composition	mol-basis															
O_2	-	0.00000	0.00000	0.00540	0.95014	0.00000	0.00000	0.00000	0.00000	0.00000	0.00000	0.01077	0.00000	0.00000	0.00000	0.00000
N_2	-	0.00000	0.00000	0.99230	0.01551	0.00000	0.00000	0.00500	0.00480	0.00315	0.00000	0.86409	0.00315	0.00315	0.00000	0.00421
Ar	-	0.00000	0.00000	0.00230	0.03435	0.00000	0.00000	0.00755	0.00725	0.00476	0.00000	0.00858	0.00476	0.00476	0.00000	0.00637
H_2	-	0.00000	0.00000	0.00000	0.00000	0.00000	0.00000	0.27132	0.26069	0.33390	0.00000	0.00000	0.36567	0.36567	0.00000	0.48888
CO	-	0.00000	0.00000	0.00000	0.00000	0.00000	0.00000	0.34260	0.32917	0.05311	0.00000	0.00000	0.02158	0.02158	0.00000	0.02885
CO_2	-	0.00000	0.00000	0.00000	0.00000	0.00000	0.00000	0.16171	0.15537	0.26493	0.00000	0.00026	0.29665	0.29665	0.00000	0.00638
H_2O	-	0.00000	0.00000	0.00000	0.00000	0.00000	1.00000	0.15369	0.18689	0.30546	1.00000	0.00122	0.27407	0.27407	0.00000	0.42207
CH_4	-	0.00000	0.00000	0.00000	0.00000	0.00000	0.00000	0.05128	0.04927	0.03233	0.00000	0.00000	0.03234	0.03234	0.00000	0.04324
H_2S	-	0.00000	0.00000	0.00000	0.00000	0.00000	0.00000	0.00289	0.00277	trace	0.00000	0.00000	trace	trace	0.00000	trace
NH_3	-	0.00000	0.00000	0.00000	0.00000	0.00000	0.00000	0.00374	0.00359	0.00236	0.00000	0.00000	0.00177	0.00177	0.00000	0.00000
COS	-	0.00000	0.00000	0.00000	0.00000	0.00000	0.00000	0.00020	0.00019	trace	0.00000	0.00000	trace	trace	0.00000	trace
HCl	-	0.00000	0.00000	0.00000	0.00000	0.00000	0.00000	trace	0.00000	0.00000	0.00000	0.00000	0.00000	0.00000	0.00000	0.00000
SO_2	-	0.00000	0.00000	0.00000	0.00000	0.00000	0.00000	0.00000	0.00000	0.00000	0.00000	0.11508	0.00000	0.00000	0.00000	0.00000
Total	-	0	0	1	1	0	1	0.99997	1	0.99999	1	1	0.99999	0.99999	0	1

Stream Number	Unit	15	16	17	18	19	20	21	22	23	24	25	26	27	28	29
Temperature	°C	203.0	145.3	187.1	35.0	32.2	69.0	105.9	5.6	5.6	565.0	151.9	32.4	5.6	20.0	43.3
Pressure	bar	32.4	20.5	9.7	152.7	8.6	41.2	26.2	0.9	0.9	0.9	0.9	0.05	0.9	0.9	0.9
Molar Flowrate	kmol/h	21863	83	14827	8645	35	92	8221	20143	100248	124102	124102	25061	285	84	768
Mass Flowrate	kg/h	234905	2663	489500	380404	1117	2590	230693	582021	2896627	3346212	3346212	451474	8248	6088	21235
Solid Flowrate	kg/h	-	-	-	-	-	-	-	-	-	-	-	-	-	-	-
Mass Vapor Fraction	-	1	1	1	1	1	1	1	1	1	1	1	0.91463	1	0	1
Composition	mol-basis															
O_2	-	0.00000	0.95001	0.00000	trace	0.95001	0.00540	0.00540	0.20810	0.20810	0.10759	0.10759	0.00000	0.20810	0.00000	0.03926
N_2	-	0.00421	0.01406	trace	0.00025	0.01406	0.99230	0.99230	0.77590	0.77590	0.68867	0.68867	0.00000	0.77590	0.00000	0.88205
Ar	-	0.00637	0.03594	trace	0.00051	0.03594	0.00230	0.00230	0.00930	0.00930	0.00878	0.00878	0.00000	0.00930	0.00000	0.01063
H_2	-	0.48888	0.00000	0.00749	trace	0.00000	0.00000	0.00000	0.00000	0.00000	0.00000	0.00000	0.00000	0.00000	0.00000	0.00000
CO	-	0.02885	0.00000	0.00044	trace	0.00000	0.00000	0.00000	0.00000	0.00000	0.00000	0.00000	0.00000	0.00000	0.00000	0.00000
CO_2	-	0.00638	0.00000	0.58148	0.99924	0.00000	0.00000	0.00000	0.00030	0.00030	0.01407	0.01407	0.00000	0.00030	0.00000	0.00034
H_2O	-	0.42207	0.00000	0.40624	0.00000	0.00000	0.00000	0.00000	0.00640	0.00640	0.18089	0.18089	1.00000	0.00640	0.31959	0.06758
CH_4	-	0.04324	0.00000	0.00066	trace	0.00000	0.00000	0.00000	0.00000	0.00000	0.00000	0.00000	0.00000	0.00000	0.00000	0.00000
H_2S	-	trace	0.00000	trace	trace	0.00000	0.00000	0.00000	0.00000	0.00000	0.00000	0.00000	0.00000	0.00000	0.00000	0.00000
NH_3	-	0.00000	0.00000	0.00352	0.00000	0.00000	0.00000	0.00000	0.00000	0.00000	0.00000	0.00000	0.00000	0.00000	0.00000	0.00000
COS	-	trace	0.00000	trace	trace	0.00000	0.00000	0.00000	0.00000	0.00000	0.00000	0.00000	0.00000	0.00000	0.00000	0.00000
HCl	-	0.00000	0.00000	0.00000	0.00000	0.00000	0.00000	0.00000	0.00000	0.00000	0.00000	0.00000	0.00000	0.00000	0.00000	0.00000
SO_2	-	0.00000	0.00000	0.00000	trace	0.00000	0.00000	0.00000	0.00000	0.00000	trace	trace	0.00000	0.00000	0.00000	0.00015
Total	-	1	1	0.99984	0.99999	1	1	1	1	1	1	1	1	1	0.31959	1

the reactors in the stable gas regime.

The whisker carbon equilibrium curves of the first shift reactor can be seen in Figure 4.32.

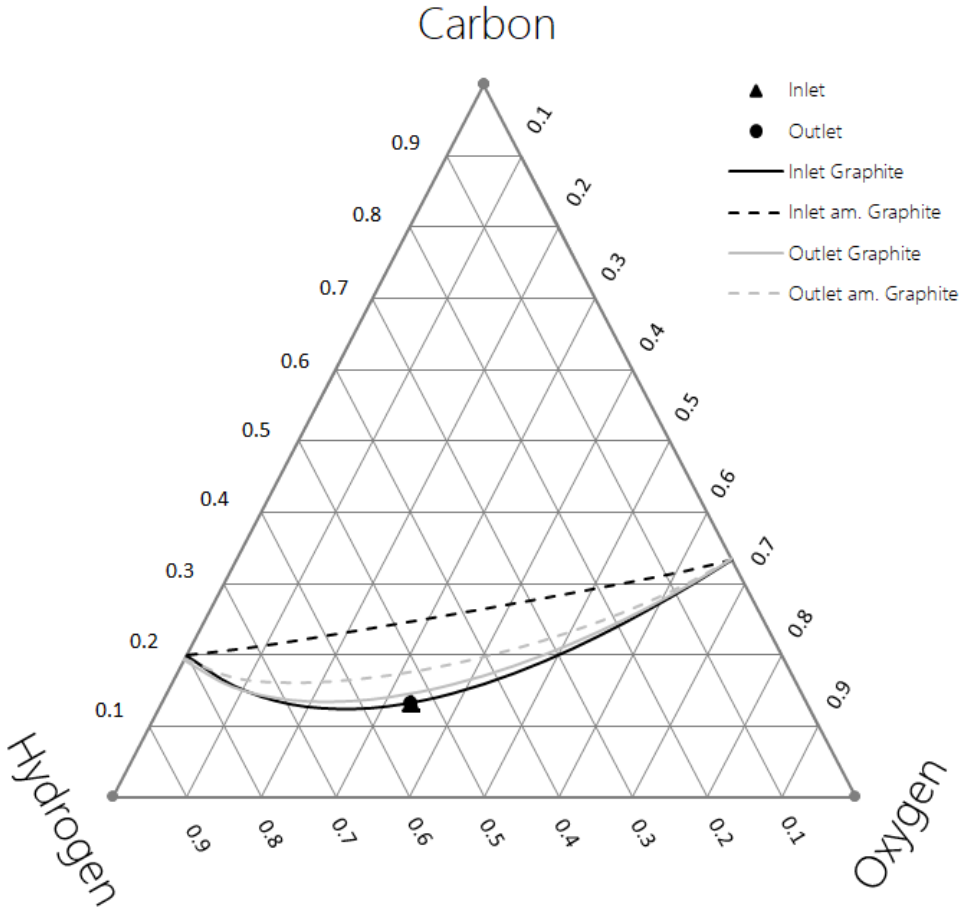

Figure 4.32: Evaluation of the carbon, hydrogen and oxygen equilibrium at inlet and outlet conditions of the 1st water-gas-shift reactor of the warm gas clean up case.

The solid black line represents the equilibrium line of graphite for reactor inlet conditions, which is 315 °C. The outlet temperature of the first shift reactor is 493 °C and is represented by the gray line. The dashed lines show the equilibrium curves for amorphous carbon but those are not relevant in this analysis. Compared to the equilibrium curve of the second shift reactor of the previous cases (Figures 4.26 and 4.30), it is visible how the equi-

librium curve has been shifted upwards. Due to the significantly higher outlet temperature of the first shift reactor, the equilibrium curve at outlet condition lies even higher than the inlet condition.

The equilibrium curves of the second shift reactor are shown in Figure 4.33.

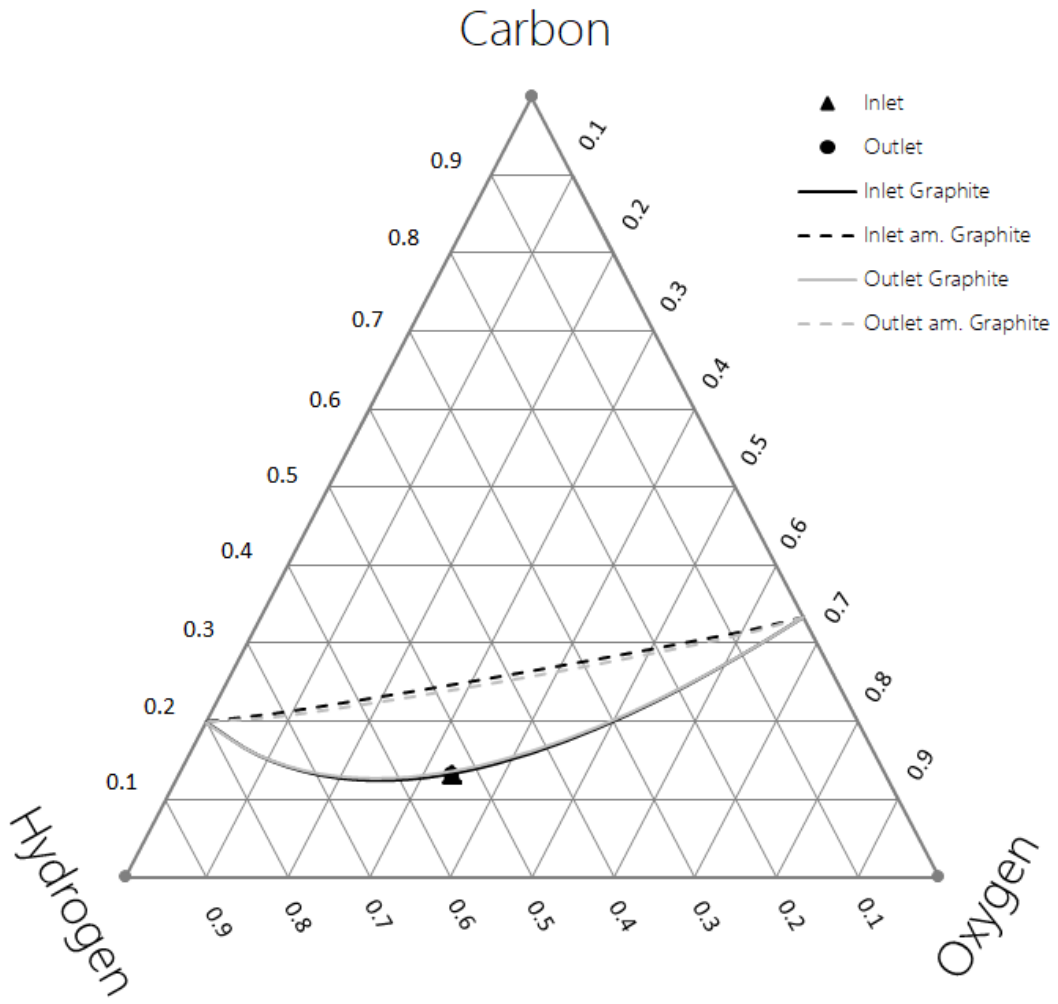

Figure 4.33: Evaluation of the carbon, hydrogen and oxygen equilibrium at inlet and outlet conditions of the 2nd water-gas-shift reactor of the warm gas clean up case.

The outlet temperature of the second shift reactor is 347 °C, which is much closer to inlet condition than the outlet temperature of the first shift reactor. Thus, the equilibrium curves are much closer to each other. The reactor inlet curves for the first shift and second

shift reactor are almost identical as well since both have the same inlet temperature. Just the lower syngas pressure causes small deviations in the equilibrium line. This shows that both reactors operate close to the minimum steam to carbon monoxide ratio. The steam to carbon monoxide ratio in this context is always referred to the point before the syngas enters the first shift reactor. Looking at the steam to carbon monoxide ratio before the second shift reactor, the true steam to carbon monoxide ratio is 5.74. However, nothing changes with respect to the atomic composition or the gases' stability as it can be seen in Figure 4.33. Often found in literature is the steam to carbon ratio, but this also does not include hydrogen, which plays an important role in the stability of a gas. Thus, it is important to always analyze gas mixtures based on the entire equilibrium and not just on a ratio of steam to carbon monoxide or steam to carbon.

The impact of raising the operating temperature of the water-gas-shift on the reactor design and its internals will be covered in the following section. The design specification of the water-gas-shift reactors operating at higher temperature is the same as it is for the previously discussed water-gas-shift reactors. Likewise, a system sizing factor of 1.25 is used for the first reactor to be less compromised by poisoning. Furthermore, an equilibrium approach temperature of 13.9 °C is applied again.

The temperature profile of the first shift reactor is shown in Figure 4.34.

Within the first half of the reactor, the temperature increases from 315 °C to 393 °C. In the second half of the reactor, the temperature remains constant after passing through 80 % of the reactor. The slope of the temperature rise increases slightly at reactor inlet until a reactor length of 0.08 is reached. Then, the slope starts to level off slowly and the temperature remains constant after reaching a reactor length of 0.8. As described earlier, the increase in the slope is an indication for an increase in the reaction kinetics. The reaction kinetics are influenced by the temperature exponentially. Later, the lowering CO partial pressure and the decreasing chemical potential induce a slowdown of the reaction

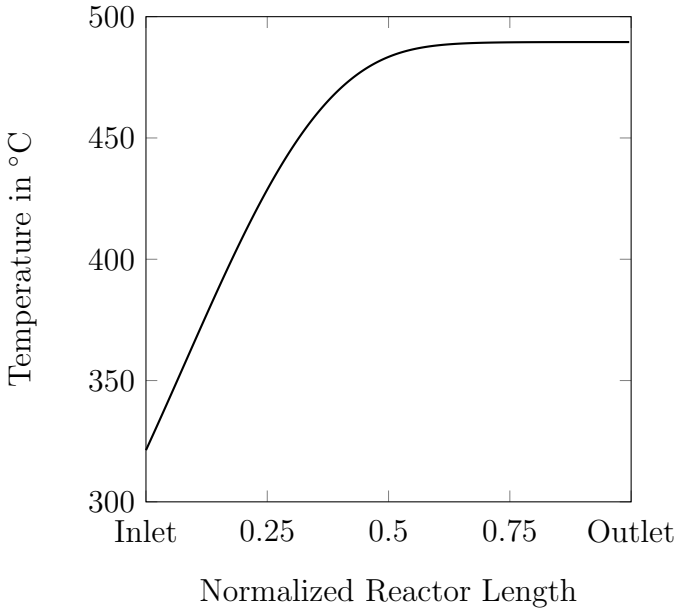

Figure 4.34: Temperature profile of the 1st shift reactor of the Optimization I CO_2-PSA warm gas cleanup scenario using a high temperature, sour shift catalyst with a system sizing factor of 1.25.

rate. Compared to the other cases, the temperature increase in the Optimization I case with 78 °C versus 151 °C is much smaller. This suggests that the CO conversion in the first shift reactor of the optimization scenario is much smaller, too. The higher inlet temperature and the lower steam partial pressure in the optimization scenario entail a lower chemical potential difference at reactor inlet compared to the other cases, which affects the kinetics, heat generation density and thermodynamic equilibrium all the way to the reactor outlet.

The CO conversion in the first reactor is 75.4 % and thus 13.7 % − points lower than in the previous cases. This can be inferred from the species profiles shown in Figure 4.35.

The species profiles of the products have a very similar shape as the temperature profile; reaction reactants follow an inverse behavior. Considering that heat can be seen as an additional reaction product – exothermic reaction – this behavior is a logical consequence. Subsequently, the explanation of the change in slope of the temperature profile can be transferred one to one. In the very first section of the reactor, the temperature increase accelerates the reaction and a faster change in species is the consequence. A buildup of product species

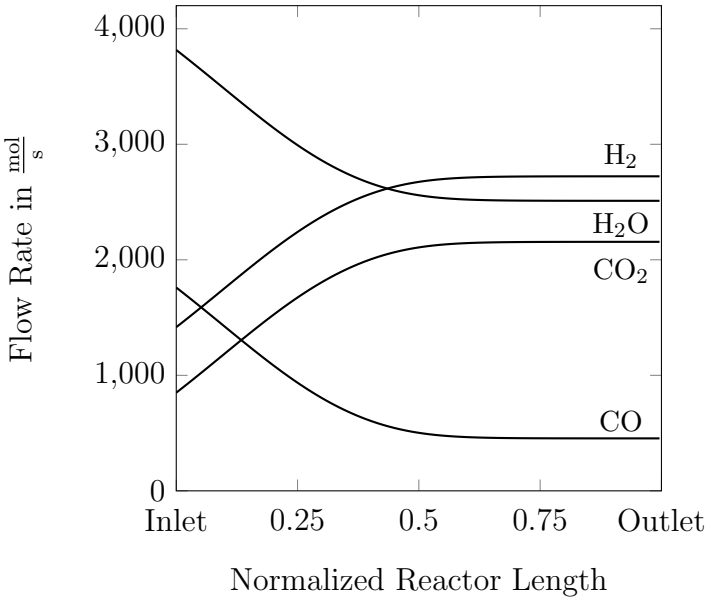

Figure 4.35: Species profiles of the 1st shift reactor of the Optimization I CO_2-PSA warm gas cleanup scenario using a high temperature, sour shift catalyst with a system sizing factor of 1.25.

and a decay of reactant species following this initially fast conversion slows down the reaction, reactant consumption and product generation, until equilibrium is established. Due to the lower water input in the optimized scenario, the water content in the syngas drops below the hydrogen content after reaching equilibrium and it no longer represents the dominant species in the syngas. This also affects the heating value of the syngas but will be further discussed after analyzing the second shift reactor.

Qualitative conclusions on the reaction rate could be already drawn from the temperature and species profiles. A quantitative analysis of the reaction rate and catalyst effectiveness is provided in Figure 4.36.

The trends in Figure 4.36 are very similar to the high temperature shift reactors previously discussed. As anticipated from the temperature and species profiles, the reaction rate increases first, reaches a maximum and decays to zero. As discussed before, the acceleration of the reaction kinetics is driven by the temperature increase, which is incorporated into the rate equation exponentially. Further downstream, the influence of the reactant and product

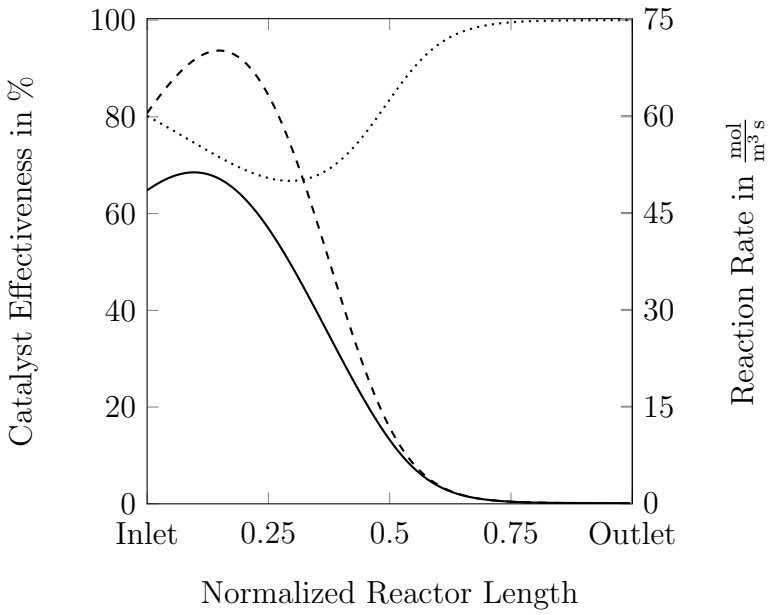

Figure 4.36: Catalyst effectiveness (·····), intrinsic reaction rate (- - -) and apparent reaction rate (——) of the 1st shift reactor of the Optimization I CO_2-PSA warm gas cleanup scenario using a high temperature, sour shift catalyst with a system sizing factor of 1.25.

partial pressures, as well as the chemical potential difference, impede the reaction. A comparison of the absolute reaction rates of apparent and intrinsic rates show that the initial and maximum reaction rates are much larger for the optimized shift reactor. The apparent rates are 2.4 times (initial) and 2.0 times (maximum) larger than those for the other cases. For the intrinsic rates the reaction rates are 2.8 times (initial) and 2.3 times (maximum) larger than those in the previous cases. As a logical consequence of these higher reaction rates, the reaction takes place close to the pore mouth and the catalyst effectiveness is lower than previously observed. The general course of the effectiveness curve from the warm gas cleanup base case is preserved in the Optimization I case since in the first shift reactor enough CO is present to generate a steep temperature increase that can accelerate the reaction kinetics faster than they are being slowed down by the decreasing CO partial pressure. At reactor inlet, the catalyst effectiveness is 80 % and drops to 67 % as reaction kinetics accelerate. The left-shift in the location of the maximum reaction rate of the apparent reaction rate compared to the intrinsic reaction rate is due to internal pore transport phenomena. The

average species concentration of CO inside the pore is smaller than in the bulk phase. Thus, the effective CO concentration for the intrinsic reaction rate is lower and leads to a faster decay in the reaction rate, which ultimately leads to this left-shift of the maximum value of the intrinsic reaction rate.

The required catalyst volume at these reaction rates is 67.3 m^3. Pressure drop caused by the bed is determined to be 1.19 bar resulting in a total pressure drop of 1.25 bar. The two high temperature sour shift reactors have a diameter of 3.51 m.

The dimensional analyses of heat transport, mass transport and reaction rate are presented in appendix C.10-C.12. Due to the increase in reaction rate, the internal mass diffusion limitation inside the catalyst particle increases significantly which has direct implications for the catalyst effectiveness as discussed above. Similarly, the external mass transfer number Ca increases also. However, the influence of the external mass transport remains negligibly small. The higher heat generation density of the faster reaction kinetics, also leads to an increase in the Mears moduli for internal and external heat transfer. Both moduli are sufficiently small to justify the model assumption of an isothermal catalyst particle. A comparison of the rate optimization number shows that the intersection with the -1 line in the Optimization I scenario is shifted to the left and that the range of the Ro number is larger than in the base case scenario indicating that with higher reactor inlet temperature cooling becomes more important in order to maximizes the reaction kinetics.

After the first shift reactor, the syngas is cooled down to 315 °C before it enters the second shift reactor. The temperature profile of the second shift reactor is given in Figure 4.37.

From inlet to outlet, the temperature increases from 315 °C to 347 °C. This is an increase by 32 °C. After the initial temperature increase, the slope levels off. The system sizing factor of the second reactor is 1.1 to ensure that equilibrium is essentially reached. A system sizing factor of 1.1 is sufficient for the second shift reactor since potential catalyst inhibitors will be trapped in the first reactor. Thus, in the last section of the reactor, equilibrium

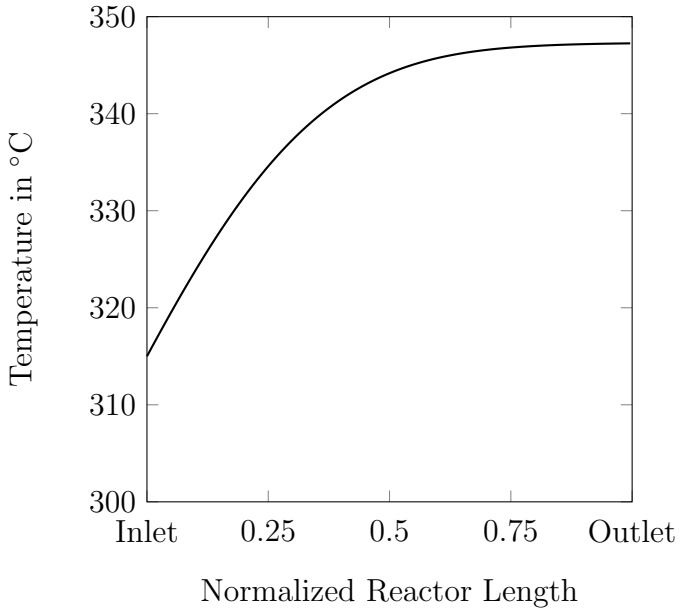

Figure 4.37: Temperature profile of the 2nd shift reactor of the Optimization I CO_2-PSA warm gas cleanup scenario using a high temperature, sweet shift catalyst with a system sizing factor of 1.1.

is established and the temperature remains constant. Due to the low CO concentration in the syngas leaving the first shift reactor, the energy released per unit volume is not enough to accelerate the reaction as in the first reactor. Thus, a steady decay of the slope of the temperature curve is observed, which is governed by the low CO partial pressure.

The total conversion after the second shift reactor is 90.0 %. This is sufficient to capture 83.4 % of the carbon dioxide for sequestration. A large amount of CO is shifted in the first reactor and only 4.6 % of the total CO entering the shift section is converted in the second shift reactor. The species profile of the second shift reactor is shown in Figure 4.38.

The reactant species decrease slowly, and product species increase inversely to the reactant decay rate. Equimolar shifting leads to a parallel profile among product and reactant species. In comparison to the lower temperature shift reactors with higher steam to carbon monoxide ratios, the reduction of water in this case is clearly visible. The higher heating value of the syngas leaving the second shift reactor is $7,580\ \frac{\text{kJ}}{\text{kg}}$ for the Optimization I case. For the cold gas cleanup Selexol$^{\text{TM}}$ case and warm gas cleanup base cases with low temperature shift

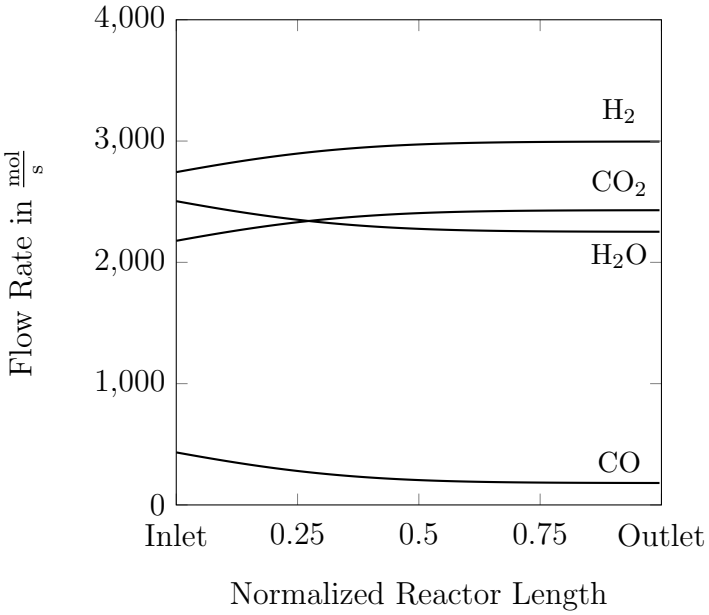

Figure 4.38: Species profiles of the 2nd shift reactor of the Optimization I CO_2-PSA warm gas cleanup scenario using a high temperature, sweet shift catalyst with a system sizing factor of 1.1.

reactor, the syngas exiting the shift reactor has a higher heating value of $6,987\ \frac{\text{kJ}}{\text{kg}}$. After decarbonization, the heating value will be upgraded but the consequence of a higher heating value is a higher nitrogen requirement for dilution of the syngas before being injected into the gas turbine.

As mentioned before, the inlet temperature of the second reactor in the Optimization I scenario is 315 °C which requires the use of a high temperature Fe/Cr catalyst. It is important to eliminate the possibility of byproduct formation, in particular Fischer-Tropsch liquids when using Fe based catalysts. The R_{FT}-values at reactor inlet and outlet conditions are 1.44 and 1.68 respectively. These values are safely below the critical value of 1.9 [104].

The catalyst effectiveness and reaction rates are shown in Figure 4.39.

The maximum value of the apparent reaction rate is $8\ \frac{\text{mol}}{\text{m}^3\,\text{s}}$ and the intrinsic rate has a maximum of $11\ \frac{\text{mol}}{\text{m}^3\,\text{s}}$. The values are much higher than those for the low temperature shift reactor in the Selexol$^{\text{TM}}$. Compared to the low temperature sweet shift reactor, the intrinsic reaction rate is much smaller, but the apparent reaction rate is more similar. Although the

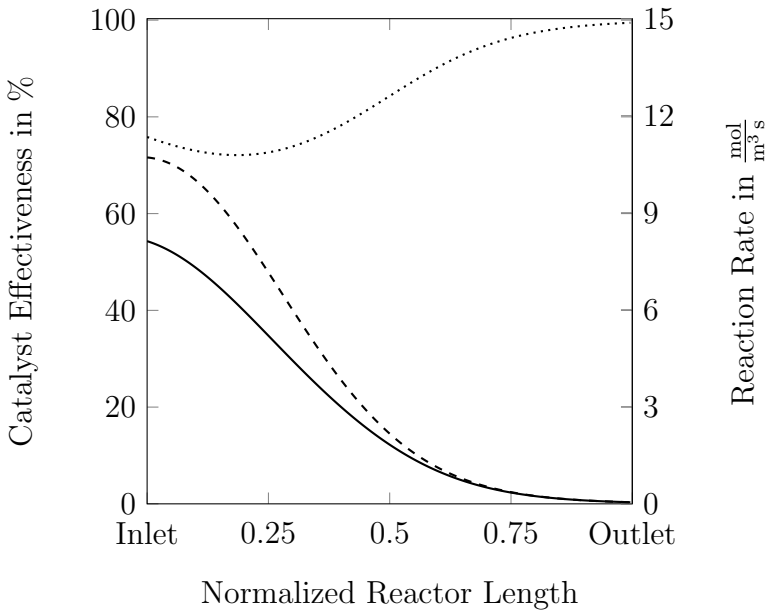

Figure 4.39: Catalyst effectiveness (·····), intrinsic ration rate (- - -) and apparent reaction rate (——) of the 2nd shift reactor of the Optimization I CO_2-PSA warm gas cleanup scenario using a high temperature, sweet shift catalyst with a system sizing factor of 1.1.

shift reactor in the Optimization I scenario is operated at higher temperature, which helps with the kinetics, the activity of the high temperature reactor is not as high as for the low temperature shift catalyst and there is no advantage over the low temperature sweet shift reactor with respect to kinetics. The low temperature sweet shift catalyst is in general more reactive but cannot be used at high temperatures and thus, an iron based catalyst has to be used. If the apparent reaction rates are equal, there will be no gains in terms of catalyst bed and vessel size. However, iron based catalysts are less expensive than copper based low temperature catalysts. Even though the apparent reaction rate is comparable to the low temperature shift catalyst, the catalyst effectiveness of the iron based catalyst is much higher. This is a result of improved species diffusion at higher temperatures.

The pressure drop of the catalyst bed is 1.13 bar totaling to an overall pressure drop of the reactor of 1.20 bar. The catalyst requirement of the second shift reactor is 89.3 m^3 (diameter of 3.66 m). This is a significant reduction from the low temperature sour shift catalyst in the Selexol^{TM} case (168.6 m^3). Relative to the low temperature sweet shift reactor, the

high temperature sweet shift reactor has a 34 % higher catalyst requirement, although the apparent reaction rates differ by only 16 %. THe origin of this is the higher CO conversion of the high temperature sweet shift reactor on an absolute mole basis.

The dimensional analyses of heat transport, mass transport and reaction rate of the second shift reactor are presented in appendices C.13-C.15. The second shift reactor uses a high temperature shift catalyst with lower intrinsic reaction rate leading to less internal diffusion limitation compared to the copper based low temperature shift catalyst. However, since the apparent reaction rates are comparable, the external diffusion limitations are in a similar range. While the internal mass transport remains considerable, the external mass transport is not significant. Internal heat transport in the high temperature shift reactor plays a bigger role than in the low temperature shift reactor, although, the apparent reaction rates are comparable. However, the HT shift catalyst pellet is larger and the catalyst has a higher activation energy. This makes it harder to compare the influence of reaction kinetics on heat transport phenomena when using two different catalysts. For the same reason the external heat transfer modulus of the HT shift reactor is higher than in the low temperature sweet shift case. Nevertheless, heat transport limitations are negligibly small and isothermal catalyst pellets are a valid assumption. For the rate optimization number, the same behavior as for the first shift reactor is observed implying that cooling of the reactor, especially in the second reactor half would lead to an considerable increase in the reaction rate.

The impact of the optimization described above on the water-gas-shift section has far-reaching implications regarding the plant performance. While maintaining the same carbon capture as in the warm gas cleanup base case, the net efficiency of the plant is increased by $1.34\,\% - \text{points}$ to $35.54\,\% - \text{HHV}$. The net electricity generated rises from $478,819\,\text{kW}$ to $497,689\,\text{kW}$. Simultaneously the water usage is reduced by over 5.0 % to $13.94\,\frac{\text{m}^3}{\text{min}}$. The normalized water usage of the warm gas cleanup scenario with optimized water-gas-shift section is $1.6806\,\frac{\text{m}^3_{\text{water}}}{\text{MWh}_{\text{Net}}}$. Comparing the water usage on a normalized basis, it becomes clear

that the real water savings are over 9.15 % compared to the warm gas cleanup base case and 14.23 % compared to the Selexol^{TM} case. Reason for the increase in efficiency, net power and a reduction of the water usage can be found in the syngas composition and the shift section. For this purpose, the following discussion will be based upon a constant coal flow rate.

The net power generated at constant coal flow rate is 515, 810 kW, which is composed of the gross power, 420, 417 kW from the gas turbine and 218, 337 kW from the steam turbine, and the auxiliary load of 122, 944 kW. Comparing these numbers to the warm gas cleanup base case, an increase in every category can be observed. The gas turbine of the base case generates 416, 436 kW, the steam turbine generates 190, 023 kW and the auxiliaries consume 110, 022 kW. The strongest increase in absolute values is for the steam turbine. The main reason is the reduction in steam usage of the water-gas-shift section and more HP steam generation. The increased operating temperature of the reactors allows a reduction in the steam to carbon monoxide ratio while still operating the reactors in a stable gas regime. This steam can now be used for electricity generation and increases the power output of the steam turbine. Increasing the inlet temperature of the shift reactor also leads to an increase in the outlet temperate and enables more HP steam generation which further increases the power output of the steam turbine. Additionally, the higher firing temperature of the gas turbine (less steam in the syngas) increases the steam generation. This higher firing temperature also implies a higher power output of the gas turbine. Furthermore, the higher power output of the gas turbine is related to the higher HHV of the syngas leaving the shift reactors. This increase is mainly due to the lower water content of the syngas but also less conversion of CO to CO_2 plays a role. In order to maintain the same level of NO_x emissions, the syngas needs to be diluted. Steam is very effective in the reduction of NO_x emissions and requires less dilution than with nitrogen. Since the syngas has a lower steam content than in the base case, a higher fraction of nitrogen needs to be injected into the syngas before it enters the gas turbine combustor. This leads to a higher mass flow through the gas turbine expander and thus to a higher power generation at the terminals. The higher nitrogen requirement

has direct implications on the auxiliary load of the plant. Between the base case and the optimized case, the only major difference in the auxiliary load lies in the ASU. As a result of the higher nitrogen requirement, more air and nitrogen have to be compressed. The oxygen compression power on the other side reduces. Nitrogen is produced at elevated pressure; increasing the nitrogen production rate results in the co-production of more high pressure oxygen. Less oxygen from the lower pressure stage is now needed, which reduces the overall compression power of oxygen.

Furthermore, it is observed that the water usage of the optimized scenario decreases. At a constant coal flow basis, the raw water consumption decreases from 15.18 $\frac{m^3}{min}$ to 14.45 $\frac{m^3}{min}$. There are two major sources for water loss in the plant: cooling tower losses and gas turbine exhaust moisture. With the increase of power generation from the steam cycle, more cooling for the Rankine cycle is required which increases the losses in the cooling tower. An indication for the higher cooling water demand of the Optimization I case is an increase in power consumption of the cooling water circulation pumps whereas this does not occur in the present case. Due to the reduction of required shift steam, less water leaves the plant through the stack and this reduction is so significant that it more than offsets the increase in water demand in the cooling tower.

A summary of the plant performance of the gas turbine air flow limited case and the constant coal flow case is provided in Table 4.18.

Table 4.18: Performance Summary of Optimization I CO_2-PSA Warm Gas Cleanup Case

Gross Power Generation	Unit	GT Air Flow Limited	Constant Coal Flow
Gas Turbine	kW	405,647	420,417
Steam Turbine	kW	210,666	218,337
Total	kW	616,313	638,754
Auxiliary Load	Unit		
Coal Handling	kW	493	511
Coal Milling	kW	706	731
Coal Dryer Circulation Blower	kW	2,475	2,565
Ash Handling & Dewatering	kW	609	631
Air Separation Unit Auxiliaries	kW	597	618
Air Separation Unit Main Compressor	kW	43,086	44,655
Oxygen Compressor	kW	10,671	11,060
Nitrogen Compressor	kW	17,537	18,175
Syngas Recycle Compressor	kW	1,498	1,553
Carbon Dioxide Purification & Compressor	kW	21,690	22,480
Boiler Feed Water & Demin. Pumps	kW	5,436	5,634
Vacuum Condensate Pump	kW	340	353
Process Condensate & SWS System	kW	72	75
BFW Circulation Pumps	kW	81	84
Cooling Water Circulation Pumps	kW	2,346	2,432
Cooling Tower Fans	kW	1,290	1,337
Air Cooled Condenser Fans	kW	2,160	2,239
Scrubber Pumps	kW	590	611
Desulfurization Unit	kW	1,673	1,734
Gas Turbine Auxiliaries	kW	951	986
Steam Turbine Auxiliaries	kW	108	112
Sulfuric Acid Plant	kW	(1,195)	(1,239)
Miscellaneous Balance of Plant	kW	2,900	3,006
Transformer Losses	kW	2,510	2,601
Total	kW	118,625	122,944
Net Power Generation	Unit		
Net Power Output	kW	497,689	515,810
Plant Performance	Unit		
Net Efficiency	%-HHV	35.54	35.53
Net Heat Rate	kJ/kWh	10129.7	10132.2
Consumables	Unit		
As-Received Coal	kg/h	253,450	262,678
Thermal Input	kW-HHV	1,400,395	1,451,385
Raw Water Usage	m^3/min	13.94	14.45
Carbon Capture	Unit		
Carbon Recovery	%	83.43	83.43

Optimization II – 3 Adiabatic High Temperature Shift Reactors.

The Optimization II scenario seeks to reduce the temperature increase in the second reactor to further raise its inlet temperature. For this purpose a third shift reactor is introduced. The implementation of the third reactor and its heat integration is similar to the 2 shift reactor design. The biggest challenge is to provide enough heat to preheat the syngas entering the first reactor. High pressure boiler feed water preheats the syngas before shift steam is introduced to meet the steam to carbon monoxide ratio and further heat the syngas to the right inlet temperature. For the operation of three shift reactors, the ideal inlet temperature is 335 °C. For the first shift reactor HP and IP steam generators are used to control the inlet temperature of the second shift reactor. Another IP steam generator is placed after the second shift reactor to control the inlet temperature of the third shift reactor. The desulfurizer in this scenario is placed before the first shift reactor since the inlet temperature of the first shift reactor is high enough that after heating the syngas to 316 °C the operating temperature of the warm gas desulfurization unit is already reached and the rest heat to heat the syngas to 335 °C can be provided by the desulfurization process. This also has the advantage that at lower operating temperature more sulfur can be removed from the syngas (see Figure 4.5).

The temperature profiles of the three shift reactors are shown in Figure 4.40.

The outlet temperatures of the first, second and third reactors are 491 °C, 367 °C and 341 °C. The shape of the temperature profile of the first reactor distinguishes from the second and third reactor. The high CO inlet concentration leads to an over proportional increase in temperature and accelerates the kinetics in the first section of the reactor before it starts to slow down as it approaches equilibrium. The second and third reactors share the same general behavior of the temperature profile. However, the temperature difference between inlet and outlet is dissimilar. In both cases, the CO concentration in the syngas is so low that the heat release is minor compared to the decrease in CO partial pressure. As a

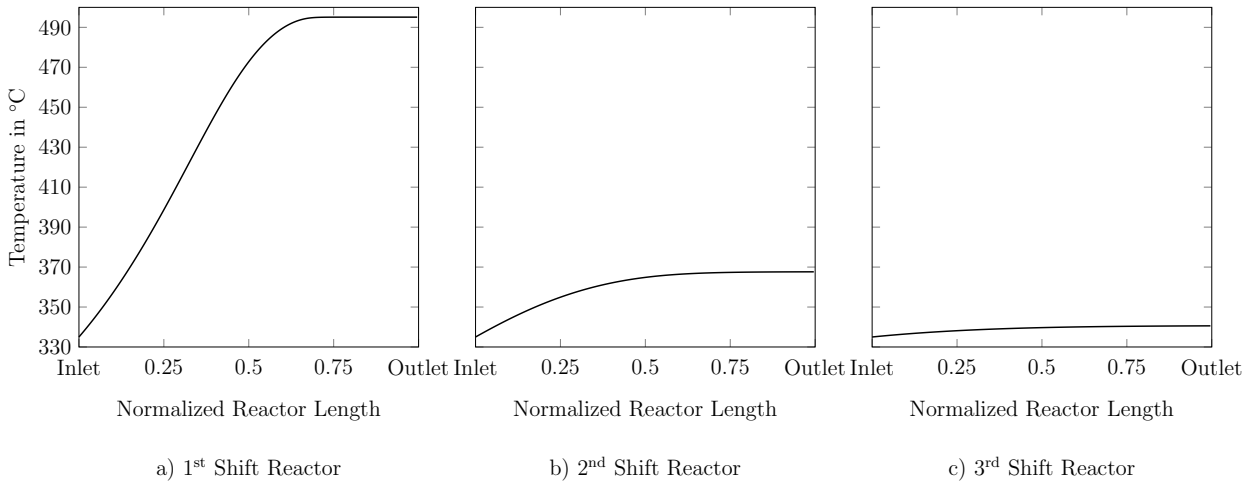

Figure 4.40: Temperature profiles of the 3 shift reactors in the Optimization II CO_2-PSA warm gas cleanup scenario using a high temperature, sweet shift catalyst (1st shift reactor), high temperature, sweet shift catalyst (2nd shift reactor) and high temperature, sweet shift catalyst (3rd shift reactor) with system sizing factors of 1.25 (1st shift reactor), 1.1 (2nd shift reactor) and 1.1 (3rd shift reactor).

result, a steady decay of the reaction temperature's slope is observed.

The concentration profiles for the three reactors are given in Figure 4.41.

In all reactors, an equimolar decrease in reactants and increase in products can be observed. The largest changes in species flows are seen in the first reactor with a conversion of 72.6 %. After the second reactor, an overall conversion of 87.4 % is reached and after the third reactor 90.1 % of the initial CO is converted. The curve shapes of the species profiles of all three reactors follow the shape of the temperature profile of the respective reactor and the same conclusions are valid. A detailed discussion on the species profiles can be found in previous sections which are equally true for the Optimization II case.

The plots of catalyst effectiveness and reaction rate are provided in Figure 4.42.

For all reactors, the catalyst effectiveness rises to approximately 100 %, which indicates that the reaction proceeds at very low speed and the gas composition is close to equilibrium. For the first reactor, this value is reached earlier as a higher system sizing factor is used. The first shift reactor has a maximum apparent reaction rate of 187 $\frac{\text{mol}}{\text{m}^3\,\text{s}}$ and a maximum

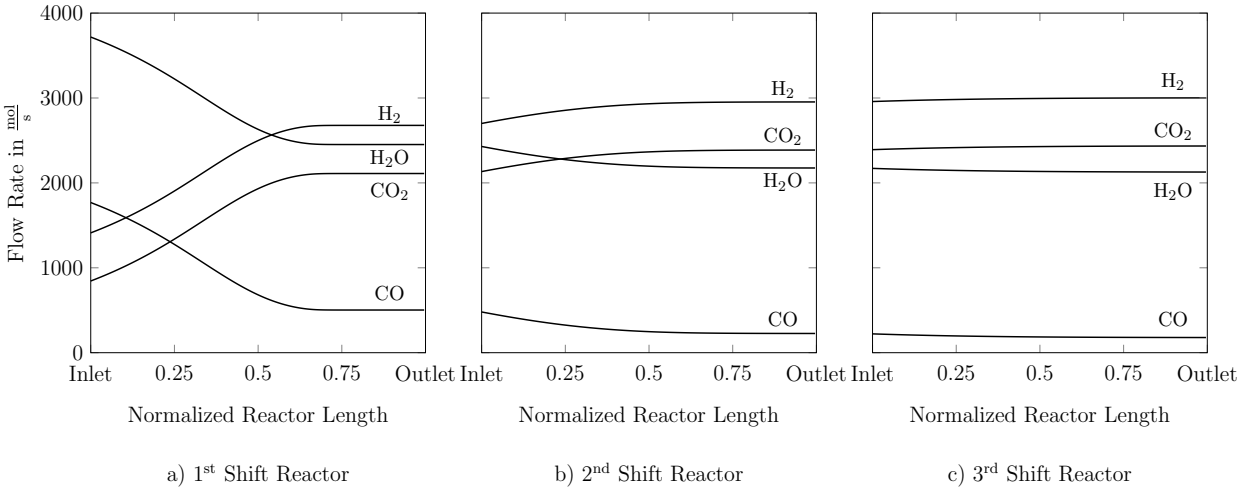

Figure 4.41: Species profile of the 3 shift reactors in the Optimization II CO_2-PSA warm gas cleanup scenario using a high temperature, sweet shift catalyst (1st shift reactor), high temperature, sweet shift catalyst (2nd shift reactor) and high temperature, sweet shift catalyst (3rd shift reactor) with system sizing factors of 1.25 (1st shift reactor), 1.1 (2nd shift reactor) and 1.1 (3rd shift reactor).

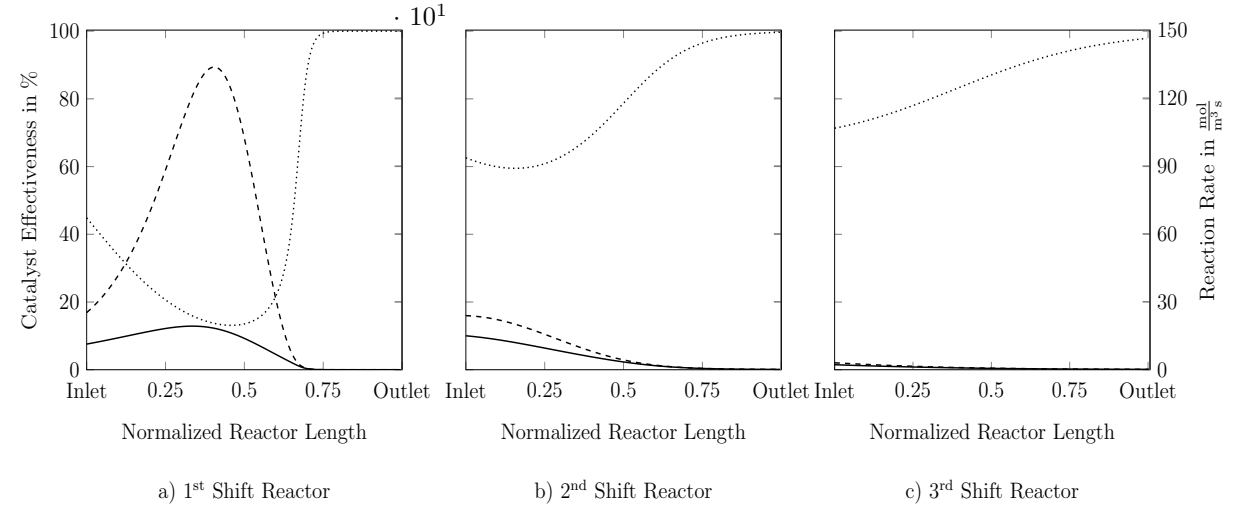

Figure 4.42: Catalyst effectiveness (·····), intrinsic ration rate (- - -) and apparent reaction rate (——) of the 3 shift reactors in the Optimization II CO_2-PSA warm gas cleanup scenario using a high temperature, sweet shift catalyst (1st shift reactor), high temperature, sweet shift catalyst (2nd shift reactor) and high temperature, sweet shift catalyst (3rd shift reactor) with system sizing factors of 1.25 (1st shift reactor), 1.1 (2nd shift reactor) and 1.1 (3rd shift reactor).

intrinsic reaction rate of 1337 $\frac{\text{mol}}{\text{m}^3\,\text{s}}$. Because of the usage of a sweet shift catalyst and the higher inlet temperature, these rates are significantly higher than in the Optimization I case. Furthermore, the difference between the two rates is larger because the reaction rate is more temperature dependent than the diffusivity resulting in a lower catalyst effectiveness. In the second reactor the reaction rate decreases monotonically. The CO concentration after the first shift reactor is not high enough to lead to an increase in reaction rate in the second reactor. However, a change in curvature indicates that the influence of temperature at the inlet is still present. The maximum apparent and intrinsic reaction rates are: 15 $\frac{\text{mol}}{\text{m}^3\,\text{s}}$ and 24 $\frac{\text{mol}}{\text{m}^3\,\text{s}}$. Before the syngas enters the third shift reactor, the CO concentration is so low that the maximum apparent and intrinsic reaction rates are 2.1 $\frac{\text{mol}}{\text{m}^3\,\text{s}}$ and 3.0 $\frac{\text{mol}}{\text{m}^3\,\text{s}}$ following an exponential decay. Due to the slow reaction rates a much higher catalyst effectiveness is reached in the third shift reactor.

The catalyst requirement for the first, second and third reactor are 13.3 m^3, 49.8 m^3 and 62.1 m^3 (with diameters 2.79 m, 3.30 m and 3.56 m). The respective pressure drops associated with the shift reactors are 1.00 bar, 1.23 bar and 1.01 bar. This represents a reduction of catalyst material of 60.1 % compared to the Selexol$^{\text{TM}}$ case and a reduction of 38.7 % compared to the warm gas cleanup base case. All reactors in this scenario use an iron based catalyst and require evaluation of the Fischer-Tropsch liquid formation. In the first reactor the R_{FT} values are 0.89 at the inlet and 1.49 at the reactor outlet. The second reactor has R_{FT} values of 1.46 and 1.71 at inlet and outlet. The third shift reactor with R_{FT} values of 1.70 and 1.71 which means that Fischer-Tropsch liquids are not a concern during regular operation.

Heat and mass transport quantities as well as the rate optimization number are shown in appendices C.16 to C.24. Because of the extremely high reaction rate in the first reactor, external mass and heat transport have an influence on the chemical conversion of CO. The external transfer coefficients can be increased by lowering the cross-sectional area and increasing the gas velocity, but the associated pressure drop would become too large. The

strongest limitations result from the internal diffusion limitation which limits the apparent reaction rate and leads to an extremely low catalyst effectiveness as seen in Figure 4.40. However, the internal heat transfer modulus is still below its critical value of 0.1 which ensures the validity of an isothermal catalyst particle approach. In reactors 2 and 3 the reaction rates are slow enough to neglect external transport phenomena. The rate optimization number shows that with increasing conversion, cooling becomes the driving force to increase the reaction rate and that the optimum reaction rate in the reactors 1 to 3 shifts to the reactor inlet. For the third reactor the optimum reaction rate is reached at the very beginning and cooling throughout the reactor is needed to accelerate the kinetics.

For the determination of the shift steam requirement, the whisker carbon equilibrium code was used. The resulting steam to carbon monoxide ratio used in the simulation is 2.09. The corresponding ternary C-O-H diagrams are provided in the appendix Figures B.2, B.3 and B.4.

The performance of the Optimization II case further improved over the Optimization I case. The net power generated in the Optimization II case is $499,548$ kW, an increase by 0.37 % compared to the first optimization and 4.33 % compared to the warm gas cleanup base case. At the same time, the efficiency increased to 35.63 %. This represents an increase of 0.09 % $-$ points compared to the Optimization I case and 1.43 % $-$ points compared to the base case solely achieved through the optimization of the water-gas-shift reaction. An increase by this amount has significant influence on the operation of the plant. Increasing the efficiency does not just affect the operating costs. In an IGCC, the efficiency has an important impact on the capital cost as it leads to a scale down of the equipment upstream of the gas turbine. Comparing the efficiency of the optimized warm gas cleanup case with the Selexol$^{\text{TM}}$ case, the warm gas cleanup case surpasses the Selexol$^{\text{TM}}$ case by 4.52 % $-$ points. The gross power generated in this case is $619,450$ kW, $408,370$ kW from the gas turbine and $211,079$ kW from the Rankine cycle. Using a constant coal flow as basis, the gross power generated is $641,335$ kW, whereby $422,798$ kW are generated in the gas turbine and

218, 537 kW in the steam turbine. These numbers are larger than those for the other warm gas cleanup cases. The explanation for this behavior is identical to the first optimization scenario. The second optimization is an amplification of the effects observed in the Optimization I case. The higher operating temperature of the shift reactors reduces the steam requirement, which leads to an increase of the heating value of the syngas. As a consequence, more nitrogen is needed for dilution which increases the mass flow through the gas turbine expander. The higher firing temperature in the gas turbine increases the power generation of the gas turbine and increases the steam production. Furthermore, the increase in power output of the Rankine cycle is coupled with lower steam consumption in the shift section of the plant. More steam in the steam turbine, ultimately leads to an increase in power generation. Due to the higher nitrogen consumption, however, the auxiliary power consumption of the ASU increases. Details can be found in previous sections. Ultimately, it would be most efficient to operate the shift reactor at isothermal conditions which would further reduce the steam requirement.

The water usage was also further reduced to 13.84 $\frac{\mathrm{m}^3}{\mathrm{min}}$. On an absolute basis, this reduction is not much but on a normalized basis, the true water use reduction becomes more obvious. The normalized water consumption of this case is 1.6623 $\frac{\mathrm{m}^3_{\mathrm{water}}}{\mathrm{MWh}_{\mathrm{Net}}}$ which is a reduction by another 1.1 % versus the Optimization I case. Compared to the Selexol$^{\mathrm{TM}}$ case, this is a reduction of 13.4 %.

A performance summary of the Optimization II case can be found in table 4.19. An overall flow sheet with stream summary at gas turbine compressor air flow limitation can be found in Figure 4.43 and Table 4.20. The stream summary at constant coal flow is provided in the appendix, Table A.3.

Table 4.19: Performance Summary of Optimization II CO_2-PSA Warm Gas Cleanup Case

Gross Power Generation	Unit	GT Air Flow Limited	Constant Coal Flow
Gas Turbine	kW	408,370	422,798
Steam Turbine	kW	211,079	218,537
Total	kW	619,450	641,335
Auxiliary Load	Unit		
Coal Handling	kW	494	511
Coal Milling	kW	707	731
Coal Dryer Circulation Blower	kW	2,478	2,565
Ash Handling & Dewatering	kW	610	631
Air Separation Unit Auxiliaries	kW	623	645
Air Separation Unit Main Compressor	kW	43,793	45,340
Oxygen Compressor	kW	10,452	10,822
Nitrogen Compressor	kW	18,273	18,918
Syngas Recycle Compressor	kW	1,500	1,553
Carbon Dioxide Purification & Compressor	kW	21,728	22,496
Boiler Feed Water & Demin. Pumps	kW	5,375	5,565
Vacuum Condensate Pump	kW	339	351
Process Condensate & SWS System	kW	71	73
BFW Circulation Pumps	kW	81	84
Cooling Water Circulation Pumps	kW	2,361	2,444
Cooling Tower Fans	kW	1,298	1,344
Air Cooled Condenser Fans	kW	2,175	2,251
Scrubber Pumps	kW	590	611
Desulfurization Unit	kW	1,683	1,743
Gas Turbine Auxiliaries	kW	958	992
Steam Turbine Auxiliaries	kW	108	112
Sulfuric Acid Plant	kW	(1,220)	(1,263)
Miscellaneous Balance of Plant	kW	2,903	3,006
Transformer Losses	kW	2,522	2,612
Total	kW	119,902	124,138
Net Power Generation	Unit		
Net Power Output	kW	499,548	517,197
Plant Performance	Unit		
Net Efficiency	%-HHV	35.63	35.63
Net Heat Rate	kJ/kWh	10102.5	10105.0
Consumables	Unit		
As-Received Coal	kg/h	253,714	262,678
Thermal Input	kW-HHV	1,401,857	1,451,385
Raw Water Usage	m^3/min	13.84	14.33
Carbon Capture	Unit		
Carbon Recovery	%	83.49	83.49

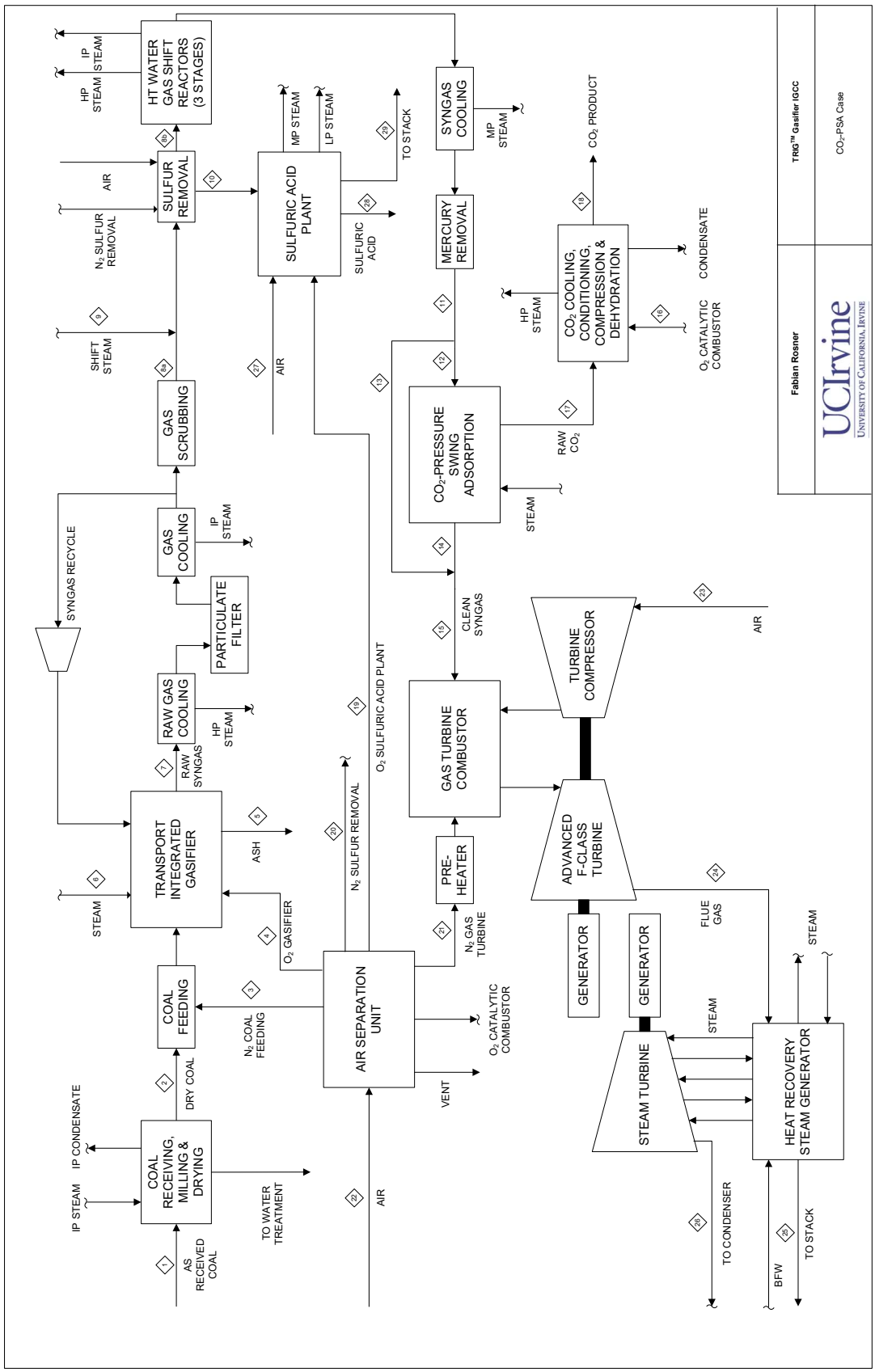

Figure 4.43: Flow sheet of the Optimization II CO_2-PSA warm gas cleanup case with 3 high temperature shift reactors.

Table 4.20: Stream Summary of Optimization II CO_2-PSA Warm Gas Cleanup Case at Fully Loaded Gas Turbine

Stream Number	Unit	1	2	3	4	5	6	7	8a	8b	9	10	11	12	13	14
Temperature	°C	5.6	71.1	105.9	73.5	982.2	397.9	982.2	161.7	334.7	394.4	760.0	199.0	199.0	0.0	203.0
Pressure	bar	0.9	0.9	56.2	50.3	3.4	51.0	41.7	38.3	36.6	51.0	35.2	31.5	31.5	0.0	31.2
Molar Flowrate	kmol/h	-	-	1637	4097	-	3442	24566	19409	29135	9726	500	29118	29118	0	21466
Mass Flowrate	kg/h	-	-	45935	131979	-	62012	527394	414043	588332	175213	16162	588036	588036	0	227464
Solid Flowrate	kg/h	253714	229673	-	-	23314	-	-	-	-	-	-	-	-	-	-
Mass Vapor Fraction	-	0	0	1	1	0	1	1	1	1	1	1	1	1	0	1
Composition	mol-basis															
O_2	-	0.00000	0.00000	0.00540	0.95013	0.00000	0.00000	0.00000	0.00000	0.00000	0.00000	0.01093	0.00000	0.00000	0.00000	0.00000
N_2	-	0.00000	0.00000	0.99230	0.01541	0.00000	0.00000	0.00498	0.00478	0.00319	0.00000	0.86405	0.00319	0.00319	0.00000	0.00428
Ar	-	0.00000	0.00000	0.00230	0.03446	0.00000	0.00000	0.00757	0.00727	0.00485	0.00000	0.00858	0.00485	0.00485	0.00000	0.00651
H_2	-	0.00000	0.00000	0.00000	0.00000	0.00000	0.00000	0.27133	0.26070	0.17367	0.00000	0.00000	0.37149	0.37149	0.00000	0.49862
CO	-	0.00000	0.00000	0.00000	0.00000	0.00000	0.00000	0.34260	0.32918	0.21929	0.00000	0.00000	0.02171	0.02171	0.00000	0.02914
CO_2	-	0.00000	0.00000	0.00000	0.00000	0.00000	0.00000	0.16170	0.15537	0.10363	0.00000	0.00026	0.30140	0.30140	0.00000	0.00650
H_2O	-	0.00000	0.00000	0.00000	0.00000	0.00000	1.00000	0.15368	0.18688	0.46016	1.00000	0.00122	0.26273	0.26273	0.00000	0.41087
CH_4	-	0.00000	0.00000	0.00000	0.00000	0.00000	0.00000	0.05128	0.04927	0.03282	0.00000	0.00000	0.03284	0.03284	0.00000	0.04408
H_2S	-	0.00000	0.00000	0.00000	0.00000	0.00000	0.00000	0.00289	0.00277	trace	0.00000	0.00000	trace	trace	0.00000	trace
NH_3	-	0.00000	0.00000	0.00000	0.00000	0.00000	0.00000	0.00374	0.00359	0.00239	0.00000	0.00000	0.00179	0.00179	0.00000	0.00000
COS	-	0.00000	0.00000	0.00000	0.00000	0.00000	0.00000	0.00020	0.00019	trace	0.00000	0.00000	trace	trace	0.00000	trace
HCl	-	0.00000	0.00000	0.00000	0.00000	0.00000	0.00000	trace	0.00000	0.00000	0.00000	0.00000	0.00000	0.00000	0.00000	0.00000
SO_2	-	0.00000	0.00000	0.00000	0.00000	0.00000	0.00000	0.00000	0.00000	0.00000	0.00000	0.11497	0.00000	0.00000	0.00000	0.00000
Total	-	0	0	1	1	0	1	0.99997	1	1	1	1	1	1	0	1
Stream Number	Unit	15	16	17	18	19	20	21	22	23	24	25	26	27	28	29
Temperature	°C	203.0	145.3	187.2	35.0	32.2	69.0	105.9	5.6	5.6	563.3	151.6	32.4	5.6	20.0	43.3
Pressure	bar	31.2	20.5	9.7	152.7	8.6	41.2	26.2	0.9	0.9	0.9	0.9	0.05	0.9	0.9	0.9
Molar Flowrate	kmol/h	21466	85	14852	8660	35	93	8591	20191	100248	124119	124119	25229	286	84	771
Mass Flowrate	kg/h	227464	2725	490291	381068	1122	2605	241078	583421	2896627	3350553	3350553	454516	8254	6116	21317
Solid Flowrate	kg/h	-	-	-	-	-	-	-	-	-	-	-	-	-	-	-
Mass Vapor Fraction	-	1	1	1	1	1	1	1	1	1	1	1	0.91474	1	0	1
Composition	mol-basis															
O_2	-	0.00000	0.95001	0.00000	trace	0.95001	0.00540	0.00540	0.20810	0.20810	0.10754	0.10754	0.00000	0.20810	0.00000	0.03928
N_2	-	0.00428	0.01406	trace	0.00025	0.01406	0.99230	0.99230	0.77590	0.77590	0.69193	0.69193	0.00000	0.77590	0.00000	0.88214
Ar	-	0.00651	0.03594	trace	0.00052	0.03594	0.00230	0.00230	0.00930	0.00930	0.00879	0.00879	0.00000	0.00930	0.00000	0.01063
H_2	-	0.49862	0.00000	0.00765	trace	0.00000	0.00000	0.00000	0.00000	0.00000	0.00000	0.00000	0.00000	0.00000	0.00000	0.00000
CO	-	0.02914	0.00000	0.00045	trace	0.00000	0.00000	0.00000	0.00000	0.00000	0.00000	0.00000	0.00000	0.00000	0.00000	0.00000
CO_2	-	0.00650	0.00000	0.58149	0.99922	0.00000	0.00000	0.00000	0.00030	0.00030	0.01403	0.01403	0.00000	0.00030	0.00000	0.00034
H_2O	-	0.41087	0.00000	0.40606	0.00000	0.00000	0.00000	0.00000	0.00640	0.00640	0.17771	0.17771	1.00000	0.00640	0.31899	0.06746
CH_4	-	0.04408	0.00000	0.00068	trace	0.00000	0.00000	0.00000	0.00000	0.00000	0.00000	0.00000	0.00000	0.00000	0.00000	0.00000
H_2S	-	trace	0.00000	trace	trace	0.00000	0.00000	0.00000	0.00000	0.00000	0.00000	0.00000	0.00000	0.00000	0.00000	0.00000
NH_3	-	0.00000	0.00000	0.00351	0.00000	0.00000	0.00000	0.00000	0.00000	0.00000	0.00000	0.00000	0.00000	0.00000	0.00000	0.00000
COS	-	trace	0.00000	trace	0.00000	0.00000	0.00000	0.00000	0.00000	0.00000	0.00000	0.00000	0.00000	0.00000	0.00000	0.00000
HCl	-	0.00000	0.00000	0.00000	0.00000	0.00000	0.00000	0.00000	0.00000	0.00000	0.00000	0.00000	0.00000	0.00000	0.00000	0.00000
SO_2	-	0.00000	0.00000	0.00000	trace	0.00000	0.00000	0.00000	0.00000	0.00000	trace	trace	0.00000	0.00000	0.00000	0.00015
Total	-	1	1	0.99983	0.99999	1	1	1	1	1	1	1	1	1	0.31899	1

Isothermal Shift I – IP Steam Generation.

Isothermal shift reactors are reactors with integrated heat exchanger. The heat exchanger is embedded in the catalyst bed and removes the reaction heat while raising steam on the tube side of the exchanger. Different heat exchanger designs have been developed for the employment in isothermal reactors, e.g. U-shaped tube heat exchangers and coil-wound heat exchangers.

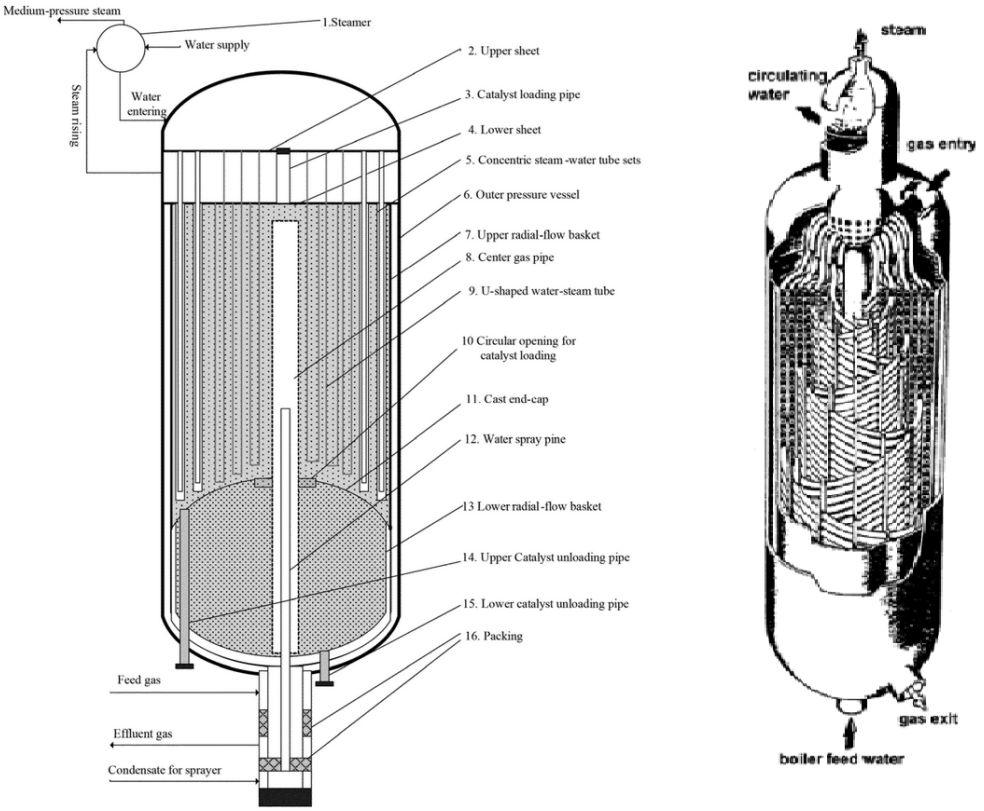

Figure 4.44: Design of isothermal shift reactors [110, 111].

Because of the complicated design of the tubes, the loading and unloading process of the catalyst becomes challenging. Therefore, most vendors offer this technology only for sweet shifting application where the replacement of the catalyst is not as frequent as in sour shift applications.

Although the reactor is commonly called an isothermal shift reactor, the temperature profile of the syngas inside the reactor is not truly isothermal. The boiler feed water is introduced at its saturation temperature and provides a constant temperature heat sink. However, the heat transport trough the tube is determined by the temperature gradient and heat transfer coefficient (at constant exchanger geometry) and will not reach thermal equilibrium in the short time the syngas is in contact with the heat exchanger surface. Thus, a rate based temperature change of the syngas will occur governed by the heat transfer rate and the heat generation rate.

The motivation of employing an isothermal shift reactor comes from the results of the Optimization I and Optimization II cases which indicate a further reduction of shift steam requirement if the reaction is conducted at isothermal conditions. Under ideal isothermal conditions a reactor outlet temperature of 340 °C would be required to achieve the desired carbon capture without the formation of whisker carbon. Current offerings of isothermal shift reactors are based on IP steam generation (typical operation range of isothermal shift reactors is $250 - 300$ °C). In this study IP steam is generated at 237 °C which is used as coolant in the isothermal shift reactor. Since the temperature gradient between the desired outlet temperature and the coolant is large (resulting in efficient cooling), the syngas can be introduced into the reactor at the same temperature as the desired outlet temperature. In the case of smaller temperature gradients between the outlet temperature and the coolant temperature (resulting in lower heat flux) sometimes lower inlet temperatures are chosen to reduce the reactor size. In order to raise the syngas temperature to 340 °C, the syngas is preheated with HP boiler feed water, shift steam addition and by the reactions occurring in the sulfur removal unit. Because of the higher operating temperature in this case compared to conventional isothermal shift reactors a less reactive high temperature sweet shift catalyst based on Fe/Cr has to be used.

The heat exchanger employed in the isothermal reactor has a specific surface area of 5.7 $\frac{\mathrm{m}^2}{\mathrm{m}^3_{\mathrm{reactor}}}$ with a volume fraction of 7.1 %. The isothermal reactor is designed with an adia-

batic section before the heat exchanger coils, which includes a guard bed which accounts for 5 % of the total catalyst volume, and an adiabatic section after the heat exchanger where only catalyst is present. The adiabatic section at the reactor outlet is needed to elevate the minimum temperature inside the reactor. Reactor cooling moves the gas mixture faster way from equilibrium than the kinetics approach equilibrium and thus a higher minimum temperature can be achieved by using an adiabatic outlet section where the gas mixture can equilibrate, although, there will be a small temperature increase in this section.

The temperature and cooling profiles of the isothermal shift reactor are plotted in Figure 4.45.

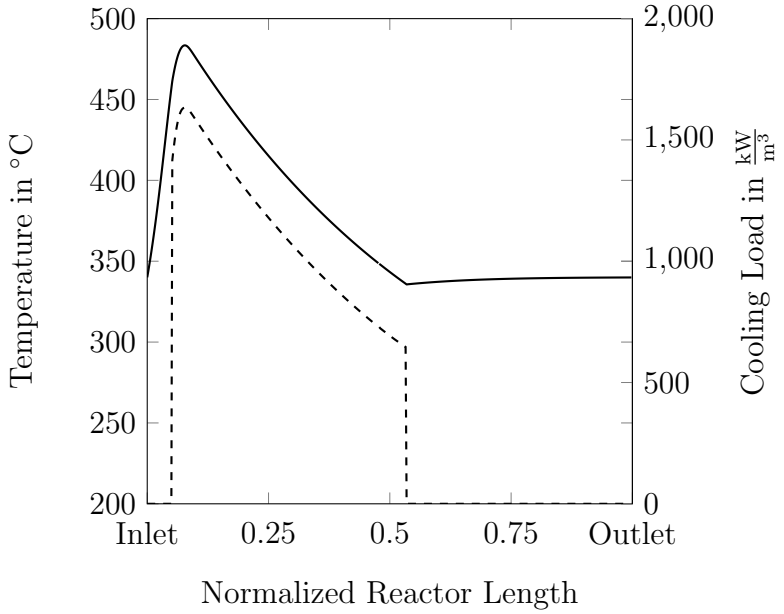

Figure 4.45: Temperature profile (——) and cooling load (- - -) of the isothermal IP shift reactor of the Isothermal Shift I scenario using a sweet shift catalyst, IP steam generation and a system sizing factor of 1.1.

At the adiabatic inlet the temperature profile has a negative curvature which changes as soon as the heat exchanger coils/cooling starts. However, the temperature still keeps increasing but it quickly reaches its maximum and starts decreasing. After the cooling section the temperature remains almost constant since most of the reactants have already

reacted and a state close to equilibrium is reached at the end of the adiabatic outlet section.

The cooling load is mostly determined by the temperature difference between the syngas and the IP boiler feed water which is constant throughout the tube (IP boiler feed water is only partially evaporated and recirculated to minimize build-up of minerals inside the tube). Nevertheless, also the heat transfer coefficient contributes to the higher heat flux at higher temperatures. Thus, the cooling load follows the temperature profile but influences the temperature profile at the same time by constantly removing heat from the syngas.

In the adiabatic inlet section, the chemical reaction proceeds fast and leads to a steep increase in temperature. After cooling comes into effect, the temperature increase can be reduced and after a reactor length of 0.09 the cooling load matches the heat released by the chemical reaction and a maximum temperature of 483 °C is reached. After that, the kinetics are too slow, because of the lower reactant concentration, and the syngas starts cooling down. While cooling down, the syngas moves away from its chemical equilibrium and the reaction kinetics are too slow to counter this process. Hence, the gas mixture is not in equilibrium. In order to reach the desired carbon monoxide conversion, the syngas temperature would drop significantly below the stable gas temperature since a much lower temperature would be needed compared to a gas mixture that is in equilibrium. As a result, an adiabatic outlet section is used to equilibrate the gas mixture and increase the lowest reactor temperature. The temperature increase in the adiabatic section is approximately 4 °C. With a required equilibrium outlet temperature of 340 °C, this means that after the cooling section a temperature of 336 °C is needed. This is not much different than the inlet temperature in the Optimization II case and ultimately results in no savings in shift steam. Thus, in the Isothermal Shift I case the steam to carbon monoxide ratio of 2.09 has to be maintained to avoid carbon deposition.

The molar flows of reactant and product species are plotted in Figure 4.46.

The molar flows of the species in the adiabatic inlet section behave very similarly to the temperature profile and general explanations as discussed before also apply here. However,

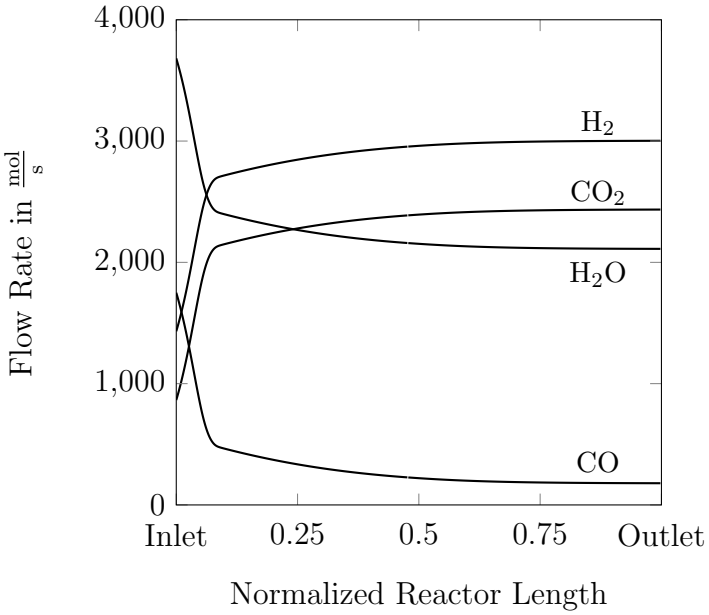

Figure 4.46: Species profiles of the isothermal IP shift reactor of the Isothermal Shift I scenario using a sweet shift catalyst, IP steam generation and a system sizing factor of 1.1.

after the maximum temperature is reached, there is a sudden change in the slope of the molar flows and the conversion continues at a much slower rate. This is due to the reduction of temperature by cooling and the continuous removal of reactants which both together result in a sharp decrease in the conversion of reactants. Throughout the cooling section a moderate slope is maintained, as cooling drives the reaction away from its equilibrium, and levels off in the adiabatic section where equilibrium is reached eventually.

The catalyst effectiveness, intrinsic reaction rate and apparent reaction rate are shown in Figure 4.47.

As discussed before, most of the conversion occurs at the inlet section of the reactor. The maximum reaction rates of 1314 $\frac{\text{mol}}{\text{m}^3\,\text{s}}$ (intrinsic) and 180 $\frac{\text{mol}}{\text{m}^3\,\text{s}}$ (apparent) are comparable to the reaction rates of the first shift reactor of the Optimization II case. However, cooling starts right before the maximum temperature is reached, which is why the reaction rates in the Isothermal Shift I case are slightly lower. Because of this high reaction rate the catalyst effectiveness goes down but recovers in the heat exchange section. In the heat exchange

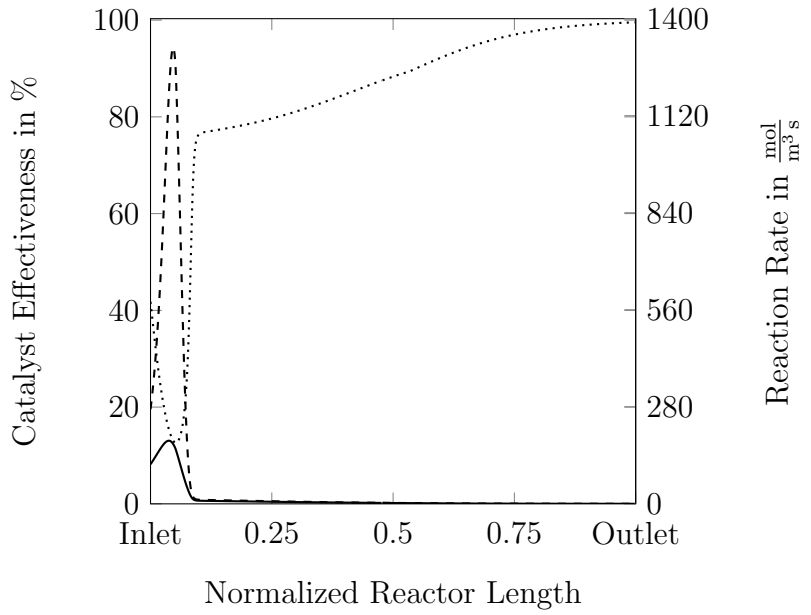

Figure 4.47: Catalyst effectiveness (·····), intrinsic reaction rate (- - -) and apparent reaction rate (——) of the isothermal IP shift reactor of the Isothermal Shift I scenario using a sweet shift catalyst, IP steam generation and a system sizing factor of 1.1.

section cooling drives the reaction as the mixture is constantly moved away from its equilibrium composition. In the adiabatic section the reaction rate levels off in the approach to equilibrium and the catalyst effectiveness moves towards a value of 100 %.

The catalyst requirement for the isothermal shift reactor is 108.6 m^3 with a reactor diameter of 3.66 m. This represents a catalyst reduction of 13.3 % compared to the Optimization II case. Most of the reaction happens in the adiabatic section where the Isothermal Shift I and Optimization II cases have similar reaction rates. Later the syngas is cooled, externally in the Optimization II case and internally in the Isothermal Shift I case. External cooling introduces the gas into the second reactor at a lower temperature and the mixture heats up while reacting. Internal cooling slowly reduces the gas temperature while it is still reacting which leads to an overall higher average gas temperature and a reduction in the catalyst requirement. The pressure drop associated with the reactor is 1.50 bar. Since an iron based catalyst is used in the isothermal shift reactor it has to be verified that the formation of Fischer-Tropsch liquids is not a concern. With R_{FT} of 0.82 and 1.84 at reactor

inlet and outlet the reactor can operate without producing Fischer-Tropsch liquids.

The analysis of the dimensionless quantities for internal and external mass and heat transport are most critical at the inlet section where high reaction rates are reached. As discussed before the internal mass transport is strongly limited at the inlet section but remains considerable throughout the reactor until the reaction slows down as it approaches equilibrium. The external mass transport plays a role only in the first section of the reactor with intrinsic reaction rates greater than 776 $\frac{\text{mol}}{\text{m}^3\,\text{s}}$. Internal heat transport never becomes limiting throughout the reactor and the assumption of an isothermal catalyst pellet is justified. External heat transfer is important in the first section of the reactor. The external heat and mass transfer coefficients are functions of the Reynolds number and can be adjusted when designing the reactor. However, a larger flow velocity increases the pressure drop which means that an acceptable compromise has to be found. Plots of the Weisz-Prater Modulus, the Carberry number and the Mears moduli are shown in appendices C.25-C.26.

The rate optimization number is plotted in Figure 4.48.

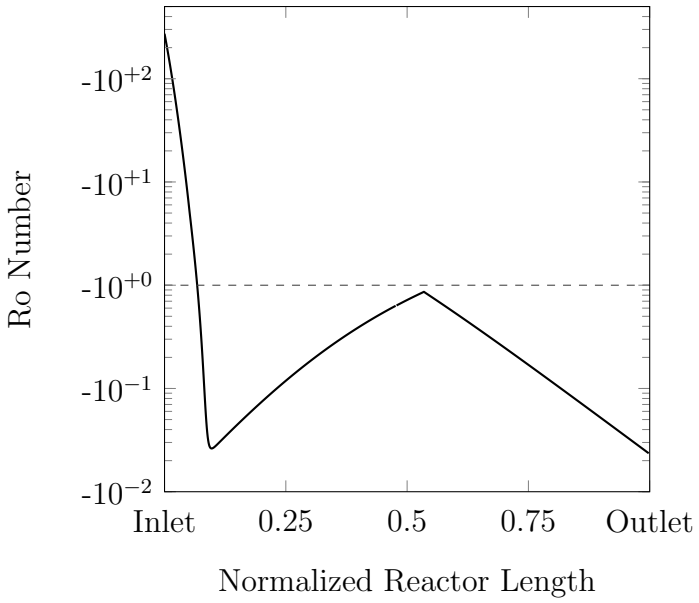

Figure 4.48: Rate optimization number of the isothermal IP shift reactor of the Isothermal Shift I scenario using a sweet shift catalyst, IP steam generation and a system sizing factor of 1.1.

At the inlet the Ro number is two orders of magnitude larger than the optimum value of -1. After that the Ro number rapidly increases to a value of -0.026 before it increases to a value of almost -1 and drops again. At the inlet the chemical potential is so large that addition of heat would lead to a significant acceleration of the kinetics. Thus, having an adiabatic inlet helps to improve the reaction kinetics. Later when most of the reactants are consumed the Ro number decreases below -1 indicating that cooling is needed to increase the chemical potential in order to accelerate the reaction rate. Cooling starts before the local minimum at the reactor length of 0.10 but is only able to provide enough cooling to accelerate the reaction after a reactor length of 0.10. At a reactor length of 0.53 a Ro-value of -0.86 is reached, however, in order to achieve the desired conversion without lowering the gas temperature, a large section without cooling is needed. This adiabatic section leads to an increase in the Ro number which represents the slowdown of the reaction in the approach to equilibrium where the chemical potential is decreasing.

The net power produced in this case is $495,150$ kW and thus less than in the Optimization I and Optimization II cases (although the steam to carbon monoxide ratio is identical to the Optimization II case) but more than in the warm gas cleanup base case. The difference originates from the steam production. While the gas turbine power output of the Isothermal Shift I and Optimization II cases are almost identical, the power generated in the Rankine cycle at $206,391$ kW is significantly lower in the Isothermal Shift I case. In the Isothermal Shift I case all the steam produced in the isothermal reactor is IP steam whereas the Optimization II case produces HP and IP. This reduced power output of the Rankine cycle is directly reflected in the efficiency at 35.31 %.

The water usage in the Isothermal Shift I case is 13.90 $\frac{\mathrm{m}^3}{\mathrm{min}}$. The normalized water consumption of this case is 1.6843 $\frac{\mathrm{m}^3_{\mathrm{water}}}{\mathrm{MWh}_{\mathrm{Net}}}$. This is higher than the Optimization I and Optimization II cases. The increase is due to the higher IP steam generation. In general the production of HP steam requires less energy input than IP steam. However, the reheat/superheat provided to the IP steam is competing with the HP steam production which

ultimately leads to more IP steam generation if more IP steam is generated in the water-gas-shift section. This leads to a higher mass flow rate through the steam turbine and condenser where all the steam needs to be condensed at the outlet of the steam turbine which leads to a higher cooling load. The higher cooling load in the cooling tower results in a higher water loss.

A summary of all performance results, Table 4.21, flow sheet, Figure 4.49, and stream summary, Table 4.22, are presented below.

Table 4.21: Performance Summary of Isothermal Shift I CO_2-PSA Warm Gas Cleanup Case

Gross Power Generation	Unit	GT Air Flow Limited	Constant Coal Flow
Gas Turbine	kW	408,503	422,815
Steam Turbine	kW	206,391	213,622
Total	kW	614,894	636,437
Auxiliary Load	Unit		
Coal Handling	kW	494	511
Coal Milling	kW	707	731
Coal Dryer Circulation Blower	kW	2,478	2,565
Ash Handling & Dewatering	kW	610	631
Air Separation Unit Auxiliaries	kW	627	649
Air Separation Unit Main Compressor	kW	43,925	45,463
Oxygen Compressor	kW	10,438	10,804
Nitrogen Compressor	kW	18,379	19,023
Syngas Recycle Compressor	kW	1,500	1,553
Carbon Dioxide Purification & Compressor	kW	21,730	22,491
Boiler Feed Water & Demin. Pumps	kW	4,911	5,083
Vacuum Condensate Pump	kW	342	354
Process Condensate & SWS System	kW	71	73
BFW Circulation Pumps	kW	81	84
Cooling Water Circulation Pumps	kW	2,386	2,469
Cooling Tower Fans	kW	1,312	1,358
Air Cooled Condenser Fans	kW	2,227	2,305
Scrubber Pumps	kW	591	611
Desulfurization Unit	kW	1,683	1,741
Gas Turbine Auxiliaries	kW	958	992
Steam Turbine Auxiliaries	kW	106	110
Sulfuric Acid Plant	kW	(1,219)	(1,262)
Miscellaneous Balance of Plant	kW	2,904	3,006
Transformer Losses	kW	2,504	2,592
Total	kW	119,743	123,938
Net Power Generation	Unit		
Net Power Output	kW	495,150	512,498
Plant Performance	Unit		
Net Efficiency	%-HHV	35.31	35.30
Net Heat Rate	kJ/kWh	10195.1	10197.7
Consumables	Unit		
As-Received Coal	kg/h	253,786	262,678
Thermal Input	kW-HHV	1,402,256	1,451,385
Raw Water Usage	m^3/min	13.90	14.39
Carbon Capture	Unit		
Carbon Recovery	%	83.47	83.47

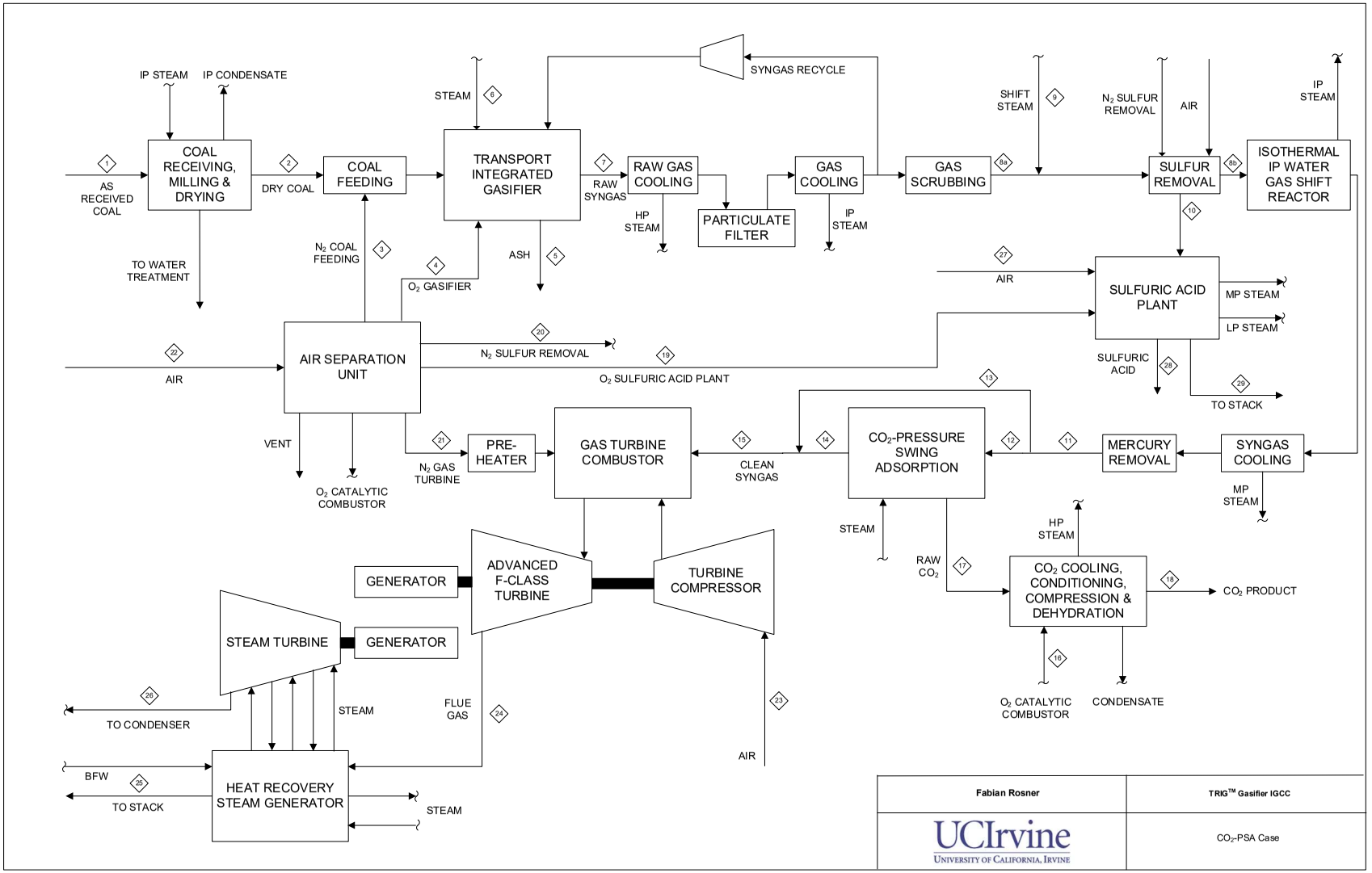

Figure 4.49: Flow sheet of the Isothermal Shift I CO_2-PSA warm gas cleanup case with an isothermal shift reactors and IP steam generation.

Table 4.22: Stream Summary of Isothermal Shift I CO_2-PSA Warm Gas Cleanup Case at Fully Loaded Gas Turbine

Stream Number	Unit	1	2	3	4	5	6	7	8a	8b	9	10	11	12	13	14
Temperature	°C	5.6	71.1	105.9	73.4	982.2	397.9	982.2	161.7	339.8	397.6	760.0	199.0	199.0	0.0	203.0
Pressure	bar	0.9	0.9	56.2	50.3	3.4	51.0	41.7	38.3	36.6	51.0	35.2	33.6	33.6	0.0	33.3
Molar Flowrate	kmol/h	-	-	1637	4098	-	3443	24573	19415	29079	9665	500	29062	29062	0	21414
Mass Flowrate	kg/h	-	-	45948	132016	-	62029	527544	414161	587349	174112	16157	587053	587053	0	226544
Solid Flowrate	kg/h	253786	229738	-	-	23320	-	-	-	-	-	-	-	-	-	-
Mass Vapor Fraction	-	0	0	1	1	0	1	1	1	1	1	1	1	1	0	1
Composition	mol-basis															
O_2	-	0.00000	0.00000	0.00540	0.95013	0.00000	0.00000	0.00000	0.00000	0.00000	0.00000	0.01091	0.00000	0.00000	0.00000	0.00000
N_2	-	0.00000	0.00000	0.99230	0.01540	0.00000	0.00000	0.00498	0.00478	0.00319	0.00000	0.86405	0.00319	0.00319	0.00000	0.00429
Ar	-	0.00000	0.00000	0.00230	0.03447	0.00000	0.00000	0.00757	0.00728	0.00486	0.00000	0.00858	0.00486	0.00486	0.00000	0.00653
H_2	-	0.00000	0.00000	0.00000	0.00000	0.00000	0.00000	0.27133	0.26070	0.17405	0.00000	0.00000	0.37223	0.37223	0.00000	0.49985
CO	-	0.00000	0.00000	0.00000	0.00000	0.00000	0.00000	0.34260	0.32918	0.21977	0.00000	0.00000	0.02183	0.02183	0.00000	0.02931
CO_2	-	0.00000	0.00000	0.00000	0.00000	0.00000	0.00000	0.16170	0.15536	0.10386	0.00000	0.00026	0.30199	0.30199	0.00000	0.00652
H_2O	-	0.00000	0.00000	0.00000	0.00000	0.00000	1.00000	0.15368	0.18688	0.45898	1.00000	0.00122	0.26118	0.26118	0.00000	0.40929
CH_4	-	0.00000	0.00000	0.00000	0.00000	0.00000	0.00000	0.05128	0.04927	0.03290	0.00000	0.00000	0.03292	0.03292	0.00000	0.04420
H_2S	-	0.00000	0.00000	0.00000	0.00000	0.00000	0.00000	0.00289	0.00277	trace	0.00000	0.00000	trace	trace	0.00000	trace
NH_3	-	0.00000	0.00000	0.00000	0.00000	0.00000	0.00000	0.00374	0.00358	0.00239	0.00000	0.00000	0.00180	0.00180	0.00000	0.00000
COS	-	0.00000	0.00000	0.00000	0.00000	0.00000	0.00000	0.00020	0.00019	trace	0.00000	0.00000	trace	trace	0.00000	trace
HCl	-	0.00000	0.00000	0.00000	0.00000	0.00000	0.00000	trace	0.00000	0.00000	0.00000	0.00000	0.00000	0.00000	0.00000	0.00000
SO_2	-	0.00000	0.00000	0.00000	0.00000	0.00000	0.00000	0.00000	0.00000	0.00000	0.00000	0.11498	0.00000	0.00000	0.00000	0.00000
Total	-	0	0	1	1	0	1	0.99997	1	1	1	1	1	1	0	1
Stream Number	Unit	15	16	17	18	19	20	21	22	23	24	25	26	27	28	29
Temperature	°C	203.0	145.3	187.2	35.0	32.2	69.0	105.9	5.6	5.6	563.3	152.4	32.4	5.6	20.0	43.3
Pressure	bar	33.3	20.5	9.7	152.7	8.6	41.2	26.2	0.9	0.9	0.9	0.9	0.05	0.9	0.9	0.9
Molar Flowrate	kmol/h	21414	85	14853	8660	35	93	8644	20219	100248	124126	124126	25841	286	84	771
Mass Flowrate	kg/h	226544	2731	490307	381088	1121	2604	242575	584226	2896627	3351329	3351329	465524	8257	6115	21316
Solid Flowrate	kg/h	-	-	-	-	-	-	-	-	-	-	-	-	-	-	-
Mass Vapor Fraction	-	1	1	1	1	1	1	1	1	1	1	1	0.91490	1	0	1
Composition	mol-basis															
O_2	-	0.00000	0.95001	0.00000	trace	0.95001	0.00540	0.00540	0.20810	0.20810	0.10752	0.10752	0.00000	0.20810	0.00000	0.03926
N_2	-	0.00429	0.01406	trace	0.00025	0.01406	0.99230	0.99230	0.77590	0.77590	0.69237	0.69237	0.00000	0.77590	0.00000	0.88212
Ar	-	0.00653	0.03594	0.00010	0.00052	0.03594	0.00230	0.00230	0.00930	0.00930	0.00879	0.00879	0.00000	0.00930	0.00000	0.01063
H_2	-	0.49985	0.00000	0.00767	trace	0.00000	0.00000	0.00000	0.00000	0.00000	0.00000	0.00000	0.00000	0.00000	0.00000	0.00000
CO	-	0.02931	0.00000	0.00045	trace	0.00000	0.00000	0.00000	0.00000	0.00000	0.00000	0.00000	0.00000	0.00000	0.00000	0.00000
CO_2	-	0.00652	0.00000	0.58149	0.99922	0.00000	0.00000	0.00000	0.00030	0.00030	0.01405	0.01405	0.00000	0.00030	0.00000	0.00034
H_2O	-	0.40929	0.00000	0.40603	0.00000	0.00000	0.00000	0.00000	0.00640	0.00640	0.17726	0.17726	1.00000	0.00640	0.31917	0.06751
CH_4	-	0.04420	0.00000	0.00068	trace	0.00000	0.00000	0.00000	0.00000	0.00000	0.00000	0.00000	0.00000	0.00000	0.00000	0.00000
H_2S	-	trace	0.00000	trace	trace	0.00000	0.00000	0.00000	0.00000	0.00000	0.00000	0.00000	0.00000	0.00000	0.00000	0.00000
NH_3	-	0.00000	0.00000	0.00351	0.00000	0.00000	0.00000	0.00000	0.00000	0.00000	0.00000	0.00000	0.00000	0.00000	0.00000	0.00000
COS	-	trace	0.00000	trace	0.00000	0.00000	0.00000	0.00000	0.00000	0.00000	0.00000	0.00000	0.00000	0.00000	0.00000	0.00000
HCl	-	0.00000	0.00000	0.00000	0.00000	0.00000	0.00000	0.00000	0.00000	0.00000	0.00000	0.00000	0.00000	0.00000	0.00000	0.00000
SO_2	-	0.00000	0.00000	0.00000	trace	0.00000	0.00000	0.00000	0.00000	0.00000	trace	trace	0.00000	0.00000	0.00000	0.00015
Total	-	1	1	0.99993	0.99999	1	1	1	1	1	1	1	1	1	0.31917	1

Isothermal Shift II – HP Steam Generation.

The production of only IP steam significantly hurts the efficiency of the Isothermal Shift I scenario. In order to improve the efficiency, it is desirable to produce only HP steam, however, HP steam is generated at a temperature of 337 °C. As mentioned before an equilibrated gas mixture at a temperature of 340 °C is needed to enable carbon capture of 83.4 %. Thus, the temperature gradient across the heat exchanger wall is not sufficient to operate the shift reactor economically. To increase the temperature difference to at least 11 °C it is necessary to increase the amount of steam added to shift the equilibrium back to the product side so that the same carbon monoxide conversion can be achieved.

Identically to the Isothermal Shift I case, the heat exchanger embedded in the catalyst bed in the Isothermal Shift II case has a specific surface area of 5.7 $\frac{\mathrm{m}^2}{\mathrm{m}^3_{\mathrm{reactor}}}$ with a volume fraction of 7.1 %. The adiabatic guard bed at the reactor inlet accounts for 5 % of the total catalyst volume.

The temperature and cooling load profiles are shown in Figure 4.50.

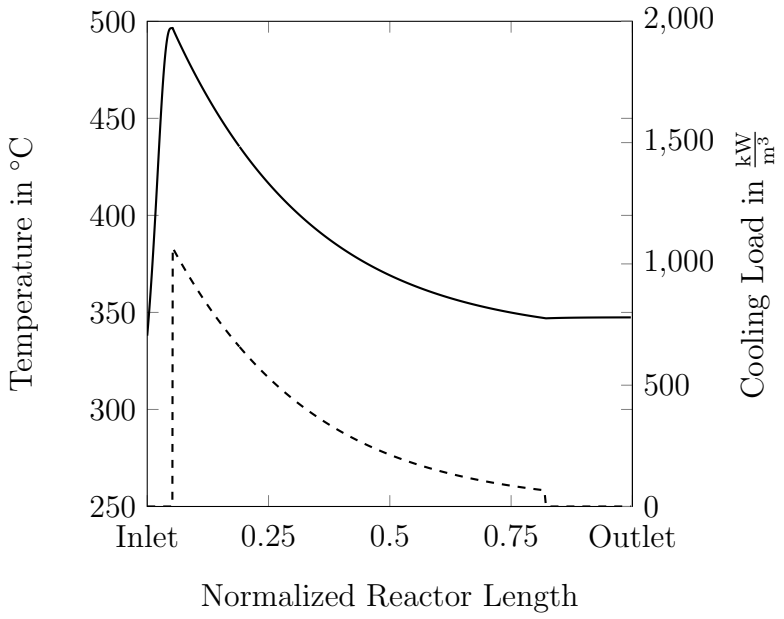

Figure 4.50: Temperature profile (——) and cooling load (- - -) of the isothermal HP shift reactor of the Isothermal Shift II scenario using a sweet shift catalyst, HP steam generation and a system sizing factor of 1.1.

The temperature increase in the guard bed is higher than in the Isothermal Shift I case. The high temperature shift catalyst significantly increases its reactivity when increasing the temperature as seen in the Optimization II case. Due to the overall larger reactor size in the Isothermal Shift II case the reaction in the adiabatic inlet section almost reaches equilibrium before the cooling section starts. The cooling load in this scenario is lower than in the previous scenario as a result of the higher operating temperature which is dictated by the coolant temperature. Thus, cooling over a longer range is needed to achieve the same heat removal as in the Isothermal Shift I case. Having less cooling per unit volume, however, decreases the length of the adiabatic section at the reactor outlet. In the Isothermal Shift I case the cooling moved the gas mixture faster away from equilibrium than the kinetics were able to catch-up with this change. Here this effect is less pronounced and only a temperature increase of approximately 1 °C is experienced in the adiabatic outlet section. However, this reduction in temperature increase in the adiabatic section cannot be utilized in this scenario since a higher steam to carbon monoxide ratio is needed regardless to maintain the conversion at the elevated outlet temperature of 348 °C.

The profiles of the flow rates of the different species are plotted in Figure 4.51.

Most of the species conversion is achieved in the adiabatic inlet section where the temperature increase helps to accelerate the reaction rate. After cooling starts, the increasing chemical potential difference drives the conversion to higher values. Eventually, the species profiles level off as the reactant concentrations and the lower temperature hinder the reaction from proceeding at high rates. In the adiabatic outlet section, the gas mixture equilibrates and no further change in the species flow profiles is observed.

The catalyst effectiveness together with intrinsic and apparent reaction rate are shown in Figure 4.52.

As mentioned before, the reaction in the adiabatic inlet section proceeds very fast at these temperatures and results in a large difference between the intrinsic and apparent re-

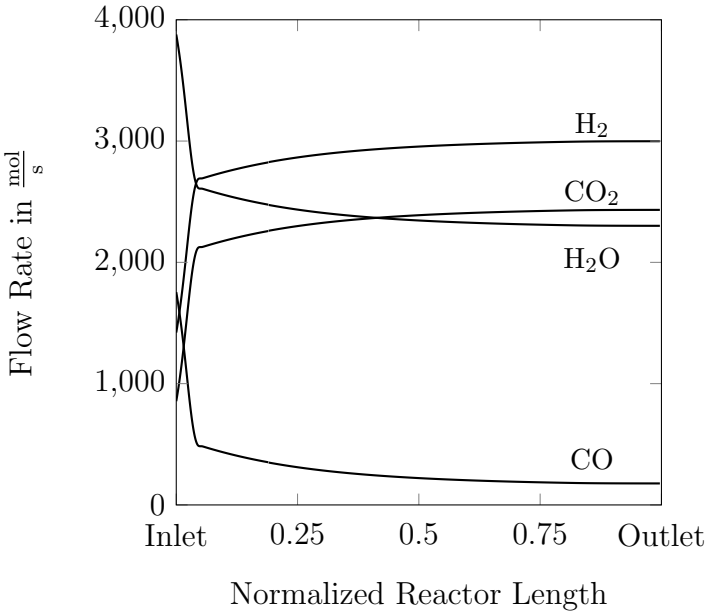

Figure 4.51: Species profiles of the isothermal HP shift reactor of the Isothermal Shift II scenario using a sweet shift catalyst, HP steam generation and a system sizing factor of 1.1.

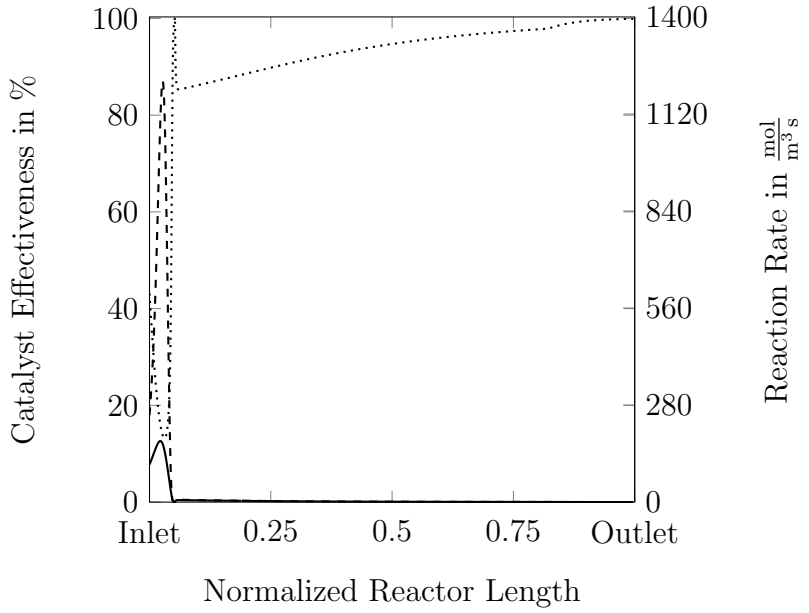

Figure 4.52: Catalyst effectiveness (·····), intrinsic reaction rate (- - -) and apparent reaction rate (——) of the isothermal HP shift reactor of the Isothermal Shift II scenario using a sweet shift catalyst, HP steam generation and a system sizing factor of 1.1.

action rate (max. intrinsic 1214 $\frac{\text{mol}}{\text{m}^3\,\text{s}}$, max. apparent 176 $\frac{\text{mol}}{\text{m}^3\,\text{s}}$). Due to this fast reaction rate the reaction temporarily approaches a state of equilibrium before it enters the cooling

section and the kinetics start slowing down at a reactor length of approximately 0.05. As a result of this the catalyst effectiveness goes up to a value of almost 100 % and drops to about 85 % at the beginning of the cooling section. The reaction rates in the cooling section are between 5 $\frac{\text{mol}}{\text{m}^3\,\text{s}}$ and 1 $\frac{\text{mol}}{\text{m}^3\,\text{s}}$ before they start approaching zero in the adiabatic section.

The catalyst volume required is 197.9 m^3 with a diameter of 3.66 m. This is a substantial increase over the Isothermal Shift I especially because of the reduced cooling density. The pressure drop associated with the shift reactor is 2.88 bar. The R_{FT} values at reactor inlet and outlet are 0.79 and 1.66 which is below the critical value of 1.9.

The dimensionless numbers for internal and external mass and heat transport are presented in appendix C.27 - C.28. For all dimensionless quantities the adiabatic inlet section represents the most critical situation. Internal mass transfer as well as external heat and mass transfer take effect on the reaction in the adiabatic inlet section. However, the Mears modulus for internal heat transfer remains below 0.1 and the assumption of an isothermal catalyst particle is valid.

The analysis of the Ro number in Figure 4.53

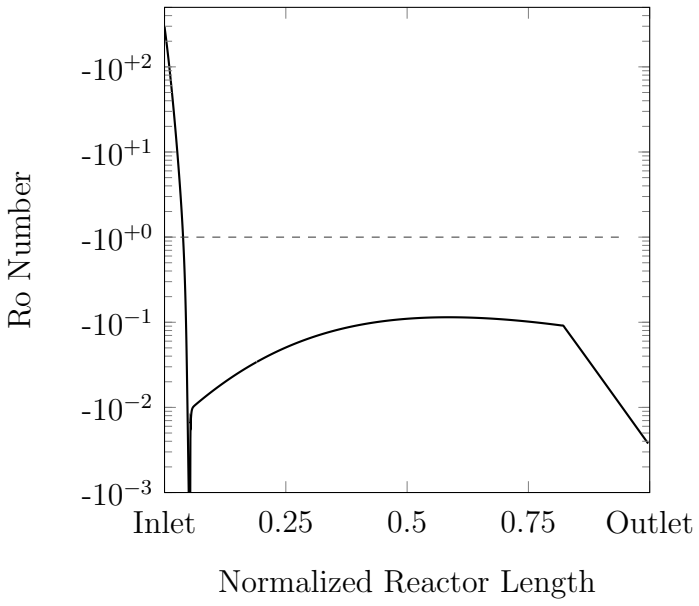

Figure 4.53: Rate optimization number of the isothermal HP shift reactor of the Isothermal Shift II scenario using a sweet shift catalyst, HP steam generation and a system sizing factor of 1.1.

shows that the provided cooling density inside the reactor is not sufficient throughout the entire cooling section and leads to an increase in the required catalyst volume. Compared to the Isothermal Shift I case it becomes obvious that the Ro number levels off much sooner and never reaches a value close to -1 (except in the adiabatic section where the Ro number increases rapidly in the approach to equilibrium). Although the heat exchanger design is identical to the Isothermal Shift I case, the higher temperature at which HP steam is generated lowers the heat flux substantially. For most of the reactor the reaction kinetics are inhibited from proceeding faster due to insufficient cooling. Only at the adiabatic inlet where a large chemical potential difference is present higher temperatures are favorable. From a reactor length of 0.04 (which is in the adiabatic bed) cooling would help to accelerate the kinetics and ultimately reduce cost.

Introducing the concept of the Ro number can help reactor designers to address this issue. In the case of the water-gas-shift reaction it is desirable to obtain a Ro number of -1 throughout the reactor. However, from a system integration point of view it does not necessarily represent the most efficient system solution to heat the syngas to extremely high temperatures at the reactor inlet in order to increase the Ro number to a value of -1. Rather it is important to avoid unnecessary reheating and reduce the steam requirement. With this in mind it is best to have an adiabatic inlet section where cooling starts when a Ro value of -1 is reached (an adiabatic inlet section is also favorable with respect to guard bed catalyst replacement). After the value of -1 is reached the cooling load has to be adjusted to maintain the Ro number at -1. Since the coolant temperature is constant, this will dictate the required surface area needed in this section of the reactor (note that: the heat transfer coefficient also varies slightly with the axial position). Making these modifications the following profile for the Ro number is obtained (Figure 4.54).

As before, the initial Ro value in the reactor is -295 and increases as the gas temperature increases in the adiabatic section. The reactor is designed to cool the syngas as soon as a Ro value of -1 is reached at a reactor length of 0.04 and the heat exchanger surface is adjusted

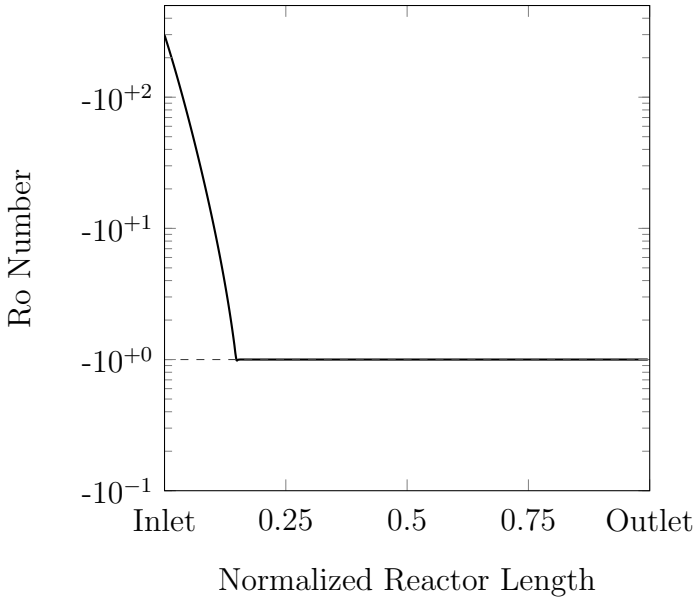

Figure 4.54: Optimized Ro number of the isothermal HP shift reactor using a sweet shift catalyst, HP steam generation and a system sizing factor of 1.1.

to maintain this value until the desired conversion is obtained.

The resulting temperature profile and cooling load are shown in Figure 4.55.

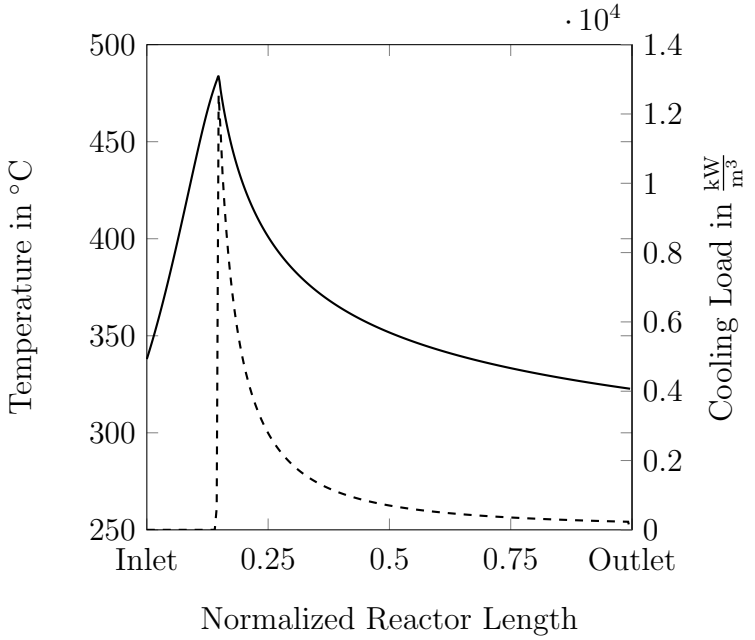

Figure 4.55: Temperature profile (——) and cooling load (- - -) of the isothermal HP shift reactor with optimized Ro number using a sweet shift catalyst, HP steam generation and a system sizing factor of 1.1.

In the adiabatic inlet section, the temperature rises to a maximum value of 484 °C before the cooling section starts at a reactor length of 0.15. In order to maintain the Ro number at a value of -1 most of the cooling is needed at the peak temperature and as the reaction proceeds less and less cooling is needed to keep the reaction rate at its optimum value. The reason for this is that as the reaction proceeds less and less carbon monoxide is converted and less heat of reaction has to be removed per volume of catalyst. By adjusting the heat transfer area in the catalyst bed accordingly, it can be ensured that the chemical potential driving force and the thermal driving force are well balanced and that the reaction proceeds as fast as possible.

The intrinsic and apparent reaction rates as well as the catalyst effectiveness are shown in Figure 4.56.

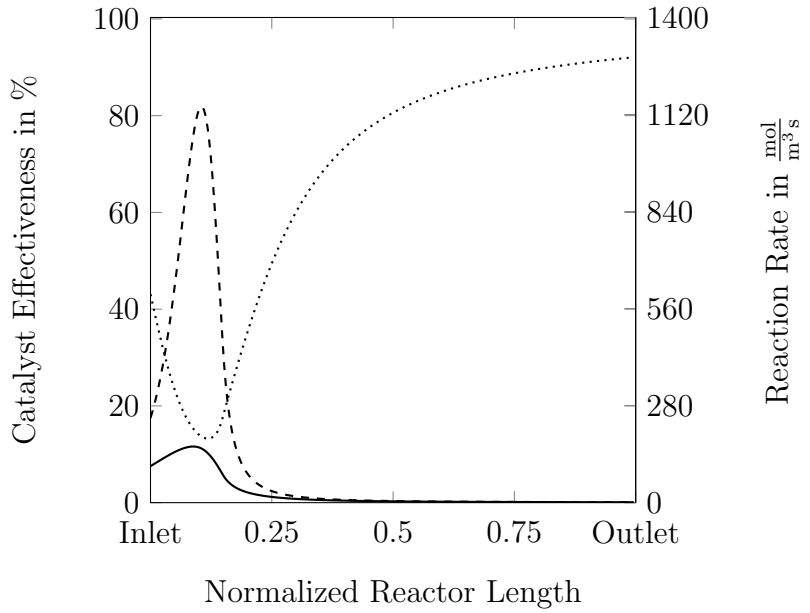

Figure 4.56: Catalyst effectiveness (·····), intrinsic reaction rate (- - -) and apparent reaction rate (——) of the isothermal HP shift reactor of the Isothermal Shift II scenario using a sweet shift catalyst, HP steam generation and a system sizing factor of 1.1.

The reaction rates in the adiabatic section including the maximum reaction rates remain unchanged. However, at beginning of the cooling section the apparent reaction rate is about 15 times faster than in the previous case with Ro number ≠ -1. Since the cooling

section was the part where the reaction was operated far away from its ideal condition this acceleration of the reaction kinetics has a significant impact on the overall catalyst volume. In the optimized case with Ro number equal to -1 the catalyst volume is reduced from 197.9 m^3 to 53.1 m^3. A faster reaction rate ultimately leads to a reduced catalyst effectiveness as the reaction occurs closer to the pore mouth and less reactants diffuse all the way into the pore. The information of catalyst effectiveness together with the application of the proposed Ro number offers a perfect combination for the reactor design engineer to optimize the reaction and minimize catalyst requirement and reactor volume. The catalyst effectiveness is a measure of how effectively the internal surface area of the pellet is used, or in other words: how much catalyst is not being used but needs to be paid for while the Ro number on the other hand optimizes the turnover that can be achieved under certain conditions per reaction site.

The following analyses are based upon the isothermal shift reactor design without optimized reaction kinetics. Common vender offerings for isothermal shift rectors are with constant heat exchange surface area throughout the reactor. Further evaluation of isothermal shift reactors with optimized heat exchange design will be part of future research.

The net power generated in this scenario is $497,436$ kW with $405,347$ kW being generated by the gas turbine and $210,228$ kW being generated by the steam cycle. The gas turbine output is less than in the Isothermal Shift I case (-0.8 %) due to the higher steam content in the syngas which requires less nitrogen diluent. This also reduces the power requirement of the air separation unit resulting in a slightly lower auxiliary load. Due to HP steam generation in the shift reactor the steam cycle power output increases from $206,391$ kW in the Isothermal Shift I case by 1.9 % which leads to an overall increase in the net power generated by 0.5 %. The resulting net efficiency of the Isothermal Shift II case is 35.53 This efficiency is higher than the Isothermal Shift I case (IP steam generation) but lower than the Optimization II case which produces HP and IP steam. The reason for the lower efficiency of the Isothermal Shift II case, although producing just HP steam, is the higher steam to carbon monoxide ratio that is needed to enable HP generation. The additional steam added

to the syngas lowers the gas turbine output as well as the steam turbine output.

The water consumption of this case is 13.94 $\frac{\mathrm{m}^3}{\mathrm{min}}$ and the normalized water consumption of this case is 1.6814 $\frac{\mathrm{m}^3_{\mathrm{water}}}{\mathrm{MWh}_{\mathrm{Net}}}$.

The performance of the Isothermal Shift II case is summarized in Table 4.23. Flow sheet and stream summary are provided in Figure 4.57 and Table 4.24.

Table 4.23: Performance Summary of Isothermal Shift II CO_2-PSA Warm Gas Cleanup Case

Gross Power Generation	Unit	GT Air Flow Limited	Constant Coal Flow
Gas Turbine	kW	405,347	420,228
Steam Turbine	kW	210,228	217,946
Total	kW	615,576	638,175
Auxiliary Load	Unit		
Coal Handling	kW	493	511
Coal Milling	kW	706	731
Coal Dryer Circulation Blower	kW	2,474	2,565
Ash Handling & Dewatering	kW	609	631
Air Separation Unit Auxiliaries	kW	585	607
Air Separation Unit Main Compressor	kW	42,813	44,385
Oxygen Compressor	kW	10,778	11,174
Nitrogen Compressor	kW	17,226	17,858
Syngas Recycle Compressor	kW	1,498	1,553
Carbon Dioxide Purification & Compressor	kW	21,686	22,483
Boiler Feed Water & Demin. Pumps	kW	5,522	5,724
Vacuum Condensate Pump	kW	339	352
Process Condensate & SWS System	kW	72	75
BFW Circulation Pumps	kW	81	84
Cooling Water Circulation Pumps	kW	2,329	2,414
Cooling Tower Fans	kW	1,280	1,327
Air Cooled Condenser Fans	kW	2,130	2,209
Scrubber Pumps	kW	590	611
Desulfurization Unit	kW	1,679	1,741
Gas Turbine Auxiliaries	kW	951	986
Steam Turbine Auxiliaries	kW	108	112
Sulfuric Acid Plant	kW	(1,217)	(1,261)
Miscellaneous Balance of Plant	kW	2,900	3,006
Transformer Losses	kW	2,507	2,599
Total	kW	118,139	122,476
Net Power Generation	Unit		
Net Power Output	kW	497,436	515,698
Plant Performance	Unit		
Net Efficiency	%-HHV	35.53	35.52
Net Heat Rate	kJ/kWh	10131.9	10134.4
Consumables	Unit		
As-Received Coal	kg/h	253,376	262,678
Thermal Input	kW-HHV	1,399,988	1,451,385
Raw Water Usage	m^3/min	13.94	14.46
Carbon Capture	Unit		
Carbon Recovery	%	83.44	83.44

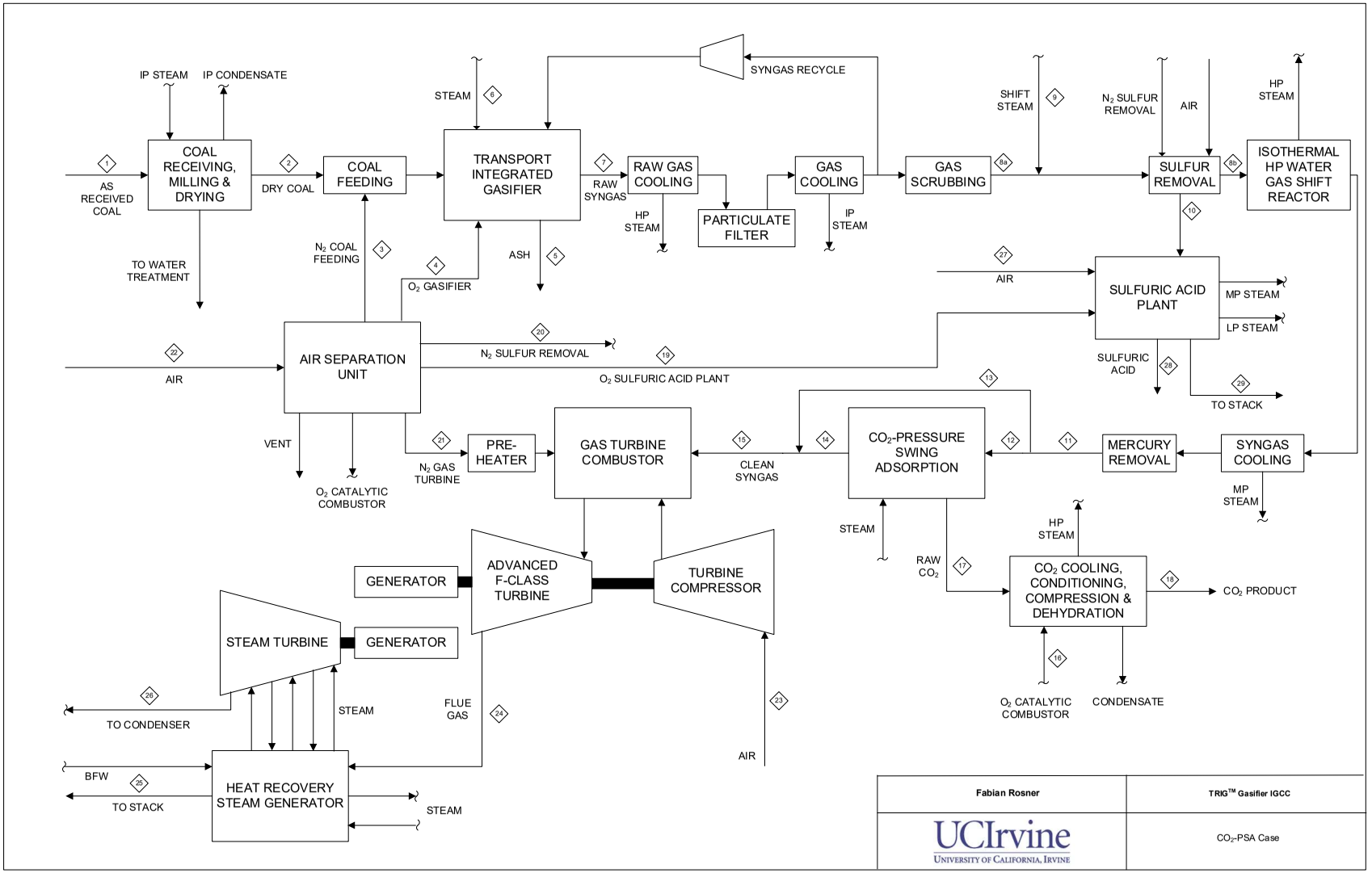

Figure 4.57: Flow sheet of the Isothermal Shift II CO_2-PSA warm gas cleanup case with an isothermal shift reactors and HP steam generation.

Table 4.24: Stream Summary of Isothermal Shift II CO_2-PSA Warm Gas Cleanup Case at Fully Loaded Gas Turbine

Stream Number	Unit	1	2	3	4	5	6	7	8a	8b	9	10	11	12	13	14
Temperature	°C	5.6	71.1	105.9	74.4	982.2	397.9	982.2	161.7	337.9	395.2	760.0	199.0	199.0	0.0	203.0
Pressure	bar	0.9	0.9	56.2	50.3	3.4	51.0	41.7	38.3	36.6	51.0	35.2	33.5	33.5	0.0	33.2
Molar Flowrate	kmol/h	-	-	1635	4092	-	3438	24534	19383	29734	10351	499	29716	29716	0	22034
Mass Flowrate	kg/h	-	-	45874	131803	-	61929	526691	413491	599037	186468	16124	598740	598740	0	237967
Solid Flowrate	kg/h	253376	229367	-	-	23283	-	-	-	-	-	-	-	-	-	-
Mass Vapor Fraction	-	0	0	1	1	0	1	1	1	1	1	1	1	1	0	1
Composition	mol-basis															
O_2	-	0.00000	0.00000	0.00540	0.95014	0.00000	0.00000	0.00000	0.00000	0.00000	0.00000	0.01088	0.00000	0.00000	0.00000	0.00000
N_2	-	0.00000	0.00000	0.99230	0.01555	0.00000	0.00000	0.00500	0.00481	0.00313	0.00000	0.86406	0.00314	0.00314	0.00000	0.00419
Ar	-	0.00000	0.00000	0.00230	0.03431	0.00000	0.00000	0.00754	0.00724	0.00472	0.00000	0.00858	0.00472	0.00472	0.00000	0.00631
H_2	-	0.00000	0.00000	0.00000	0.00000	0.00000	0.00000	0.27132	0.26069	0.16994	0.00000	0.00000	0.36336	0.36336	0.00000	0.48506
CO	-	0.00000	0.00000	0.00000	0.00000	0.00000	0.00000	0.34260	0.32917	0.21458	0.00000	0.00000	0.02139	0.02139	0.00000	0.02855
CO_2	-	0.00000	0.00000	0.00000	0.00000	0.00000	0.00000	0.16171	0.15538	0.10141	0.00000	0.00026	0.29480	0.29480	0.00000	0.00633
H_2O	-	0.00000	0.00000	0.00000	0.00000	0.00000	1.00000	0.15369	0.18689	0.47174	1.00000	0.00122	0.27870	0.27870	0.00000	0.42667
CH_4	-	0.00000	0.00000	0.00000	0.00000	0.00000	0.00000	0.05127	0.04927	0.03212	0.00000	0.00000	0.03213	0.03213	0.00000	0.04290
H_2S	-	0.00000	0.00000	0.00000	0.00000	0.00000	0.00000	0.00289	0.00277	trace	0.00000	0.00000	trace	trace	0.00000	trace
NH_3	-	0.00000	0.00000	0.00000	0.00000	0.00000	0.00000	0.00375	0.00359	0.00234	0.00000	0.00000	0.00176	0.00176	0.00000	0.00000
COS	-	0.00000	0.00000	0.00000	0.00000	0.00000	0.00000	0.00020	0.00019	trace	0.00000	0.00000	trace	trace	0.00000	trace
HCl	-	0.00000	0.00000	0.00000	0.00000	0.00000	0.00000	trace	0.00000	0.00000	0.00000	0.00000	0.00000	0.00000	0.00000	0.00000
SO_2	-	0.00000	0.00000	0.00000	0.00000	0.00000	0.00000	0.00000	0.00000	0.00000	0.00000	0.11500	0.00000	0.00000	0.00000	0.00000
Total	-	0	0	1	1	0	1	0.99997	1	1	1	1	1	1	0	1

Stream Number	Unit	15	16	17	18	19	20	21	22	23	24	25	26	27	28	29
Temperature	°C	203.0	145.3	187.2	35.0	32.2	69.0	105.9	5.6	5.6	564.9	151.6	32.4	5.6	20.0	43.3
Pressure	bar	33.2	20.5	9.7	152.7	8.6	41.2	26.2	0.9	0.9	0.9	0.9	0.05	0.9	0.9	0.9
Molar Flowrate	kmol/h	22034	82	14826	8644	35	93	8064	20141	100248	124095	124095	24716	285	84	770
Mass Flowrate	kg/h	237967	2644	489461	380352	1119	2599	226298	581959	2896627	3344265	3344265	445270	8243	6102	21271
Solid Flowrate	kg/h	-	-	-	-	-	-	-	-	-	-	-	-	-	-	-
Mass Vapor Fraction	-	1	1	1	1	1	1	1	1	1	1	1	0.91454	1	0	1
Composition	mol-basis															
O_2	-	0.00000	0.95001	0.00000	trace	0.95001	0.00540	0.00540	0.20810	0.20810	0.10760	0.10760	0.00000	0.20810	0.00000	0.03924
N_2	-	0.00419	0.01406	trace	0.00024	0.01406	0.99230	0.99230	0.77590	0.77590	0.68729	0.68729	0.00000	0.77590	0.00000	0.88231
Ar	-	0.00631	0.03594	trace	0.00051	0.03594	0.00230	0.00230	0.00930	0.00930	0.00877	0.00877	0.00000	0.00930	0.00000	0.01063
H_2	-	0.48506	0.00000	0.00744	trace	0.00000	0.00000	0.00000	0.00000	0.00000	0.00000	0.00000	0.00000	0.00000	0.00000	0.00000
CO	-	0.02855	0.00000	0.00044	trace	0.00000	0.00000	0.00000	0.00000	0.00000	0.00000	0.00000	0.00000	0.00000	0.00000	0.00000
CO_2	-	0.00633	0.00000	0.58147	0.99924	0.00000	0.00000	0.00000	0.00030	0.00030	0.01405	0.01405	0.00000	0.00030	0.00000	0.00033
H_2O	-	0.42667	0.00000	0.40631	0.00000	0.00000	0.00000	0.00000	0.00640	0.00640	0.18229	0.18229	1.00000	0.00640	0.31856	0.06733
CH_4	-	0.04290	0.00000	0.00066	trace	0.00000	0.00000	0.00000	0.00000	0.00000	0.00000	0.00000	0.00000	0.00000	0.00000	0.00000
H_2S	-	trace	0.00000	trace	trace	0.00000	0.00000	0.00000	0.00000	0.00000	0.00000	0.00000	0.00000	0.00000	0.00000	0.00000
NH_3	-	0.00000	0.00000	0.00352	0.00000	0.00000	0.00000	0.00000	0.00000	0.00000	0.00000	0.00000	0.00000	0.00000	0.00000	0.00000
COS	-	trace	0.00000	trace	0.00000	0.00000	0.00000	0.00000	0.00000	0.00000	0.00000	0.00000	0.00000	0.00000	0.00000	0.00000
HCl	-	0.00000	0.00000	0.00000	0.00000	0.00000	0.00000	0.00000	0.00000	0.00000	0.00000	0.00000	0.00000	0.00000	0.00000	0.00000
SO_2	-	0.00000	0.00000	0.00000	trace	0.00000	0.00000	0.00000	0.00000	0.00000	trace	trace	0.00000	0.00000	0.00000	0.00015
Total	-	1	1	0.99984	0.99999	1	1	1	1	1	1	1	1	1	0.31856	1

4.5 Pathways to 90 % Carbon Capture

The Selexol^{TM} case was limited to a maximum carbon capture of 83.4 %. In the warm gas cleanup case, improvements in the maximum carbon capture were observed due to the higher CO_2 yield of the PSA. However, with a maximum capture of 88.6 %, it is still limited to a value below the DoE target of 90 % capture. This section is devoted to exploring options to increase the carbon capture for the TRIG^{TM} gasifier to comply with this target.

The TRIG^{TM} gasifier is a low temperature, low rank coal gasifier which has great potential because low rank coal reserves are plentiful and the lower operation temperature positively affects the efficiency. However, operating at lower temperatures impacts the gas composition and shifts the equilibrium conditions toward forming more to methane. The TRIG^{TM} gasifier produces a syngas with a methane content of 5.1 mol $-$ %. Methane passes through the shift reactor section and CO_2-PSA and is converted to CO_2 in the gas turbine and released into the atmosphere. In order to achieve a carbon capture greater than 88.6 %, methane has to be utilized in a different way to enable its capturing.

In the following, three pathways to 90 % carbon capture are investigated. In these cases, two new technologies are introduced, steam methane reforming and hydrogen pressure swing adsorption, which will be discussed prior to the analysis.

4.5.1 Hydrogen Pressure Swing Adsorption

Hydrogen pressure swing adsorption is a technology used to produce high purity hydrogen. Since its development in the 1950's, capacities of hydrogen-PSA units have increased and can be found in many refineries, chemical plants and power plants. The operating principle is based upon adsorption and operates on a discontinuous cycle. Similarly to the CO_2-PSA, the H_2-PSA can be set up in such a manner that a continuous operation can

be achieved, whereby various adsorption vessels operate at different stages of the cycle. A general illustration of the process is depicted in Figure 4.58.

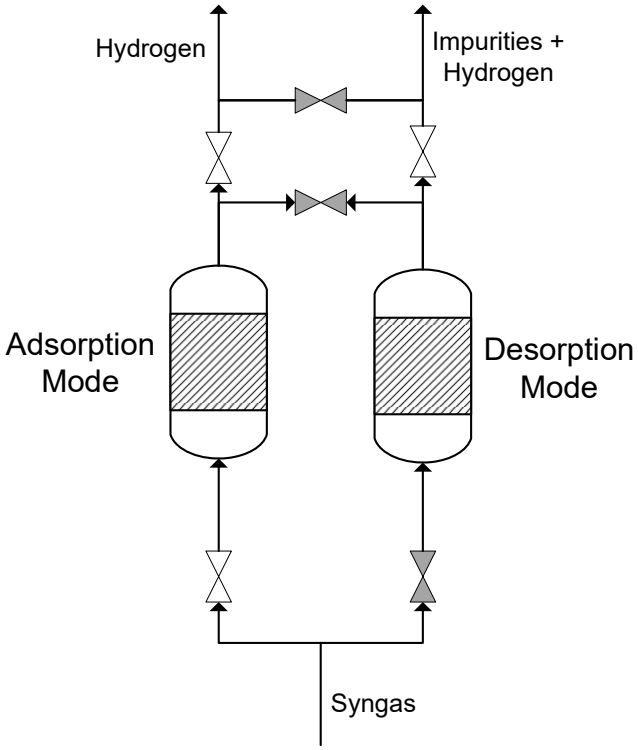

Figure 4.58: Simplified flow sheet of a hydrogen PSA.

High pressure syngas enters the adsorption vessel and impurities such as CO, CO_2, N_2 and CH_4 are adsorbed onto the bed material together with small amounts of H_2. However, most of the H_2 passes through the bed without being adsorbed. H_2 is a very small molecule and has only weak Van der Waals interactions with the bed's surface. After the bed material is fully loaded, its operation is switched into desorption mode. In order to desorb all the adsorbed molecules, the pressure is lowered and the molecules transition into the gas phase. With a hydrogen PSA, purities >99.9 % can be achieved at a recovery rate of $80 - 90$ %. Operating pressures of PSAs are typically in the range from 11 bar to 41 bar. The hydrogen product stream usually has a pressure similar to the incoming pressure (10 bar to 40 bar)

diminished by the pressure drop of the bed. The outlet stream of the impurities is close to ambient pressure in order to restore the capacity of the bed [112].

4.5.2 Steam Methane Reformer

Steam methane reformers are reactors that operate at high temperatures ($700 - 1000$ °C) converting methane to hydrogen, carbon monoxide and carbon dioxide. Steam methane reforming is most widely used as hydrogen supply for refineries or ammonia synthesis plants. The reactions occurring inside the reactor are the endothermic steam methane reforming reaction (4.122) and the mildly exothermic water-gas-shift reaction (4.123).

$$CH_4 + H_2O \longrightarrow CO + 3H_2 \tag{4.122}$$

$$CO + H_2O \longrightarrow CO_2 + H_2 \tag{4.123}$$

From an equilibrium point of view, it is advantageous to operate the reactor at comparatively low pressures. However, due to economic reasons influenced by the low mass to volume ratio at ambient condition, reformers are typically operated in a pressure range from 3 bar to 25 bar. In large scale applications, in order to reach the operating temperature and provide the endothermic heat, some of the methane is partially or completely oxidized. Many different reformer designs, for example side fired or top fired, are commercially available, each with its advantages and disadvantages. Even though the reformer operating temperature is between $700 - 1000$ °C, a nickel catalyst is required to improve the reaction kinetics of the reforming reaction. In some applications, an adiabatic pre-reformer is used to improve the economics of the plant and to convert higher hydrocarbons giving the plant feedstock flexibility. Pre-reformers are adiabatic reactors that operate at a temperature around 500 °C

and do not involve any type of firing. These low temperature reformers use a highly reactive nickel catalyst in order to obtain reasonable reactor space times. Additional to hydrogen plants, adiabatic reformers are commonly used in fuel cell applications. For small scale and unconventional applications where complete conversion is not crucial to the process, adiabatic low temperature reformer reactors offer an effective compromise between conversion and cost. In this study, only the integration of an adiabatic low temperature reformer has been evaluated. Nevertheless, the chemistry in both types of reactors are the same. The biggest difference between the high temperature and low temperature reactors is the thermodynamic equilibrium. A higher operating temperature leads to a lower CH_4 equilibrium concentration in the product gas.

4.5.3 Pathway I – Methane Combustion

In order to increase the carbon capture, methane needs to be separated from the syngas or converted to CO_2 before the carbon removal unit. The base scenario for Pathway I is the warm gas cleanup base case with sour shift high temperature and sweet shift low temperature reactors without bypassing any of the syngas. This base case has a carbon capture efficiency of 88.6 % which is increased to 90.0 % by installing a hydrogen PSA. Selective methane separation from syngas remains a challenge and no commercially available technology could be identified that can achieve this task. Hence, a hydrogen PSA is used to enrich methane in a split stream. The major components of the syngas are hydrogen, carbon monoxide, carbon dioxide, methane and steam. After shifting and decarbonization of the syngas, mostly hydrogen, steam and methane are left. PSAs operate at low temperatures (26 °C in this case), which further eliminates most of the water through condensation during the cooling process (some of the high temperature condensate is used to increase the moisture content of the syngas while the rest is sent to the water treatment plant). As a result, a stream

containing 88.8 mol − % hydrogen and 7.5 mol − % methane enters the hydrogen PSA. The hydrogen PSA produces a very pure high pressure hydrogen stream which can be reinjected into the syngas. The low pressure stream leaving the PSA is enriched in methane and contains 31.5 mol − % of CH_4. Because of the hydrogen yield of the PSA, the low pressure stream (tail gas) further contains 56.1 mol − % H_2. In Pathway I case, the methane rich stream is compressed and sent to the combustor in the CO_2 conditioning system. This way, methane can still contribute to the electricity generation by raising additional steam for the Rankine cycle. By using oxygen as oxidant instead of air, the generated CO_2 is not diluted, and no further purification is needed. After dehydration and compression to 152.7 bar, a high purity carbon dioxide stream carrying 90.0 % of the carbon dioxide is obtained ready for sequestration. A flow sheet of the Pathway I integration of the hydrogen PSA is shown in Figure 4.59. A table with information on major streams shown in the flow sheet is provided in Table 4.25. A steam summary at constant coal flow rate is provided in the appendix Table A.6.

Alternatively, the shifted non-decarbonized syngas could be fed into the hydrogen PSA directly by a split stream. Thus, the H_2-PSA and CO_2-PSA would operate in parallel. This would lead to a lower steam requirement and a size reduction in the CO_2-PSA but at the same time lead to an increase in capital cost of the H_2-PSA. The lower steam requirement in this arrangement increases the power output of Rankine cycle. However, this power is completely offset by the increase in the power requirement of the H_2-PSA tail gas compressor. With this parallel PSA design, the CO_2 content of the methane rich stream is significantly higher. Thus, the total volume flow through the H_2-PSA and its tail gas compressor is much higher. In the CO_2-PSA, carbon dioxide is recovered at a higher pressure than in the H_2-PSA. This pressure difference has to be closed by the tail gas compressor in a parallel setup. The net efficiencies of both setups are almost identical but the parallel setup has a higher water requirement than the setup shown in Figure 4.59. The steam requirement by the CO_2-PSA is internally recycled and does not affect the net water balance. However, in

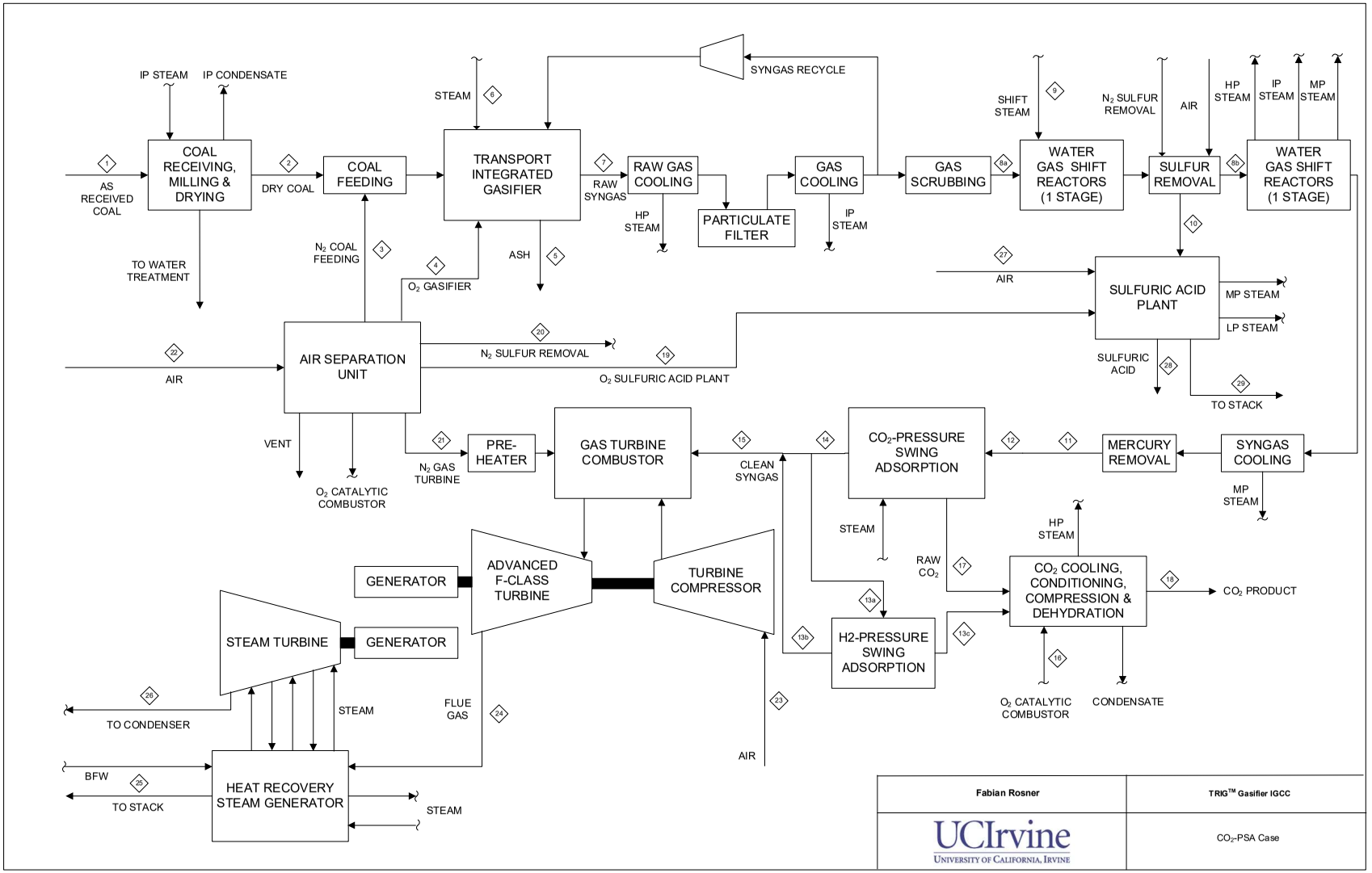

Figure 4.59: Flow sheet of the Pathway I CO_2-PSA warm gas cleanup case with hydrogen PSA and combustor injection for 90 % carbon capture.

Table 4.25: Stream Summary of the Pathway I CO_2-PSA Warm Gas Cleanup Case with 90 % Carbon Capture at Fully Loaded Gas Turbine

Stream Number	Unit	1	2	3	4	5	6	7	8a	8b	9	10	11	12	13a	13b	13c
Temperature	°C	5.6	71.1	105.9	82.7	982.2	397.9	982.2	161.7	408.5	328.9	760.0	199.0	199.0	203.0	26.0	130.8
Pressure	bar	0.9	0.9	56.2	50.3	3.4	51.0	41.7	38.3	35.7	51.0	34.3	32.8	32.8	32.4	31.4	20.5
Molar Flowrate	kmol/h	-	-	1698	4252	-	3571	25484	20134	34924	14790	519	34906	34906	3225	1233	384
Mass Flowrate	kg/h	-	-	47649	136903	-	64325	547071	429488	694984	266455	16761	694669	694669	35992	2965	4054
Solid Flowrate	kg/h	263180	238242	-	-	24183	-	-	-	-	-	-	-	-	-	-	-
Mass Vapor Fraction	-	0	0	1	1	0	1	1	1	1	1	1	1	1	1	1	1
Composition	mol-basis																
O_2	-	0.00000	0.00000	0.00540	0.95026	0.00000	0.00000	0.00000	0.00000	0.00000	0.00000	0.01091	0.00000	0.00000	0.00000	0.00000	0.00000
N_2	-	0.00000	0.00000	0.99230	0.01680	0.00000	0.00000	0.00524	0.00503	0.00290	0.00000	0.86405	0.00290	0.00290	0.00383	0.00080	0.02961
Ar	-	0.00000	0.00000	0.00230	0.03294	0.00000	0.00000	0.00724	0.00696	0.00401	0.00000	0.00858	0.00401	0.00401	0.00529	0.00968	0.01334
H_2	-	0.00000	0.00000	0.00000	0.00000	0.00000	0.00000	0.27125	0.26062	0.31940	0.00000	0.00000	0.33764	0.33764	0.44517	0.98951	0.56139
CO	-	0.00000	0.00000	0.00000	0.00000	0.00000	0.00000	0.34255	0.32913	0.02058	0.00000	0.00000	0.00253	0.00253	0.00334	0.00000	0.02806
CO_2	-	0.00000	0.00000	0.00000	0.00000	0.00000	0.00000	0.16181	0.15547	0.25890	0.00000	0.00026	0.27710	0.27710	0.00587	0.00000	0.04939
H_2O	-	0.00000	0.00000	0.00000	0.00000	0.00000	1.00000	0.15376	0.18695	0.36372	1.00000	0.00122	0.34585	0.34585	0.49908	0.00000	0.00366
CH_4	-	0.00000	0.00000	0.00000	0.00000	0.00000	0.00000	0.05120	0.04919	0.02836	0.00000	0.00000	0.02838	0.02838	0.03741	0.00000	0.31454
H_2S	-	0.00000	0.00000	0.00000	0.00000	0.00000	0.00000	0.00289	0.00277	trace	0.00000	0.00000	trace	trace	trace	0.00000	trace
NH_3	-	0.00000	0.00000	0.00000	0.00000	0.00000	0.00000	0.00383	0.00368	0.00212	0.00000	0.00000	0.00159	0.00159	0.00000	0.00000	0.00000
COS	-	0.00000	0.00000	0.00000	0.00000	0.00000	0.00000	0.00020	0.00019	trace	0.00000	0.00000	trace	trace	trace	0.00000	trace
HCl	-	0.00000	0.00000	0.00000	0.00000	0.00000	0.00000	trace	0.00000	0.00000	0.00000	0.00000	0.00000	0.00000	0.00000	0.00000	0.00000
SO_2	-	0.00000	0.00000	0.00000	0.00000	0.00000	0.00000	0.00000	0.00000	0.00000	0.00000	0.11498	0.00000	0.00000	0.00000	0.00000	0.00000
Total	-	0	0	1	1	0	1	0.99997	1	1	1	1	1	1	1	1	0.99999
Stream Number	Unit	14	15	16	17	18	19	20	21	22	23	24	25	26	27	28	29
Temperature	°C	203.0	240.6	145.3	187.2	35.0	32.2	69.0	105.9	5.6	5.6	560.3	151.9	32.4	5.6	20.0	43.3
Pressure	bar	32.4	31.1	20.5	9.7	152.7	8.6	41.2	26.2	0.9	0.9	0.9	0.9	0.05	0.9	0.9	0.9
Molar Flowrate	kmol/h	26222	25507	453	16370	9721	36	96	4804	22426	100248	123674	123674	23383	216	76	703
Mass Flowrate	kg/h	292621	282597	14593	540517	427410	1165	2701	134823	647992	2896627	3282669	3282669	421246	6239	6135	19619
Solid Flowrate	kg/h	-	-	-	-	-	-	-	-	-	-	-	-	-	-	-	-
Mass Vapor Fraction	-	1	1	1	1	1	1	1	1	1	1	1	1	0.92051	1	0	1
Composition	mol-basis																
O_2	-	0.00000	0.00000	0.95001	0.00000	trace	0.95001	0.00540	0.00540	0.20810	0.20810	0.10830	0.10830	0.00000	0.20810	0.00000	0.04468
N_2	-	0.00383	0.00349	0.01406	trace	0.00192	0.01406	0.99230	0.99230	0.77590	0.77590	0.65923	0.65923	0.00000	0.77590	0.00000	0.89873
Ar	-	0.00529	0.00524	0.03594	trace	0.00234	0.03594	0.00230	0.00230	0.00930	0.00930	0.00869	0.00869	0.00000	0.00930	0.00000	0.01103
H_2	-	0.44517	0.44921	0.00000	0.00686	trace	0.00000	0.00000	0.00000	0.00000	0.00000	0.00000	0.00000	0.00000	0.00000	0.00000	0.00000
CO	-	0.00334	0.00301	0.00000	trace	trace	0.00000	0.00000	0.00000	0.00000	0.00000	0.00000	0.00000	0.00000	0.00000	0.00000	0.00000
CO_2	-	0.00587	0.00530	0.00000	0.58145	0.99571	0.00000	0.00000	0.00000	0.00030	0.00030	0.00891	0.00891	0.00000	0.00030	0.00000	0.00048
H_2O	-	0.49908	0.50003	0.00000	0.40753	0.00000	0.00000	0.00000	0.00000	0.00640	0.00640	0.21487	0.21487	1.00000	0.00640	0.21517	0.04491
CH_4	-	0.03741	0.03373	0.00000	0.00058	trace	0.00000	0.00000	0.00000	0.00000	0.00000	0.00000	0.00000	0.00000	0.00000	0.00000	0.00000
H_2S	-	trace	trace	0.00000	trace	trace	0.00000	0.00000	0.00000	0.00000	0.00000	0.00000	0.00000	0.00000	0.00000	0.00000	0.00000
NH_3	-	0.00000	0.00000	0.00000	0.00339	0.00000	0.00000	0.00000	0.00000	0.00000	0.00000	0.00000	0.00000	0.00000	0.00000	0.00000	0.00000
COS	-	trace	trace	0.00000	trace	0.00000	0.00000	0.00000	0.00000	0.00000	0.00000	0.00000	0.00000	0.00000	0.00000	0.00000	0.00000
HCl	-	0.00000	0.00000	0.00000	0.00000	0.00000	0.00000	0.00000	0.00000	0.00000	0.00000	0.00000	0.00000	0.00000	0.00000	0.00000	0.00000
SO_2	-	0.00000	0.00000	0.00000	0.00000	trace	0.00000	0.00000	0.00000	0.00000	0.00000	trace	trace	0.00000	0.00000	0.00000	0.00017
Total	-	1	1	1	0.99981	0.99997	1	1	1	1	1	1	1	1	1	0.21517	1

the parallel setup more steam is available for power generation in the Rankine cycle which increases the cooling water demand. The increased flow through the methane compressor further increases the cooling load. This increase in cooling load induces higher evaporative losses in the cooling tower and a higher overall water consumption. Thus, the flow sheet shown in Figure 4.59 has been chosen over the parallel PSA setup, although the net efficiencies are almost the same.

The carbon capture in Pathway I is 90.03 % at a net plant efficiency of 33.17 HHV − %. As mentioned before, in order to achieve this carbon capture, an additional process unit is integrated into the plant. Due to this process integration, a significant drop in efficiency occurs. An efficiency of 33.82 HHV − % would be expected for a carbon capture of 90 % by applying a simple linear extrapolation to the efficiency of the warm gas cleanup base scenario at its maximum carbon capture of 88.6 %. Extrapolating the efficiency of the Optimization II scenario to 90 % carbon capture a value of 33.43 HHV − % would result. These extrapolated efficiencies can be seen as ideal values without the integration losses of any additional equipment. The Pathway I efficiency lies about $0.65 - 0.26$ % − points below these ideal values. The two main reasons of this are the power generation as well as the heating value of the syngas.

The power generated by the gas turbine is $400,919$ kW (66.9 %) and an additional $198,645$ kW (33.1 %) are generated by the steam turbine. The gas turbine generates slightly less power than that in the warm gas cleanup base scenario ($401,657$ kW). With 0 % bypass and H_2-PSA, the syngas heating value is upgraded from $15,245$ $\frac{\text{kJ}}{\text{kg}}$ to $16,400$ $\frac{\text{kJ}}{\text{kg}}$. Typically, a higher heating value means a higher turbine output when being scaled to full turbine load. However, in contrast to the previous optimization cases, the integration of the H_2-PSA leads to an increase in heating value of the syngas as well as to a higher water content. Water is more effective in suppressing NO_x formation. Because of this, a relatively small quantity of nitrogen is needed (however, still more than in the base case), which means that the heating value after diluent addition is still higher ($12,005$ $\frac{\text{kJ}}{\text{kg}}$ vs. $11,444$ $\frac{\text{kJ}}{\text{kg}}$). Since the air flow is lim-

iting the turbine operation, the required fuel flow to the gas turbine is lower when its higher heating value is higher. A consequence of this lower fuel mass flow is less mass flow through the turbine expander and less power generation. The turbine firing temperature of the Pathway I case is almost identical to the base case and does not influence the power output of the gas turbine (less carbon dioxide but more water). The comparison of the gas turbine power output above is conducted on the basis of air flow limitation. If comparing the gas turbine power output on the basis of a constant coal flow rate, a significant reduction can be observed, which is related to the lesser fuel input because of the split stream. Consequently, it is more appropriate to compare the steam turbine performance on the basis of constant coal flow. When scaling the Pathway I scenario, a higher coal flow rate in the fully loaded gas turbine case is observed due to the split stream even though the efficiency is higher than in the base case. A higher coal flow rate as in the scaled Pathway I case ultimately leads to a higher heat input to the Rankine cycle skewing the observations. The steam turbine in the Pathway I scenario generates more power, $198,266\,\mathrm{kW}$ versus $190,023\,\mathrm{kW}$ in the warm gas cleanup base scenario. In general, there is a shift from gas turbine power generation to Rankine cycle power generation. Reason for this shift is that in order to achieve a higher carbon capture, methane and some of the hydrogen is separated from the syngas and combusted in the CO_2-conditioner which generates high pressure steam for the Rankine cycle. Comparison of the auxiliary load is again conduced on the basis of air flow limitation. A substantial increase in three major parts of the plant is noticed. First: the higher carbon capture leads to an increase in compression power of CO_2. Second: the low pressure steam leaving the H_2-PSA has to be compressed in order to be fed it into the combustor. Third: the increase in ASU power is mostly related to the higher oxygen requirement for the CO_2-conditioner combustor. The nitrogen compression power almost remains constant since there is only a minor increase in nitrogen demand for coal preparation and gas turbine diluent. The oxygen demand is higher due to an increased mass flow of combustibles into the CO_2-conditioner combustor which requires more oxygen intake. The additional oxygen

demand for the gasifier due to the increase coal flow is small. Together with the increase in oxygen demand, the compression power of the main ASU compressor increases.

The net power output of the Pathway I scenario is greater than that for the warm gas cleanup base case, which is caused by the higher coal flow rate. On the basis of constant coal flow, it is clear that the power generation from the Pathway I scenario is significantly less, which is reflected in the lower efficiency.

The water consumption of the Pathway I scenario at 15.61 $\frac{\mathrm{m}^3}{\mathrm{min}}$ is higher than that in the warm gas cleanup base case. Even if considering the higher net power of the Pathway I scenario, the relative water consumption is 1.9420 $\frac{\mathrm{m}^3_{\mathrm{water}}}{\mathrm{MWh}_{\mathrm{Net}}}$ and thus still higher than the warm gas cleanup base scenario with a relative water consumption of 1.8345 $\frac{\mathrm{m}^3_{\mathrm{water}}}{\mathrm{MWh}_{\mathrm{Net}}}$. Origin of the higher water demand is the higher cooling water requirement, mostly due to the higher power output of the Rankine cycle as well as the cooling water for the methane compressor.

A summary of the performance data of the Pathway I scenario is presented in Table 4.26. The table includes the results for full turbine load and constant coal flow rate.

Table 4.26: Performance Summary of the Pathway I CO_2-PSA Warm Gas Cleanup Case with 90 % Carbon Capture

Gross Power Generation	Unit	GT Air Flow Limited	Constant Coal Flow
Gas Turbine	kW	400,919	400,154
Steam Turbine	kW	198,645	198,266
Total	kW	599,564	598,420
Auxiliary Load	Unit		
Coal Handling	kW	512	511
Coal Milling	kW	733	731
Coal Dryer Circulation Blower	kW	2,570	2,565
Ash Handling & Dewatering	kW	633	631
Air Separation Unit Auxiliaries	kW	349	348
Air Separation Unit Main Compressor	kW	40,481	40,404
Oxygen Compressor	kW	14,615	14,587
Nitrogen Compressor	kW	10,804	10,784
Syngas Recycle Compressor	kW	1,556	1,553
Carbon Dioxide Purification & Compressor	kW	24,171	24,125
Boiler Feed Water & Demin. Pumps	kW	5,904	5,892
Vacuum Condensate Pump	kW	368	367
Process Condensate & SWS System	kW	122	121
BFW Circulation Pumps	kW	87	87
Cooling Water Circulation Pumps	kW	2,383	2,379
Cooling Tower Fans	kW	1,310	1,308
Air Cooled Condenser Fans	kW	2,015	2,012
Scrubber Pumps	kW	612	611
Desulfurization Unit	kW	1,745	1,742
Gas Turbine Auxiliaries	kW	940	938
Steam Turbine Auxiliaries	kW	102	102
Sulfuric Acid Plant	kW	(1,263)	(1,261)
Miscellaneous Balance of Plant	kW	3,012	3,006
Transformer Losses	kW	2,441	2,437
Methane Compressor	kW	1,087	1,085
Total	kW	117,290	117,066
Net Power Generation	Unit		
Net Power Output	kW	482,274	481,354
Plant Performance	Unit		
Net Efficiency	%-HHV	33.17	33.16
Net Heat Rate	kJ/kWh	10854.8	10857.5
Consumables	Unit		
As-Received Coal	kg/h	263,180	262,678
Thermal Input	kW-HHV	1,454,159	1,451,385
Raw Water Usage	m^3/min	15.61	15.58
Carbon Capture	Unit		
Carbon Recovery	%	90.03	90.03

4.5.4 Pathway II – Adiabatic Methane Reforming

The Pathway II scenario is similar to the Pathway I scenario and uses an adiabatic reformer reactor in addition to the H_2-PSA but instead of sending the methane rich stream leaving the H_2-PSA to the CO_2-conditioner combustor, the methane rich stream is sent to a reformer reactor and recycled back to the CO_2-PSA. The reforming reaction (Equation 4.122) is endothermic and converts heat into chemical energy while reducing the methane content. Converting heat to chemical energy has the potential of increasing the efficiency of the plant. Combusting a fuel component in the gas turbine has a higher efficiency than converting it to heat, raising steam and utilizing the steam in a Rankine cycle. Thus, this setup could potentially increase the carbon capture to the desired value of 90 % while increasing the plant efficiency at the same time. The integration of the reformer reactor requires steam input to adjust the steam to carbon ratio to a value that ensures gas stability with respect to carbon formation under the operating conditions, and heat input to preheat the gas to 500 °C. As in the Pathway I scenario, the syngas has to be cooled to 26 °C before it can enter the H_2-PSA. In the Pathway II scenario, a majority of the high temperature condensate as well as the low temperature condensate is used to humidify the low pressure methane rich steam leaving the H_2-PSA. The rest of the high temperature condensate is used to humidify the gas turbine fuel. The heat for preheating the methane rich stream is provided by the reheated steam from the HRSG. After reforming, the syngas is cooled, compressed and recycled to the CO_2-PSA.

A simplified flow sheet of the Pathway II scenario is shown in Figure 4.60. The corresponding stream summary at gas turbine inlet flow limitations is given in Table 4.27. A steam summary at constant coal flow rate is provided in the appendix Table A.7.

The analysis of the whisker carbon equilibrium inside the reformer reactor is shown in appendix Figure B.5. In this scenario, no water is being sent to the water treatment, all the condensate is used to re-humidify the syngas. By adding more steam to the gas stream

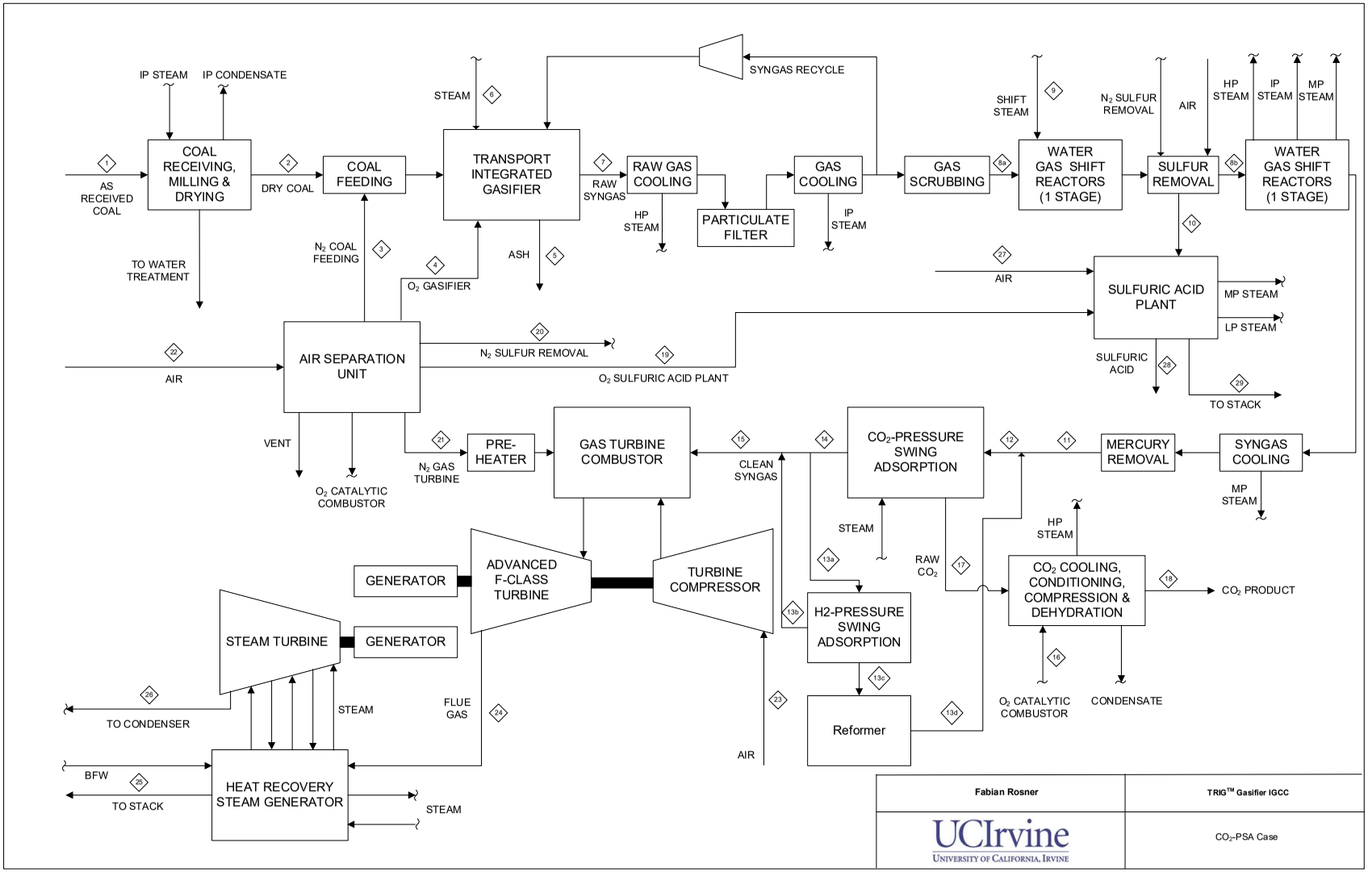

Figure 4.60: Flow sheet of the Pathway II CO_2-PSA warm gas cleanup case with hydrogen PSA and reformer for 90 % carbon capture.

Table 4.27: Stream Summary of the Pathway II CO_2-PSA Warm Gas Cleanup Case with 90 % Carbon Capture at Fully Loaded Gas Turbine

Stream Number	Unit	1	2	3	4	5	6	7	8a	8b	9	10	11	13a	13b	13c	13d
Temperature	°C	5.6	71.1	105.9	76.6	982.2	397.9	982.2	161.7	408.6	329.0	760.0	199.0	203.0	26.0	500.0	165.5
Pressure	bar	0.9	0.9	56.2	50.3	3.4	51.0	41.7	38.3	35.7	51.0	34.3	32.8	32.4	31.4	1.3	35.0
Molar Flowrate	kmol/h	-	-	1634	4090	-	3435	24519	19372	33605	14233	499	35336	10746	4201	3637	1749
Mass Flowrate	kg/h	-	-	45846	131722	-	61891	526367	413236	668726	256412	16126	687938	118166	10249	55523	19510
Solid Flowrate	kg/h	253220	229226	-	-	23268	-	-	-	-	-	-	-	-	-	-	-
Mass Vapor Fraction	-	0	0	1	1	0	1	1	1	1	1	1	1	1	1	1	1
Composition	mol-basis																
O_2	-	0.00000	0.00000	0.00540	0.95017	0.00000	0.00000	0.00000	0.00000	0.00000	0.00000	0.01091	0.00000	0.00000	0.00000	0.00000	0.00000
N_2	-	0.00000	0.00000	0.99230	0.01588	0.00000	0.00000	0.00507	0.00487	0.00281	0.00000	0.86405	0.00420	0.00547	0.00112	0.01488	0.03094
Ar	-	0.00000	0.00000	0.00230	0.03395	0.00000	0.00000	0.00746	0.00717	0.00413	0.00000	0.00858	0.00446	0.00581	0.01041	0.00515	0.01071
H_2	-	0.00000	0.00000	0.00000	0.00000	0.00000	0.00000	0.27130	0.26067	0.31942	0.00000	0.00000	0.34879	0.45460	0.98847	0.20147	0.56253
CO	-	0.00000	0.00000	0.00000	0.00000	0.00000	0.00000	0.34258	0.32916	0.02059	0.00000	0.00000	0.00264	0.00344	0.00000	0.01016	0.00468
CO_2	-	0.00000	0.00000	0.00000	0.00000	0.00000	0.00000	0.16174	0.15540	0.25885	0.00000	0.00026	0.26743	0.00560	0.00000	0.01656	0.08267
H_2O	-	0.00000	0.00000	0.00000	0.00000	0.00000	1.00000	0.15371	0.18691	0.36373	1.00000	0.00122	0.32888	0.47018	0.00000	0.58958	0.00304
CH_4	-	0.00000	0.00000	0.00000	0.00000	0.00000	0.00000	0.05126	0.04925	0.02839	0.00000	0.00000	0.04212	0.05489	0.00000	0.16219	0.30541
H_2S	-	0.00000	0.00000	0.00000	0.00000	0.00000	0.00000	0.00289	0.00277	trace	0.00000	0.00000	trace	trace	0.00000	trace	trace
NH_3	-	0.00000	0.00000	0.00000	0.00000	0.00000	0.00000	0.00377	0.00362	0.00208	0.00000	0.00000	0.00149	0.00000	0.00000	0.00000	0.00000
COS	-	0.00000	0.00000	0.00000	0.00000	0.00000	0.00000	0.00020	0.00019	trace	0.00000	0.00000	trace	trace	0.00000	trace	trace
HCl	-	0.00000	0.00000	0.00000	0.00000	0.00000	0.00000	trace	0.00000	0.00000	0.00000	0.00000	0.00000	0.00000	0.00000	0.00000	0.00000
SO_2	-	0.00000	0.00000	0.00000	0.00000	0.00000	0.00000	0.00000	0.00000	0.00000	0.00000	0.11498	0.00000	0.00000	0.00000	0.00000	0.00000
Total	-	0	0	1	1	0	1	0.99997	1	1	1	1	1	1	1	0.99999	0.99999
Stream Number	Unit	14	15	16	17	18	19	20	21	22	23	24	25	26	27	28	29
Temperature	°C	203.0	240.6	145.3	187.4	35.0	32.2	69.0	105.9	5.6	5.6	563.1	152.4	32.4	5.6	20.0	43.3
Pressure	bar	32.4	31.1	20.5	9.7	152.7	8.6	41.2	26.2	0.9	0.9	0.9	0.9	0.05	0.9	0.9	0.9
Molar Flowrate	kmol/h	26866	23229	88	15992	9321	35	93	6880	20087	100248	123831	123831	21152	278	83	761
Mass Flowrate	kg/h	295415	239891	2831	528028	410155	1120	2599	193077	580402	2896627	3308320	3308320	381052	8028	6085	21046
Solid Flowrate	kg/h	-	-	-	-	-	-	-	-	-	-	-	-	-	-	-	-
Mass Vapor Fraction	-	1	1	1	1	1	1	1	1	1	1	1	1	0.91558	1	0	1
Composition	mol-basis																
O_2	-	0.00000	0.00000	0.95001	0.00000	trace	0.95001	0.00540	0.00540	0.20810	0.20810	0.10787	0.10787	0.00000	0.20810	0.00000	0.03970
N_2	-	0.00547	0.00400	0.01406	trace	0.00028	0.01406	0.99230	0.99230	0.77590	0.77590	0.67794	0.67794	0.00000	0.77590	0.00000	0.88354
Ar	-	0.00581	0.00592	0.03594	trace	0.00049	0.03594	0.00230	0.00230	0.00930	0.00930	0.00875	0.00875	0.00000	0.00930	0.00000	0.01066
H_2	-	0.45460	0.49423	0.00000	0.00699	trace	0.00000	0.00000	0.00000	0.00000	0.00000	0.00000	0.00000	0.00000	0.00000	0.00000	0.00000
CO	-	0.00344	0.00239	0.00000	trace	trace	0.00000	0.00000	0.00000	0.00000	0.00000	0.00000	0.00000	0.00000	0.00000	0.00000	0.00000
CO_2	-	0.00560	0.00389	0.00000	0.58149	0.99922	0.00000	0.00000	0.00000	0.00030	0.00030	0.00857	0.00857	0.00000	0.00030	0.00000	0.00034
H_2O	-	0.47018	0.45148	0.00000	0.40716	0.00000	0.00000	0.00000	0.00000	0.00640	0.00640	0.19687	0.19687	1.00000	0.00640	0.31050	0.06560
CH_4	-	0.05489	0.03809	0.00000	0.00084	trace	0.00000	0.00000	0.00000	0.00000	0.00000	0.00000	0.00000	0.00000	0.00000	0.00000	0.00000
H_2S	-	trace	trace	0.00000	trace	trace	0.00000	0.00000	0.00000	0.00000	0.00000	0.00000	0.00000	0.00000	0.00000	0.00000	0.00000
NH_3	-	0.00000	0.00000	0.00000	0.00329	0.00000	0.00000	0.00000	0.00000	0.00000	0.00000	0.00000	0.00000	0.00000	0.00000	0.00000	0.00000
COS	-	trace	trace	0.00000	trace	0.00000	0.00000	0.00000	0.00000	0.00000	0.00000	0.00000	0.00000	0.00000	0.00000	0.00000	0.00000
HCl	-	0.00000	0.00000	0.00000	0.00000	0.00000	0.00000	0.00000	0.00000	0.00000	0.00000	0.00000	0.00000	0.00000	0.00000	0.00000	0.00000
SO_2	-	0.00000	0.00000	0.00000	0.00000	trace	0.00000	0.00000	0.00000	0.00000	0.00000	trace	trace	0.00000	0.00000	0.00000	0.00015
Total	-	1	1	1	0.99977	0.99999	1	1	1	1	1	1	1	1	1	0.31050	1

entering the reformer reactor than that required to avoid carbon deposition, the equilibrium is shifted towards the product side, which helps to lower the methane content in the syngas. Although there is only little water from the syngas lost through condensation in the H_2-PSA split stream, the water content of the syngas fed to the gas turbine is about $3\ \text{mol} - \% -$ points lower than that in the warm gas cleanup base case. This is caused by the reforming reaction, which consumes water and produces more molecules than it consumes which leads to a further reduction of the water content expressed in mol-%. The real effect of water reduction through the reformer is even greater since the carbon capture in this case is higher than that in the base case which further increases the relative water content in the syngas. The methane conversion in the reformer is 9.4 %. This conversion is not very high and thus, a very high recycle rate of 40 % is needed to achieve the targeted carbon capture of 90 %. Further addition of steam would help to improve the conversion of methane, but a higher steam content would lead to a significant amount of condensation during reformate compression and would increase the conversion only marginally. Furthermore, a lower water content in the syngas has to be compensated with more nitrogen diluent, which ultimately leads to a higher ASU compression power. The reformer equilibrium is also influenced by the reactor pressure. The gas volume of the products is higher than that of the reactants. Thus, lower the pressure, the higher the equilibrium conversion. However, the reactor pressure and piping system pressure at all times, has to be maintained above ambient pressure in order to avoid ambient oxygen leaking into the syngas.

The net power generation of the Pathway II scenario at $457,251$ kW is lower than that in the warm gas cleanup base scenario and the Pathway I scenario. Although, the power of $403,623$ kW generated by the gas turbine is the largest among the above-mentioned cases, the total gross power generated ($580,302$ kW) is considerably less than that in the other two cases. The steam turbine in the Pathway II scenario generates $176,679$ kW of power which is 3.6 % less than that in the warm gas cleanup base case and 11.1 % less than that in the Pathway I scenario. The reason for higher power output of the gas turbine lies in

the syngas composition and a slightly higher gas turbine firing temperature. The water content in the gas turbine fuel was reduced by $4.9\,\% - \text{points}$ compared to the Pathway I scenario and the hydrogen content was increased by $4.5\,\% - \text{points}$. This leads to a significant increase in heating value which is $18,991\,\frac{\text{kJ}}{\text{kg}}$ in the Pathway II scenario. The lower water content combined with higher heating value syngas results in a significant increase in nitrogen requirement in the gas turbine. The reduction in steam turbine power generation of the Pathway II scenario compared to the Pathway I scenario can be explained by the reduction in steam generation from the CO_2-conditioner combustor (in the Pathway I scenario additional methane combustion). Furthermore, the heat consumption of the reformer reduces the power output of the steam turbine in comparison with the warm gas cleanup base case or the Pathway I scenario. Major differences in the auxiliary load result from the ASU and the methane compressors. Based upon a constant coal flow, the ASU auxiliary load is much higher than that in the warm gas cleanup base case. This increase is due to the higher nitrogen requirement, which increases the main compression power and nitrogen compression power. The oxygen compression power is reduced since more high pressure nitrogen is required, which shifts the entire production to more high pressure products including oxygen. Thus, less oxygen from the low pressure stage has to be compressed, leading to a reduction in oxygen compression power. Compared to the Pathway I scenario, the ASU auxiliary load increases by only a small amount since the Pathway I scenario has a higher oxygen requirement than the warm gas cleanup base case, which also results in a higher air compression power. However, large differences in the oxygen and nitrogen compression power are recognizable due to the differences in oxygen and nitrogen demand of the individual cases. Another major item in the auxiliary load is the compression of the reformate stream. Because of the low methane conversion in the reformer, the resulting recycle rate and the higher compression ratio compared to the Pathway I scenario lead to an almost 7 times higher compression power of the recycle stream. This takes a major hit on the efficiency of the plant – $32.68\,\% - \text{HHV}$ – and thus $0.49\,\% - \text{points}$ lower than that in the Pathway I

scenario.

The water usage of the plant is 15.08 $\frac{\mathrm{m}^3}{\mathrm{min}}$ which is lower than that in the Pathway I scenario. However, the net power in the Pathway I scenario is higher making the Pathway I scenario more water efficient. The specific water usage of the Pathway II scenario is 1.9788 $\frac{\mathrm{m}^3_{\mathrm{water}}}{\mathrm{MWh}_{\mathrm{Net}}}$ versus 1.9420 $\frac{\mathrm{m}^3_{\mathrm{water}}}{\mathrm{MWh}_{\mathrm{Net}}}$ for the Pathway I scenario.

A performance summary of the Pathway II scenario is given in Table 4.28.

Table 4.28: Performance Summary of the Pathway II CO_2-PSA Warm Gas Cleanup Case with 90 % Carbon Capture

Gross Power Generation	Unit	GT Air Flow Limited	Constant Coal Flow
Gas Turbine	kW	403,623	418,698
Steam Turbine	kW	176,679	183,278
Total	kW	580,302	601,977
Auxiliary Load	Unit		
Coal Handling	kW	493	511
Coal Milling	kW	705	731
Coal Dryer Circulation Blower	kW	2,473	2,565
Ash Handling & Dewatering	kW	609	631
Air Separation Unit Auxiliaries	kW	499	518
Air Separation Unit Main Compressor	kW	40,697	42,217
Oxygen Compressor	kW	11,551	11,982
Nitrogen Compressor	kW	14,876	15,431
Syngas Recycle Compressor	kW	1,497	1,553
Carbon Dioxide Purification & Compressor	kW	23,449	24,325
Boiler Feed Water & Demin. Pumps	kW	5,394	5,596
Vacuum Condensate Pump	kW	345	358
Process Condensate & SWS System	kW	83	86
BFW Circulation Pumps	kW	78	81
Cooling Water Circulation Pumps	kW	2,418	2,508
Cooling Tower Fans	kW	1,330	1,379
Air Cooled Condenser Fans	kW	1,823	1,891
Scrubber Pumps	kW	589	611
Desulfurization Unit	kW	1,679	1,742
Gas Turbine Auxiliaries	kW	947	982
Steam Turbine Auxiliaries	kW	91	94
Sulfuric Acid Plant	kW	(1,206)	(1,251)
Miscellaneous Balance of Plant	kW	2,898	3,006
Transformer Losses	kW	2,363	2,451
Methane Compressor	kW	7,372	7,648
Total	kW	123,052	127,648
Net Power Generation	Unit		
Net Power Output	kW	457,251	474,329
Plant Performance	Unit		
Net Efficiency	%-HHV	32.68	32.67
Net Heat Rate	kJ/kWh	11015.5	11018.3
Consumables	Unit		
As-Received Coal	kg/h	253,220	262,678
Thermal Input	kW-HHV	1,399,128	1,451,385
Raw Water Usage	m^3/min	15.08	15.64
Carbon Capture	Unit		
Carbon Recovery	%	90.04	90.04

4.5.5 Pathway III – Methane Recycling to the Gasifier

Problematic for the Pathway II scenario is the low operating temperature of the reformer reactor. A low operating temperature thermodynamically favors methane formation. In order to achieve higher CH_4 conversion, a higher operating temperature is essential but challenging with respect to the heat integration of the plant. A reactor that operates at higher temperatures and promotes reforming and water-gas-shift reaction is the gasifier. In Pathway III, the methane tail gas from the H_2-PSA is recycled to the gasifier instead of feeding it into a separate reformer reactor. As a result, the compression ratio is increased to gasifier injection pressure, which affects the auxiliary power consumption of the plant negatively. Furthermore, the recycle stream leads to an increased mass flow rate between the point where the steam is split from the main stream and the mixer where the recycle stream is re-injected. Consequently, the equipment upstream of the split and downstream of the mix has to be scaled up to handle the increased flow rate. In order to minimize this effect, some of the gasifier raw syngas recycle is offset by the methane recycle. The raw syngas recycle in the TRIG^{TM} gasifier is required to entrain the coal particles in the gas flow. To maintain the momentum of the raw syngas recycle stream, the mass flow of the raw gas recycle stream is held constant.

A flow sheet of the Pathway III scenario is illustrated in Figure 4.61. A stream summary of the major streams at gas turbine air inlet flow limitations is provided in Table 4.29. The corresponding stream summary at constant coal flow rate is given in appendix Table A.8.

A higher methane content in the gasifier recycle stream changes the heat balance of the gasifier. The endothermicity of the steam methane reforming reaction requires a higher oxygen injection to increase the heat release by oxidation in order to maintain the same operating temperature. The heat loss is a function of temperature and gasifier size and is held constant in this off-design operation of the gasifier. For the same coal input, the oxygen

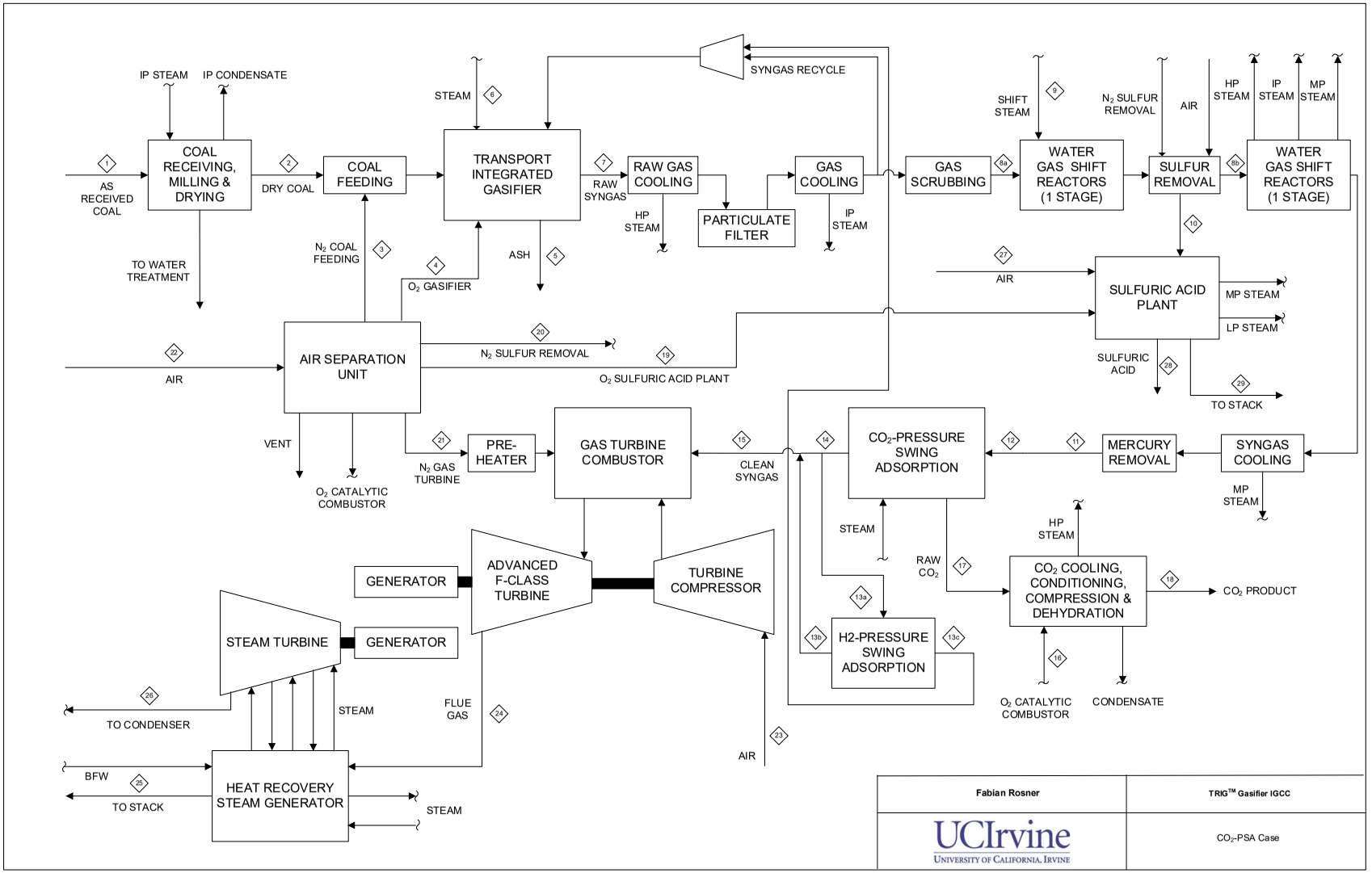

Figure 4.61: Flow sheet of the Pathway III CO_2-PSA warm gas cleanup case with hydrogen PSA and gasifier recycle for 90 % carbon capture.

Table 4.29: Stream Summary of the Pathway III CO_2-PSA Warm Gas Cleanup Case with 90 % Carbon Capture at Fully Loaded Gas Turbine

Stream Number	Unit	1	2	3	4	5	6	7	8a	8b	9	10	11	12	13a	13b	13c
Temperature	°C	5.6	71.1	105.9	79.5	982.2	397.9	982.2	161.6	408.0	331.8	760.0	199.0	199.0	203.0	26.0	178.0
Pressure	bar	0.9	0.9	56.2	50.3	3.4	51.0	41.7	38.3	35.6	51.0	34.2	32.6	32.6	32.2	31.2	46.0
Molar Flowrate	kmol/h	-	-	1644	4199	-	3458	25398	20452	34805	14353	503	34784	34784	5855	2287	733
Mass Flowrate	kg/h	-	-	46140	135191	-	62288	533296	427050	684687	258566	16232	684330	684330	64492	5547	7870
Solid Flowrate	kg/h	254844	230696	-	-	23417	-	-	-	-	-	-	-	-	-	-	-
Mass Vapor Fraction	-	0	0	1	1	0	1	1	1	1	1	1	1	1	1	1	1
Composition	mol-basis																
O_2	-	0.00000	0.00000	0.00540	0.95022	0.00000	0.00000	0.00000	0.00000	0.00000	0.00000	0.01091	0.00000	0.00000	0.00000	0.00000	0.00000
N_2	-	0.00000	0.00000	0.99230	0.01632	0.00000	0.00000	0.00584	0.00561	0.00330	0.00000	0.86405	0.00330	0.00330	0.00433	0.00089	0.03181
Ar	-	0.00000	0.00000	0.00230	0.03346	0.00000	0.00000	0.00766	0.00736	0.00432	0.00000	0.00858	0.00433	0.00433	0.00568	0.01018	0.01361
H_2	-	0.00000	0.00000	0.00000	0.00000	0.00000	0.00000	0.28137	0.27035	0.32739	0.00000	0.00000	0.34618	0.34618	0.45448	0.98894	0.54459
CO	-	0.00000	0.00000	0.00000	0.00000	0.00000	0.00000	0.33609	0.32293	0.02123	0.00000	0.00000	0.00265	0.00265	0.00348	0.00000	0.02783
CO_2	-	0.00000	0.00000	0.00000	0.00000	0.00000	0.00000	0.15239	0.14642	0.25467	0.00000	0.00026	0.27342	0.27342	0.00577	0.00000	0.04611
H_2O	-	0.00000	0.00000	0.00000	0.00000	0.00000	1.00000	0.15310	0.18630	0.35488	1.00000	0.00122	0.33650	0.33650	0.48448	0.00000	0.00235
CH_4	-	0.00000	0.00000	0.00000	0.00000	0.00000	0.00000	0.05632	0.05411	0.03180	0.00000	0.00000	0.03182	0.03182	0.04177	0.00000	0.33368
H_2S	-	0.00000	0.00000	0.00000	0.00000	0.00000	0.00000	0.00276	0.00265	trace	0.00000	0.00000	trace	trace	trace	0.00000	trace
NH_3	-	0.00000	0.00000	0.00000	0.00000	0.00000	0.00000	0.00427	0.00410	0.00241	0.00000	0.00000	0.00181	0.00181	0.00000	0.00000	0.00000
COS	-	0.00000	0.00000	0.00000	0.00000	0.00000	0.00000	0.00018	0.00017	trace	0.00000	0.00000	trace	trace	trace	0.00000	trace
HCl	-	0.00000	0.00000	0.00000	0.00000	0.00000	0.00000	trace	0.00000	0.00000	0.00000	0.00000	0.00000	0.00000	0.00000	0.00000	0.00000
SO_2	-	0.00000	0.00000	0.00000	0.00000	0.00000	0.00000	0.00000	0.00000	0.00000	0.00000	0.11498	0.00000	0.00000	0.00000	0.00000	0.00000
Total	-	0	0	1	1	0	1	0.99997	1	1	1	1	1	1	1	1	0.99999
Stream Number	Unit	14	15	16	17	18	19	20	21	22	23	24	25	26	27	28	29
Temperature	°C	203.0	240.6	145.3	187.1	35.0	32.2	69.0	105.9	5.6	5.6	563.0	152.3	32.4	5.6	20.0	43.3
Pressure	bar	32.2	30.9	20.5	9.7	152.7	8.6	41.2	26.2	0.9	0.9	0.9	0.9	0.05	0.9	0.9	0.9
Molar Flowrate	kmol/h	26257	24900	78	16095	9376	35	93	5363	20449	100248	123725	123725	21743	314	89	807
Mass Flowrate	kg/h	289201	270080	2526	531481	412587	1126	2616	150505	590870	2896627	3289635	3289635	391703	9074	6213	22248
Solid Flowrate	kg/h	-	-	-	-	-	-	-	-	-	-	-	-	-	-	-	-
Mass Vapor Fraction	-	1	1	1	1	1	1	1	1	1	1	1	1	0.91905	1	0	1
Composition	mol-basis																
O_2	-	0.00000	0.00000	0.95001	0.00000	trace	0.95001	0.00540	0.00540	0.20810	0.20810	0.10813	0.10813	0.00000	0.20810	0.00000	0.03763
N_2	-	0.00433	0.00363	0.01406	trace	0.00023	0.01406	0.99230	0.99230	0.77590	0.77590	0.66453	0.66453	0.00000	0.77590	0.00000	0.87737
Ar	-	0.00568	0.00559	0.03594	trace	0.00044	0.03594	0.00230	0.00230	0.00930	0.00930	0.00874	0.00874	0.00000	0.00930	0.00000	0.01051
H_2	-	0.45448	0.46323	0.00000	0.00672	trace	0.00000	0.00000	0.00000	0.00000	0.00000	0.00000	0.00000	0.00000	0.00000	0.00000	0.00000
CO	-	0.00348	0.00285	0.00000	trace	trace	0.00000	0.00000	0.00000	0.00000	0.00000	0.00000	0.00000	0.00000	0.00000	0.00000	0.00000
CO_2	-	0.00577	0.00473	0.00000	0.58147	0.99932	0.00000	0.00000	0.00000	0.00030	0.00030	0.00866	0.00866	0.00000	0.00030	0.00000	0.00033
H_2O	-	0.48448	0.48575	0.00000	0.40709	0.00000	0.00000	0.00000	0.00000	0.00640	0.00640	0.20994	0.20994	1.00000	0.00640	0.34872	0.07402
CH_4	-	0.04177	0.03423	0.00000	0.00062	trace	0.00000	0.00000	0.00000	0.00000	0.00000	0.00000	0.00000	0.00000	0.00000	0.00000	0.00000
H_2S	-	trace	trace	0.00000	trace	trace	0.00000	0.00000	0.00000	0.00000	0.00000	0.00000	0.00000	0.00000	0.00000	0.00000	0.00000
NH_3	-	0.00000	0.00000	0.00000	0.00391	0.00000	0.00000	0.00000	0.00000	0.00000	0.00000	0.00000	0.00000	0.00000	0.00000	0.00000	0.00000
COS	-	trace	trace	0.00000	trace	0.00000	0.00000	0.00000	0.00000	0.00000	0.00000	0.00000	0.00000	0.00000	0.00000	0.00000	0.00000
HCl	-	0.00000	0.00000	0.00000	0.00000	0.00000	0.00000	0.00000	0.00000	0.00000	0.00000	0.00000	0.00000	0.00000	0.00000	0.00000	0.00000
SO_2	-	0.00000	0.00000	0.00000	0.00000	trace	0.00000	0.00000	0.00000	0.00000	0.00000	trace	trace	0.00000	0.00000	0.00000	0.00014
Total	-	1	1	1	0.99980	0.99999	1	1	1	1	1	1	1	1	1	0.34872	1

demand rose by 1.02 %. As a result of this increased overall mass flow, the amount of raw gas recycle in the Pathway III scenario is minimally higher than that in the other cases when comparing on a constant coal flow basis.

The change in atomic composition of the syngas is small. However, the increase of oxygen in the syngas allows a lower steam to carbon monoxide ratio in the shift section of 2.75 from initially 2.80. The higher mass flow and lower CO and H_2O partial pressure in the syngas in the Pathway III scenario require more shift catalyst. Changes in reactor design of the first reactor are small because of its high operating temperature and fast kinetics. The catalyst in the first reactor requires a volume of 140.5 m^3 (diameter 3.51 m). Because of the higher mass flow and velocity, the resulting pressure drop is 1.33 bar. The low temperature sweet shift reactor requires 61.2 m^3 catalyst (diameter 3.15 m), a 3.6 % increase. The pressure drop associate with the catalyst bed is 1.62 bar. The design of the shift reactors is based on the kinetic evaluation of the reaction which can be found in appendix C.29 - C.40. The corresponding whisker carbon equilibrium curves can be found in appendix B.6 and B.7.

Recycling a methane rich stream back to the gasifier reduces the amount of recycled gas to 22.3 % compared to 40 % in the Pathway II scenario which indicates a much higher methane conversion efficiency in the gasifier than in the reformer reactor. As a result of this higher methane content in the gasifier feed, the product stream's methane concentration rises too. The methane is then carried through the shift reactors and CO_2-PSA. A reduction of the methane content of the syngas fed to the gas turbine is achieved after the H_2-PSA. A portion of the syngas is split off and the majority of its hydrogen is re-injected into the syngas fed to the gas turbine. This hydrogen injection causes the methane content in the syngas to decrease below the required level to enable a carbon capture of 90 %. Since the methane recycle replaces some of the raw syngas recycle, the compression power of the raw syngas recycle compressor would be expected to decrease (on a constant coal flow basis). However, the methane recycle stream is small compared to the raw syngas recycle and the pressure ratio is not significant which reduces the power consumption of the gasifier recycle compressor by

only 2.4 %. The methane recycle compressor has a greater impact on the plant performance. In order to recycle the methane rich stream back to the gasifier it is compressed from 1.3 bar to 46.0 bar. Although the stream is comparatively small, the pressure ratio is so large that the compression power is more than double as much as the compression power of the raw syngas recycle. Drawing an analogy to the Pathway II scenario, the methane compression power could be cut in half due to the higher methane conversion in the gasifier and the resulting lower recycle requirement. Other major losses include the increased compression power for CO_2 compression as well as an increase in compression power for the ASU main compressor and nitrogen compressor. The compression power for CO_2 is the same for all 90 % capture cases since they use the same capture technology. The ASU auxiliary load, including main air compressor, nitrogen compressor and oxygen compressor, in the Pathway III scenario is the lowest among all 90 % capture cases. Pathway I requires more oxygen for methane combustion and Pathway II has a higher nitrogen demand for syngas dilution. The Pathway III scenario produces syngas with a heating value of $17,099\ \frac{\text{kJ}}{\text{kg}}$ which is between those in the Pathway I and Pathway II scenarios. Furthermore, the water concentration in the Pathway III syngas is at a medium level, in between those of Pathway I and Pathway II, which results in a modest nitrogen requirement for syngas dilution. Thus, the Pathway III scenario offers the best compromise between high heating value and high water content syngas to effectively reduce the auxiliary load of the ASU.

The power generated by the gas turbine is $400,992$ kW which is more than that in the Pathway I and less than that in the Pathway II scenario and is very much related to the nitrogen diluent (GT firing temperature is the same as in Pathway I). The steam turbine power output is $182,912$ kW. This is less than in the Pathway I scenario since the methane reforming consumes heat instead of producing heat by methane combustion. However, the Rankine cycle power output is significantly higher than that in the Pathway II case which also uses reforming. Reforming methane in the gasifier consumes only the amount of heat needed supplied by partial oxidation. In the separate adiabatic reformer reactor, a signif-

icant amount of heat is lost due to cooling and reheating since the heat is supplied by an external source. Furthermore, the reforming case uses reheat steam to preheat the reformer feed which reduces the power output of the steam cycle. The net power generated in the Pathway III scenario is $468,886$ kW resulting in an efficiency of 33.30 %. This is the highest efficiency among the 90 % carbon capture cases and $0.52 - 0.13$ % $-$ points away from the ideal values using this CO_2-PSA technology. The net power in the Pathway III scenario is higher than that in the Pathway II scenario, which has a particularly low net power generation because of the high power consumption of the methane compressor and the low power output of the steam cycle. The net power of the Pathway I scenario is much higher than that for the Pathway III scenario because the plant is scaled to full turbine load. Splitting off a portion of the syngas to produce steam helps to increase the net power generation but increases the coal flow rate too.

The water consumption of the plant at fully loaded gas turbine is 15.21 $\frac{\mathrm{m}^3}{\mathrm{min}}$. This is a specific water consumption of 1.9463 $\frac{\mathrm{m}^3_{\mathrm{water}}}{\mathrm{MWh}_{\mathrm{Net}}}$ which makes it almost as water efficient as the Pathway I scenario. Pathway I has the greatest cooling requirement in the Rankine cycle, followed by the Pathway III scenario and the Pathway II scenario. The syngas split fraction to the H_2-PSA in the Pathway III scenario is much larger than that in the Pathway I scenario. Before the syngas enters the H_2-PSA, it has to be cooled to 26 °C. The higher mass flow to the H_2-PSA in the Pathway III scenario raises the cooling load to the same level as in the Pathway I scenario but the higher water content in the syngas in the Pathway III scenario ultimately increases the water losses through the stack, leading to an overall higher water consumption than in the Pathway II case. The Pathway II case has a low cooling demand of the Ranking cycle but the methane compression in the Pathway II case (40 % recycle) increases the cooling demand significantly making it the highest water consumer among the tested scenarios.

A summary on the Pathway III IGCC performance is provided in Table 4.30.

Table 4.30: Performance Summary of the Pathway III CO_2-PSA Warm Gas Cleanup Case with 90 % Carbon Capture

Gross Power Generation	Unit	GT Air Flow Limited	Constant Coal Flow
Gas Turbine	kW	400,992	413,318
Steam Turbine	kW	182,912	188,534
Total	kW	583,904	601,853
Auxiliary Load	Unit		
Coal Handling	kW	496	511
Coal Milling	kW	710	731
Coal Dryer Circulation Blower	kW	2,489	2,565
Ash Handling & Dewatering	kW	613	631
Air Separation Unit Auxiliaries	kW	389	401
Air Separation Unit Main Compressor	kW	38,605	39,791
Oxygen Compressor	kW	12,908	13,304
Nitrogen Compressor	kW	11,873	12,238
Syngas Recycle Compressor	kW	1,471	1,516
Carbon Dioxide Purification & Compressor	kW	23,499	24,221
Boiler Feed Water & Demin. Pumps	kW	5,462	5,630
Vacuum Condensate Pump	kW	351	361
Process Condensate & SWS System	kW	85	88
BFW Circulation Pumps	kW	81	84
Cooling Water Circulation Pumps	kW	2,310	2,381
Cooling Tower Fans	kW	1,270	1,309
Air Cooled Condenser Fans	kW	1,874	1,932
Scrubber Pumps	kW	593	611
Desulfurization Unit	kW	1,690	1,742
Gas Turbine Auxiliaries	kW	940	969
Steam Turbine Auxiliaries	kW	94	97
Sulfuric Acid Plant	kW	(1,208)	(1,246)
Miscellaneous Balance of Plant	kW	2,916	3,006
Transformer Losses	kW	2,378	2,451
Methane Compressor	kW	3,129	3,226
Total	kW	115,018	118,553
Net Power Generation	Unit		
Net Power Output	kW	468,886	483,299
Plant Performance	Unit		
Net Efficiency	%-HHV	33.30	33.29
Net Heat Rate	kJ/kWh	10811.1	10813.8
Consumables	Unit		
As-Received Coal	kg/h	254,844	262,678
Thermal Input	kW-HHV	1,408,101	1,451,385
Raw Water Usage	m^3/min	15.21	15.68
Carbon Capture	Unit		
Carbon Recovery	%	90.00	90.00

4.6 Techno-Economic Analysis

The techno-economic analysis is conducted in accordance with the methodology described in 4.1.4. The Selexol^{TM} case TPC is estimated to be \$ 1,738,374,000. With a net power generation of 452 MW the specific plant cost is 3,849 $\frac{\$}{kW}$. Compared to the CO_2-PSA base case with a TPC of \$ 1,631,377,000, the plant cost of the Selexol^{TM} case is 6.6 % higher. The cost of gas turbine equipment and associated equipment for both cases are very similar because in both cases the gas turbine is operated at fully loaded conditions. Small deviation in costs are seen in HRSG, feed water systems, water makeup and other feedwater systems, service water, fuel gas systems miscellaneous power plant equipment, instrumentations, site improvements and building costs. Since the gas turbine is operated at full load, the HRSG operates at similar conditions. However, the steam generation side differs as the in-plant steam usage changes. Water system related costs are also very similar since the total raw water usage of both plants (14.45 $\frac{m^3}{min}$ vs. 14.64 $\frac{m^3}{min}$) is almost identical. Nevertheless, the warm gas cleanup technology is more water efficient because of its higher net power generation. Equipment associated with the Rankine cycle, steam turbine, condensers and cooling water systems, have a higher cost in the Selexol^{TM} case due to its higher power generation by the Rankine cycle. Because of the higher efficiency of the CO_2-PSA base case, less coal is needed to operate the turbine at full load and thus equipment upstream of the gas turbine can be down scaled. This effect has especially strong impact on expensive equipment like the ASU, fuel preparation and gasifier. Large savings are also seen in the shift reactor expenses, which can be traced back to the replacement of the low temperature sour shift catalyst with a more reactive sweet shift catalyst. The reduction in catalyst volume significantly lowers the cost of the shift reactors by 31.4 %. A further cost reduction of the CO_2-PSA case is associated with omission of the syngas humidification. The increase in fuel gas piping cost is a result of the higher water content in the PSA case syngas. Compared to the syngas humidifying equipment this cost increase is negligible. Although, the costs associated with

the sulfuric acid unit are higher than that of the Claus unit, the CO_2-PSA and warm gas desulfurization are less expensive than the dual stage Selexol^{TM} unit. Furthermore, CO_2 compression and purification in the CO_2-PSA case are more expensive. Overall comparing desulfurization, decarbonization, CO_2 compression and purification, savings of 17.0 % are seen by moving from the Selexol^{TM} process to the CO_2-PSA process.

Comparing the CO_2-PSA base case with the Optimization I scenario, a small increase in TPC is observed ($\$\ 1,641,255,000$). However, the specific plant cost decreased to $3,298\ \frac{\$}{kW}$ because of the higher net power generation. Although the optimization of the shift section in the Optimization I case leads to a reduction in the shift reactor costs, the TPC increases because of the higher steam availability. Higher steam availability is achieved by reduction of shift steam. This ultimately leads to an increase in cost of the steam turbine generator, steam condensers and other boiler systems. Less shift steam injection into the syngas, which eventually leaves through the stack, reduces the water consumption and thus, the costs of the feedwater system. The same effects become visible when looking into the Optimization II case. However, a decrease in TPC in the Optimization II case is observed ($\$\ 1,639,866,000$) because of the reduced rector size originating at faster reaction kinetics by using only sweet shifting in this case.

Similar observations are made for the Isothermal Shift I and II cases. Differences in these cases are the steam to carbon ratio and the cost of the shift reactors. In the Isothermal Shift I case the TPC drops to $\$\ 1,631,648,000$ due to the savings made in the shift section. Using IP steam generation for cooling the reactor significantly reduces the reactor size. The cost increases in steam condenser and feed water system are small compared to the cost reduction of the shift section. For the Isothermal Shift II case the TPC increases again to $\$\ 1,637,543,000$ as a result of the larger rector size needed in this scenario. The production of more HP steam increases the cost of the steam turbine but reduces the cost of the condensers compared to the Isothermal Shift I case due to a lower mass flow when producing HP steam only.

In the 90 % carbon capture scenarios, Pathway I, Pathway II and Pathway III, the TPC increases to $ 1,695,892,000, $ 1,680,768,000 and $ 1,667,609,000. The specific plant cost among the Pathway scenarios is the lowest for the Pathway I case with $3,516 \frac{\$}{kW}$ versus $3,676 \frac{\$}{kW}$ for the Pathway II case and $3,557 \frac{\$}{kW}$ for the Pathway III case. Due to the higher carbon capture in the Pathway scenarios, the cost for the CO_2-PSA equipment increases as well as the CO_2 purification and compression equipment. Furthermore, the Pathway scenarios use extra equipment, e.g. H_2-PSA and recycle gas compressor (Pathway I, II & III), reformer (Pathway II) which add costs to the TPC. Other plant costs are very similar to the CO_2-PSA base case except the equipment upstream of the gas turbine in the Pathway I case and the ASU cost in the Pathway III case. In the Pathway I case some of the syngas is combusted in the CO_2 purification system with oxygen to raise steam which leads to an increase in coal flow in order to operate the gas turbine at full load. Thus, all the equipment upstream of the gas turbine has to be scaled up. In the Pathway III case the gasifier is operated under different conditions using the methane rich stream from the H_2-PSA to replace some of the gasifier recycle steam. Methane reforming is endothermic and requires a higher oxygen input to balance the energy in the gasifier. The higher oxygen demand directly impacts the ASU size and its cost as it can be seen from the cost analysis.

A detailed listing of all individual plant parts with their associated costs are presented in Table 4.31.

Fix annual operating costs in the Selexol^{TM} case are $ 66,736,000 and are slightly higher than those in the CO_2-PSA base case with $ 63,642,000. Differences in the fix operating costs are due to property tax and maintenance labor cost. Also, the maintenance cost of the Selexol^{TM} case is higher ($ 34,056,000) than that in the CO_2-PSA base case ($ 32,640,000) because of the more expensive equipment used in the Selexol^{TM} case. Total cost of raw water is similar as well as the costs for CO_2 TS&M. Annual cost for coal in the Selexol^{TM} case is higher ,$ 39,833,000 versus $ 38,419,000, due to the improved plant efficiency. In general, the Selexol^{TM} case requires less chemicals/catalysts but the high

Table 4.31: Summary of Total Plant Costs

Equipment	Total Plant Cost ($1000)								
	Selexol^{TM}	CO_2-PSA Base	Optimization I	Optimization II	Isoth. Shift I	Isoth. Shift II	Pathway I	Pathway II	Pathway III
Air Separation Unit	187,569	183,044	183,027	183,121	183,166	182,990	187,984	182,911	186,313
Fuel Receiving, Preparation & Feeding	201,734	196,980	197,028	197,164	197,201	196,990	201,988	196,910	197,743
Gasifier, Syngas Cooler & Auxiliaries	337,927	328,654	328,747	329,012	329,084	328,674	338,424	328,518	330,140
Gasification Foundations	23,264	22,847	22,852	22,864	22,867	22,848	23,286	22,841	22,914
Ash Handling Systems	46,341	45,429	45,439	45,465	45,472	45,431	46,390	45,416	45,576
Flare Stack System	2,290	2,250	2,250	2,251	2,252	2,250	2,293	2,249	2,256
Shift Reactor	37,787	25,927	21,611	19,145	11,563	18,697	26,728	25,916	26,604
LTGC + Syngas Humidification	22,795	-	-	-	-	-	-	-	-
Warm Gas Desulfurization	-	14,501	14,505	14,517	14,520	14,502	14,943	14,495	14,568
Sulfuric Acid Plant	-	30,942	30,950	30,971	30,977	30,944	31,741	30,931	31,064
Blowback Gas Systems	3,402	3,366	3,366	3,367	3,367	3,366	3,404	3,365	3,372
Fuel Gas Piping	1,863	2,459	2,187	2,158	2,154	2,199	2,444	2,284	2,402
Gas Cleanup Foundations	2,159	2,098	1,895	1,874	1,871	1,904	2,162	2,097	2,156
Mercury & Trace Contaminant Removal (Cold Gas)	3,855	-	-	-	-	-	-	-	-
Mercury & Trace Contaminant Removal (Warm Gas)	-	3,341	3,342	3,344	3,345	3,341	3,440	3,339	3,356
Selexol Unit	217,734	-	-	-	-	-	-	-	-
CO_2 Compression, Dehydration & Pumping (Selexol)	60,478	-	-	-	-	-	-	-	-
Claus Plant & TG Recycle	19,866	-	-	-	-	-	-	-	-
Carbon Dioxide PSA	-	141,817	141,897	142,085	142,092	141,882	154,887	150,367	151,062
Carbon Dioxide Purification & Heat Recovery	-	24,477	24,475	24,511	24,512	24,473	27,252	26,159	26,308
CO_2 Compression, Dehydration & Pumping (CO_2-PSA)	-	50,114	50,326	50,404	50,407	50,318	55,358	53,900	54,002
Hydrogen PSA	-	-	-	-	-	-	6,250	14,735	9,628
Adiabatic Reformer	-	-	-	-	-	-	-	12,148	-
Recycle Compressor	-	-	-	-	-	-	2,067	8,644	2,346
Gas Turbine, Generator & Auxiliaries	159,009	159,009	159,009	159,009	159,009	159,009	159,009	159,009	159,009
HRSG, Ducting & Stack	51,524	50,890	51,114	50,971	50,947	51,112	50,583	50,871	50,832
Steam Turbine, Generator & Auxiliaries	70,548	68,247	75,235	75,338	74,163	75,125	72,203	66,517	68,151
Steam Condensers	41,992	37,262	41,852	42,055	42,744	41,443	40,017	37,128	37,960
Feedwater System	25,166	25,367	22,765	22,501	22,466	22,880	26,383	25,746	25,878
Water Makeup & Pretreating	1,719	1,733	1,675	1,667	1,672	1,675	1,815	1,771	1,782
Other Feedwater Subsystems	3,849	3,722	4,108	4,114	4,049	4,102	3,940	3,626	3,716
Service Water Systems	4,481	4,367	4,368	4,372	4,373	4,368	4,487	4,366	4,386
Other Boiler Plant Systems	5,104	4,930	5,458	5,466	5,377	5,450	5,229	4,800	4,923
Fuel Oil System & Natural Gas	2,134	2,106	2,111	2,114	2,114	2,110	2,105	2,108	2,105
Waste Water Treatment	1,704	1,661	1,661	1,662	1,663	1,661	1,706	1,660	1,668
Misc. Power Plant Equipment	2,824	2,789	2,824	2,827	2,822	2,823	2,805	2,783	2,787
Cooling Water System	29,778	24,146	26,024	26,133	26,335	25,875	26,315	26,595	25,730
Accessory Electric Plant	96,851	94,558	96,808	97,029	96,708	96,756	95,615	94,220	94,483
Instrumentation & Controls	31,163	31,017	31,018	31,022	31,023	31,017	31,170	31,014	31,040
Improvement to Site	21,824	21,761	21,761	21,763	21,764	21,761	21,827	21,760	21,771
Buildings & Structures	19,638	19,568	19,568	19,570	19,571	19,568	19,642	19,567	19,579
Total	1,738,374	1,631,377	1,641,255	1,639,866	1,631,648	1,637,543	1,695,892	1,680,768	1,667,609
Specific Plant Cost in $/kW	3,849	3,407	3,298	3,283	3,295	3,292	3,516	3,676	3,557

costs for the sour shift catalyst and the Selexol^{TM} solvent lead to an overall higher cost for the initial fill costs ($\$ 15,202,000$ vs. $\$ 14,683,000$). However, on an annual basis, the Selexol^{TM} case has a lower cost for chemicals/catalysts and waste disposal ($\$ 11,152,000$ vs. $\$ 13,180,000$) mainly due to the high cost of the high temperature trace component sorbent and its need for quarterly replacement. A large difference is seen in the annual byproduct credit. The Selexol^{TM} based plant with Claus process generates a byproduct value of $\$ 1,459,000$, whereas the warm gas cleanup IGCC with the sulfuric acid unit generates a byproduct value of $\$ 4,494,000$.

In the Optimization I & II cases, the variable cost is lowered by the usage of a less expensive high temperature sweet shift catalyst and a reduction in catalyst volume. This leads to a reduction in initial fill cost in the Optimization I case to $\$ 12,995,000$ and $\$ 12,060,000$ in the Optimization II case. Furthermore, the annual costs for chemicals/catalysts and waste disposal are reduced to $\$ 12,404,000$ and $\$ 11,901,000$ but because of the high cost of the trace contaminant sorbent, the costs were not able to drop below the Selexol^{TM} case levels.

The Isothermal Shift I case has the lowest shift reactor costs and the initial fill costs are $\$ 11,952,000$. The initial fill cost for the Isothermal Shift II case are $\$ 12,530,000$. Annual costs for chemicals/catalysts and waste disposal are $\$ 11,867,000$ and $\$ 12,050,000$.

The Pathway scenarios are more similar to the CO_2-PSA base case, however, have additional demand for catalyst/chemicals due the employment of a H_2-PSA and/or reformer and/or larger catalytic combustor in the CO_2 purification section. As a result, the initial fill as well as the annual costs for chemicals/catalysts and waste disposal are higher compared to the other cases.

Some characteristic numbers of the financial analysis are summarized in Table 4.32 and Table 4.34.

TPC and operating cost have a direct impact on the cost-of-electricity (COE). The COE of the Selexol^{TM} case without TS&M is 129.4 $\frac{\$}{\text{MWh}}$ and with TS&M 148.6 $\frac{\$}{\text{MWh}}$. The lower TPC and operating cost in the CO_2-PSA base case lead to a COE of 115.1 $\frac{\$}{\text{MWh}}$ and

Table 4.32: Summary I of Operating and Maintenance Costs

Item	Unit	Selexol™	Base Case CO_2-PSA	Optimization I	Optimization II	Isothermal Shift I	Isothermal Shift II
Net Power	MW	452	479	498	500	495	497
Net Efficiency	HHV-%	31.11	34.20	35.54	35.63	35.31	35.53
Capacity Factor (CF)	%	80	80	80	80	80	80
Total Plant Cost (TPC)	$1000	1,738,374	1,631,377	1,641,255	1,639,866	1,631,648	1,637,543
6 Month Labor Cost	$1000	15,984	15,507	15,583	15,579	15,567	15,606
1 Month Maintenance Materials	$1000	2,838	2,720	2,739	2,738	2,735	2,745
1 Month Non-Fuel Consumables	$1000	719	881	803	758	757	774
1 Month Waste Disposal	$1000	490	500	500	501	501	500
25% of 1 Month Fuel Cost at 100% CF	$1000	1,037	1,001	1,001	1,002	1,002	1,001
2% of TPC	$1000	34,767	32,628	32,825	32,797	32,633	32,751
60 Day Supply of Fuel & Consumables at 100% CF	$1000	9,602	9,632	9,481	9,402	9,400	9,421
0.5% of TPC (Spare Parts)	$1000	8,692	8,157	8,206	8,199	8,158	8,188
Initial Catalyst & Chemicals Cost	$1000	15,202	14,683	12,995	12,060	11,952	12,530
Land	$1000	900	900	900	900	900	900
Other Owner's Costs (15% of TPC)	$1000	260,756	244,706	246,188	245,980	244,747	245,631
Financing Costs	$1000	46,936	44,047	44,314	44,276	44,054	44,214
Total Overnight Cost (TOC)	$1000	2,136,298	2,006,738	2,016,790	2,014,060	2,004,054	2,011,802
Fixed Operating Cost for Initial Year of Operation (OCF)	$1000	66,736	63,642	63,991	63,955	63,767	63,963
Annual Feed Cost at above CF for Initial Year (OCV1)	$1000	39,833	38,419	38,434	38,474	38,485	38,422
Other Annual Variable Operating Cost at above CF for Initial Year (OCV2)	$1000	38,853	39,372	38,806	38,376	38,330	38,577
Annual CO_2 Transporting, Storing, and Monitoring Cost at above CF for Initial Year (OCV3)	$1000	60,714	58,562	58,605	58,706	58,709	58,597
Annual Byproduct Revenues at above CF for Initial Year (OCV4)	$1000	1,459	4,494	4,496	4,501	4,502	4,495

Table 4.33: Summary I of Carbon Capture Costs and Avoided Costs

Item	Unit	Selexol™	CO_2-PSA Base	Optimization I	Optimization II	Isothermal Shift I	Isothermal Shift II
1st Year Cost of Electricity (COE) w/o CO_2 TS&M	$/MWh	129.4	115.1	111.1	110.4	111.0	110.9
1st Year Cost of Electricity (COE)	$/MWh	148.6	132.6	127.9	127.2	127.9	127.7
1st Year CO_2 Capture Cost with CO_2 TS&M Compared to Corresponding IGCC (w/o CO_2 Capture)	$/tonne	66.0	52.4	48.3	47.5	48.0	48.0
1st yearCO_2 Capture Cost with CO_2 TS&M Compared to SCPC (w/oCO_2 Capture)	$/tonne	88.0	76.6	73.4	72.7	73.0	73.2
1st Year CO_2 Avoided Cost with CO_2 TS&M Compared to Corresponding IGCC (w/o CO_2 Capture)	$/tonne	89.4	63.0	55.4	54.3	55.5	55.1
1st year CO_2 Avoided Cost with CO_2 TS&M Compared to SCPC (w/o CO_2 Capture)	$/tonne	112.2	86.8	79.4	78.3	79.5	79.1

Table 4.34: Summary II of Operating and Maintenance Costs

Item	Unit	Pathway I	Pathway II	Pathway III
Net Power	MW	482	457	469
Net Efficiency	HHV-%	33.17	32.68	33.30
Capacity Factor (CF)	%	80	80	80
Total Plant Cost (TPC)	$1000	1,695,892	1,680,768	1,667,609
6 Month Labor Cost	$1000	15,863	15,775	15,680
1 Month Maintenance Materials	$1000	2,809	2,787	2,763
1 Month Non-Fuel Consumables	$1000	922	907	904
1 Month Waste Disposal	$1000	522	502	505
25% of 1 Month Fuel Cost at 100% CF	$1000	1,039	1,000	1,006
2% of TPC	$1000	33,918	33,615	33,352
60 Day Supply of Fuel & Consumables at 100% CF	$1000	10,020	9,679	9,724
0.5% of TPC (Spare Parts)	$1000	8,479	8,404	8,338
Initial Catalyst & Chemicals Cost	$1000	15,530	15,364	15,147
Land	$1000	900	900	900
Other Owner's Costs (15% of TPC)	$1000	254,384	252,115	250,141
Financing Costs	$1000	45,789	45,381	45,025
Total Overnight Cost (TOC)	$1000	2,086,069	2,067,197	2,051,096
Fixed Operating Cost for Initial Year of Operation (OCF)	$1000	65,645	65,166	64,713
Annual Feed Cost at above CF for Initial Year (OCV1)	$1000	39,909	38,399	38,645
Other Annual Variable Operating Cost at above CF for Initial Year (OCV2)	$1000	40,828	40,277	40,058
Annual CO_2 Transporting, Storing, and Monitoring Cost at above CF for Initial Year (OCV3)	$1000	65,666	63,188	63,567
Annual Byproduct Revenues at above CF for Initial Year (OCV4)	$1000	4,669	4,492	4,521

Table 4.35: Summary II of Carbon Capture Costs and Avoided Costs

Item	Unit	Pathway I	Pathway II	Pathway III
1st Year Cost of Electricity (COE) w/o CO_2 TS&M	$/MWh	118.7	123.7	119.9
1st Year Cost of Electricity (COE)	$/MWh	138.1	143.4	139.2
1st Year CO_2 Capture Cost with CO_2 TS&M Compared to Corresponding IGCC (w/o CO_2 Capture)	$/tonne	53.3	58.5	54.8
1st year CO_2 Capture Cost with CO_2 TS&M Compared to SCPC (w/oCO_2 Capture)	$/tonne	75.0	79.9	76.7
1st Year CO_2 Avoided Cost with CO_2 TS&M Compared to Corresponding IGCC (w/o CO_2 Capture)	$/tonne	65.4	72.9	66.9
1st year CO_2 Avoided Cost with CO_2 TS&M Compared to SCPC (w/o CO_2 Capture)	$/tonne	87.2	94.3	88.6

132.6 $\frac{\$}{\text{MWh}}$ with TS&M. After optimization of this case, the COE drops to 111.1 $\frac{\$}{\text{MWh}}$ for Optimization I, 110.4 $\frac{\$}{\text{MWh}}$ for Optimization II, and 127.9 $\frac{\$}{\text{MWh}}$ for Optimization I, 127.2 $\frac{\$}{\text{MWh}}$ for Optimization II with TS&M. The Isothermal Shift I and II scenarios COEs are close to the Optimization I and II cases but the efficiency penalty is too large despite the reduced plant cost. The Isothermal Shift I case has a COE of 111.0 $\frac{\$}{\text{MWh}}$ without TS&M and a COE of 127.9 $\frac{\$}{\text{MWh}}$ with TS&M. The Isothermal Shift II case has a COE of 110.9 $\frac{\$}{\text{MWh}}$ without TS&M and a COE of 127.7 $\frac{\$}{\text{MWh}}$ with TS&M. Among the Pathway scenarios, Pathway I is the most effective solution to reaching a carbon capture of 90 %. Although Pathway I has the highest TPC and operating costs among the Pathway scenarios and not the highest plant efficiency, the higher power output can compensate for these additional costs leading to a COE of 118.7 $\frac{\$}{\text{MWh}}$ and 138.1 $\frac{\$}{\text{MWh}}$ with TS&M. The second best option for 90 % carbon capture is the Pathway III scenario with a COE of 119.9 $\frac{\$}{\text{MWh}}$ and 139.2 $\frac{\$}{\text{MWh}}$ with TS&M. Highest COE while achieving 90 % carbon capture is obtained with the separate reformer reactor resulting in a COE of 123.7 $\frac{\$}{\text{MWh}}$ and 143.4 $\frac{\$}{\text{MWh}}$ with TS&M.

Cost of carbon capture and avoided cost are compared to a corresponding TRIG™ IGCC plant without carbon capture and a supercritical PC plant without carbon capture. The COE for the IGCC was estimated with 91.00 $\frac{\$}{\text{MWh}}$ and that for the PC plant with 71.80 $\frac{\$}{\text{MWh}}$. Basis of the COE is 2011$ and is escalated from [24, 25]. CO_2 emissions for these reference plants are 859 $\frac{\text{kg}}{\text{MWh}}$ and 818 $\frac{\text{kg}}{\text{MWh}}$ respectively [24, 25].

The cost of carbon capture as well as avoided cost are the lowest for the Optimization II case, which also has the lowest COE. The cost for carbon capture with TS&M is reduced from 66.0 $\frac{\$}{\text{tonne}}$ to 47.5 $\frac{\$}{\text{tonne}}$ compared to a corresponding IGCC without carbon capture. In comparison to a PC plant, the cost of capture is reduced from 88.0 $\frac{\$}{\text{tonne}}$ to 72.7 $\frac{\$}{\text{tonne}}$. A similar behavior is observed for the avoided costs which are reduced from 89.4 $\frac{\$}{\text{tonne}}$/112.2 $\frac{\$}{\text{tonne}}$ to 54.3 $\frac{\$}{\text{tonne}}$/78.3 $\frac{\$}{\text{tonne}}$. All results are summarized in Table 4.33 and Table 4.35. The overall trend shows that the plants with the lowest carbon capture cost or avoided cost have the lowest COE. This illustrates the importance of finding more efficient and cost effective ways

of removing CO_2 from the syngas or exhaust stream.

Chapter 5

Summary, Conclusions and Recommendations

5.1 Summary

A design basis for IGCC plants facilitating a highly efficient, low temperature TRIG™ gasifier utilizing low rank coal was established. Feedstock and site characteristics were identified, and critical operating parameters were determined. Implemented models were validated with literature, internal data and experimental data. A methodology for the techno-economic evaluation of the plant design was identified and a financing structure based on financial risk analysis was selected. For the estimation of the capital cost, scaling exponents based on individual scaling parameters were derived from literature and a basis for individual maintenance cost relationships was established. Furthermore, a basis for operational costs was created to account for viable and fixed operating cost.

A state-of-the-art IGCC power plant with dual-stage Selexol™ unit for carbon capture (cold gas cleanup) was designed, evaluated and compared to available literature. Based

upon the plant design of the cold gas cleanup, a novel PSA-based CO_2-removal technology (warm gas cleanup) was integrated into the plant replacing the dual-stage Selexol^{TM} unit with a warm gas sulfur removal unit and the novel warm gas CO_2-removal unit. Further adjustments to the plant design were made to meet the criteria laid down in the design basis, e.g. warm gas mercury removal and CO_2 conditioning system. Installation of the warm gas sulfur removal unit also required a reevaluation of the Claus process and the heat integration of the plant. A detailed comparison between the two carbon capture systems was conducted with respect to their performance, water usage and economics.

In order to optimize the performance of the IGCC and reduce the impact of carbon capture on the efficiency, the water-gas-shift section of the plant was optimized. For this purpose an equilibrium-based, thermodynamic gas stability analysis code was used to predict the optimum steam to carbon monoxide ratio. Furthermore, a kinetic model for the analysis of the water-gas-shift reactors was developed based upon intrinsic power law kinetics. The analysis and optimization were conducted at constant carbon capture to maintain comparability. Based upon the process integration of the shift reactors, sour high-temperature shifting, sour low-temperature shifting, sweet high-temperature shifting, and sweet low-temperature shifting were analyzed with respect to their specific pressure drop, temperature profile, species profiles, apparent reaction rate, intrinsic reaction rate, catalyst effectiveness, capital cost, maintenance cost and operating cost.

Next with respect to the optimization scenarios using adiabatic shift reactors, two cases incorporating isothermal shifting were investigated. Central to the analysis is the above-mentioned kinetic model which has been modified to simulate real reactor behavior of an isothermal water-gas-shift reactor with heat transfer from the gas mixture to the coolant.

In the course of designing the isothermal reactor's vessel and heat exchanger, a novel dimensionless quantity, the rate optimization number (Ro), has been developed to optimize the reaction kinetics. The Ro number provides a measure for the importance of thermal driving force versus chemical driving force and can be used to optimize the reaction rate.

To increase the carbon capture, methods to convert methane to CO_2 were investigated. Three new process schemes have been developed and integrated into the CO_2-PSA warm gas cleanup IGCC: (1) combustion of syngas in the CO_2 purification section while raising steam, (2) syngas reforming in an external adiabatic reformer and (3) syngas recycling to the gasifier.

A techno-economic analysis was conducted for all cases presented in this work. The techno-economic analysis involved a detailed itemized capital cost evaluation with respect to the individual equipment capacity, a detailed analysis of maintenance cost and a detailed analysis of fixed and variable operating costs. Based on the thermodynamic plant performance and the total plant cost, the cost of electricity was determined according to the financing structure presented in Section 4.1.4. Cost of Capture and Avoided Cost were determined with performance and emission values from literature using a corresponding IGCC without carbon capture and a supercritical pulverized coal power plant without carbon capture.

5.2 Conclusions

A state-of-the-art IGCC power plant with a dual-stage Selexol^{TM} unit for carbon capture has been compared to a novel PSA-based warm gas CO_2-removal technology. The analyses revealed the following conclusions:

Low Temperature Gasification (TRIG^{TM}) and its Resulting High Methane Syngas Limits Carbon Capture

Due to the low-temperature gasification technology selected for this IGCC study, the carbon capture is limited as a consequence of the high methane content in the syngas pro-

duced by the TRIG^{TM} gasifier. In the raw syngas from the TRIG^{TM} gasifier, 9.2 mol $-$ % of the carbon is in the form of methane. The Selexol^{TM} case reaches a mximum carbon capture of 83.40 % while achieving a thermal plant efficiency of 31.11 % $-$ HHV. With the implementation of the warm gas CO_2-removal unit the carbon capture limit rises to 88.6 % as a result of a higher capture yield of the PSA-technology. The plant efficiency with the PSA-based CO_2-removal unit increases at the same time to 34.2 % $-$ HHV.

Warm Gas Cleanup Using a CO_2-PSA Significantly Improves Plant Performance

A state-of-the-art TRIG^{TM} IGCC with Selexol^{TM} CO_2-removal unit was developed. With a carbon capture of 83.40 % and a net plant efficiency of 31.11 % $-$ HHV the resulting COE is 129.4 $\frac{\$}{\text{MWh}}$ without taking costs for carbon dioxide sequestration into consideration and 148.6 $\frac{\$}{\text{MWh}}$ with carbon dioxide TS&M costs. The integration of the warm gas CO_2-removal technology into the plant increases the efficiency to 34.20 % $-$ HHV. The analysis of the power requirement shows that the CO_2-PSA itself has a 4.5 % lower energy input than the Selexol^{TM} process on a per kg of captured CO_2 basis. Further energy savings are achieved in the ASU and syngas humidification. This illustrates that it is important to evaluate technologies in the context of the whole system and not just on a stand-alone basis. The complex interconnections between various components in the plant can have significant influence on the overall efficiency. The COE in the warm gas cleanup base case is lowered to 115.1 $\frac{\$}{\text{MWh}}$ without taking costs for carbon dioxide sequestration into consideration and 132.6 $\frac{\$}{\text{MWh}}$ with carbon dioxide TS&M costs.

Optimization of Water-Gas-Shift Reaction Increases Profitability

After optimization of the water-gas-shift reactor section using kinetic reaction analysis

and thermodynamic gas stability analysis results in an increase in efficiency and a higher profitability. Moving from sour shifting to more reactive sweet shifting reduces the cost of reaction vessels by up to 49.3 % (Selexol^{TM} case to Optimization II). Initial catalyst and operating cost of the shift reactors are reduced by up to 85.0 % and 90.0 % (Selexol^{TM} case to Optimization II). With a simultaneous reduction of the steam consumption in the shift section the resulting efficiency of the Optimization II case is 35.63 % which this makes it the most efficient and cost effective case leading to a COE of 110.4 $\frac{\$}{\text{MWh}}$ without TS&M and 127.2 $\frac{\$}{\text{MWh}}$ with TS&M.

Isothermal Shifting Can Reduce Reactor Cost, Catalyst Volume and Operating Cost

Important for the economic performance of an isothermal water-gas-shift reactor is the cooling load. The case studies of the Isothermal Shift I and Isothermal Shift II cases have shown that most of the reactor volume is needed to sufficiently cool the syngas. Furthermore, the analysis revealed that after the adiabatic inlet section intensive cooling is desirable to increase the chemical driving force and accelerate the kinetics. Both effects together can lead to a reduction of reactor cost, catalyst cost and operating cost. In the Optimization II case with 3 adiabatic high temperature reactors the total catalyst volume is 125.2 m^3 whereas the catalyst volume in the Isothermal Shift I case is 108.6 m^3 (without optimization of the Ro number). In the Isothermal Shift II case with optimized Ro number the catalyst volume can be reduced to 51.3 m^3.

Using the Ro Number in the Reactor Design Leads to a Significant Reduction in Reactor Size

The here introduced Ro number which compares the impact of temperature on the

thermal driving force to the chemical driving force can help reactor engineers to make effective use of the catalyst. For the water-gas-shift reaction, a value of -1 represents the optimum reaction rate. By designing the heat exchanger in the isothermal shift reactor in accordance with the Ro number a reduction of the required catalyst volume from initially 197.9 m^3 to 51.3 m^3 was possible (Isothermal Shift II case). The optimization with the Ro number has shown that most of the cooling is needed after the adiabatic inlet length and the ideal cooling profile follows an exponential decay along the reactor axis.

For the Water-Gas-Shift Reaction, the Assumption of an Isothermal Catalyst Pellet is a Valid Assumption

The importance of internal mass transfer, internal heat transfer, external mass transfer and external heat transfer were investigated for all water-gas-shift reactors in this study including high temperature sour shift, low temperature sour shift, high temperature sweet shift and low temperature sweet shift. While internal mass transport limitations have found to limit the reaction rate in all cases, external mass transfer and external heat transfer were important only for the high temperature sweet shift catalyst with inlet temperature of greater 335 °C. However, internal heat transport was never found to be a considerable factor throughout this study and the assumption of an isothermal catalyst particle was justified under all encountered conditions.

In IGCC Power Plants, Efficiency is an Important Indicator of Economic Performance

The cost analysis shows that for IGCC power plants, the efficiency is a very important measure, more important than in conventional power plants. A higher plant efficiency reduces the equipment size upstream of the gas turbine and cannot just lower the operating

cost but also has a significant influence on the overall TPC. The economic evaluation shows that a higher cost of e.g. the shift reactor section (Optimization I to Optimization II) can be justified by an increase in efficiency and ultimately a reduction in the COE.

Among the Studied Scenarios, Combustion of Methane Enriched Syngas in the CO_2 Purification Section while Raising Steam is the Most Cost Effective Solution for Increasing the Carbon Capture to 90 %

Maximum carbon capture after implementation of the warm gas CO_2-removal unit is 88.6 % as a result of a higher capture yield of the PSA-technology. In order to reach the DoE target of 90 % carbon capture, three options have been studied: (1) combustion of syngas in the CO_2 purification section while raising steam, (2) syngas reforming in an external adiabatic reformer and (3) syngas recycling to the gasifier. All scenarios are able to reach the desired carbon capture of 90 %; however, the economics of these three approaches are very different. Although the recycling option (3) has the highest efficiency, the combustor option (1) is the most economical with a COE of 118.7 $\frac{\$}{\text{MWh}}$ without TS&M and 138.1 $\frac{\$}{\text{MWh}}$ with TS&M.

5.3 Recommendations

This study showed that using a sorbent-based CO_2-PSA technology for carbon capture is a highly attractive solution for near future carbon capture increasing the relative pant efficiency by more than 14.5 % and decreasing the COE by more than 14.7 %. The obtained results from the Optimization I and II cases suggest that it would be most efficient to operate the shift reactors at isothermal conditions. However, the isothermal cases in this study were not able to surpass the performance of the setup with three individual adiabatic water-gas-

shift reactors. Important factors for the performance of the isothermal shift reactor are the carbon monoxide conversion and temperature at which steam is generated. Further research in this area is needed to fully comprehend the impact of these factors. Furthermore, the optimization of the reactor using the Ro number can lead to a significant improvement. It has been shown in this study that the reactor size can be reduced when the reaction rate is optimized with the Ro number. Another area of future research is the improvement of carbon capture in high methane content syngas applications. Especially in the field of highly efficient low temperature gasification processes which will gain importance in the future with the increasing interest in low rank coals and biomass, new technologies for selective methane separation could play an important role in the improvement of the herein investigated strategies for increased carbon capture.

Bibliography

[1] IEA. CO2 Emissions from Fuel Combustion. Technical report, 2014.

[2] IEA. WORLD ENERGY OUTLOOK 2011. Technical report, 2011.

[3] NETL. U.S. Department of Energy - Pre-Combustion Capture Focus Area, 2018.

[4] H. Nalbandian. Performance and Risks of Advanced Pulverized-Coal Plants. *Energeia*, 20(1):1–6, 2009.

[5] U.S. Department of Energy. *Cost and Performance Baseline for Fossil Energy Plants Volume 1 : Bituminous Coal and Natural Gas to Electricity*, volume 1. 2013.

[6] ClimateTechWiki. Integrated gasification combined-cycle, 2017.

[7] Christopher Higman and Maarten J Van Der Burgt. *Gasification*. 2008.

[8] Hartmut Spliethoff. *Power Generation from Solid Fuels*. 2010.

[9] Ashok Rao. *Sustainable Energy Conversion for Electricity and Coproducts*. 2015.

[10] Johann Stichlmair and Sebastian Rehfeld. *Skript zur Vorlesung: Konzeptuelle Prozesssynthese, Technische Universität München*. 2013.

[11] UOP. UOP Selexol Technology for Acid Gas Removal Main. 2009.

[12] Christopher Munson, Pradeep Indrakanti, Massood Ramezan, Evan Granite, and Jenny Tennant. Evaluation of Palladium-Based Sorbents for Trace Mercury Removal in Electricity Generation. *International Journal of Clean Coal and Energy*, 3(4):65–76, 2014.

[13] Brian Turk and Jerry Schlather. Gas Desulfurization Process in a Pilot-scale Transport Reactor System. *Gasification Technologies Conference 2006*, 2006.

[14] Neville a.H. Holt. Integrated Gasification Combined Cycle Power Plants. *Encyclopedia of Physical Science and Technology*, (September):897–924, 2004.

[15] Ian Barnes. Recent operating experience and improvement of commercial IGCC. Technical report, IEA, 2013.

[16] Agnieszka Leśniak and Marek Bieniecki. Energy production in selected integrated gas-steam IGCC systems powered by gas from coal gasification processes. *Chemik*, 68(12):1080–1085, 2014.

[17] A. Van Dongen and M. Kanaar. Co-gasification at the Buggenum IGCC power plant. *DGMK Tagungsbericht*, (2):57–58, 2006.

[18] T. Hashimoto, S. Sakamoto, Y. Kitagawa, Y. Hyakutake, and N. Setani. Development of IGCC commercial plant with air-blown gasifier. *Mitsubishi Heavy Industries Technical Review*, 46(2):1–5, 2009.

[19] The U.S. Department of Energy and Tampa Electric Company. The Tampa Electric Integrated Gasification Combined-Cycle Project - An Update. 19(7):28, 2000.

[20] Report from Vresová : 12 years of operating experience with the world ' s largest coal-fuelled IGCC. *Modern Power Systems*, (October):1–8, 2008.

[21] The U.S. Department of Energy. The Wabash River Coal Gasification Repowering Project. *Clean Coal Technology*, (20):28, 2000.

[22] Sadao Wasaka. Overview of NEDO's High-efficiency High efficiency Clean Coal Technology Development. *Clean Coal Day, in Tokyo*, 2012.

[23] Kohgami Kyoichi. Concept of NEDO ' s Clean Coal Technology Strategy Multi Purpose Coal Gasification Technology Development. In *Third International Conference on Clean Coal Technologies for our Future*, pages 1–32, 2007.

[24] U.S. Department of Energy. *Cost and Performance Baseline for Fossil Energy Plants Volume 3a: Low Rank Coal to Electricity: IGCC Cases*, volume 3a. 2011.

[25] U.S. Department of Energy. Low Rank Coal to Electricity : Combustion Cases. *Combustion*, 3(March), 2011.

[26] R. Strube and G. Manfrida. CO2 capture in coal-fired power plants-Impact on plant performance. *International Journal of Greenhouse Gas Control*, 5(4):710–726, 2011.

[27] Mohammad Mansouri Majoumerd and Mohsen Assadi. Techno-economic assessment of fossil fuel power plants with CO2 capture - Results of EU H2-IGCC project. *International Journal of Hydrogen Energy*, 39(30):16771–16784, 2014.

[28] Anamaria Padurean, Calin-Cristian Cormos, and Paul-Serban Agachi. Pre-combustion carbon dioxide capture by gas–liquid absorption for Integrated Gasification Combined Cycle power plants. *International Journal of Greenhouse Gas Control*, 7:1–11, 2012.

[29] Usama Ahmed, Umer Zahid, Yeong Su Jeong, Chul Jin Lee, and Chonghun Han. IGCC process intensification for simultaneous power generation and CO2 capture. *Chemical Engineering and Processing: Process Intensification*, 101:72–86, 2016.

[30] Jeremy Urech, Laurence Tock, Trent Harkin, Andrew Hoadley, and François Maréchal. An assessment of different solvent-based capture technologies within an IGCC-CCS power plant. *Energy*, 64:268–276, 2014.

[31] Jerry Schlather and Brian Turk. Desulfurization Process versus Traditional Scrubbers for a Warm Syngas Cleanup Technologies. In *Gasification Technologies Conference*, 2007.

[32] Johannes Franz, Pascal Maas, and Viktor Scherer. Economic evaluation of pre-combustion CO2-capture in IGCC power plants by porous ceramic membranes. *Applied Energy*, 130:532–542, 2014.

[33] David J. Couling, Kshitij Prakash, and William H. Green. Analysis of membrane and adsorbent processes for warm syngas cleanup in integrated gasification combined-cycle power with CO 2 capture and sequestration. *Industrial and Engineering Chemistry Research*, 50(19):11313–11336, 2011.

[34] D. Sofia, A. Giuliano, M. Poletto, and D. Barletta. *Techno-economic analysis of power and hydrogen co-production by an IGCC plant with CO2 capture based on membrane technology*, volume 37. Elsevier, 2015.

[35] Letitia Petrescu and Calin-Cristian Cormos. Environmental assessment of IGCC power plants with pre-combustion CO 2 capture by chemical & calcium looping methods. *Journal of Cleaner Production*, 158:233–244, 2017.

[36] Jinling Chi, Lifeng Zhao, Bo Wang, Zhen Li, Yunhan Xiao, and Yuhua Duan. Thermodynamic performance assessment and comparison of IGCC with solid cycling process for CO2 capture at high and medium temperatures. *International Journal of Hydrogen Energy*, 39(12):6479–6491, 2014.

[37] Stefano Campanari, Luca Mastropasqua, Matteo Gazzani, Paolo Chiesa, and Matteo C. Romano. Predicting the ultimate potential of natural gas SOFC power cycles with CO2 capture - Part B: Applications. *Journal of Power Sources*, 325:194–208, 2016.

[38] Mehdi Mehrpooya, Reza Esfilar, and S. M.Ali Moosavian. Introducing a novel air separation process based on cold energy recovery of LNG integrated with coal gasification, transcritical carbon dioxide power cycle and cryogenic CO2 capture. *Journal of Cleaner Production*, 142:1749–1764, 2017.

[39] S. García, M. V. Gil, J. J. Pis, F. Rubiera, and C. Pevida. Cyclic operation of a fixed-bed pressure and temperature swing process for CO2 capture: Experimental and statistical analysis. *International Journal of Greenhouse Gas Control*, 12:35–43, 2013.

[40] Nabil Tlili, Georges Grévillot, and Cécile Vallières. Carbon dioxide capture and recovery by means of TSA and/or VSA. *International Journal of Greenhouse Gas Control*, 3(5):519–527, 2009.

[41] U.S. Department of Energy. Current and Future Technologies for Gasification- Based Power Generation. Technical Report November 2009, 2010.

[42] US Department of Energy. 2014 Technology Readiness Assessment. Technical Report January, 2015.

[43] Shigeo Ito and Hisao Makino. Carbon dioxide separation from coal gas by physical adsorption at warm temperatures. *Greenhouse Gas Control Technologies*, 1999.

[44] Luca Riboldi and Olav Bolland. Comprehensive analysis on the performance of an IGCC plant with a PSA process integrated for CO2 capture. *International Journal of Greenhouse Gas Control*, 43:57–69, 2015.

[45] Zan Liu and William H Green. Analysis of Adsorbent-Based Warm CO 2 Capture Technology for Integrated Gasification Combined Cycle (IGCC) Power Plants. *Industrial & Engineering Chemistry Research*, 53(27):11145–11158, 2014.

[46] David J. Couling, Ujjal Das, and William H. Green. Analysis of hydroxide sorbents for CO 2 capture from warm syngas. *Industrial and Engineering Chemistry Research*, 51(41):13473–13481, 2012.

[47] Xuancan Zhu, Yixiang Shi, Ningsheng Cai, Shuang Li, and Yi Yang. Techno-economic evaluation of an elevated temperature pressure swing adsorption process in a 540 MW IGCC power plant with CO2 capture. *Energy Procedia*, 63:2016–2022, 2014.

[48] Xuancan Zhu, Yixiang Shi, and Ningsheng Cai. Integrated gasification combined cycle with carbon dioxide capture by elevated temperature pressure swing adsorption. *Applied Energy*, 176:196–208, 2016.

[49] Qin Chen, Ashok Rao, and Scott Samuelsen. H 2 coproduction in IGCC with CCS via coal and biomass mixture using advanced technologies. *Applied Energy*, 118:258–270, 2014.

[50] Qin Chen, Ashok Rao, and Scott Samuelsen. Coproduction of transportation fuels in advanced IGCCs via coal and biomass mixtures. *Applied Energy*, mar 2015.

[51] Qianlin Zhuang, Mitch Biondi, Shihong Yan, Kishna Bhagat, Randy Vansickle, Chao Chen, Hongjun Tan, Yan Zhu, Wei You, and Wu Xia. TRIG^{TM}: An advanced gasification technology to utilize low rank coals for power. *Fuel*, 152:103–109, 2015.

[52] Alexander K Bonsu, Joseph D Eiland, Benjamin F Gardner, Charles A Powell, Luke H Rogers, George S Booras, Ronald W Breault, and Nicola Salazar. Impact of CO2 Capture on Transport Gasifier IGCC Power Plant. *Southern Company*.

[53] Luke H Rogers, Alexander K Bonsu, Joseph D Eiland, Benjamin F Gardner, Charles A Powell, George S Booras, and Nicola Salazar. Power from PRB – Four Conceptual IGCC Plant Designs Using the Transport Gasifier. In *Twenty-Second Annual International Pittsburgh Coal Conference 13-Sep-2005*, pages 1–22, 2005.

[54] Christopher J. Arthur, Muhammad Tajammal Munir, Brent R. Young, and Wei Yu. Process simulation of the transport gasifier. *Fuel*, 115:479–489, 2014.

[55] Siva Ariyapadi, Philip Shires, Manish Bhargava, and David Ebbern. KBR'S TRANSPORT GASIFIER (TRIG^{TM}) – AN ADVANCED GASIFICATION TECHNOLOGY FOR SNG PRODUCTION FROM LOW-RANK COALS. In *Twenty-fifth Annual International Pittsburgh Coal Conference Pittsburgh, PA*, 2008.

[56] John C. Hensley. Cooling Tower Fundamentals. *Mrarley an SPX Brand*, (Second):133, 2011.

[57] B Bock, P Goldberg, R Rhudy, Howard J Herzog, Gemma Heddle, Mike Klett, John Davison, Dale Simbeck, J David Wallace, and Danial G De La Torre Ugarte. Economic evaluation of CO2 storage and sink enhancement options. Technical Report December, 2003.

[58] Lawrence A Smith, Neeraj Gupta, Bruce M Sass, Thomas A Bubenik, Charles Byrer, and Perry Bergman. Engineering and Economic Assessment of Carbon Dioxide Sequestration in Saline Formations National Energy Technology Laboratory (a) P . O . Box 880 , Morgantown , WV , 26507-0880. *Journal Of Energy*, 2(February):5–22, 2002.

[59] Qianlin Zhuang. TRIG^{TM}: ADVANCED GASIFICATION TECHNOLOGY UTILIZING LOW RANK COALS FOR POWER. In *The 12th European Gasification Conference*, pages 1–26, 2014.

[60] Ping Wang, Sheila W Hedges, Kent Casleton, and Chris Guenther. Thermal Behavior of Coal and Biomass Blends in Inert and Oxidizing Gaseous Environments. *International Journal of Clean Coal and Energy*, 1:35–42, 2012.

[61] Haiying Qi and Bo Zhao. *Cleaner Combustion and Sustainable World*.

[62] Frank Morton, Tim Pinkston, Nicola Salazar, and Denise Stalls. Orlando Gasification Project: Demonstration of a Nominal 285 MW Coal-Based Transport Gasifier. In *Pittsburgh Coal Conference*, pages 1–42, 2006.

[63] Correspondance with Chao Chen from Southern Company, 2016.

[64] Gokhan Alptekin, Steve Dietz, Ambal Jayaraman, Margarita Dubovik, and Inc TDA Research. A Low Cost , High Capacity Regenerable Sorbent for CO 2 Capture. pages 5–8, 2012.

[65] Personal Conversation with Ashok Rao, Ph.D., P.E.

[66] Calgon Carbon. PRODUCT BULLETIN - HGR® P for Mercury Removal. *Product Bulletin*, page 38989, 2015.

[67] Jeffrey W. Portzer, John R. Albritton, C. Clark Allen, and Raghubir P. Gupta. Development of novel sorbents for mercury control at elevated temperatures in coal-derived syngas: Results of initial screening of candidate materials. *Fuel Processing Technology*, 85(6-7):621–630, 2004.

[68] US Department of Energy. Doe/netl-341/013113. 2010.

[69] G. Manzolini, E. Macchi, J.W. Dijkstra, and D. Jansen. Technical economic evaluation of a system for electricity production with CO2 capture using a membrane reformer with permeate side combustion. *Proceedings of the ASME Turbo Expo*, 4:1–11, 2006.

[70] Prateek Mall, Taufeeq Ahmad, and Mohd Qasim. Ammonia Plant Design for 1 MTPA, 2012.

[71] DOE/NETL. NETL Updated Costs (2011 Basis) for selected Bituminous Baseline Cases. *NETL Report DOE/NETL-341/082312*, (June 2011), 2012.

[72] William Steen, Carl Richardson, Yongqi Lu, Hong Lu, and Massoud Rostam-Abadi. Sorbent enhanced water gas shift-rethinking carbon capture in IGCC. *Energy Procedia*, 63:1686–1702, 2014.

[73] Raghubir Gupta. High-Temperature Sulfur Removal in Gasification Applications. *Center for Energy Technology RTI International*, 2007.

[74] Gökhan Alptekin. Pilot Testing of a Highly Efficient Pre-combustion Sorbent-based Carbon Capture System (Contract No. DE-FE-0013105). *TDA Research Inc.*, 2013.

[75] Gokhan Alptekin, Ambal Jayaraman, Matt Cates, Mike Bonnema, Jim Dippo, David Gribble, and Kerry Libberton. Pilot Testing of a Highly Efficient Pre-combustion Sorbent-based Carbon Capture System (Contract No. DE-FE-0013105). 2017.

[76] J. W. Colton. Pinpoint Carbon Deposition. *Hydrocarbon Processing*, 1981.

[77] Werner Kast, Hermann Nirschl, Edward S. Gaddis, Karl-Ernst Wirth, and Johann Stichlmair. *VDI Wärmeatlas - L1 - Einphasige Strömungen*. 2013.

[78] James M. Moe. Design of water-gas shift reactors. *Chemical Engineering Progress*, page 33, 1962.

[79] Mark E. Davis and Robert J. Davis. *Fundamentals of Chemical Reaction Engineering*. Davis2013, 2013.

[80] W He, W Lu, and J H Dickerson. *Transport in Solid Oxide Fuel Cells*. 2014.

[81] H. Robert Perry. *Perry's Chemical Engineers' Handbook*, volume 19. 7th edition, 1997.

[82] Bruce E. Poling, John M. Prausnitz, and John P. O'Connell. *THE PROPERTIES OF GASES AND LIQUIDS*. 2004.

[83] James B. Rawlings and John G. Ekerdt. *Chemical Reactor Analysis and Design Fundamentals*. 2015.

[84] H. Scott Fogler. *Elements of Chemical Reaction Engineering*. 3rd edition, 2004.

[85] P. N. Dwivedi and S. N. Upadhyay. Particle-Fluid Mass Transfer in Fixed and Fluidized Beds. *Industrial and Engineering Chemistry Process Design and Development*, 16(2):157–165, 1977.

[86] Javier Pérez-Ramírez, Rob J. Berger, Guido Mul, Freek Kapteijn, and Jacob A. Moulijn. Six-flow reactor technology a review on fast catalyst screening and kinetic studies. *Catalysis Today*, 60(1):93–109, 2000.

[87] Thomas A. Adams and Paul I. Barton. A dynamic two-dimensional heterogeneous model for water gas shift reactors. *International Journal of Hydrogen Energy*, 34(21):8877–8891, 2009.

[88] Chi-Hsiung Li and B. A. Finlayson. Heat transfer in packed beds - A reevaluation. *Chemical Engineering Science*, 32:1055–1066, 1977.

[89] C. F. Chu and K. M. Ng. Flow in packed tubes with a small tube to particle diameter ratio. *AIChE Journal*, 35(1):148–158, 1989.

[90] David E. Mears. The role of axial dispersion in trickle-flow laboratory reactors. *Chemical Engineering Science*, 26(9):1361–1366, 1971.

[91] Rahman S. Abdulmohsin and Muthanna H. Al-Dahhan. Axial dispersion and mixing phenomena of the gas phase in a packed pebble-bed reactor. *Annals of Nuclear Energy*, 88:100–111, 2016.

[92] J. M.P.Q. Delgado. A critical review of dispersion in packed beds. *Heat and Mass Transfer/Waerme- und Stoffuebertragung*, 42(4):279–310, 2006.

[93] P. Y. Lanfrey, Z. V. Kuzeljevic, and M. P. Dudukovic. Tortuosity model for fixed beds randomly packed with identical particles. *Chemical Engineering Science*, 65(5):1891–1896, 2010.

[94] David E. Mears. Diagnostic criteria for heat transport limitations in fixed bed reactors. *Journal of Catalysis*, 20(2):127–131, 1971.

[95] Fumitake Yoshida, D Ramaswami, and A Hougen. Termperatures and Partial Pressures at the Surfaces of Catalyst Particles. *A.I.Ch.E. Journal*, 8(1):5–11, 1962.

[96] Theodore Bergman, Adrienne Lavine, Frank Incropera, and David Dewitt. *Fundamentals of Heat an Mass Transfer*. 7th edition, 2011.

[97] D. M. Spillman. *An Investigation of the High Pressure Kinetics of the Water-Gas Shift Reaction over a Sulfided Molybdenum Oxide-Alumina Catalyst Promoted by Cobalt Oxide and an Alkali Metal or Rare Earth Oxide.* PhD thesis, 1988.

[98] Silvester Fail. *Biohydrogen Production Based on the Catalyzed Water Gas Shift Reaction in Wood Gas*. PhD thesis, 2014.

[99] Katarzyna Antoniak-Jurak, Paweł Kowalik, Marcin Konkol, Wiesław Próchniak, Robert Bicki, Wioletta Raróg-Pilecka, Piotr Kuśtrowski, and Janusz Ryczkowski. Sulfur tolerant Co-Mo-K catalysts supported on carbon materials for sour gas shift process - Effect of support modification. *Fuel Processing Technology*, 144:305–311, 2016.

[100] Diogo Mendes and Luis M Madeira. Determination of the Low-Temperature Water-Gas Shift Reaction Kinetics Using a Cu-Based Catalyst. *Ind. Eng. Chem. Res.*, 49:11269–11279, 2010.

[101] Ernst Lorenz, Friedrich Wodtcke, Franz Ludwig Ebenhoech, and Erich Giesler. Catalytic Reaction of Carbon Monoxide with Steam, 1970.

[102] Bonan Liu, Qiuyun Zong, Xian Du, Zhaoxi Zhang, Tiancun Xiao, and Hamid Almegren. Novel sour water gas shift catalyst (SWGS) for lean steam to gas ratio applications. *Fuel Processing Technology*, 134:65–72, 2015.

[103] A. Plaza, S. Fail, J. A. Cortés, K. Föttinger, N. Diaz, R. Rauch, and H. Hofbauer. Apparent kinetics of the catalyzed water–gas shift reaction in synthetic wood gas. *Chemical Engineering Journal*, 301:222–228, 2016.

[104] Johnson Matthey. HiFUEL ® Base Metal Water Gas Shift Catalysts Catalogue. 2016.

[105] Johnson Matthey. Delivering world class ammonia plant performance. *Katalco (JM) Performance*, pages 1–20, 2008.

[106] Hans Bohlbro, Erik Mogensen, Mogens Jørgensen, and Kristian Søndergaard. *An Investigation on the Kinetics of the Conversion of Carbon Monoxide with Water Vapour Over Iron Oxide Based Catalysts*. 1969.

[107] Clariant. Catalysts for SYNGAS. 2010.

[108] Yongtaek Choi and Harvey G. Stenger. Water gas shift reaction kinetics and reactor modeling for fuel cell grade hydrogen. *Journal of Power Sources*, 124(2):432–439, 2003.

[109] Gökhan Alptekin. Progress Review for DE-PS26-08NT00258-03: Investigation of Effects of Coal and Biomass Contaminants on the Performance of Water-Gas- Shift and Fischer-Tropsch Catalysts. Technical report, 2011.

[110] Dingzhong XIE. ISOTHERMAL CONVERSION REACTOR WITH HIGH CO AND HIGH CONVERSION RATE, AND PROCESS THEREFOR, 2016.

[111] I. L. Leites, D. A. Sama, and N. Lior. The theory and practice of energy saving in the chemical industry: Some methods for reducing thermodynamic irreversibility in chemical technology processes. *Energy*, 28(1):55–97, 2003.

[112] Honeywell UOP. 50 Years of PSA Technology for H2 Purification. pages 1–5, 2016.

Appendix A

Stream Summaries

Table A.1: Stream Summary of the CO_2-PSA Warm Gas Cleanup Base Case at Constant Coal Flow Rate

Stream Number	Unit	1	2	3	4	5	6	7	8a	8b	9	10	11	12	13	14
Temperature	°C	5.6	71.1	105.9	80.5	982.2	397.9	982.2	161.7	408.5	328.9	760.0	199.0	199.0	199.0	203.0
Pressure	bar	0.9	0.9	56.2	50.3	3.4	51.0	41.7	38.3	35.7	51.0	34.3	32.8	32.8	32.8	32.4
Molar Flowrate	kmol/h	-	-	1695	4244	-	3564	25435	20095	34858	14763	518	34840	32786	2054	24631
Mass Flowrate	kg/h	-	-	47558	136642	-	64203	546027	428669	693675	265962	16720	693362	652490	40872	274886
Solid Flowrate	kg/h	262678	237787	-	-	24137	-	-	-	-	-	-	-	-	-	-
Mass Vapor Fraction	-	0	0	1	1	0	1	1	1	1	1	1	1	1	1	1
Composition	mol-basis															
O_2	-	0.00000	0.00000	0.00540	0.95023	0.00000	0.00000	0.00000	0.00000	0.00000	0.00000	0.01093	0.00000	0.00000	0.00000	0.00000
N_2	-	0.00000	0.00000	0.99230	0.01647	0.00000	0.00000	0.00518	0.00497	0.00287	0.00000	0.86405	0.00287	0.00287	0.00287	0.00378
Ar	-	0.00000	0.00000	0.00230	0.03330	0.00000	0.00000	0.00732	0.00703	0.00405	0.00000	0.00858	0.00406	0.00406	0.00406	0.00535
H_2	-	0.00000	0.00000	0.00000	0.00000	0.00000	0.00000	0.27127	0.26064	0.31941	0.00000	0.00000	0.33764	0.33764	0.33764	0.44517
CO	-	0.00000	0.00000	0.00000	0.00000	0.00000	0.00000	0.34256	0.32914	0.02059	0.00000	0.00000	0.00253	0.00253	0.00253	0.00334
CO_2	-	0.00000	0.00000	0.00000	0.00000	0.00000	0.00000	0.16179	0.15545	0.25888	0.00000	0.00026	0.27708	0.27708	0.27708	0.00587
H_2O	-	0.00000	0.00000	0.00000	0.00000	0.00000	1.00000	0.15374	0.18694	0.36372	1.00000	0.00122	0.34585	0.34585	0.34585	0.49906
CH_4	-	0.00000	0.00000	0.00000	0.00000	0.00000	0.00000	0.05122	0.04921	0.02837	0.00000	0.00000	0.02839	0.02839	0.02839	0.03743
H_2S	-	0.00000	0.00000	0.00000	0.00000	0.00000	0.00000	0.00289	0.00277	trace	0.00000	0.00000	trace	trace	trace	trace
NH_3	-	0.00000	0.00000	0.00000	0.00000	0.00000	0.00000	0.00381	0.00365	0.00211	0.00000	0.00000	0.00158	0.00158	0.00158	0.00000
COS	-	0.00000	0.00000	0.00000	0.00000	0.00000	0.00000	0.00020	0.00019	trace	0.00000	0.00000	trace	trace	trace	trace
HCl	-	0.00000	0.00000	0.00000	0.00000	0.00000	0.00000	trace	0.00000	0.00000	0.00000	0.00000	0.00000	0.00000	0.00000	0.00000
SO_2	-	0.00000	0.00000	0.00000	0.00000	0.00000	0.00000	0.00000	0.00000	0.00000	0.00000	0.11497	0.00000	0.00000	0.00000	0.00000
Total	-	0	0	1	1	0	1	0.99997	1	1	1	1	1	1	1	1
Stream Number	Unit	15	16	17	18	19	20	21	22	23	24	25	26	27	28	29
Temperature	°C	202.6	145.3	187.3	35.0	32.2	69.0	105.9	5.6	5.6	562.6	151.9	32.4	5.6	20.0	43.3
Pressure	bar	32.4	20.5	9.7	152.7	8.6	41.2	26.2	0.9	0.9	0.9	0.9	0.05	0.9	0.9	0.9
Molar Flowrate	kmol/h	26685	75	15374	8955	36	96	4847	20607	103936	128486	128486	22147	283	85	783
Mass Flowrate	kg/h	315759	2401	507655	394079	1161	2695	136013	595427	3003205	3423864	3423864	398993	8181	6292	21664
Solid Flowrate	kg/h	-	-	-	-	-	-	-	-	-	-	-	-	-	-	-
Mass Vapor Fraction	-	1	1	1	1	1	1	1	1	1	1	1	0.91096	1	0	1
Composition	mol-basis															
O_2	-	0.00000	0.95001	0.00000	trace	0.95001	0.00540	0.00540	0.20810	0.20810	0.10753	0.10753	0.00000	0.20810	0.00000	0.04020
N_2	-	0.00371	0.01406	trace	0.00022	0.01406	0.99230	0.99230	0.77590	0.77590	0.65729	0.65729	0.00000	0.77590	0.00000	0.88466
Ar	-	0.00525	0.03594	trace	0.00044	0.03594	0.00230	0.00230	0.00930	0.00930	0.00868	0.00868	0.00000	0.00930	0.00000	0.01069
H_2	-	0.43689	0.00000	0.00685	trace	0.00000	0.00000	0.00000	0.00000	0.00000	0.00000	0.00000	0.00000	0.00000	0.00000	0.00000
CO	-	0.00328	0.00000	trace	trace	0.00000	0.00000	0.00000	0.00000	0.00000	0.00000	0.00000	0.00000	0.00000	0.00000	0.00000
CO_2	-	0.02675	0.00000	0.58148	0.99934	0.00000	0.00000	0.00000	0.00030	0.00030	0.01411	0.01411	0.00000	0.00030	0.00000	0.00033
H_2O	-	0.48727	0.00000	0.40754	0.00000	0.00000	0.00000	0.00000	0.00640	0.00640	0.21237	0.21237	1.00000	0.00640	0.30349	0.06397
CH_4	-	0.03673	0.00000	0.00058	trace	0.00000	0.00000	0.00000	0.00000	0.00000	0.00000	0.00000	0.00000	0.00000	0.00000	0.00000
H_2S	-	trace	0.00000	trace	trace	0.00000	0.00000	0.00000	0.00000	0.00000	0.00000	0.00000	0.00000	0.00000	0.00000	0.00000
NH_3	-	0.00012	0.00000	0.00337	0.00000	0.00000	0.00000	0.00000	0.00000	0.00000	trace	trace	0.00000	0.00000	0.00000	0.00000
COS	-	trace	0.00000	trace	0.00000	0.00000	0.00000	0.00000	0.00000	0.00000	0.00000	0.00000	0.00000	0.00000	0.00000	0.00000
HCl	-	0.00000	0.00000	0.00000	0.00000	0.00000	0.00000	0.00000	0.00000	0.00000	0.00000	0.00000	0.00000	0.00000	0.00000	0.00000
SO_2	-	0.00000	0.00000	0.00000	trace	0.00000	0.00000	0.00000	0.00000	0.00000	trace	trace	0.00000	0.00000	0.00000	0.00015
Total	-	1	1	0.99981	0.99999	1	1	1	1	1	0.99997	0.99997	1	1	0.30349	1

Table A.2: Stream Summary of the Optimization I CO_2-PSA Warm Gas Cleanup Case at Constant Coal Flow Rate

Stream Number	Unit	1	2	3	4	5	6	7	8a	8b	9	10	11	12	13	14
Temperature	°C	5.6	71.1	105.9	74.2	982.2	397.9	982.2	161.7	492.9	382.0	760.0	199.0	199.0	0.0	203.0
Pressure	bar	0.9	0.9	56.2	50.3	3.4	51.0	41.7	38.3	35.3	51.0	33.9	32.7	32.7	0.0	32.4
Molar Flowrate	kmol/h	-	-	1695	4242	-	3564	25434	20095	30627	10532	516	30609	30609	0	22659
Mass Flowrate	kg/h	-	-	47558	136642	-	64203	546027	428671	617459	189741	16656	617151	617151	0	243458
Solid Flowrate	kg/h	262678	237787	-	-	24137	-	-	-	-	-	-	-	-	-	-
Mass Vapor Fraction	-	0	0	1	1	0	1	1	1	1	1	1	1	1	0	1
Composition	mol-basis															
O_2	-	0.00000	0.00000	0.00540	0.95014	0.00000	0.00000	0.00000	0.00000	0.00000	0.00000	0.01077	0.00000	0.00000	0.00000	0.00000
N_2	-	0.00000	0.00000	0.99230	0.01551	0.00000	0.00000	0.00500	0.00480	0.00315	0.00000	0.86409	0.00315	0.00315	0.00000	0.00421
Ar	-	0.00000	0.00000	0.00230	0.03435	0.00000	0.00000	0.00755	0.00725	0.00476	0.00000	0.00858	0.00476	0.00476	0.00000	0.00637
H_2	-	0.00000	0.00000	0.00000	0.00000	0.00000	0.00000	0.27132	0.26069	0.33390	0.00000	0.00000	0.36567	0.36567	0.00000	0.48888
CO	-	0.00000	0.00000	0.00000	0.00000	0.00000	0.00000	0.34260	0.32917	0.05311	0.00000	0.00000	0.02158	0.02158	0.00000	0.02885
CO_2	-	0.00000	0.00000	0.00000	0.00000	0.00000	0.00000	0.16171	0.15537	0.26493	0.00000	0.00026	0.29665	0.29665	0.00000	0.00638
H_2O	-	0.00000	0.00000	0.00000	0.00000	0.00000	1.00000	0.15369	0.18689	0.30546	1.00000	0.00122	0.27407	0.27407	0.00000	0.42207
CH_4	-	0.00000	0.00000	0.00000	0.00000	0.00000	0.00000	0.05128	0.04927	0.03233	0.00000	0.00000	0.03234	0.03234	0.00000	0.04324
H_2S	-	0.00000	0.00000	0.00000	0.00000	0.00000	0.00000	0.00289	0.00277	trace	0.00000	0.00000	trace	trace	0.00000	trace
NH_3	-	0.00000	0.00000	0.00000	0.00000	0.00000	0.00000	0.00374	0.00359	0.00236	0.00000	0.00000	0.00177	0.00177	0.00000	0.00000
COS	-	0.00000	0.00000	0.00000	0.00000	0.00000	0.00000	0.00020	0.00019	trace	0.00000	0.00000	trace	trace	0.00000	trace
HCl	-	0.00000	0.00000	0.00000	0.00000	0.00000	0.00000	trace	0.00000	0.00000	0.00000	0.00000	0.00000	0.00000	0.00000	0.00000
SO_2	-	0.00000	0.00000	0.00000	0.00000	0.00000	0.00000	0.00000	0.00000	0.00000	0.00000	0.11508	0.00000	0.00000	0.00000	0.00000
Total	-	0	0	1	1	0	1	0.99997	1	0.99999	1	1	0.99999	0.99999	0	1
Stream Number	Unit	15	16	17	18	19	20	21	22	23	24	25	26	27	28	29
Temperature	°C	203.0	145.3	187.1	35.0	32.2	69.0	105.9	5.6	5.6	565.0	151.9	32.4	5.6	20.0	43.3
Pressure	bar	32.4	20.5	9.7	152.7	8.6	41.2	26.2	0.9	0.9	0.9	0.9	0.05	0.9	0.9	0.9
Molar Flowrate	kmol/h	22659	86	15367	8960	36	96	8520	20876	103898	128620	128620	25973	296	87	796
Mass Flowrate	kg/h	243458	2760	507324	394255	1158	2684	239093	603214	3002097	3468052	3468052	467912	8548	6310	22008
Solid Flowrate	kg/h	-	-	-	-	-	-	-	-	-	-	-	-	-	-	-
Mass Vapor Fraction	-	1	1	1	1	1	1	1	1	1	1	1	0.91463	1	0	1
Composition	mol-basis															
O_2	-	0.00000	0.95001	0.00000	trace	0.95001	0.00540	0.00540	0.20810	0.20810	0.10759	0.10759	0.00000	0.20810	0.00000	0.03926
N_2	-	0.00421	0.01406	trace	0.00025	0.01406	0.99230	0.99230	0.77590	0.77590	0.68867	0.68867	0.00000	0.77590	0.00000	0.88205
Ar	-	0.00637	0.03594	trace	0.00051	0.03594	0.00230	0.00230	0.00930	0.00930	0.00878	0.00878	0.00000	0.00930	0.00000	0.01063
H_2	-	0.48888	0.00000	0.00749	trace	0.00000	0.00000	0.00000	0.00000	0.00000	0.00000	0.00000	0.00000	0.00000	0.00000	0.00000
CO	-	0.02885	0.00000	0.00044	trace	0.00000	0.00000	0.00000	0.00000	0.00000	0.00000	0.00000	0.00000	0.00000	0.00000	0.00000
CO_2	-	0.00638	0.00000	0.58148	0.99924	0.00000	0.00000	0.00000	0.00030	0.00030	0.01407	0.01407	0.00000	0.00030	0.00000	0.00034
H_2O	-	0.42207	0.00000	0.40624	0.00000	0.00000	0.00000	0.00000	0.00640	0.00640	0.18089	0.18089	1.00000	0.00640	0.31959	0.06758
CH_4	-	0.04324	0.00000	0.00066	trace	0.00000	0.00000	0.00000	0.00000	0.00000	0.00000	0.00000	0.00000	0.00000	0.00000	0.00000
H_2S	-	trace	0.00000	trace	trace	0.00000	0.00000	0.00000	0.00000	0.00000	0.00000	0.00000	0.00000	0.00000	0.00000	0.00000
NH_3	-	0.00000	0.00000	0.00352	0.00000	0.00000	0.00000	0.00000	0.00000	0.00000	0.00000	0.00000	0.00000	0.00000	0.00000	0.00000
COS	-	trace	0.00000	trace	trace	0.00000	0.00000	0.00000	0.00000	0.00000	0.00000	0.00000	0.00000	0.00000	0.00000	0.00000
HCl	-	0.00000	0.00000	0.00000	0.00000	0.00000	0.00000	0.00000	0.00000	0.00000	0.00000	0.00000	0.00000	0.00000	0.00000	0.00000
SO_2	-	0.00000	0.00000	0.00000	trace	0.00000	0.00000	0.00000	0.00000	0.00000	trace	trace	0.00000	0.00000	0.00000	0.00015
Total	-	1	1	0.99984	0.99999	1	1	1	1	1	1	1	1	1	0.31959	1

Table A.3: Stream Summary of Optimization II CO_2-PSA Warm Gas Cleanup Case Coal Flow Rate

Stream Number	Unit	1	2	3	4	5	6	7	8a	8b	9	10	11	12	13	14
Temperature	°C	5.6	71.1	105.9	73.5	982.2	397.9	982.2	161.7	334.7	394.4	760.0	199.0	199.0	0.0	203.0
Pressure	bar	0.9	0.9	56.2	50.3	3.4	51.0	41.7	38.3	36.6	51.0	35.2	31.5	31.5	0.0	31.2
Molar Flowrate	kmol/h	-	-	1695	4242	-	3564	25434	20095	30164	10069	518	30146	30146	0	22224
Mass Flowrate	kg/h	-	-	47558	136642	-	64203	546027	428672	609118	181403	16733	608811	608811	0	235500
Solid Flowrate	kg/h	262678	237787	-	-	24137	-	-	-	-	-	-	-	-	-	-
Mass Vapor Fraction	-	0	0	1	1	0	1	1	1	1	1	1	1	1	0	1
Composition	mol-basis															
O_2	-	0.00000	0.00000	0.00540	0.95013	0.00000	0.00000	0.00000	0.00000	0.00000	0.00000	0.01093	0.00000	0.00000	0.00000	0.00000
N_2	-	0.00000	0.00000	0.99230	0.01541	0.00000	0.00000	0.00498	0.00478	0.00319	0.00000	0.86405	0.00319	0.00319	0.00000	0.00428
Ar	-	0.00000	0.00000	0.00230	0.03446	0.00000	0.00000	0.00757	0.00727	0.00485	0.00000	0.00858	0.00485	0.00485	0.00000	0.00651
H_2	-	0.00000	0.00000	0.00000	0.00000	0.00000	0.00000	0.27133	0.26070	0.17367	0.00000	0.00000	0.37149	0.37149	0.00000	0.49862
CO	-	0.00000	0.00000	0.00000	0.00000	0.00000	0.00000	0.34260	0.32918	0.21929	0.00000	0.00000	0.02171	0.02171	0.00000	0.02914
CO_2	-	0.00000	0.00000	0.00000	0.00000	0.00000	0.00000	0.16170	0.15537	0.10363	0.00000	0.00026	0.30140	0.30140	0.00000	0.00650
H_2O	-	0.00000	0.00000	0.00000	0.00000	0.00000	1.00000	0.15368	0.18688	0.46016	1.00000	0.00122	0.26273	0.26273	0.00000	0.41087
CH_4	-	0.00000	0.00000	0.00000	0.00000	0.00000	0.00000	0.05128	0.04927	0.03282	0.00000	0.00000	0.03284	0.03284	0.00000	0.04408
H_2S	-	0.00000	0.00000	0.00000	0.00000	0.00000	0.00000	0.00289	0.00277	trace	0.00000	0.00000	trace	trace	0.00000	trace
NH_3	-	0.00000	0.00000	0.00000	0.00000	0.00000	0.00000	0.00374	0.00359	0.00239	0.00000	0.00000	0.00179	0.00179	0.00000	0.00000
COS	-	0.00000	0.00000	0.00000	0.00000	0.00000	0.00000	0.00020	0.00019	trace	0.00000	0.00000	trace	trace	0.00000	trace
HCl	-	0.00000	0.00000	0.00000	0.00000	0.00000	0.00000	trace	0.00000	0.00000	0.00000	0.00000	0.00000	0.00000	0.00000	0.00000
SO_2	-	0.00000	0.00000	0.00000	0.00000	0.00000	0.00000	0.00000	0.00000	0.00000	0.00000	0.11497	0.00000	0.00000	0.00000	0.00000
Total	-	0	0	1	1	0	1	0.99997	1	1	1	1	1	1	0	1
Stream Number	Unit	15	16	17	18	19	20	21	22	23	24	25	26	27	28	29
Temperature	°C	203.0	145.3	187.2	35.0	32.2	69.0	105.9	5.6	5.6	563.3	151.6	32.4	5.6	20.0	43.3
Pressure	bar	31.2	20.5	9.7	152.7	8.6	41.2	26.2	0.9	0.9	0.9	0.9	0.05	0.9	0.9	0.9
Molar Flowrate	kmol/h	22224	88	15377	8966	36	96	8894	20905	103790	128504	128504	26121	296	87	799
Mass Flowrate	kg/h	235500	2821	507613	394531	1162	2697	249595	604033	2998965	3468928	3468928	470575	8546	6332	22071
Solid Flowrate	kg/h	-	-	-	-	-	-	-	-	-	-	-	-	-	-	-
Mass Vapor Fraction	-	1	1	1	1	1	1	1	1	1	1	1	0.91474	1	0	1
Composition	mol-basis															
O_2	-	0.00000	0.95001	0.00000	trace	0.95001	0.00540	0.00540	0.20810	0.20810	0.10754	0.10754	0.00000	0.20810	0.00000	0.03928
N_2	-	0.00428	0.01406	trace	0.00025	0.01406	0.99230	0.99230	0.77590	0.77590	0.69193	0.69193	0.00000	0.77590	0.00000	0.88214
Ar	-	0.00651	0.03594	trace	0.00052	0.03594	0.00230	0.00230	0.00930	0.00930	0.00879	0.00879	0.00000	0.00930	0.00000	0.01063
H_2	-	0.49862	0.00000	0.00765	trace	0.00000	0.00000	0.00000	0.00000	0.00000	0.00000	0.00000	0.00000	0.00000	0.00000	0.00000
CO	-	0.02914	0.00000	0.00045	trace	0.00000	0.00000	0.00000	0.00000	0.00000	0.00000	0.00000	0.00000	0.00000	0.00000	0.00000
CO_2	-	0.00650	0.00000	0.58149	0.99922	0.00000	0.00000	0.00000	0.00030	0.00030	0.01403	0.01403	0.00000	0.00030	0.00000	0.00034
H_2O	-	0.41087	0.00000	0.40606	0.00000	0.00000	0.00000	0.00000	0.00640	0.00640	0.17771	0.17771	1.00000	0.00640	0.31899	0.06746
CH_4	-	0.04408	0.00000	0.00068	trace	0.00000	0.00000	0.00000	0.00000	0.00000	0.00000	0.00000	0.00000	0.00000	0.00000	0.00000
H_2S	-	trace	0.00000	trace	trace	0.00000	0.00000	0.00000	0.00000	0.00000	0.00000	0.00000	0.00000	0.00000	0.00000	0.00000
NH_3	-	0.00000	0.00000	0.00351	0.00000	0.00000	0.00000	0.00000	0.00000	0.00000	0.00000	0.00000	0.00000	0.00000	0.00000	0.00000
COS	-	trace	0.00000	trace	0.00000	0.00000	0.00000	0.00000	0.00000	0.00000	0.00000	0.00000	0.00000	0.00000	0.00000	0.00000
HCl	-	0.00000	0.00000	0.00000	0.00000	0.00000	0.00000	0.00000	0.00000	0.00000	0.00000	0.00000	0.00000	0.00000	0.00000	0.00000
SO_2	-	0.00000	0.00000	0.00000	trace	0.00000	0.00000	0.00000	0.00000	0.00000	trace	trace	0.00000	0.00000	0.00000	0.00015
Total	-	1	1	0.99983	0.99999	1	1	1	1	1	1	1	1	1	0.31899	1

Table A.4: Stream Summary of Isothermal Shift I CO_2-PSA Warm Gas Cleanup Case at Constant Coal Flow Rate

Stream Number	Unit	1	2	3	4	5	6	7	8a	8b	9	10	11	12	13	14
Temperature	°C	5.6	71.1	105.9	73.4	982.2	397.9	982.2	161.7	339.8	397.6	760.0	199.0	199.0	0.0	203.0
Pressure	bar	0.9	0.9	56.2	50.3	3.4	51.0	41.7	38.3	36.6	51.0	35.2	33.6	33.6	0.0	33.3
Molar Flowrate	kmol/h	-	-	1691	4234	-	3557	25383	20055	30038	9983	517	30020	30020	0	22120
Mass Flowrate	kg/h	-	-	47463	136368	-	64074	544933	427812	606709	179851	16689	606403	606403	0	234012
Solid Flowrate	kg/h	262152	237311	-	-	24089	-	-	-	-	-	-	-	-	-	-
Mass Vapor Fraction	-	0	0	1	1	0	1	1	1	1	1	1	1	1	0	1
Composition	mol-basis															
O_2	-	0.00000	0.00000	0.00540	0.95013	0.00000	0.00000	0.00000	0.00000	0.00000	0.00000	0.01091	0.00000	0.00000	0.00000	0.00000
N_2	-	0.00000	0.00000	0.99230	0.01540	0.00000	0.00000	0.00498	0.00478	0.00319	0.00000	0.86405	0.00319	0.00319	0.00000	0.00429
Ar	-	0.00000	0.00000	0.00230	0.03447	0.00000	0.00000	0.00757	0.00728	0.00486	0.00000	0.00858	0.00486	0.00486	0.00000	0.00653
H_2	-	0.00000	0.00000	0.00000	0.00000	0.00000	0.00000	0.27133	0.26070	0.17405	0.00000	0.00000	0.37223	0.37223	0.00000	0.49985
CO	-	0.00000	0.00000	0.00000	0.00000	0.00000	0.00000	0.34260	0.32918	0.21977	0.00000	0.00000	0.02183	0.02183	0.00000	0.02931
CO_2	-	0.00000	0.00000	0.00000	0.00000	0.00000	0.00000	0.16170	0.15536	0.10386	0.00000	0.00026	0.30199	0.30199	0.00000	0.00652
H_2O	-	0.00000	0.00000	0.00000	0.00000	0.00000	1.00000	0.15368	0.18688	0.45898	1.00000	0.00122	0.26118	0.26118	0.00000	0.40929
CH_4	-	0.00000	0.00000	0.00000	0.00000	0.00000	0.00000	0.05128	0.04927	0.03290	0.00000	0.00000	0.03292	0.03292	0.00000	0.04420
H_2S	-	0.00000	0.00000	0.00000	0.00000	0.00000	0.00000	0.00289	0.00277	trace	0.00000	0.00000	trace	trace	0.00000	trace
NH_3	-	0.00000	0.00000	0.00000	0.00000	0.00000	0.00000	0.00374	0.00358	0.00239	0.00000	0.00000	0.00180	0.00180	0.00000	0.00000
COS	-	0.00000	0.00000	0.00000	0.00000	0.00000	0.00000	0.00020	0.00019	trace	0.00000	0.00000	trace	trace	0.00000	trace
HCl	-	0.00000	0.00000	0.00000	0.00000	0.00000	0.00000	trace	0.00000	0.00000	0.00000	0.00000	0.00000	0.00000	0.00000	0.00000
SO_2	-	0.00000	0.00000	0.00000	0.00000	0.00000	0.00000	0.00000	0.00000	0.00000	0.00000	0.11498	0.00000	0.00000	0.00000	0.00000
Total	-	0	0	1	1	0	1	0.99997	1	1	1	1	1	1	0	1
Stream Number	Unit	15	16	17	18	19	20	21	22	23	24	25	26	27	28	29
Temperature	°C	203.0	145.3	187.2	35.0	32.2	69.0	105.9	5.6	5.6	563.3	152.4	32.4	5.6	20.0	43.3
Pressure	bar	33.3	20.5	9.7	152.7	8.6	41.2	26.2	0.9	0.9	0.9	0.9	0.05	0.9	0.9	0.9
Molar Flowrate	kmol/h	22120	88	15343	8946	36	96	8929	20886	103552	128218	128218	26692	295	87	797
Mass Flowrate	kg/h	234012	2821	506468	393649	1158	2690	250570	603483	2992104	3461794	3461794	480869	8530	6317	22018
Solid Flowrate	kg/h	-	-	-	-	-	-	-	-	-	-	-	-	-	-	-
Mass Vapor Fraction	-	1	1	1	1	1	1	1	1	1	1	1	0.91490	1	0	1
Composition	mol-basis															
O_2	-	0.00000	0.95001	0.00000	trace	0.95001	0.00540	0.00540	0.20810	0.20810	0.10752	0.10752	0.00000	0.20810	0.00000	0.03926
N_2	-	0.00429	0.01406	trace	0.00025	0.01406	0.99230	0.99230	0.77590	0.77590	0.69237	0.69237	0.00000	0.77590	0.00000	0.88212
Ar	-	0.00653	0.03594	0.00010	0.00052	0.03594	0.00230	0.00230	0.00930	0.00930	0.00879	0.00879	0.00000	0.00930	0.00000	0.01063
H_2	-	0.49985	0.00000	0.00767	trace	0.00000	0.00000	0.00000	0.00000	0.00000	0.00000	0.00000	0.00000	0.00000	0.00000	0.00000
CO	-	0.02931	0.00000	0.00045	trace	0.00000	0.00000	0.00000	0.00000	0.00000	0.00000	0.00000	0.00000	0.00000	0.00000	0.00000
CO_2	-	0.00652	0.00000	0.58149	0.99922	0.00000	0.00000	0.00000	0.00030	0.00030	0.01405	0.01405	0.00000	0.00030	0.00000	0.00034
H_2O	-	0.40929	0.00000	0.40603	0.00000	0.00000	0.00000	0.00000	0.00640	0.00640	0.17726	0.17726	1.00000	0.00640	0.31917	0.06751
CH_4	-	0.04420	0.00000	0.00068	trace	0.00000	0.00000	0.00000	0.00000	0.00000	0.00000	0.00000	0.00000	0.00000	0.00000	0.00000
H_2S	-	trace	0.00000	trace	trace	0.00000	0.00000	0.00000	0.00000	0.00000	0.00000	0.00000	0.00000	0.00000	0.00000	0.00000
NH_3	-	0.00000	0.00000	0.00351	0.00000	0.00000	0.00000	0.00000	0.00000	0.00000	0.00000	0.00000	0.00000	0.00000	0.00000	0.00000
COS	-	trace	0.00000	trace	0.00000	0.00000	0.00000	0.00000	0.00000	0.00000	0.00000	0.00000	0.00000	0.00000	0.00000	0.00000
HCl	-	0.00000	0.00000	0.00000	0.00000	0.00000	0.00000	0.00000	0.00000	0.00000	0.00000	0.00000	0.00000	0.00000	0.00000	0.00000
SO_2	-	0.00000	0.00000	0.00000	trace	0.00000	0.00000	0.00000	0.00000	0.00000	trace	trace	0.00000	0.00000	0.00000	0.00015
Total	-	1	1	0.99993	0.99999	1	1	1	1	1	1	1	1	1	0.31917	1

Table A.5: Stream Summary of Isothermal Shift II CO_2-PSA Warm Gas Cleanup Case at Constant Coal Flow Rate

Stream Number	Unit	1	2	3	4	5	6	7	8a	8b	9	10	11	12	13	14
Temperature	°C	5.6	71.1	105.9	74.4	982.2	397.9	982.2	161.7	337.9	395.2	760.0	199.0	199.0	0.0	203.0
Pressure	bar	0.9	0.9	56.2	50.3	3.4	51.0	41.7	38.3	36.6	51.0	35.2	33.5	33.5	0.0	33.2
Molar Flowrate	kmol/h	-	-	1695	4242	-	3564	25434	20095	30825	10731	518	30807	30807	0	22843
Mass Flowrate	kg/h	-	-	47558	136642	-	64203	546027	428671	621029	193314	16716	620721	620721	0	246703
Solid Flowrate	kg/h	262678	237787	-	-	24137	-	-	-	-	-	-	-	-	-	-
Mass Vapor Fraction	-	0	0	1	1	0	1	1	1	1	1	1	1	1	0	1
Composition	mol-basis															
O_2	-	0.00000	0.00000	0.00540	0.95014	0.00000	0.00000	0.00000	0.00000	0.00000	0.00000	0.01088	0.00000	0.00000	0.00000	0.00000
N_2	-	0.00000	0.00000	0.99230	0.01555	0.00000	0.00000	0.00500	0.00481	0.00313	0.00000	0.86406	0.00314	0.00314	0.00000	0.00419
Ar	-	0.00000	0.00000	0.00230	0.03431	0.00000	0.00000	0.00754	0.00724	0.00472	0.00000	0.00858	0.00472	0.00472	0.00000	0.00631
H_2	-	0.00000	0.00000	0.00000	0.00000	0.00000	0.00000	0.27132	0.26069	0.16994	0.00000	0.00000	0.36336	0.36336	0.00000	0.48506
CO	-	0.00000	0.00000	0.00000	0.00000	0.00000	0.00000	0.34260	0.32917	0.21458	0.00000	0.00000	0.02139	0.02139	0.00000	0.02855
CO_2	-	0.00000	0.00000	0.00000	0.00000	0.00000	0.00000	0.16171	0.15538	0.10141	0.00000	0.00026	0.29480	0.29480	0.00000	0.00633
H_2O	-	0.00000	0.00000	0.00000	0.00000	0.00000	1.00000	0.15369	0.18689	0.47174	1.00000	0.00122	0.27870	0.27870	0.00000	0.42667
CH_4	-	0.00000	0.00000	0.00000	0.00000	0.00000	0.00000	0.05127	0.04927	0.03212	0.00000	0.00000	0.03213	0.03213	0.00000	0.04290
H_2S	-	0.00000	0.00000	0.00000	0.00000	0.00000	0.00000	0.00289	0.00277	trace	0.00000	0.00000	trace	trace	0.00000	trace
NH_3	-	0.00000	0.00000	0.00000	0.00000	0.00000	0.00000	0.00375	0.00359	0.00234	0.00000	0.00000	0.00176	0.00176	0.00000	0.00000
COS	-	0.00000	0.00000	0.00000	0.00000	0.00000	0.00000	0.00020	0.00019	trace	0.00000	0.00000	trace	trace	0.00000	trace
HCl	-	0.00000	0.00000	0.00000	0.00000	0.00000	0.00000	trace	0.00000	0.00000	0.00000	0.00000	0.00000	0.00000	0.00000	0.00000
SO_2	-	0.00000	0.00000	0.00000	0.00000	0.00000	0.00000	0.00000	0.00000	0.00000	0.00000	0.11500	0.00000	0.00000	0.00000	0.00000
Total	-	0	0	1	1	0	1	0.99997	1	1	1	1	1	1	0	1

Stream Number	Unit	15	16	17	18	19	20	21	22	23	24	25	26	27	28	29
Temperature	°C	203.0	145.3	187.2	35.0	32.2	69.0	105.9	5.6	5.6	564.9	151.6	32.4	5.6	20.0	43.3
Pressure	bar	33.2	20.5	9.7	152.7	8.6	41.2	26.2	0.9	0.9	0.9	0.9	0.05	0.9	0.9	0.9
Molar Flowrate	kmol/h	22843	85	15370	8961	36	96	8360	20880	103928	128651	128651	25624	296	87	798
Mass Flowrate	kg/h	246703	2741	507430	394315	1160	2694	234606	603324	3002969	3467041	3467041	461617	8545	6326	22052
Solid Flowrate	kg/h	-	-	-	-	-	-	-	-	-	-	-	-	-	-	-
Mass Vapor Fraction	-	1	1	1	1	1	1	1	1	1	1	1	0.91454	1	0	1
Composition	mol-basis															
O_2	-	0.00000	0.95001	0.00000	trace	0.95001	0.00540	0.00540	0.20810	0.20810	0.10760	0.10760	0.00000	0.20810	0.00000	0.03924
N_2	-	0.00419	0.01406	trace	0.00024	0.01406	0.99230	0.99230	0.77590	0.77590	0.68729	0.68729	0.00000	0.77590	0.00000	0.88231
Ar	-	0.00631	0.03594	trace	0.00051	0.03594	0.00230	0.00230	0.00930	0.00930	0.00877	0.00877	0.00000	0.00930	0.00000	0.01063
H_2	-	0.48506	0.00000	0.00744	trace	0.00000	0.00000	0.00000	0.00000	0.00000	0.00000	0.00000	0.00000	0.00000	0.00000	0.00000
CO	-	0.02855	0.00000	0.00044	trace	0.00000	0.00000	0.00000	0.00000	0.00000	0.00000	0.00000	0.00000	0.00000	0.00000	0.00000
CO_2	-	0.00633	0.00000	0.58147	0.99924	0.00000	0.00000	0.00000	0.00030	0.00030	0.01405	0.01405	0.00000	0.00030	0.00000	0.00033
H_2O	-	0.42667	0.00000	0.40631	0.00000	0.00000	0.00000	0.00000	0.00640	0.00640	0.18229	0.18229	1.00000	0.00640	0.31856	0.06733
CH_4	-	0.04290	0.00000	0.00066	trace	0.00000	0.00000	0.00000	0.00000	0.00000	0.00000	0.00000	0.00000	0.00000	0.00000	0.00000
H_2S	-	trace	0.00000	trace	trace	0.00000	0.00000	0.00000	0.00000	0.00000	0.00000	0.00000	0.00000	0.00000	0.00000	0.00000
NH_3	-	0.00000	0.00000	0.00352	0.00000	0.00000	0.00000	0.00000	0.00000	0.00000	0.00000	0.00000	0.00000	0.00000	0.00000	0.00000
COS	-	trace	0.00000	trace	0.00000	0.00000	0.00000	0.00000	0.00000	0.00000	0.00000	0.00000	0.00000	0.00000	0.00000	0.00000
HCl	-	0.00000	0.00000	0.00000	0.00000	0.00000	0.00000	0.00000	0.00000	0.00000	0.00000	0.00000	0.00000	0.00000	0.00000	0.00000
SO_2	-	0.00000	0.00000	0.00000	trace	0.00000	0.00000	0.00000	0.00000	0.00000	trace	trace	0.00000	0.00000	0.00000	0.00015
Total	-	1	1	0.99984	0.99999	1	1	1	1	1	1	1	1	1	0.31856	1

Table A.6: Stream Summary of the Pathway I CO_2-PSA Warm Gas Cleanup Case with 90 % Carbon Capture at Constant Coal Flow Rate

Stream Number	Unit	1	2	3	4	5	6	7	8a	8b	9	10	11	12	13a	13b	13c
Temperature	°C	5.6	71.1	105.9	82.7	982.2	397.9	982.2	161.7	408.5	328.9	760.0	199.0	199.0	203.0	26.0	130.8
Pressure	bar	0.9	0.9	56.2	50.3	3.4	51.0	41.7	38.3	35.7	51.0	34.3	32.8	32.8	32.4	31.4	20.5
Molar Flowrate	kmol/h	-	-	1695	4244	-	3564	25435	20095	34858	14762	518	34839	34839	3219	1231	383
Mass Flowrate	kg/h	-	-	47558	136642	-	64203	546027	428668	693658	265947	16729	693344	693344	35924	2959	4046
Solid Flowrate	kg/h	262678	237787	-	-	24137	-	-	-	-	-	-	-	-	-	-	-
Mass Vapor Fraction	-	0	0	1	1	0	1	1	1	1	1	1	1	1	1	1	1
Composition	mol-basis																
O_2	-	0.00000	0.00000	0.00540	0.95026	0.00000	0.00000	0.00000	0.00000	0.00000	0.00000	0.01091	0.00000	0.00000	0.00000	0.00000	0.00000
N_2	-	0.00000	0.00000	0.99230	0.01680	0.00000	0.00000	0.00524	0.00503	0.00290	0.00000	0.86405	0.00290	0.00290	0.00383	0.00080	0.02961
Ar	-	0.00000	0.00000	0.00230	0.03294	0.00000	0.00000	0.00724	0.00696	0.00401	0.00000	0.00858	0.00401	0.00401	0.00529	0.00968	0.01334
H_2	-	0.00000	0.00000	0.00000	0.00000	0.00000	0.00000	0.27125	0.26062	0.31940	0.00000	0.00000	0.33764	0.33764	0.44517	0.98951	0.56139
CO	-	0.00000	0.00000	0.00000	0.00000	0.00000	0.00000	0.34255	0.32913	0.02058	0.00000	0.00000	0.00253	0.00253	0.00334	0.00000	0.02806
CO_2	-	0.00000	0.00000	0.00000	0.00000	0.00000	0.00000	0.16181	0.15547	0.25890	0.00000	0.00026	0.27710	0.27710	0.00587	0.00000	0.04939
H_2O	-	0.00000	0.00000	0.00000	0.00000	0.00000	1.00000	0.15376	0.18695	0.36372	1.00000	0.00122	0.34585	0.34585	0.49908	0.00000	0.00366
CH_4	-	0.00000	0.00000	0.00000	0.00000	0.00000	0.00000	0.05120	0.04919	0.02836	0.00000	0.00000	0.02838	0.02838	0.03741	0.00000	0.31454
H_2S	-	0.00000	0.00000	0.00000	0.00000	0.00000	0.00000	0.00289	0.00277	trace	0.00000	0.00000	trace	trace	trace	0.00000	trace
NH_3	-	0.00000	0.00000	0.00000	0.00000	0.00000	0.00000	0.00383	0.00368	0.00212	0.00000	0.00000	0.00159	0.00159	0.00000	0.00000	0.00000
COS	-	0.00000	0.00000	0.00000	0.00000	0.00000	0.00000	0.00020	0.00019	trace	0.00000	0.00000	trace	trace	trace	0.00000	trace
HCl	-	0.00000	0.00000	0.00000	0.00000	0.00000	0.00000	trace	0.00000	0.00000	0.00000	0.00000	0.00000	0.00000	0.00000	0.00000	0.00000
SO_2	-	0.00000	0.00000	0.00000	0.00000	0.00000	0.00000	0.00000	0.00000	0.00000	0.00000	0.11498	0.00000	0.00000	0.00000	0.00000	0.00000
Total	-	0	0	1	1	0	1	0.99997	1	1	1	1	1	1	1	1	0.99999
Stream Number	Unit	14	15	16	17	18	19	20	21	22	23	24	25	26	27	28	29
Temperature	°C	203.0	240.6	145.3	187.2	35.0	32.2	69.0	105.9	5.6	5.6	560.3	151.9	32.4	5.6	20.0	43.3
Pressure	bar	32.4	31.1	20.5	9.7	152.7	8.6	41.2	26.2	0.9	0.9	0.9	0.9	0.05	0.9	0.9	0.9
Molar Flowrate	kmol/h	26172	25458	452	16339	9702	36	96	4795	22383	100057	123438	123438	23338	215	76	702
Mass Flowrate	kg/h	292063	282058	14565	539485	426595	1162	2696	134566	646756	2891101	3276406	3276406	420442	6227	6124	19581
Solid Flowrate	kg/h	-	-	-	-	-	-	-	-	-	-	-	-	-	-	-	-
Mass Vapor Fraction	-	1	1	1	1	1	1	1	1	1	1	1	1	0.92051	1	0	1
Composition	mol-basis																
O_2	-	0.00000	0.00000	0.95001	0.00000	trace	0.95001	0.00540	0.00540	0.20810	0.20810	0.10830	0.10830	0.00000	0.20810	0.00000	0.04468
N_2	-	0.00383	0.00349	0.01406	trace	0.00192	0.01406	0.99230	0.99230	0.77590	0.77590	0.65923	0.65923	0.00000	0.77590	0.00000	0.89873
Ar	-	0.00529	0.00524	0.03594	trace	0.00234	0.03594	0.00230	0.00230	0.00930	0.00930	0.00869	0.00869	0.00000	0.00930	0.00000	0.01103
H_2	-	0.44517	0.44921	0.00000	0.00686	trace	0.00000	0.00000	0.00000	0.00000	0.00000	0.00000	0.00000	0.00000	0.00000	0.00000	0.00000
CO	-	0.00334	0.00301	0.00000	trace	trace	0.00000	0.00000	0.00000	0.00000	0.00000	0.00000	0.00000	0.00000	0.00000	0.00000	0.00000
CO_2	-	0.00587	0.00530	0.00000	0.58145	0.99571	0.00000	0.00000	0.00000	0.00030	0.00030	0.00891	0.00891	0.00000	0.00030	0.00000	0.00048
H_2O	-	0.49908	0.50003	0.00000	0.40753	0.00000	0.00000	0.00000	0.00000	0.00640	0.00640	0.21487	0.21487	1.00000	0.00640	0.21517	0.04491
CH_4	-	0.03741	0.03373	0.00000	0.00058	trace	0.00000	0.00000	0.00000	0.00000	0.00000	0.00000	0.00000	0.00000	0.00000	0.00000	0.00000
H_2S	-	trace	trace	0.00000	trace	trace	0.00000	0.00000	0.00000	0.00000	0.00000	0.00000	0.00000	0.00000	0.00000	0.00000	0.00000
NH_3	-	0.00000	0.00000	0.00000	0.00339	0.00000	0.00000	0.00000	0.00000	0.00000	0.00000	0.00000	0.00000	0.00000	0.00000	0.00000	0.00000
COS	-	trace	trace	0.00000	trace	0.00000	0.00000	0.00000	0.00000	0.00000	0.00000	0.00000	0.00000	0.00000	0.00000	0.00000	0.00000
HCl	-	0.00000	0.00000	0.00000	0.00000	0.00000	0.00000	0.00000	0.00000	0.00000	0.00000	0.00000	0.00000	0.00000	0.00000	0.00000	0.00000
SO_2	-	0.00000	0.00000	0.00000	0.00000	trace	0.00000	0.00000	0.00000	0.00000	0.00000	trace	trace	0.00000	0.00000	0.00000	0.00017
Total	-	1	1	1	0.99981	0.99997	1	1	1	1	1	1	1	1	1	0.21517	1

Table A.7: Stream Summary of the Pathway II CO_2-PSA Warm Gas Cleanup Case with 90 % Carbon Capture at Constant Coal Flow Rate

Stream Number	Unit	1	2	3	4	5	6	7	8a	8b	9	10	11	13a	13b	13c	13d
Temperature	°C	5.6	71.1	105.9	76.6	982.2	397.9	982.2	161.7	408.6	329.0	760.0	199.0	203.0	26.0	500.0	165.5
Pressure	bar	0.9	0.9	56.2	50.3	3.4	51.0	41.7	38.3	35.7	51.0	34.3	32.8	32.4	31.4	1.3	35.0
Molar Flowrate	kmol/h	-	-	1695	4243	-	3564	25435	20095	34860	14765	518	36656	11148	4358	3773	1815
Mass Flowrate	kg/h	-	-	47558	136642	-	64203	546027	428670	693703	265989	16729	713632	122579	10632	57597	20238
Solid Flowrate	kg/h	262678	237787	-	-	24137	-	-	-	-	-	-	-	-	-	-	-
Mass Vapor Fraction	-	0	0	1	1	0	1	1	1	1	1	1	1	1	1	1	1
Composition	mol-basis																
O_2	-	0.00000	0.00000	0.00540	0.95017	0.00000	0.00000	0.00000	0.00000	0.00000	0.00000	0.01091	0.00000	0.00000	0.00000	0.00000	0.00000
N_2	-	0.00000	0.00000	0.99230	0.01588	0.00000	0.00000	0.00507	0.00487	0.00281	0.00000	0.86405	0.00420	0.00547	0.00112	0.01488	0.03094
Ar	-	0.00000	0.00000	0.00230	0.03395	0.00000	0.00000	0.00746	0.00717	0.00413	0.00000	0.00858	0.00446	0.00581	0.01041	0.00515	0.01071
H_2	-	0.00000	0.00000	0.00000	0.00000	0.00000	0.00000	0.27130	0.26067	0.31942	0.00000	0.00000	0.34879	0.45460	0.98847	0.20147	0.56253
CO	-	0.00000	0.00000	0.00000	0.00000	0.00000	0.00000	0.34258	0.32916	0.02059	0.00000	0.00000	0.00264	0.00344	0.00000	0.01016	0.00468
CO_2	-	0.00000	0.00000	0.00000	0.00000	0.00000	0.00000	0.16174	0.15540	0.25885	0.00000	0.00026	0.26743	0.00560	0.00000	0.01656	0.08267
H_2O	-	0.00000	0.00000	0.00000	0.00000	0.00000	1.00000	0.15371	0.18691	0.36373	1.00000	0.00122	0.32888	0.47018	0.00000	0.58958	0.00304
CH_4	-	0.00000	0.00000	0.00000	0.00000	0.00000	0.00000	0.05126	0.04925	0.02839	0.00000	0.00000	0.04212	0.05489	0.00000	0.16219	0.30541
H_2S	-	0.00000	0.00000	0.00000	0.00000	0.00000	0.00000	0.00289	0.00277	trace	0.00000	0.00000	trace	trace	0.00000	trace	trace
NH_3	-	0.00000	0.00000	0.00000	0.00000	0.00000	0.00000	0.00377	0.00362	0.00208	0.00000	0.00000	0.00149	0.00000	0.00000	0.00000	0.00000
COS	-	0.00000	0.00000	0.00000	0.00000	0.00000	0.00000	0.00020	0.00019	trace	0.00000	0.00000	trace	trace	0.00000	trace	trace
HCl	-	0.00000	0.00000	0.00000	0.00000	0.00000	0.00000	trace	0.00000	0.00000	0.00000	0.00000	0.00000	0.00000	0.00000	0.00000	0.00000
SO_2	-	0.00000	0.00000	0.00000	0.00000	0.00000	0.00000	0.00000	0.00000	0.00000	0.00000	0.11498	0.00000	0.00000	0.00000	0.00000	0.00000
Total	-	0	0	1	1	0	1	0.99997	1	1	1	1	1	1	1	0.99999	0.99999
Stream Number	Unit	14	15	16	17	18	19	20	21	22	23	24	25	26	27	28	29
Temperature	°C	203.0	240.6	145.3	187.4	35.0	32.2	69.0	105.9	5.6	5.6	563.1	152.4	32.4	5.6	20.0	43.3
Pressure	bar	32.4	31.1	20.5	9.7	152.7	8.6	41.2	26.2	0.9	0.9	0.9	0.9	0.05	0.9	0.9	0.9
Molar Flowrate	kmol/h	27869	24096	91	16590	9669	36	96	7137	20837	103992	128456	128456	21942	288	86	789
Mass Flowrate	kg/h	306449	248851	2936	547750	425474	1162	2696	200288	602080	3004816	3431885	3431885	395284	8328	6312	21833
Solid Flowrate	kg/h	-	-	-	-	-	-	-	-	-	-	-	-	-	-	-	-
Mass Vapor Fraction	-	1	1	1	1	1	1	1	1	1	1	1	1	0.91558	1	0	1
Composition	mol-basis																
O_2	-	0.00000	0.00000	0.95001	0.00000	trace	0.95001	0.00540	0.00540	0.20810	0.20810	0.10787	0.10787	0.00000	0.20810	0.00000	0.03970
N_2	-	0.00547	0.00400	0.01406	trace	0.00028	0.01406	0.99230	0.99230	0.77590	0.77590	0.67794	0.67794	0.00000	0.77590	0.00000	0.88354
Ar	-	0.00581	0.00592	0.03594	trace	0.00049	0.03594	0.00230	0.00230	0.00930	0.00930	0.00875	0.00875	0.00000	0.00930	0.00000	0.01066
H_2	-	0.45460	0.49423	0.00000	0.00699	trace	0.00000	0.00000	0.00000	0.00000	0.00000	0.00000	0.00000	0.00000	0.00000	0.00000	0.00000
CO	-	0.00344	0.00239	0.00000	trace	trace	0.00000	0.00000	0.00000	0.00000	0.00000	0.00000	0.00000	0.00000	0.00000	0.00000	0.00000
CO_2	-	0.00560	0.00389	0.00000	0.58149	0.99922	0.00000	0.00000	0.00000	0.00030	0.00030	0.00857	0.00857	0.00000	0.00030	0.00000	0.00034
H_2O	-	0.47018	0.45148	0.00000	0.40716	0.00000	0.00000	0.00000	0.00000	0.00640	0.00640	0.19687	0.19687	1.00000	0.00640	0.31050	0.06560
CH_4	-	0.05489	0.03809	0.00000	0.00084	trace	0.00000	0.00000	0.00000	0.00000	0.00000	0.00000	0.00000	0.00000	0.00000	0.00000	0.00000
H_2S	-	trace	trace	0.00000	trace	trace	0.00000	0.00000	0.00000	0.00000	0.00000	0.00000	0.00000	0.00000	0.00000	0.00000	0.00000
NH_3	-	0.00000	0.00000	0.00000	0.00329	0.00000	0.00000	0.00000	0.00000	0.00000	0.00000	0.00000	0.00000	0.00000	0.00000	0.00000	0.00000
COS	-	trace	trace	0.00000	trace	0.00000	0.00000	0.00000	0.00000	0.00000	0.00000	0.00000	0.00000	0.00000	0.00000	0.00000	0.00000
HCl	-	0.00000	0.00000	0.00000	0.00000	0.00000	0.00000	0.00000	0.00000	0.00000	0.00000	0.00000	0.00000	0.00000	0.00000	0.00000	0.00000
SO_2	-	0.00000	0.00000	0.00000	0.00000	trace	0.00000	0.00000	0.00000	0.00000	0.00000	trace	trace	0.00000	0.00000	0.00000	0.00015
Total	-	1	1	1	0.99977	0.99999	1	1	1	1	1	1	1	1	1	0.31050	1

Table A.8: Stream Summary of the Pathway III CO_2-PSA Warm Gas Cleanup Case with 90 % Carbon Capture at Constant Coal Flow Rate

Stream Number	Unit	1	2	3	4	5	6	7	8a	8b	9	10	11	12	13a	13b	13c
Temperature	°C	5.6	71.1	105.9	79.5	982.2	397.9	982.2	161.6	408.0	331.8	760.0	199.0	199.0	203.0	26.0	178.0
Pressure	bar	0.9	0.9	56.2	50.3	3.4	51.0	41.7	38.3	35.6	51.0	34.2	32.6	32.6	32.2	31.2	46.0
Molar Flowrate	kmol/h	-	-	1695	4328	-	3564	26179	21081	35875	14794	518	35853	35853	6035	2358	756
Mass Flowrate	kg/h	-	-	47558	139347	-	64203	549689	440177	705734	266514	16731	705366	705366	66474	5717	8112
Solid Flowrate	kg/h	262678	237787	-	-	24137	-	-	-	-	-	-	-	-	-	-	-
Mass Vapor Fraction	-	0	0	1	1	0	1	1	1	1	1	1	1	1	1	1	1
Composition	mol-basis																
O_2	-	0.00000	0.00000	0.00540	0.95022	0.00000	0.00000	0.00000	0.00000	0.00000	0.00000	0.01091	0.00000	0.00000	0.00000	0.00000	0.00000
N_2	-	0.00000	0.00000	0.99230	0.01632	0.00000	0.00000	0.00584	0.00561	0.00330	0.00000	0.86405	0.00330	0.00330	0.00433	0.00089	0.03181
Ar	-	0.00000	0.00000	0.00230	0.03346	0.00000	0.00000	0.00766	0.00736	0.00432	0.00000	0.00858	0.00433	0.00433	0.00568	0.01018	0.01361
H_2	-	0.00000	0.00000	0.00000	0.00000	0.00000	0.00000	0.28137	0.27035	0.32739	0.00000	0.00000	0.34618	0.34618	0.45448	0.98894	0.54459
CO	-	0.00000	0.00000	0.00000	0.00000	0.00000	0.00000	0.33609	0.32293	0.02123	0.00000	0.00000	0.00265	0.00265	0.00348	0.00000	0.02783
CO_2	-	0.00000	0.00000	0.00000	0.00000	0.00000	0.00000	0.15239	0.14642	0.25467	0.00000	0.00026	0.27342	0.27342	0.00577	0.00000	0.04611
H_2O	-	0.00000	0.00000	0.00000	0.00000	0.00000	1.00000	0.15310	0.18630	0.35488	1.00000	0.00122	0.33650	0.33650	0.48448	0.00000	0.00235
CH_4	-	0.00000	0.00000	0.00000	0.00000	0.00000	0.00000	0.05632	0.05411	0.03180	0.00000	0.00000	0.03182	0.03182	0.04177	0.00000	0.33368
H_2S	-	0.00000	0.00000	0.00000	0.00000	0.00000	0.00000	0.00276	0.00265	trace	0.00000	0.00000	trace	trace	trace	0.00000	trace
NH_3	-	0.00000	0.00000	0.00000	0.00000	0.00000	0.00000	0.00427	0.00410	0.00241	0.00000	0.00000	0.00181	0.00181	0.00000	0.00000	0.00000
COS	-	0.00000	0.00000	0.00000	0.00000	0.00000	0.00000	0.00018	0.00017	trace	0.00000	0.00000	trace	trace	trace	0.00000	trace
HCl	-	0.00000	0.00000	0.00000	0.00000	0.00000	0.00000	trace	0.00000	0.00000	0.00000	0.00000	0.00000	0.00000	0.00000	0.00000	0.00000
SO_2	-	0.00000	0.00000	0.00000	0.00000	0.00000	0.00000	0.00000	0.00000	0.00000	0.00000	0.11498	0.00000	0.00000	0.00000	0.00000	0.00000
Total	-	0	0	1	1	0	1	0.99997	1	1	1	1	1	1	1	1	0.99999
Stream Number	Unit	14	15	16	17	18	19	20	21	22	23	24	25	26	27	28	29
Temperature	°C	203.0	240.6	145.3	187.1	35.0	32.2	69.0	105.9	5.6	5.6	563.0	152.3	32.4	5.6	20.0	43.3
Pressure	bar	32.2	30.9	20.5	9.7	152.7	8.6	41.2	26.2	0.9	0.9	0.9	0.9	0.05	0.9	0.9	0.9
Molar Flowrate	kmol/h	27064	25665	81	16590	9664	36	96	5528	21078	103329	127529	127529	22411	324	91	832
Mass Flowrate	kg/h	298091	278382	2604	547818	425270	1160	2696	155131	609033	2985666	3390755	3390755	403744	9353	6404	22932
Solid Flowrate	kg/h	-	-	-	-	-	-	-	-	-	-	-	-	-	-	-	-
Mass Vapor Fraction	-	1	1	1	1	1	1	1	1	1	1	1	1	0.91905	1	0	1
Composition	mol-basis																
O_2	-	0.00000	0.00000	0.95001	0.00000	trace	0.95001	0.00540	0.00540	0.20810	0.20810	0.10813	0.10813	0.00000	0.20810	0.00000	0.03763
N_2	-	0.00433	0.00363	0.01406	trace	0.00023	0.01406	0.99230	0.99230	0.77590	0.77590	0.66453	0.66453	0.00000	0.77590	0.00000	0.87737
Ar	-	0.00568	0.00559	0.03594	trace	0.00044	0.03594	0.00230	0.00230	0.00930	0.00930	0.00874	0.00874	0.00000	0.00930	0.00000	0.01051
H_2	-	0.45448	0.46323	0.00000	0.00672	trace	0.00000	0.00000	0.00000	0.00000	0.00000	0.00000	0.00000	0.00000	0.00000	0.00000	0.00000
CO	-	0.00348	0.00285	0.00000	trace	trace	0.00000	0.00000	0.00000	0.00000	0.00000	0.00000	0.00000	0.00000	0.00000	0.00000	0.00000
CO_2	-	0.00577	0.00473	0.00000	0.58147	0.99932	0.00000	0.00000	0.00000	0.00030	0.00030	0.00866	0.00866	0.00000	0.00030	0.00000	0.00033
H_2O	-	0.48448	0.48575	0.00000	0.40709	0.00000	0.00000	0.00000	0.00000	0.00640	0.00640	0.20994	0.20994	1.00000	0.00640	0.34872	0.07402
CH_4	-	0.04177	0.03423	0.00000	0.00062	trace	0.00000	0.00000	0.00000	0.00000	0.00000	0.00000	0.00000	0.00000	0.00000	0.00000	0.00000
H_2S	-	trace	trace	0.00000	trace	trace	0.00000	0.00000	0.00000	0.00000	0.00000	0.00000	0.00000	0.00000	0.00000	0.00000	0.00000
NH_3	-	0.00000	0.00000	0.00000	0.00391	0.00000	0.00000	0.00000	0.00000	0.00000	0.00000	0.00000	0.00000	0.00000	0.00000	0.00000	0.00000
COS	-	trace	trace	0.00000	trace	0.00000	0.00000	0.00000	0.00000	0.00000	0.00000	0.00000	0.00000	0.00000	0.00000	0.00000	0.00000
HCl	-	0.00000	0.00000	0.00000	0.00000	0.00000	0.00000	0.00000	0.00000	0.00000	0.00000	0.00000	0.00000	0.00000	0.00000	0.00000	0.00000
SO_2	-	0.00000	0.00000	0.00000	0.00000	trace	0.00000	0.00000	0.00000	0.00000	0.00000	trace	trace	0.00000	0.00000	0.00000	0.00014
Total	-	1	1	1	0.99980	0.99999	1	1	1	1	1	1	1	1	1	0.34872	1

Appendix B

Whisker Carbon Equilibria

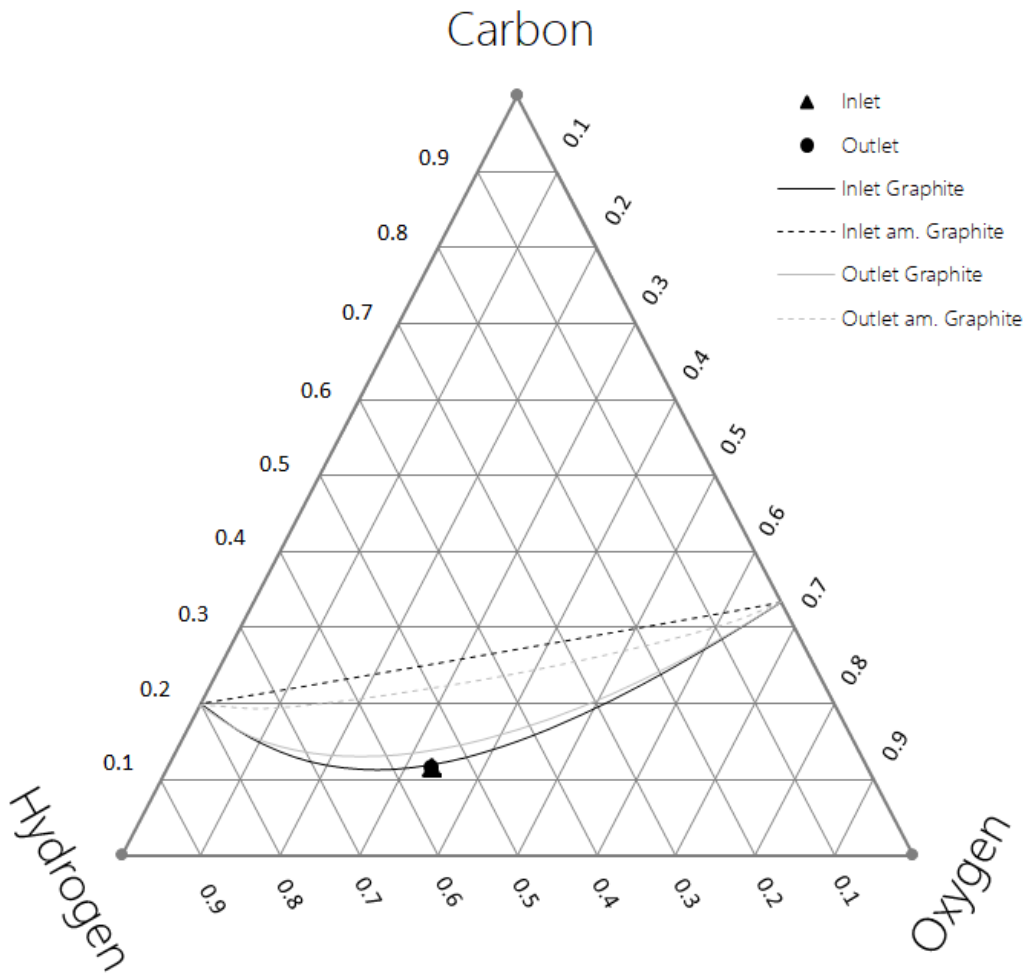

Figure B.1: Evaluation of the carbon, hydrogen and oxygen equilibrium at inlet and outlet conditions of the 1st water gas shift reactor of the CO_2-PSA warm gas cleanup base case.

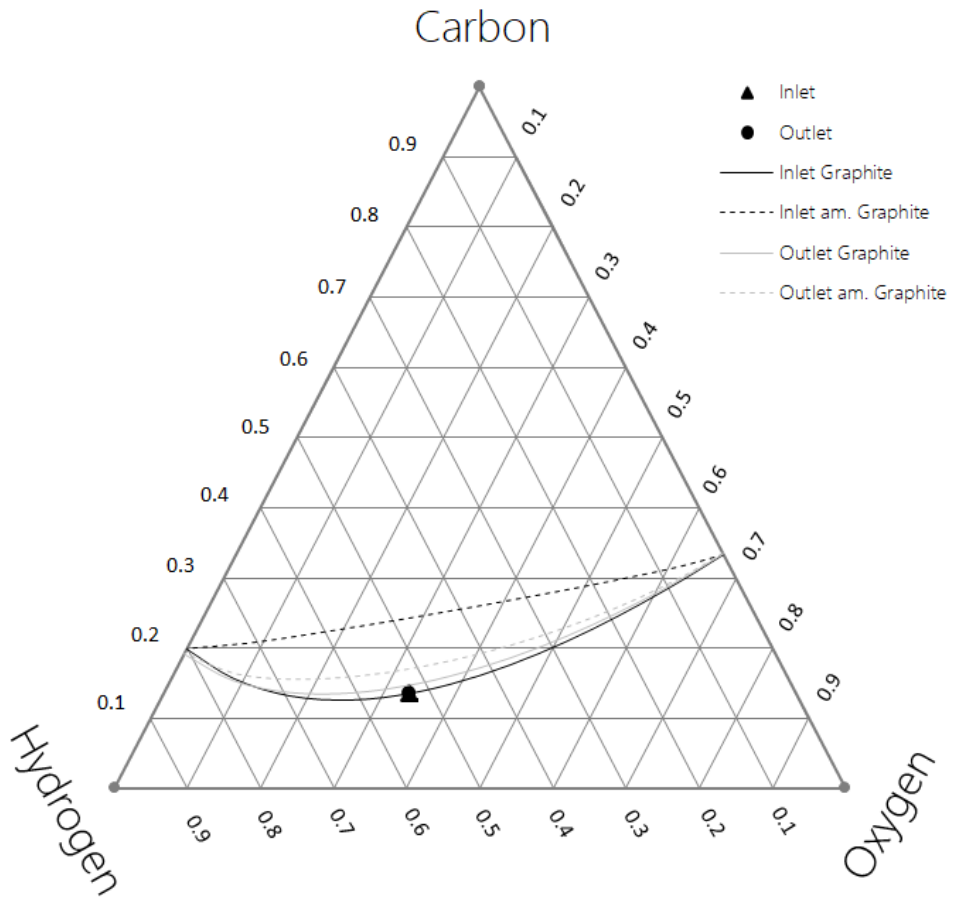

Figure B.2: Evaluation of the carbon, hydrogen and oxygen equilibrium at inlet and outlet conditions of the 1st water gas shift reactor of the Optimization II CO_2-PSA warm gas cleanup case.

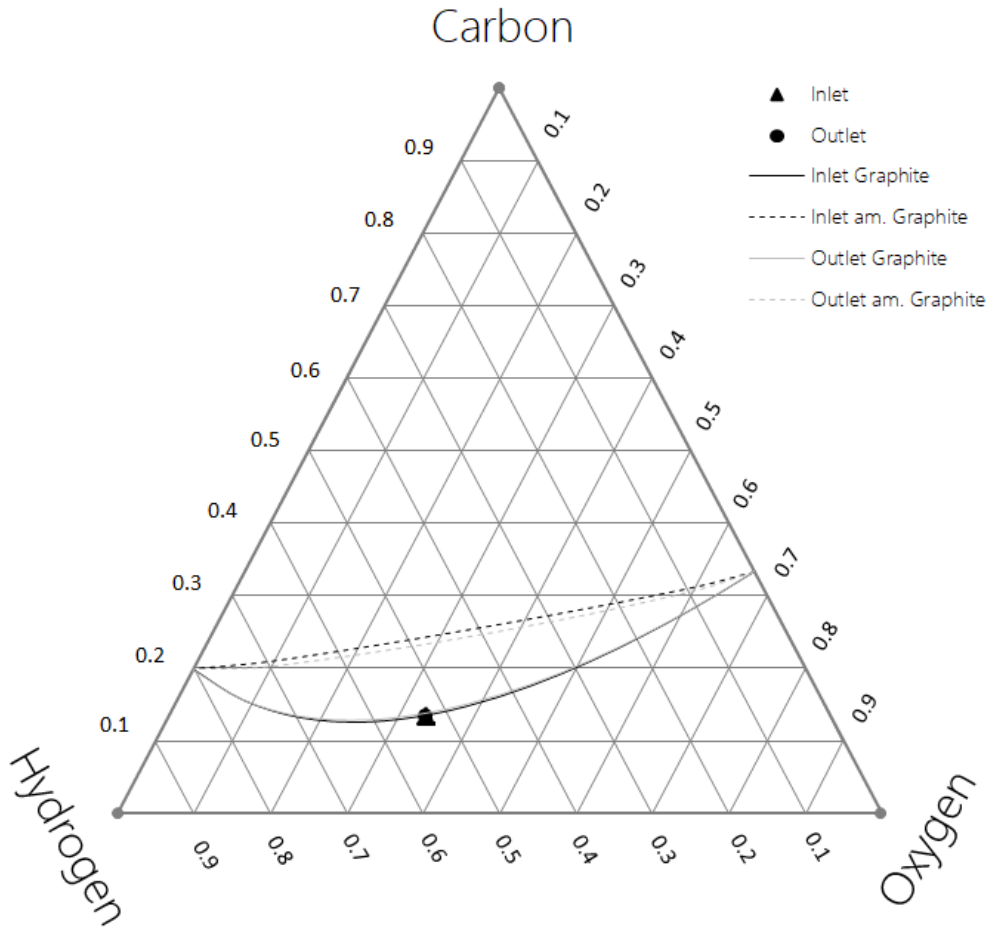

Figure B.3: Evaluation of the carbon, hydrogen and oxygen equilibrium at inlet and outlet conditions of the 2nd water gas shift reactor of the Optimization II CO_2-PSA warm gas cleanup case.

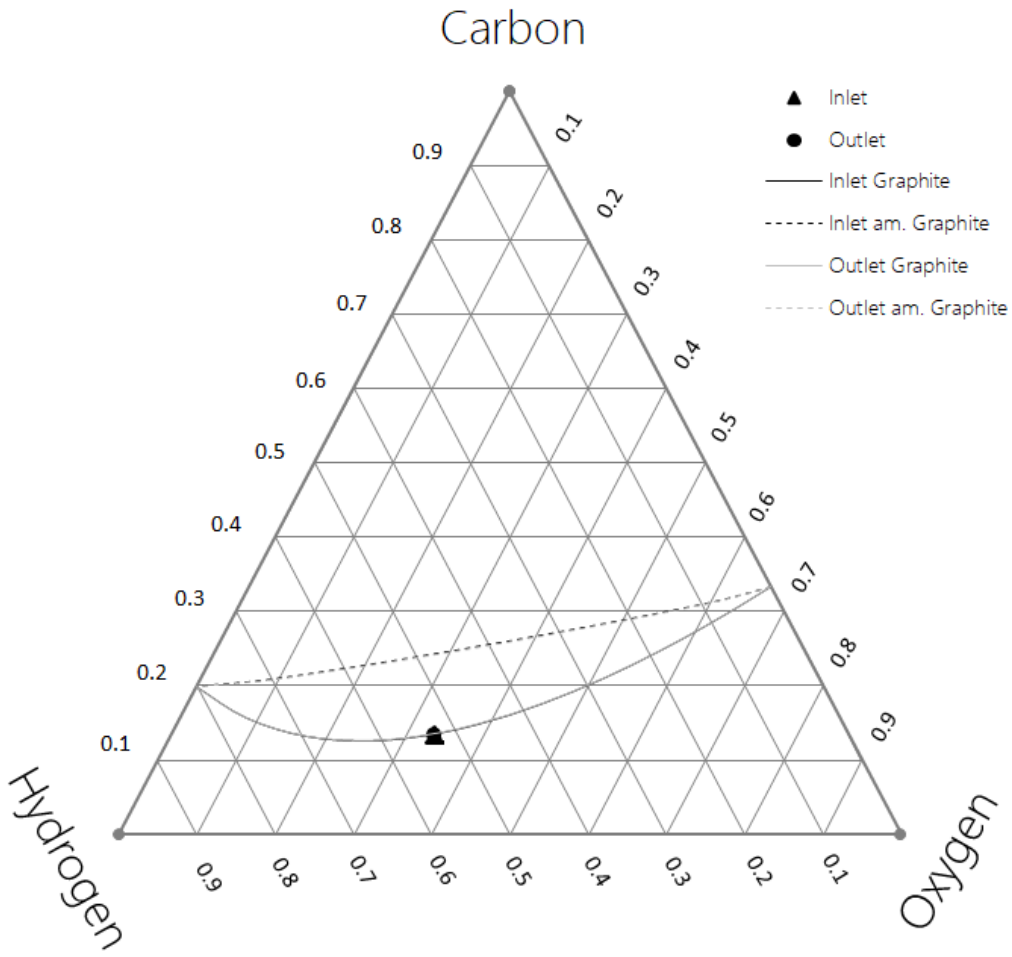

Figure B.4: Evaluation of the carbon, hydrogen and oxygen equilibrium at inlet and outlet conditions of the 3rd water gas shift reactor of the Optimization II CO_2-PSA warm gas cleanup case.

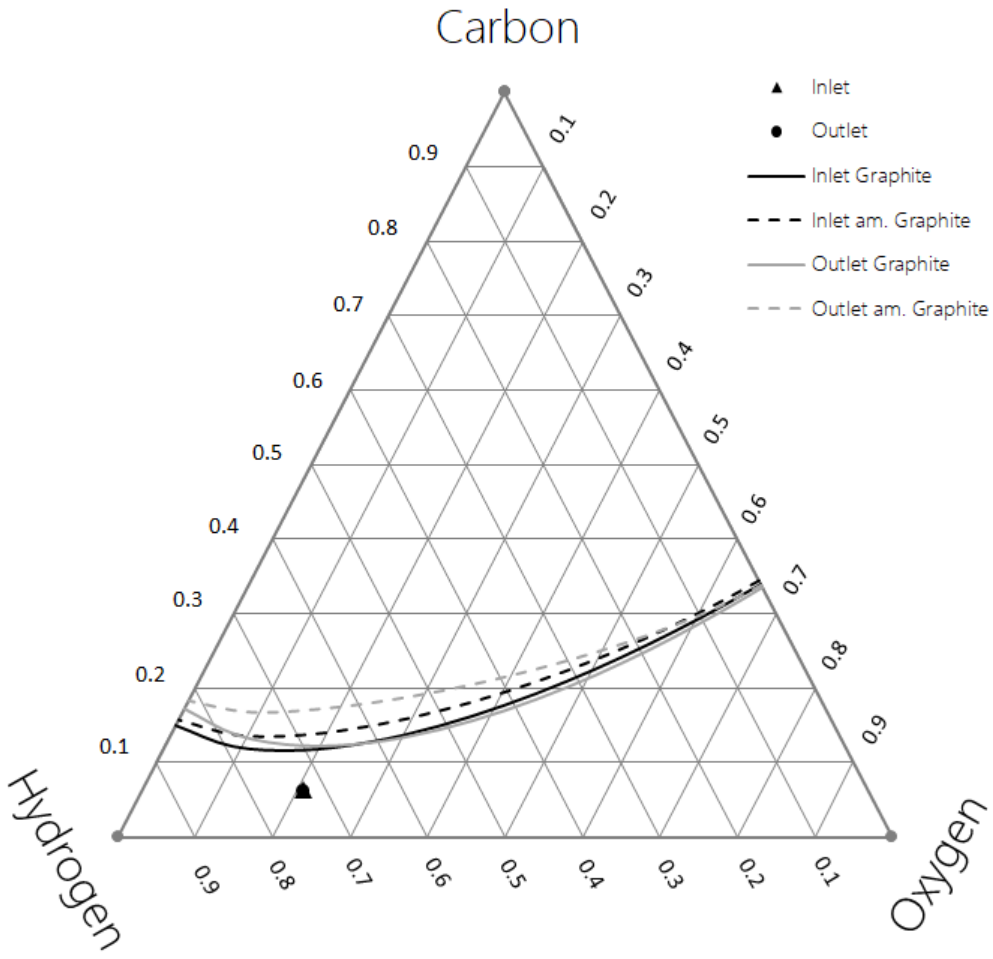

Figure B.5: Evaluation of the carbon, hydrogen and oxygen equilibrium at inlet and outlet conditions of the reformer reactor in the Pathway II case.

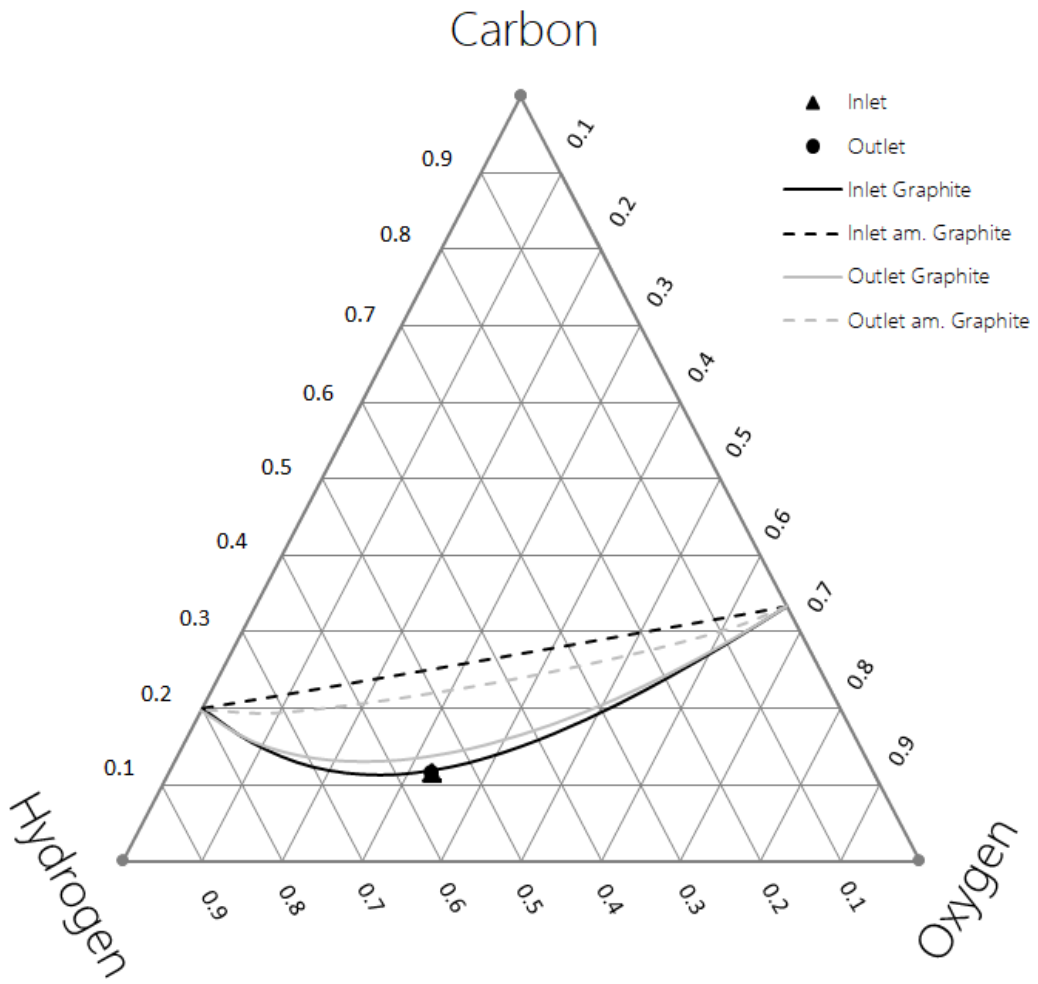

Figure B.6: Evaluation of the carbon, hydrogen and oxygen equilibrium at inlet and outlet conditions of the 1st water gas shift reactor of the Pathway III CO_2-PSA warm gas cleanup case.

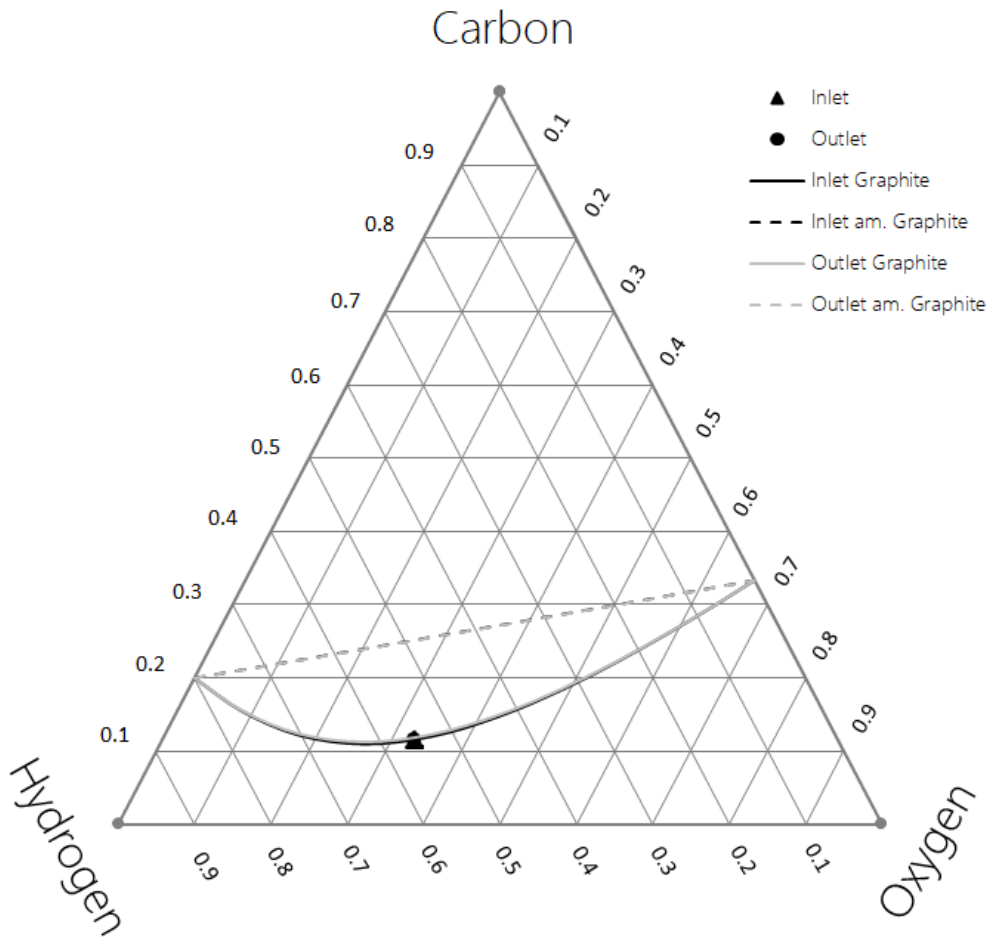

Figure B.7: Evaluation of the carbon, hydrogen and oxygen equilibrium at inlet and outlet conditions of the 2nd water gas shift reactor of the Pathway III CO_2-PSA warm gas cleanup case.

Appendix C

Shift Reactor Analyses

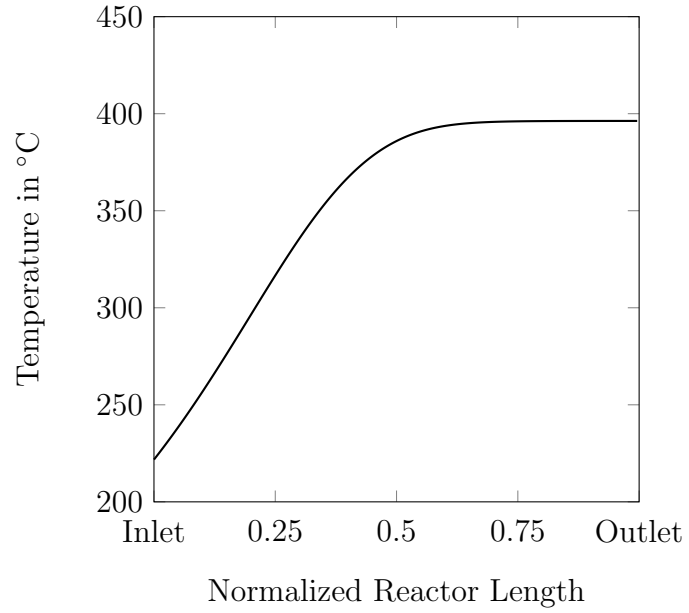

Figure C.1: Temperature profile of the 1st shift reactor of the CO_2-PSA warm gas cleanup base scenario using a sour shift catalyst with a system sizing factor of 1.25.

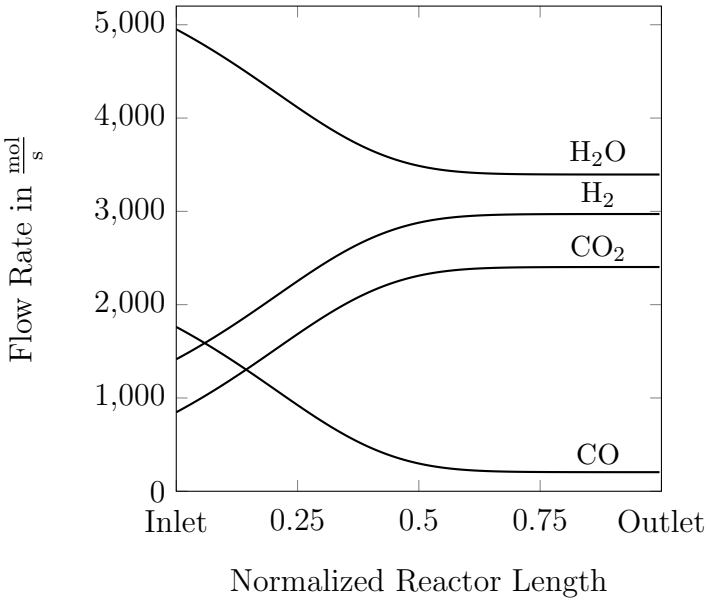

Figure C.2: Species profiles of the 1st shift reactor of the CO_2-PSA warm gas cleanup base scenario using a sour shift catalyst with a system sizing factor of 1.25.

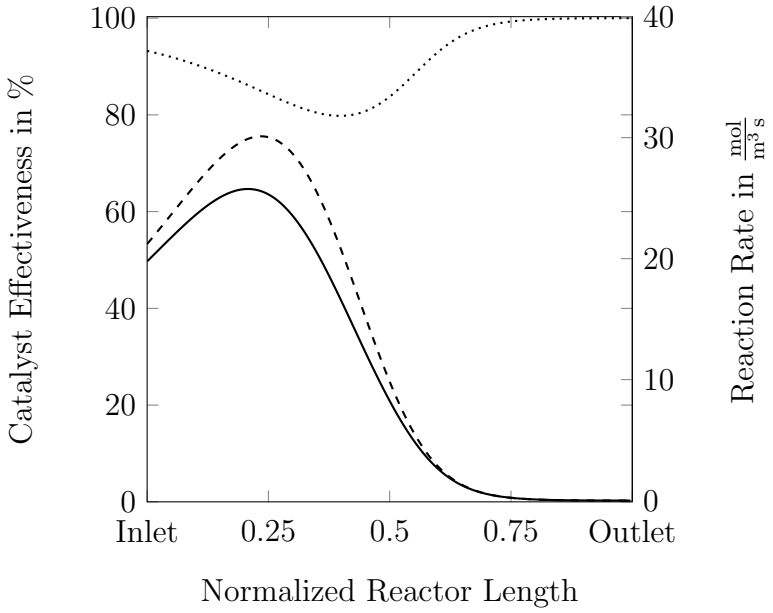

Figure C.3: Catalyst effectiveness (·····), intrinsic reaction rate (- - -) and apparent reaction rate (——) of the 1st shift reactor of the CO_2-PSA warm gas cleanup base scenario using a sour shift catalyst with a system sizing factor of 1.25.

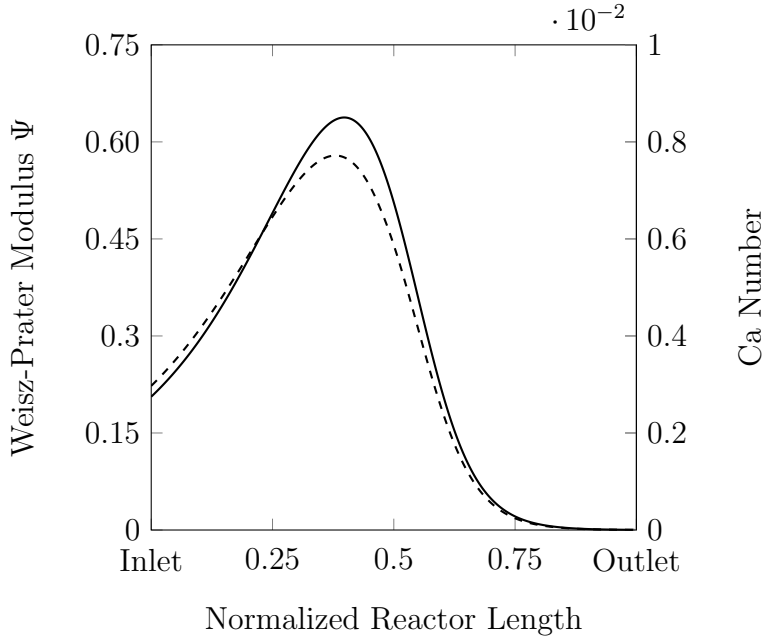

Figure C.4: Prater-Weisz modulus (——) and Carberry number (- - -) of the 1st shift reactor of the CO_2-PSA warm gas cleanup base scenario using a sour shift catalyst with a system sizing factor of 1.25.

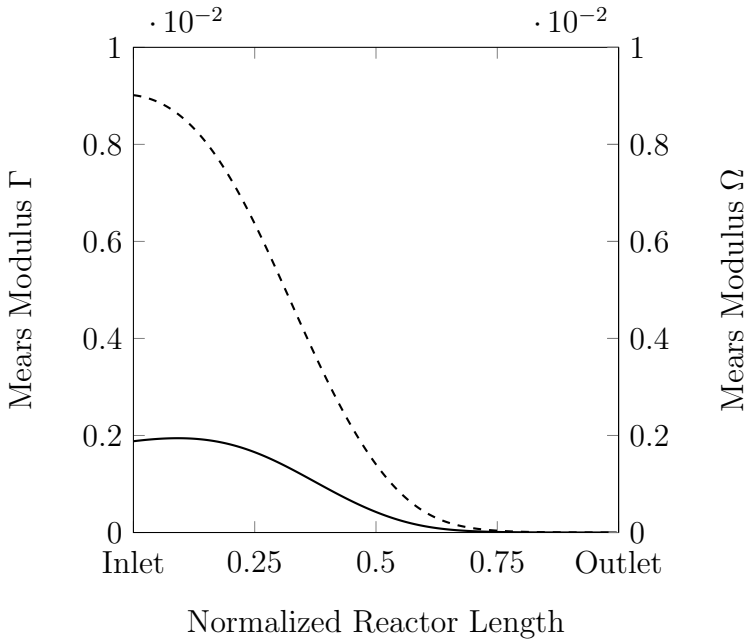

Figure C.5: Mears Modulus for internal heat transfer Γ (——) and Mears Modulus for external heat transfer Ω (- - -) of the 1st shift reactor of the CO_2-PSA warm gas cleanup base scenario using a sour shift catalyst with a system sizing factor of 1.25.

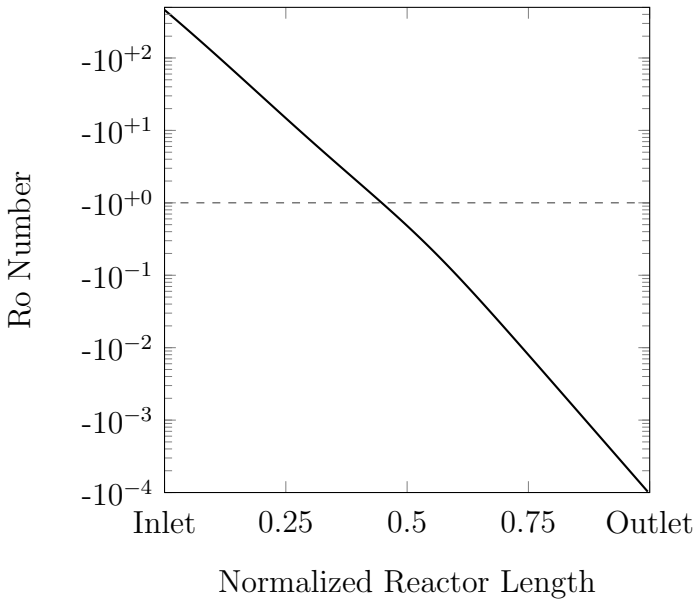

Figure C.6: Rate optimization number of the 1st shift reactor of the CO_2-PSA warm gas cleanup base scenario using a sour shift catalyst with a system sizing factor of 1.25.

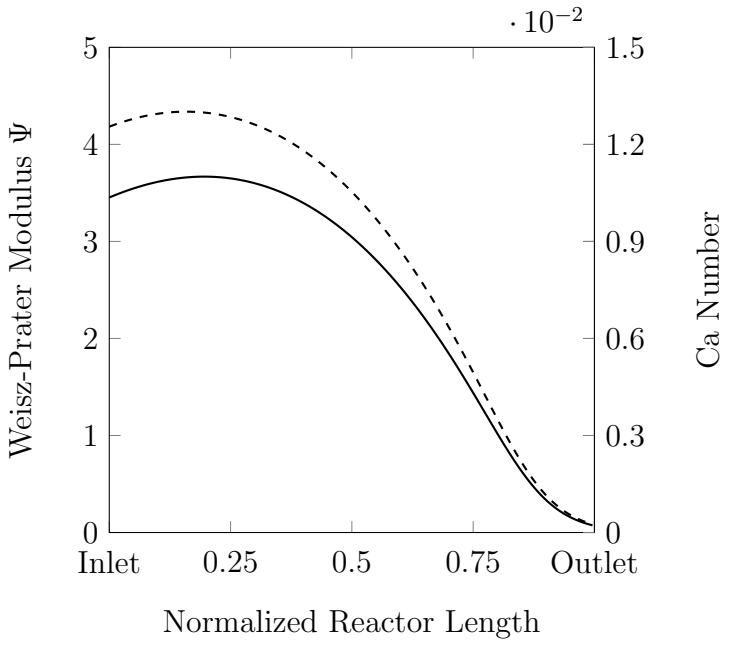

Figure C.7: Prater-Weisz modulus (——) and Carberry number (- - -) of the 2nd shift reactor of the CO_2-PSA warm gas cleanup base scenario using a low temperature, sweet shift catalyst with a system sizing factor of 1.1.

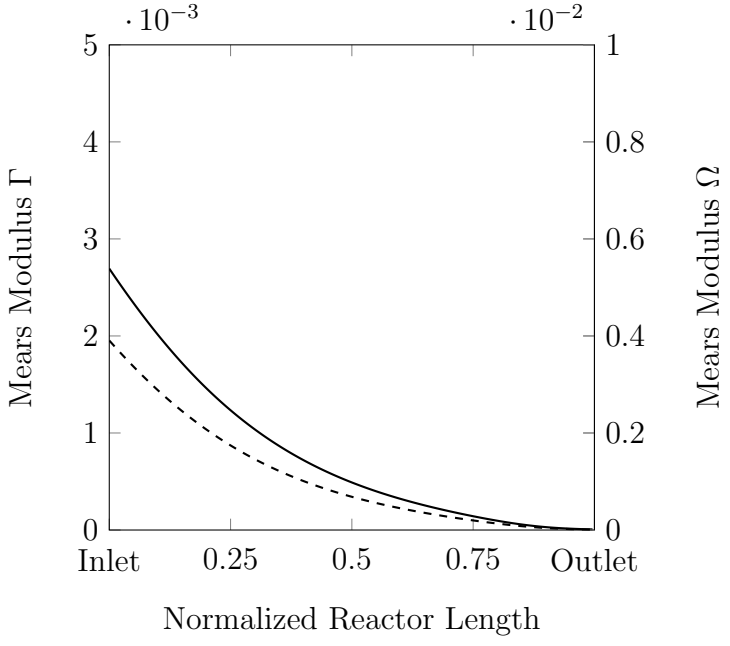

Figure C.8: Mears Modulus for internal heat transfer Γ (——) and Mears Modulus for external heat transfer Ω (- - -) of the 2nd shift reactor of the CO_2-PSA warm gas cleanup base scenario using a low temperature, sweet shift catalyst with a system sizing factor of 1.1.

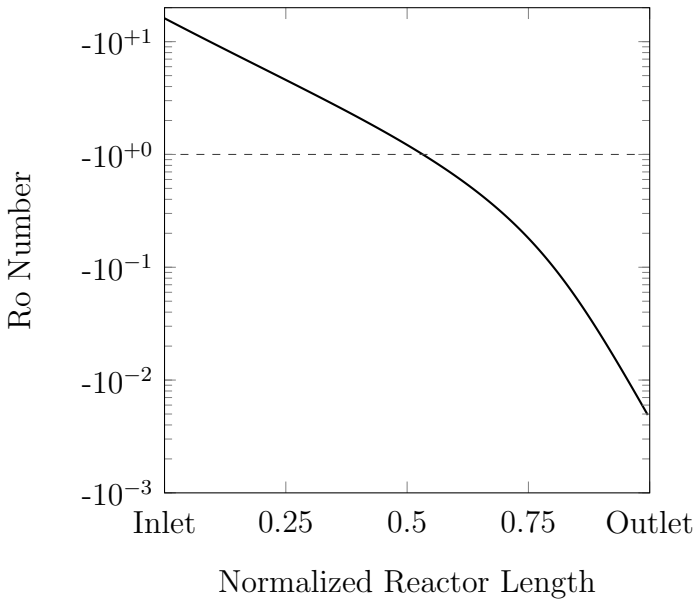

Figure C.9: Rate optimization number of the 2nd shift reactor of the CO_2-PSA warm gas cleanup base scenario using a low temperature, sweet shift catalyst with a system sizing factor of 1.1.

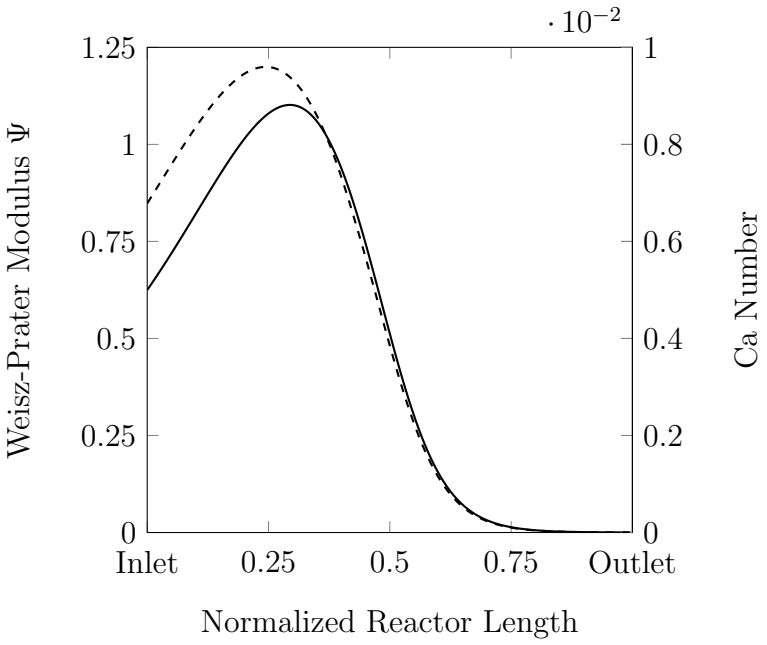

Figure C.10: Prater-Weisz modulus (——) and Carberry number (- - -) of the 1st shift reactor of the Optimization I CO_2-PSA warm gas cleanup scenario using a high temperature, sour shift catalyst with a system sizing factor of 1.25.

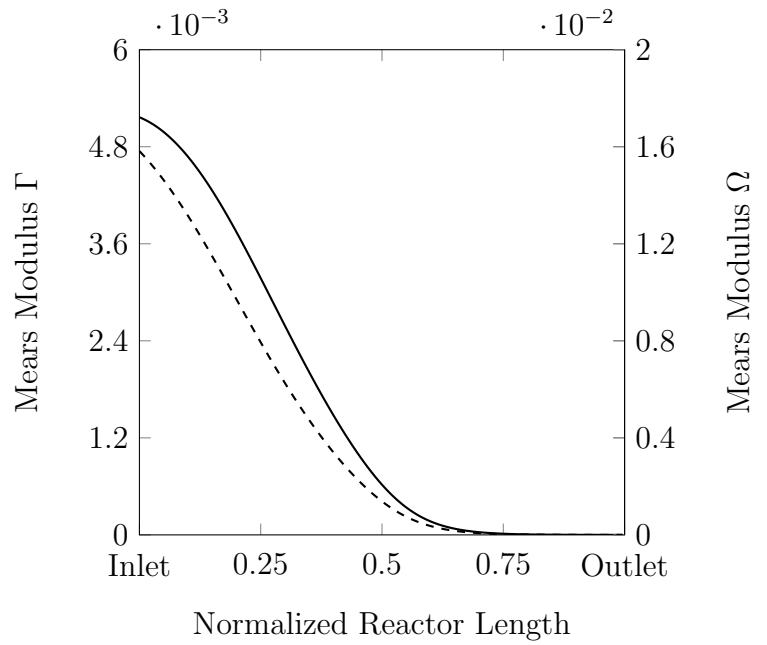

Figure C.11: Mears Modulus for internal heat transfer Γ (——) and Mears Modulus for external heat transfer Ω (- - -) of the 1st shift reactor of the Optimization I CO_2-PSA warm gas cleanup scenario using a high temperature, sour shift catalyst with a system sizing factor of 1.25.

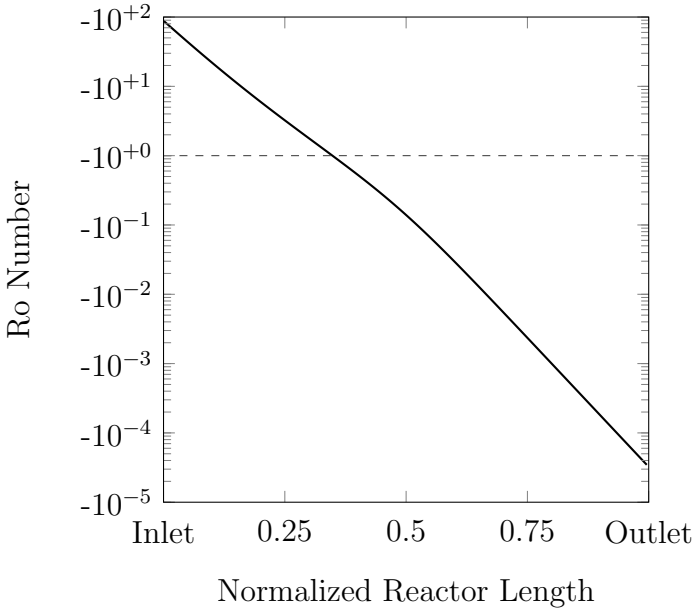

Figure C.12: Rate optimization number of the 1st shift reactor of the Optimization I CO_2-PSA warm gas cleanup scenario using a high temperature, sour shift catalyst with a system sizing factor of 1.25.

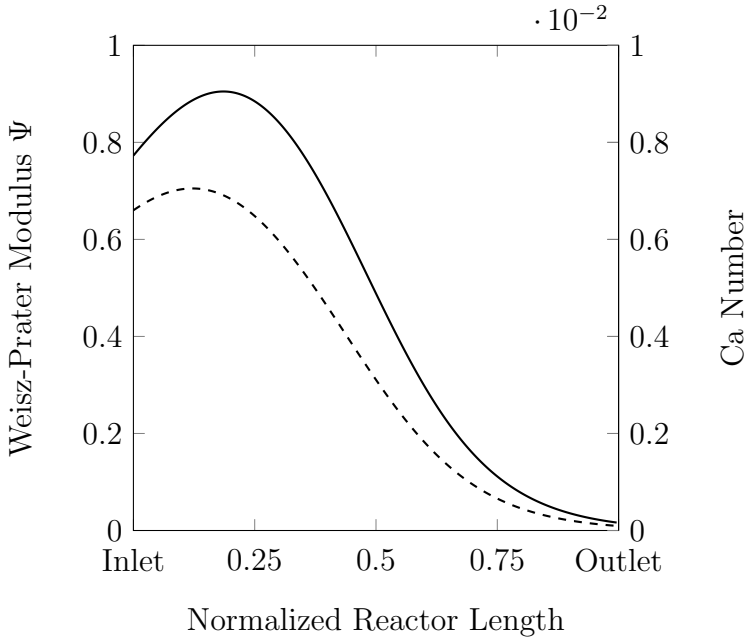

Figure C.13: Prater-Weisz modulus (——) and Carberry number (- - -) of the 2nd shift reactor of the Optimization I CO_2-PSA warm gas cleanup scenario using a high temperature, sweet shift catalyst with a system sizing factor of 1.1.

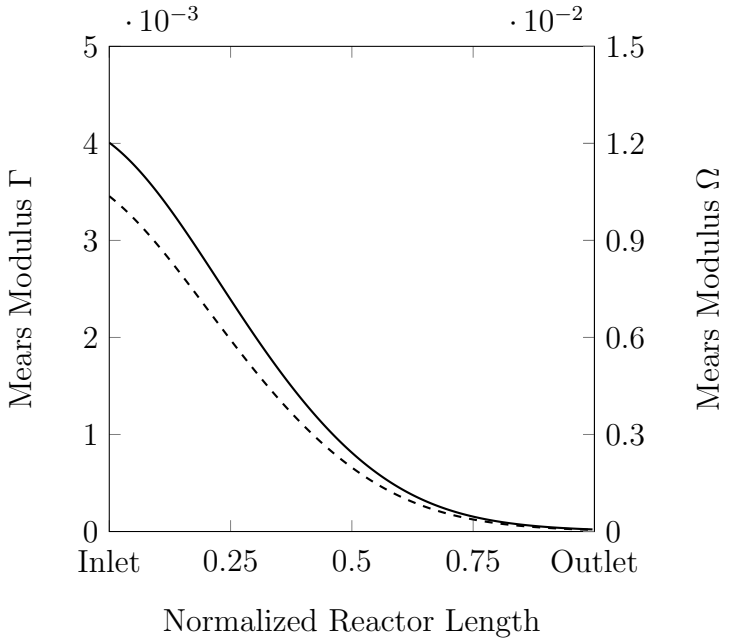

Figure C.14: Mears Modulus for internal heat transfer Γ (——) and Mears Modulus for external heat transfer Ω (- - -) of the 2nd shift reactor of the Optimization I CO_2-PSA warm gas cleanup scenario using a high temperature, sweet shift catalyst with a system sizing factor of 1.1.

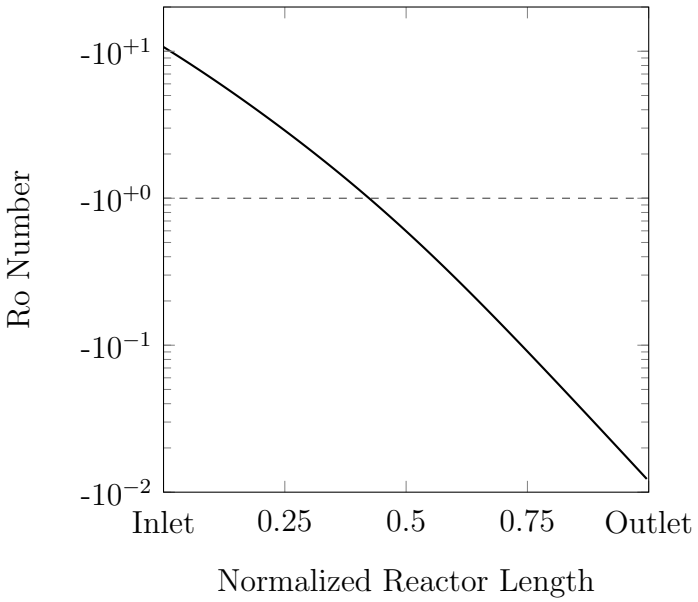

Figure C.15: Rate optimization number of the 2nd shift reactor of the Optimization I CO_2-PSA warm gas cleanup scenario using a high temperature, sweet shift catalyst with a system sizing factor of 1.1.

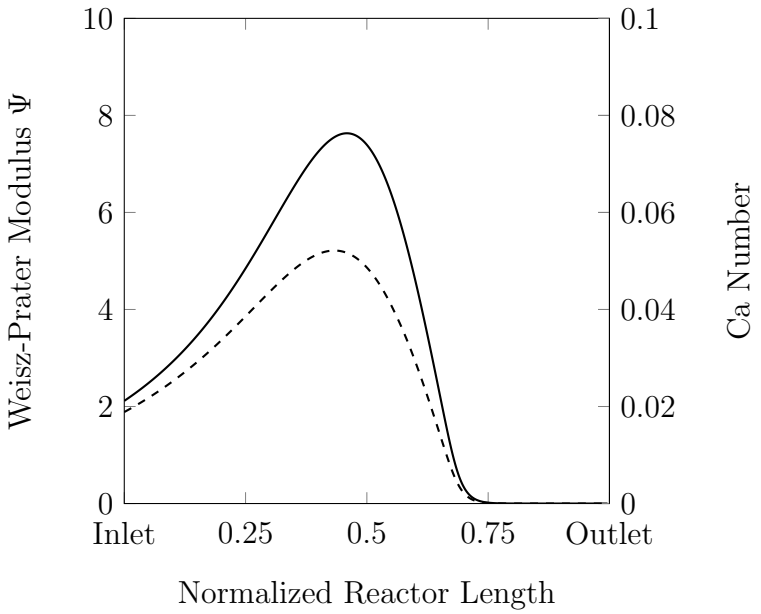

Figure C.16: Prater-Weisz modulus (——) and Carberry number (- - -) of the 1st shift reactor of the Optimization II CO_2-PSA warm gas cleanup scenario using a high temperature, sweet shift catalyst with a system sizing factor of 1.25.

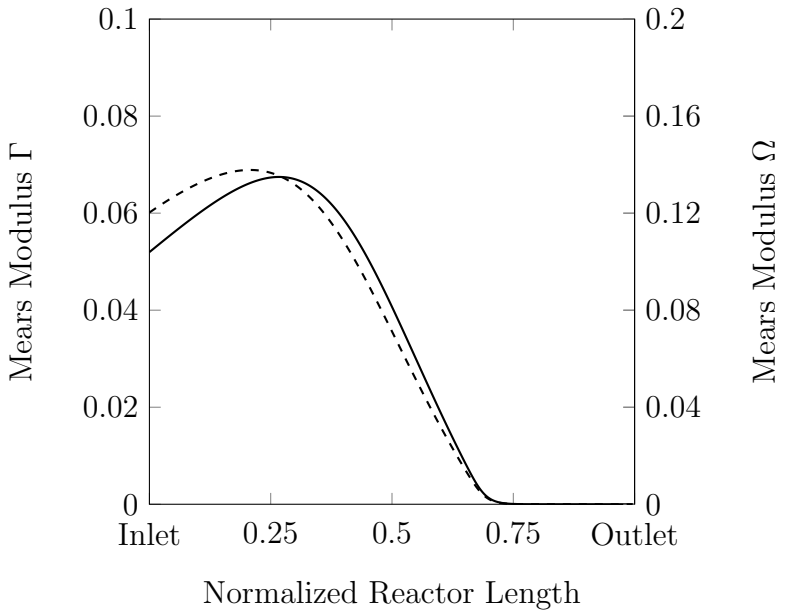

Figure C.17: Mears Modulus for internal heat transfer Γ (——) and Mears Modulus for external heat transfer Ω (- - -) of the 1st shift reactor of the Optimization II CO_2-PSA warm gas cleanup scenario using a high temperature, sweet shift catalyst with a system sizing factor of 1.25.

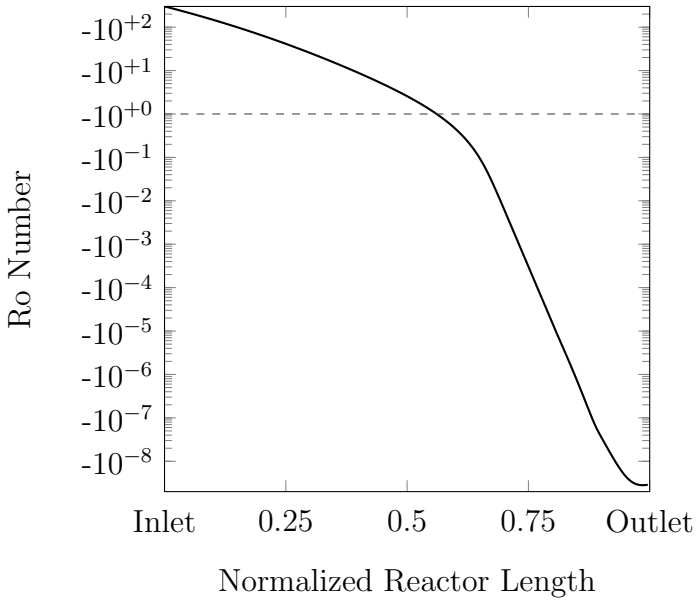

Figure C.18: Rate optimization number of the 1st shift reactor of the Optimization II CO_2-PSA warm gas cleanup scenario using a high temperature, sweet shift catalyst with a system sizing factor of 1.25.

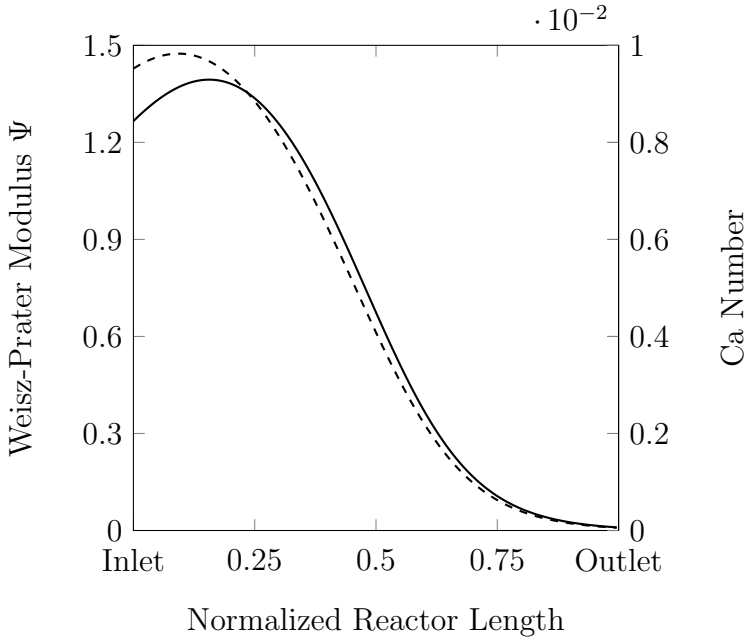

Figure C.19: Prater-Weisz modulus (——) and Carberry number (- - -) of the 2nd shift reactor of the Optimization II CO_2-PSA warm gas cleanup scenario using a high temperature, sweet shift catalyst with a system sizing factor of 1.1.

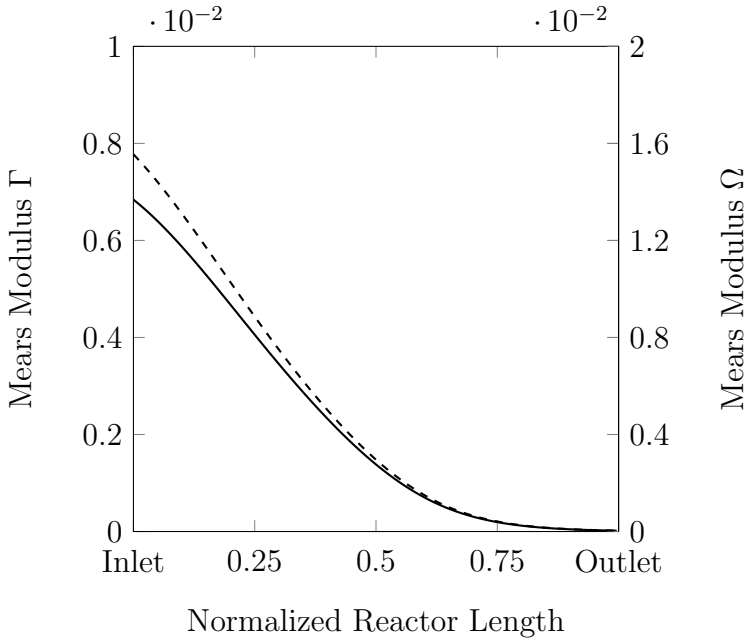

Figure C.20: Mears Modulus for internal heat transfer Γ (——) and Mears Modulus for external heat transfer Ω (- - -) of the 2nd shift reactor of the Optimization II CO_2-PSA warm gas cleanup scenario using a high temperature, sweet shift catalyst with a system sizing factor of 1.1.

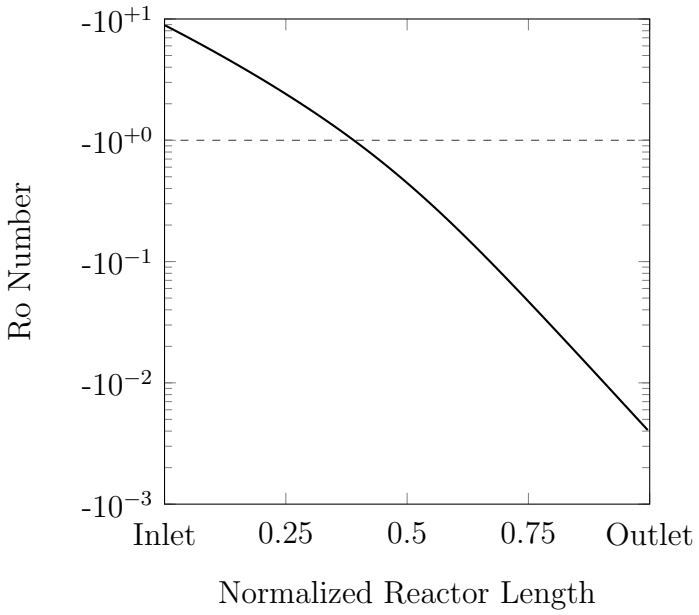

Figure C.21: Rate optimization number of the 2nd shift reactor of the Optimization II CO_2-PSA warm gas cleanup scenario using a high temperature, sweet shift catalyst with a system sizing factor of 1.1.

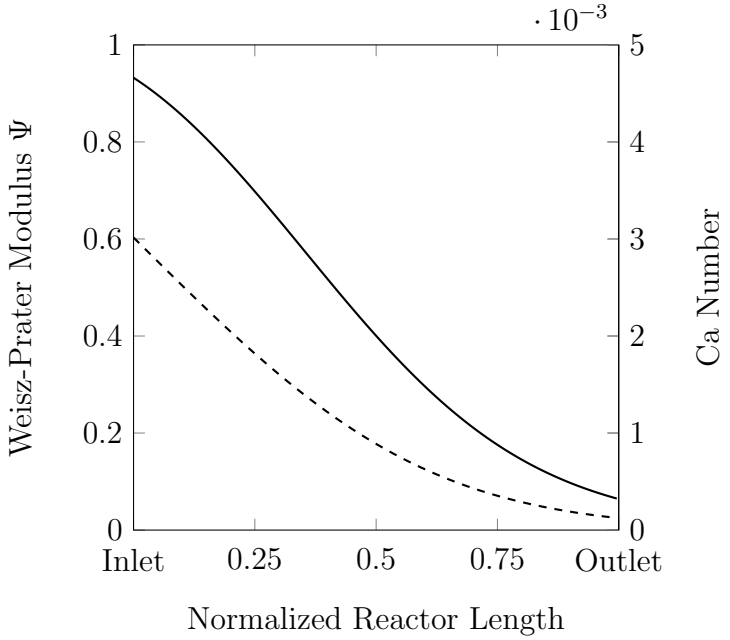

Figure C.22: Prater-Weisz modulus (——) and Carberry number (- - -) of the 3rd shift reactor of the Optimization II CO_2-PSA warm gas cleanup scenario using a high temperature, sweet shift catalyst with a system sizing factor of 1.1.

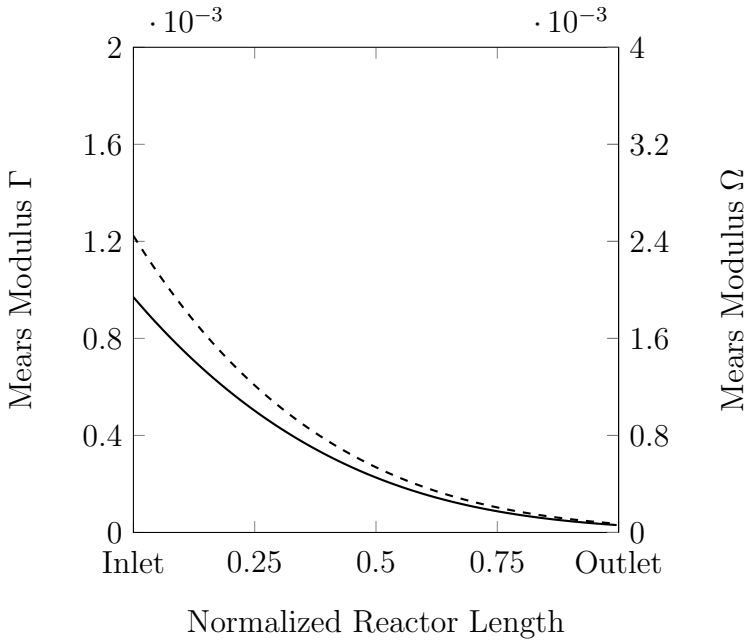

Figure C.23: Mears Modulus for internal heat transfer Γ (——) and Mears Modulus for external heat transfer Ω (- - -) of the 3rd shift reactor of the Optimization II CO_2-PSA warm gas cleanup scenario using a high temperature, sweet shift catalyst with a system sizing factor of 1.1.

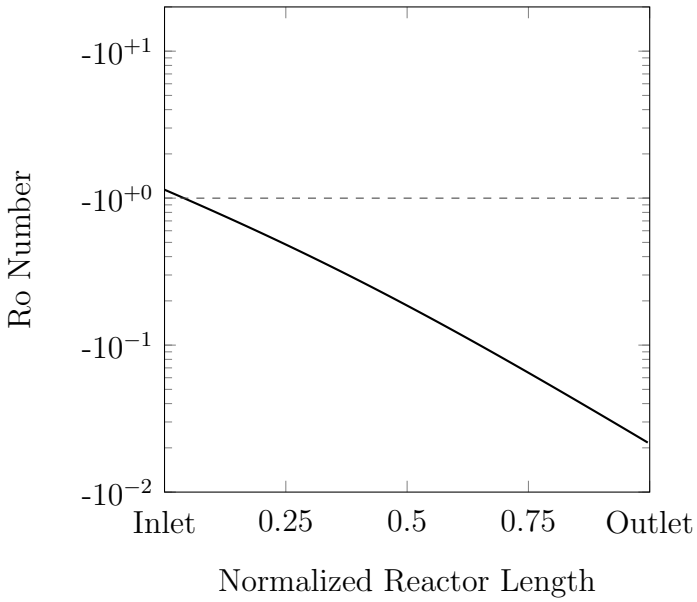

Figure C.24: Rate optimization number of the 3rd shift reactor of the Optimization II CO_2-PSA warm gas cleanup scenario using a high temperature, sweet shift catalyst with a system sizing factor of 1.1.

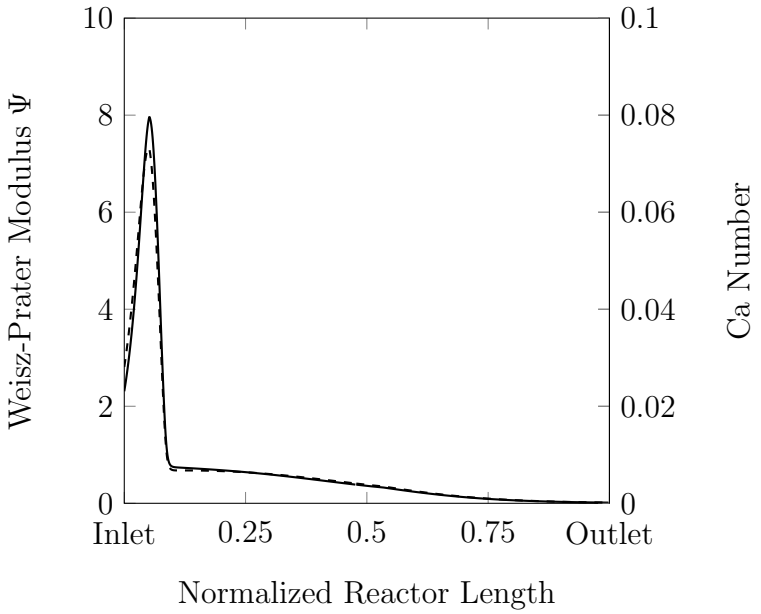

Figure C.25: Prater-Weisz modulus (——) and Carberry number (- - -) of the isothermal IP shift reactor of the Isothermal Shift I scenario using a sweet shift catalyst, IP steam generation and a system sizing factor of 1.1.

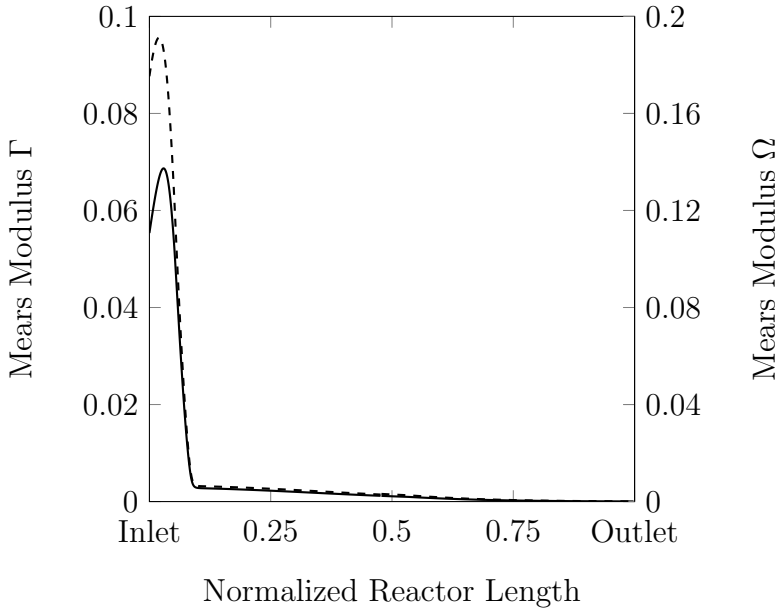

Figure C.26: Mears Modulus for internal heat transfer Γ (——) and Mears Modulus for external heat transfer Ω (- - -) of the isothermal IP shift reactor of the Isothermal Shift I scenario using a sweet shift catalyst, IP steam generation and a system sizing factor of 1.1.

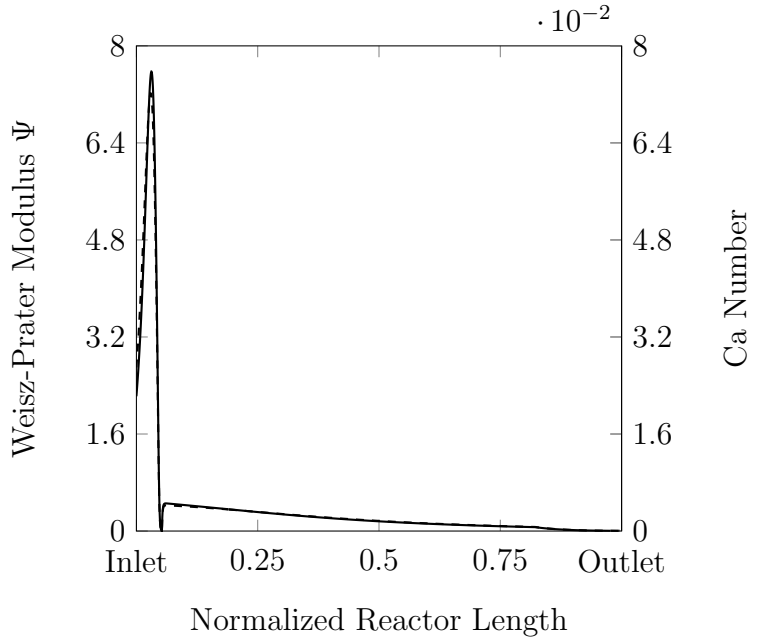

Figure C.27: Prater-Weisz modulus (——) and Carberry number (- - -) of the isothermal HP shift reactor of the Isothermal Shift II scenario using a sweet shift catalyst, HP steam generation and a system sizing factor of 1.1.

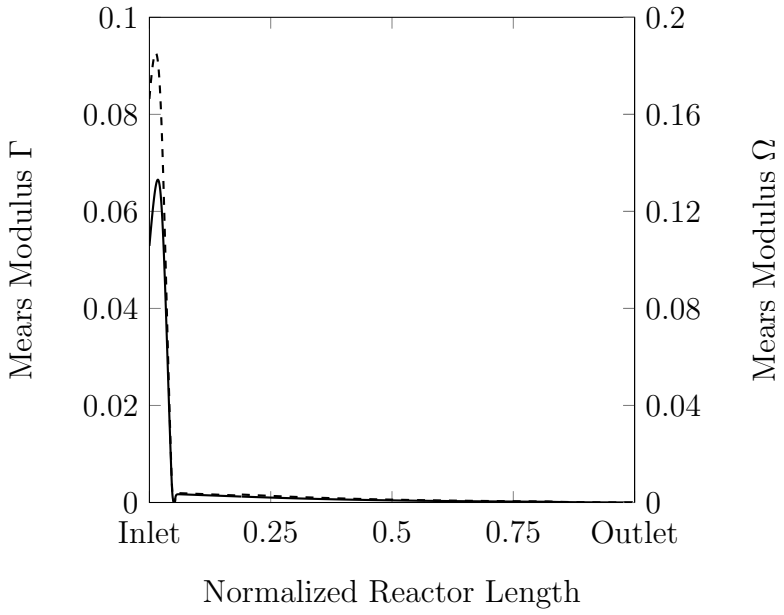

Figure C.28: Mears Modulus for internal heat transfer Γ (——) and Mears Modulus for external heat transfer Ω (- - -) of the isothermal HP shift reactor of the Isothermal Shift II scenario using a sweet shift catalyst, HP steam generation and a system sizing factor of 1.1.

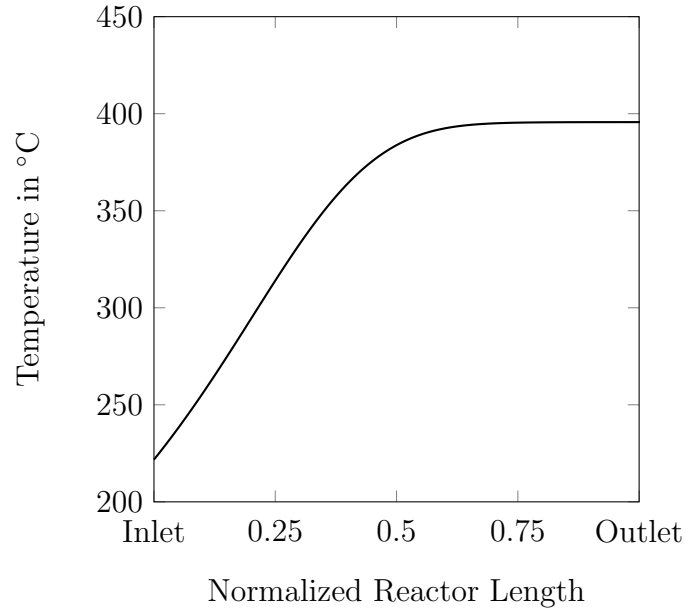

Figure C.29: Temperature profile of the 1st shift reactor of the Pathway III scenario using a sour shift catalyst with a system sizing factor of 1.25.

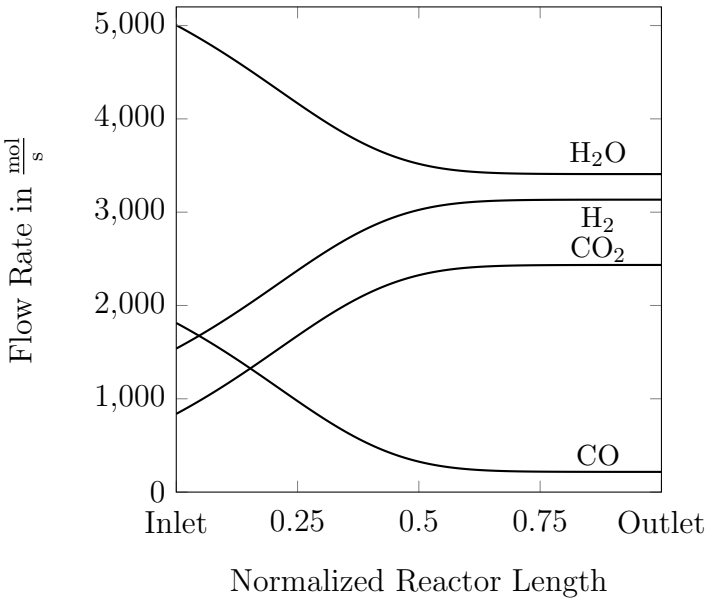

Figure C.30: Species profiles of the 1st shift reactor of the Pathway III scenario using a sour shift catalyst with a system sizing factor of 1.25.

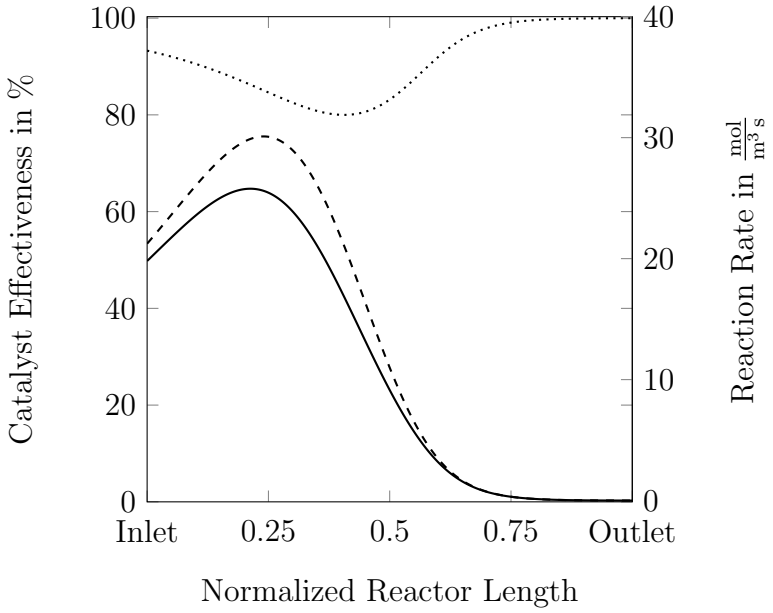

Figure C.31: Catalyst effectiveness (·····), intrinsic reaction rate (- - -) and apparent reaction rate (——) of the 1st shift reactor of the Pathway III scenario using a sour shift catalyst with a system sizing factor of 1.25.

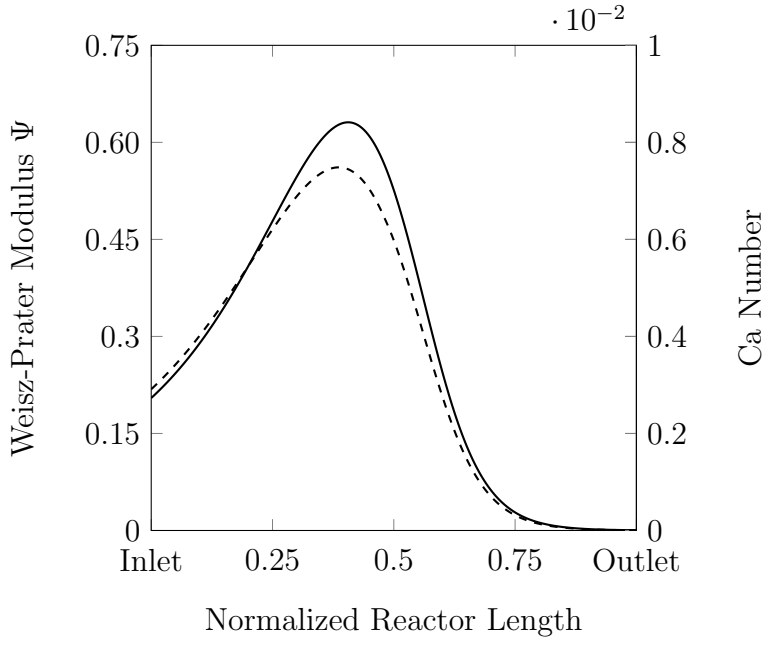

Figure C.32: Prater-Weisz modulus (——) and Carberry number (- - -) of the 1st shift reactor of the 1st shift reactor of the Pathway III scenario using a sour shift catalyst with a system sizing factor of 1.25.

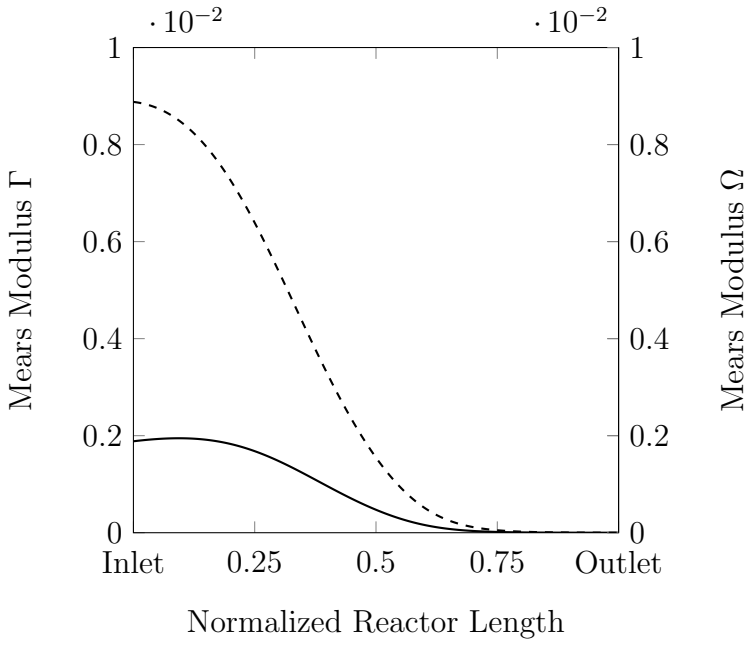

Figure C.33: Mears Modulus for internal heat transfer Γ (——) and Mears Modulus for external heat transfer Ω (- - -) of the 1st shift reactor of the Pathway III scenario using a sour shift catalyst with a system sizing factor of 1.25.

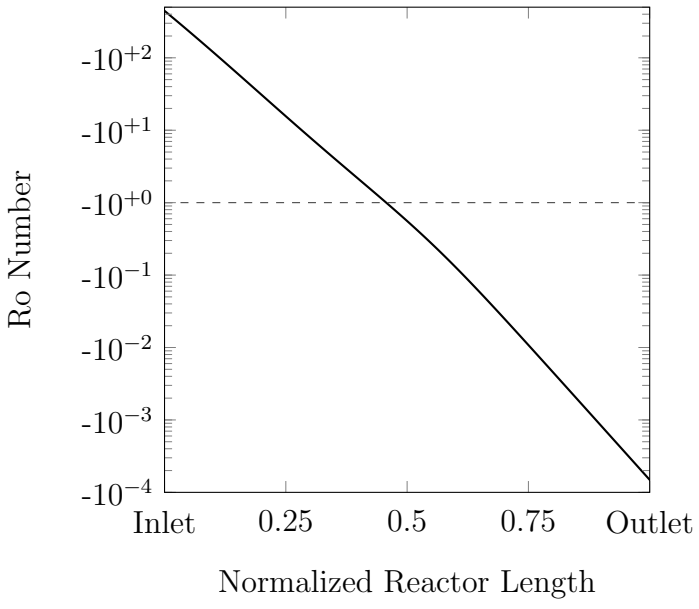

Figure C.34: Rate optimization number of the 1st shift reactor of the Pathway III scenario using a sour shift catalyst with a system sizing factor of 1.25.

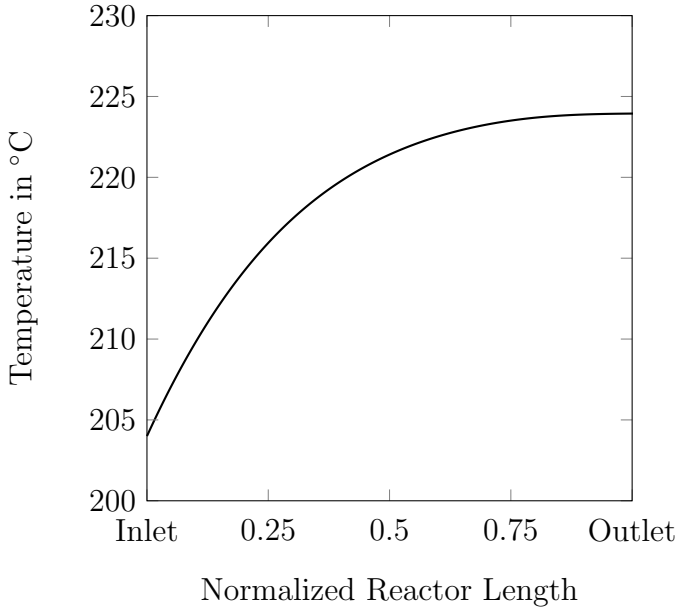

Figure C.35: Temperature profile of the 2nd shift reactor of the Pathway III scenario using a low temperature, sweet shift catalyst with a system sizing factor of 1.1.

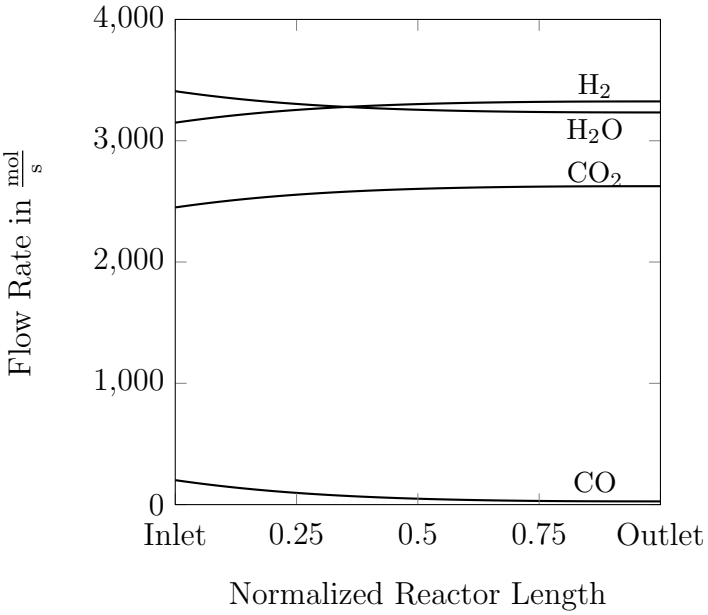

Figure C.36: Species profiles of the 2nd shift reactor of the Pathway III scenario using a low temperature, sweet shift catalyst with a system sizing factor of 1.1.

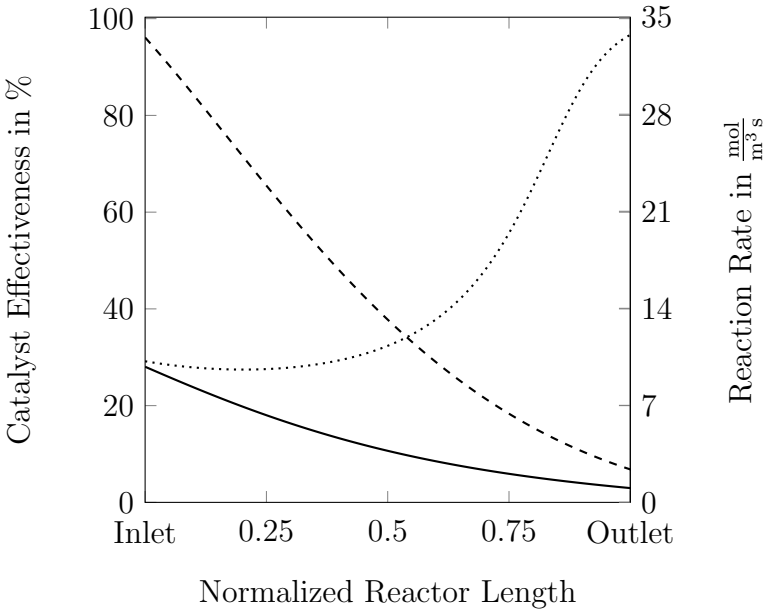

Figure C.37: Catalyst effectiveness (·····), intrinsic ration rate (- - -) and apparent reaction rate (——) of the 2nd shift reactor of the Pathway III scenario using a low temperature, sweet shift catalyst with a system sizing factor of 1.1.

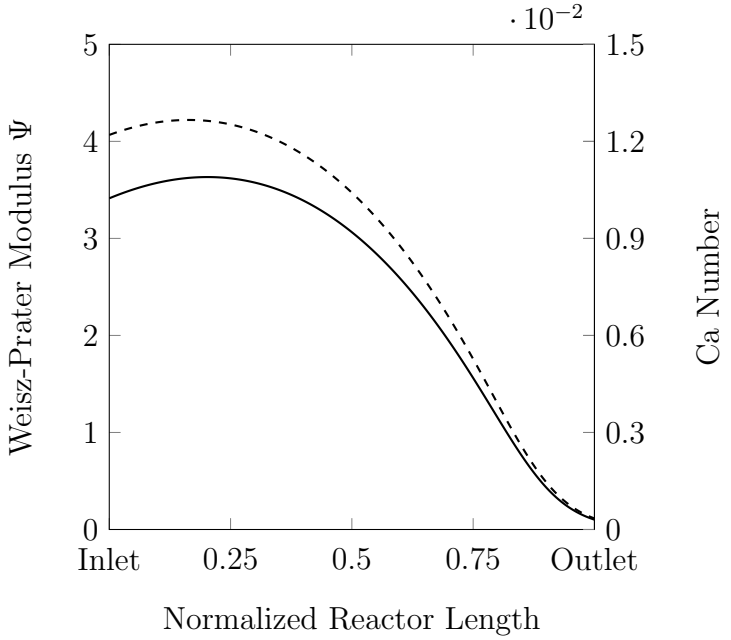

Figure C.38: Prater-Weisz modulus (——) and Carberry number (- - -) of the 2nd shift reactor of the Pathway III scenario using a low temperature, sweet shift catalyst with a system sizing factor of 1.1.

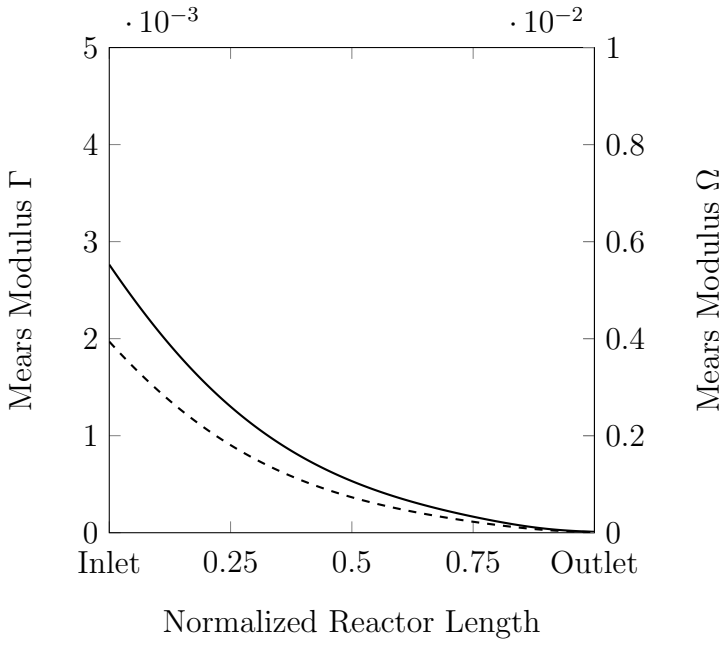

Figure C.39: Mears Modulus for internal heat transfer Γ (——) and Mears Modulus for external heat transfer Ω (- - -) of the 2nd shift reactor of the Pathway III scenario using a low temperature, sweet shift catalyst with a system sizing factor of 1.1.

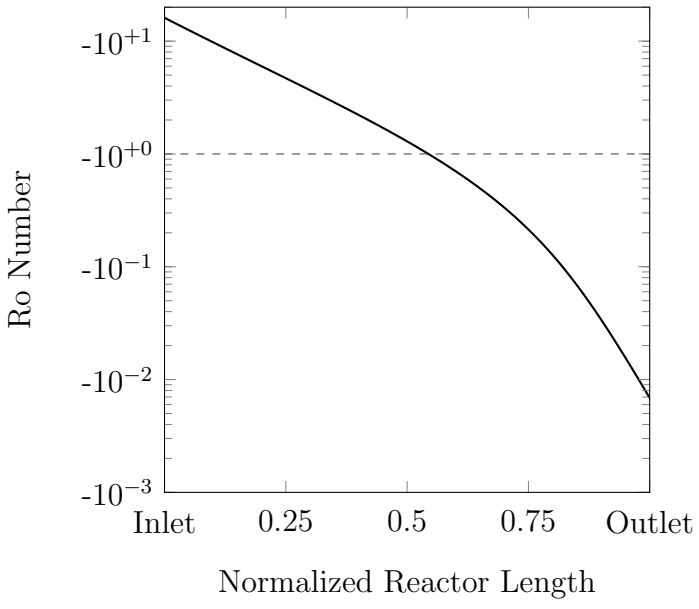

Figure C.40: Rate optimization number of the 2nd shift reactor of the Pathway III scenario using a low temperature, sweet shift catalyst with a system sizing factor of 1.1.